Universidade de Aveiro Departamento de Química
2020

ANA MARGARIDA SILVA COSTA

Hidrogeis Multiestruturais obtidos através de Estratégias Biomiméticas para Aplicações Biomédicas

Biomimetic Design of Multistructural Hydrogels for Biomedical Purposes

Universidade de Aveiro Departamento de Química
2020

ANA MARGARIDA SILVA COSTA

Hidrogeis Multiestruturais obtidos através de Estratégias Biomiméticas para Aplicações Biomédicas

Biomimetic Design of Multistructural Hydrogels for Biomedical Purposes

Tese apresentada à Universidade de Aveiro para cumprimento dos requisitos necessários à obtenção do grau de Doutor em Química, realizada sob a orientação científica do Doutor João Filipe Colardelle da Luz Mano, Professor Catedrático do Departamento de Química da Universidade de Aveiro

Apoio Financeiro pela Fundação para a Ciência e Tecnologia (FCT), através do projeto Marine Biotechnology ERA-NET "BLUETEETH" (ERA-MBT/0002/2015) e da concessão da bolsa de doutoramento SFRH/BD/101748/2014, no âmbito do Programa Operacional Potencial Humano (POPH) – Formação Avançada, comparticipada pelo Fundo Social Europeu (FSE) e por fundos nacionais do Ministério da Educação (MEC).

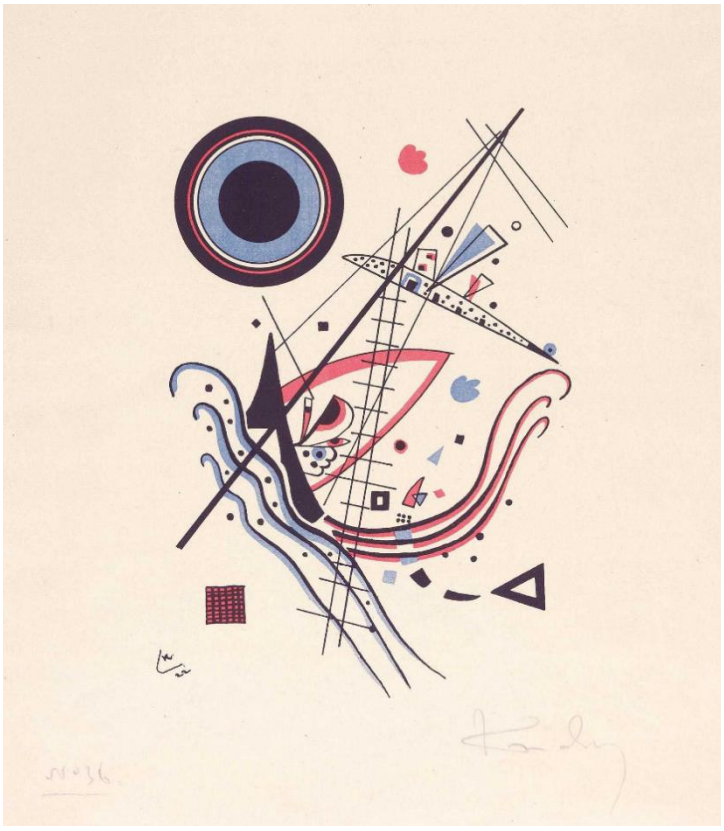

Wassily Kandinsky, *Blau* -**1922**

o júri

Presidente

Prof. Doutor Vitor Brás Sequeira Amaral
professor catedrático da Universidade de Aveiro

Arguentes

Prof. Doutor Manuel Salmeron-Sanchez
professor (Chair) da Universidade de Glasgow

Prof. Doutora Cristina Maria Santos Alves de Carvalho Barrias
professor associado da Universidade do Porto

Prof. Doutor Jorge Fernando Jordão Coelho
professor catedrático da Universidade de Coimbra

Prof. Doutor João Carlos Matias Celestino Gomes da Rocha
professor catedrático da Universidade de Aveiro

Prof. Doutor João Filipe Colardelle da Luz Mano
professor catedrático da Universidade de Aveiro

agradecimentos I would like to express my deeply gratitude and dedicate this dissertation to several people and institutions that helped me during my PhD.

Gostaria de começar por agradecer ao meu supervisor, Professor João Mano. Irei sempre recordar-me do seu entusiasmo pela ciência e das suas ideias originais e inspiradoras, que eram sempre acompanhadas por várias gargalhadas. Obrigada pelos desafios e oportunidades que me proporcionou. Tudo isto, ajudou-me a crescer profissional e pessoalmente e, a querer fazer melhor todos os dias. Agradeço a todos os meus extraordinários colegas do COMPASS RG, a.k.a. Texugos, que com o tempo foram crescendo exponencialmente, todo o apoio e por tornarem os meus dias mais felizes. Acreditem que todos vocês têm algo único e especial, e que aprendi com todos vocês. Às minhas colegas/amigas do trabalho/casa, Maria e Sofia, obrigada por tudo, vocês ajudaram-me muito mais do que imaginam. Em especial, gostava de deixar o meu maior obrigado ao meu amigo João pela sua boa-disposição, pelas conversas infindáveis e por estar sempre presente.

Gostava também de agradecer a todas as pessoas do CICECO (Aveiro Institute of Materials) e do Departamento de Química da Universidade de Aveiro, com as quais tive a sorte de me cruzar durante estes anos, toda a valiosa ajuda dada na resolução de todos os meus problemas científicos, técnicos e administrativos.

I would like to acknowledge Professor Andrew Dove from University of Warwick (now University of Birmingham) for the opportunity of working in his laboratory. It was maybe the most challenging experience of my PhD as I never worked in Organic Chemistry before, but it was also very rewarding as I truly learned so much. During my stay, I was lucky to meet wonderful people that I will always remember. Gracias Mar for all the support in the laboratory, you were the best post-doc I worked with, as well as for the valuable advices and friendship. Thank you, Laura for introducing me to the Organic Chemistry world. Obrigada Paula e Felipe por todos os momentos juntos, pela vossa amizade e por me deixarem descansar falando em português (apesar de com um sotaquezinho). Danke Patrick, “the other foreign PhD student”, for all the laughs and travels! Eskerrik asko Noé for all the conversations and the company on the late-night experiments. And to all the other colleagues that made me feel welcome. You are all amazing!

I would like to express my deeply felt thanks to Professor David Mooney for the opportunity to work with him and be part of his group, the Wyss Institute and Harvard University. It was a dream come true! I joined the most enthusiastic group ever, thanks to Miguel, Christina, Hua, Alberto, Meadhbh and Alex. Your love for science was an inspiration and thank you all for making me feel part of the group. My deepest gratitude goes to Ben that accompanied my research project (and always told me where the free food was)! A special thanks goes to the “Lab LOOsers” group - Raphael, Alena, Carola and Sangmin - for all the cooking, trips and friendship! And, of course, to all the fantastic friends I made outside the lab with whom I shared unforgettable moments, including the most wonderful Christmas Dinner outside Portugal. Thanks Carlos, Mitsue, Liza, Guillaume, Manav and Laura.

Gostaria, ainda, de agradecer a toda a equipa dos 3Bs da Universidade do Minho pela amizade e profissionalismo. Recordo com saudade o tempo que passei nesta instituição, onde iniciei o meu doutoramento e conheci pessoas maravilhosas. Lembro-me das conversas científicas e não científicas durante os almoços no exterior, as festas surpresa

de aniversário e as nossas saídas depois do trabalho. Em especial, gostava de agradecer ao Luca, à Joana, ao Rui Costa, ao Álvaro e ao Nuno, foi um prazer trabalhar convosco. E, claro, ao grupo SSMSS - Sofia, Sílvia, Sónia e Silvia – são das melhores amizades que levo destes anos. Obrigada por tudo!

Obrigada Sofia, Nádia, Francisca e Joana Raquel pela vossa longa e valiosa amizade, imenso respeito e preciosos conselhos e, acima de tudo, por poder contar sempre convosco. Apesar de estarmos mais longe, quando estamos juntas parece que o tempo não passou.

Por último, mas são as pessoas mais importantes da minha vida, quero agradecer à minha família excecional, em especial à minha mãe, ao meu pai e às minhas irmãs, pelo apoio incondicional, por me aturarem todos os dias e por serem verdadeiros exemplos de vida.

Vasco, fizeste toda a diferença neste período da minha vida, contribuindo para o meu equilíbrio. Obrigada pelo teu sorriso, pelas tuas palavras, pelo teu amor e pela tua paciência.

palavras-chave hidrogel, double-network, polissacarídeos, superfícies superanfifóbicas, microesferas, partículas hierárquicas, cápsulas

resumo

A matriz extracelular dos tecidos moles é caraterizada por uma estrutura definida e complexa, sendo responsável pelas suas extraordinárias propriedades mecânicas. Usando a matriz extracelular como inspiração, foi demonstrada a possibilidade de produzir hidrogéis robustos e citocompatíveis sob condições fisiológicas. Os materiais obtidos foram sintetizados através de uma adaptação da metodologia Double-network (DN), combinando mecanismos de reticulação físicos e químicos. Estes sistemas multifuncionais são capazes de suportar tensões mecânicas na mesma ordem de grandeza das encontradas nos tecidos estruturais do corpo, o que reforça o potencial destes biomateriais hidratados para reparar estes mesmos tecidos. Estes géis DN foram melhorados de modo a obter materiais com outras características importantes para aplicações biomédicas, nomeadamente a capacidade de se autorrepararem e serem administrados através de estratégias minimamente invasivas, como por injeção.

Adicionalmente, o nosso grupo desenvolveu uma nova metodologia, inspirada pela capacidade de a folha de lótus repelir líquidos, para produzir partículas poliméricas com uma forma esférica. Esta técnica consiste em dispensar uma solução polimérica sobre uma superfície com extrema repelência a líquidos e, de seguida, um processo de reticulação é aplicado à gota polimérica de modo a reter a sua forma esférica. Nesta tese, esta estratégia biomimética foi usada para fabricar diversos sistemas esféricos com variadas estruturas macroscópicas. Primeiro, superfícies reversíveis e superanfifóbicas (SA) foram criadas através da deposição de microcápsulas contendo partículas magnéticas no seu interior sobre um suporte sólido. A principal vantagem de usar partículas sensíveis a campos magnéticos é a possibilidade de controlar a sua posição e fixação a um suporte usando um íman. Estas superfícies SA foram usadas como suportes para produzir partículas esféricas e canais de microfluídica. De seguida, partículas poliméricas com tamanhos na escala micrométrica foram obtidos, pela primeira vez, usando superfícies SA. A estratégia desenvolvida consiste em dispensar, sob uma superfície SA, uma solução polimérica usando um pulverizador e, de seguida, um mecanismo de reticulação é aplicado de modo a obter hidrogéis esféricos. Adicionalmente, foram também criadas partículas multicompartimentalizadas com uma estrutura hierárquica incorporando as micropartículas produzidas anteriormente.

Finalmente, as superfícies SA foram também usadas para obter cápsulas esféricas compostas por uma camada externa polimérica e um núcleo no estado líquido. Diferentes objetos como células e moléculas bioativas podem ser encapsulados no interior das partículas anteriores, reforçando o seu potencial biomédico.

É antecipado que todas estas estratégias biomiméticas sejam importantes para o desenvolvimento da nova geração de hidrogéis com potencial em biomedicina e engenharia de tecidos.

keywords

hydrogel, double-network, polysaccharides, microspheres, hierarchical particles, capsules, superamphiphobic surfaces

abstract

The extracellular matrix (ECM) of load-bearing soft tissues is characterized by a well-defined and complex architecture which is responsible for its high mechanical performance. Inspired by the native ECM of living tissues, we demonstrate the possibility to fabricate tough and cytocompatible hydrogels from a single polymeric precursor formulation and under physiological conditions. The designed systems were synthesized through an adapted Double-network (DN)-based methodology combining chemical and physical crosslinking mechanisms. Such multifunctional devices were able to withstand an impressive compressive stress in the same order of magnitude as the ones found in native load-bearing soft tissues, highlighting their potential for the repair of these tissues. Further improvements on the former DN-based hydrogel were made in order to achieve highly hydrated biomaterials with other advantageous properties for biomedical purposes, including self-healing and injectability.

Inspired by the lotus-leaf liquid-repellence, our group proposed a simple, straightforward and cost-effective tool to produce spherical polymeric particles above artificial superantiwetting surfaces. In this thesis, this biomimetic strategy was used to fabricate a large variety of natural-based hydrogel spherical systems with distinct macroscopic structures. First, reversible superamphiphobic (SA) surfaces were fabricated by covering a substrate with specifically designed microcapsules entrapping magnetic particles. The main advantage of using magnetic responsive particles is the ability to control their arrangement and fixation over the substrate by applying an external magnetic field. The produced non-permanent SA surfaces were successfully employed to fabricate water/oil repellent surfaces, liquid marbles and microfluidic channels and, also used as templates for the fabrication of spherical particles. Second, SA surfaces were successfully employed as supports to produce spherical polymeric microparticles with potential as cell and drug carriers. The proposed strategy consists in spraying a hydrogel precursor solution over a SA surface followed by a crosslinking mechanism. Next, hierarchical systems were also created via the assembly of polymeric spherical particles induced by these artificial SA substrates under physiological conditions. Finally, SA surfaces were successfully employed to fabricate ready-to-use and stable liquefied capsules enclosing different objects, such as cells and drugs.

All these bioinspired strategies are poised to usher the development of the next generation of engineered hydrogel devices for biomedicine and tissue engineering.

Contents

List of Abbreviations and Acronyms

0-9	
3D	Tridimensional
A	
AAm	Acrylamide
AAP	Anionic Polymerization
AFM	Atomic Force Microscopy
ALG	Alginate
AP	Average pitch
ASAP	Sodium polyacrylate
B	
BC	Bacterial cellulose
BSA	Bovine Serum Albumin
C	
C	Carbon
$CaCl_2$	Calcium chloride
$CaCO_3$	Calcium carbonate
CCb	Click Chemistry-based
CD	Crosslinking Degree
CH_2Cl_2	Methylene chloride
CH_3COOH	Acetic acid glacial
CHI	Chitosan
CTA	Cetyltrimethylammonium
CVD	Chemical Vapor Deposition
α-CD	α-Cyclodextrin
D	
D_2O	Deuterium oxide
DAAm	N, N-Dimethylacrylamide
DC	Double-Crosslinked
DEXT	Dextran
DGI	Dodecyl Glycerol Itaconate
DMAP	Dimethylamine Pyridine
DMEM	Dulbecco's Modified Eagle's Medium
DMSO	Dimethyl sulfoxide
DN	Double-Network
DNA	Deoxyribonucleic Acid
D-NC	Dendritic Nanocomposite
DOPA	3,4-Dihydroxy-L-phenylalanine
DOPA-CHI	DOPA-functionalized CHI
E	
ECH	Epichlorohydrin
ECL	ε-Caprolactam
ECM	Extracellular Matrix
EDC	N-(3-dimethylaminopropyl)-N'-ethylcarbodiimide hydrochloride
EDS	Energy-Dispersive X-Ray Spectroscopy
EDTA	Ethylenediamine tetraacetic acid
EthD-1	Ethidium homodimer
EtOH	Ethanol
F	
FA	Fractional area
FBS	Fetal bovine serum
$FeCl_3 \cdot 6H_2O$	Iron(II) chloride tetrahydrate
FITC	Fluorescein-isothiocyanate
FTIR	Fourier Transformed Infrared Spectroscopy
G	
G	α-L-guluronic acid
GEL	Gelatin

GelMA	Gelatin Methacrylamide
GGMA	Gellan Gum Methacrylate
GluN	Glucosamine
GMA	Glicidyl Methacrylate
GP	Genipin
β-GP	β-glycerophosphate

H

HA	Hyaluronan
HCl	Hydrochloric acid
Hib	Hydrophobic interactions-based

I

I2959	2-hydroxy-4'-(2-hydroxyethoxy)-2-methylpropiophenone
IC	Iota-Carrageenan
IPN	Interpenetrating Networks
ITC	Ionically crosslinked Triblock Copolymer

J

JF	Jellyfish

K

KC	Kappa-Carrageenan
KPS	Potassium Peroxodisulfate

L

Lb	Lamellar bilayer
LC	Lambda-Carrageenan
LMW-CHI	Low Molecular Weight-Chitosan
LMW-MACHI	Low Molecular Weight-Methacrylamide Chitosan
L-NC	Layered Nanocomposite
LPD	Liquid Phase Deposition

M

M	β-D-Mannuronic acid
MA	Methacrylic Anhydride
MACHI	Methacrylamide Chitosan
MA-DEXT	Methacrylate-Dextran
MBAAm	N,N-methylenebisacrylamide
MES	2-(N-morpholino) Ethanesulfonic acid hydrate
MIC	Microcapsules
MMC	Macromolecular Microspheres Composite
MMW-CHI	Medium Molecular Weight Chitosan
MPTC	3-(methacryloylamino) Propyl-Trimethylammonium Chloride
MTS	3-(4,5-dimethylthiazol-2-yl)5-(3-carboxymethoxy-phenyl)-2-4-sulfophenyl)-2-4-sulfophenyl)-2H-tetrazolium

N

Na_2CO_3	Sodium carbonate
NaCl	Sodium chloride
NaOH	Sodium hydroxide
NASS	Sodium pstyrenesulphonate
NC	Nanocomposite
NH_4OH	Ammonium hydroxide
NHS	N-hydroxysuccinimide
NIPAM	N-Isopropyl Acrylamide
NMR	Nuclear Magnetic Resonance

O

OD	Optical density

P

P	Phosphorus
PA	Polyampholytes
PAA	Poly(acrylic acid)
PAAc	Hydrophobically-modified poly(acrylic acid)
PAAm	Poly(acrylamide)
PAMPS	Poly(2-acrylamido-2-methylpropanesulfonic) acid
PBA	Phenylboronic Acid
PBS	Phosphate Buffer Saline
PDMS	Polydimethylsiloxane
PEG	Poly-ethylene glycol
PFDTS	1H,1H,2H,2H-perfluorodecyl triethoxysilane
PHA	Methacrylate Hyaluronan
PI	Propidium iodide
PLLA	Poly(L-lactic acid)
PMMA	Poly(methyl methacrylate)
PNIPAAm	Poly(N-isopropyl acrylamide)
PtBMA	Poly(tert-butyl methacrylate)
PVA	Polyvinyl alcohol

R

RMS	Root mean square
RT	Room temperature

S

SA	Superamphiphobic
SCA	Surface Contact Area
SBF	Simulated Body Fluid
SD	Substitution Degree
SEM	Scanning Electron Microscope
SF	Shape Factor
SH	Superhydrophobic
SI	Supplementary information
SiI-MIC	Fluorosilane-coated microcapsules

T

TAPEG	Tetraamine-terminated PEG
TCPS	Tissue Culture Polystyrene Plates
TE	Tissue Engineering
TEOS	Tetraethyl Orthosilicate
TFA	Trifluoroacetic acid
THPEG	Tetrahydroxyl-terminated PEG
TP	Topological
TPP	Sodium tripolyphosphate
Treta-PEG	Tetra-poly(ethylene)glycol

U

UG	Untreated glass
UV	Ultraviolet

W

WCA	Water contact angles

List of Tables

CHAPTER IV

CHAPTER VI

CHAPTER IX

List of Figures

SECTION 1: Design of Double-network (DN) hydrogels using natural polysaccharides

CHAPTER I

CHAPTER II

CHAPTER III

CHAPTER IV

CHAPTER V

SECTION 2: Superantiwetting Platforms to produce Spherical-Shaped Particles

CHAPTER VI

CHAPTER VII

CHAPTER VIII

CHAPTER IX

CHAPTER X

CHAPTER XI

CHAPTER XII

List of Publications

A – Publications resulting from the work performed during the present PhD thesis in:

A1 – International peer-reviewed journals

Sara Azevedo#, Ana M. S. Costa#, Amanda Andersen, Insung S. Choi, Henrik Birkedal, João F. Mano, (#authors contributed equally), Bioinspired Ultratough Hydrogel with Fast Recovery, Self-Healing, Injectability and Cytocompatibility, *Advanced Materials* **2017**, 29(28), pp. 1700759,

DOI: 10.1002/adma.201700759

URL: http://onlinelibrary.wiley.com/doi/10.1002/adma.201700759

Ana M. S. Costa, João F. Mano, Solvent-Free Strategy Yields Size and Shape-Uniform Capsules, *Journal of American Chemical Society* **2017**, 139(3), pp. 1057-1060,

DOI: 10.1021/jacs.6b11925

URL: https://pubs.acs.org/doi/10.1021/jacs.6b11925

Ana M. S. Costa, Nadya V. Dencheva, Sofia G. Caridade, Zlatan Z. Denchev, João F. Mano, Moldable Superhydrophobic Surfaces, *Advanced Materials Interfaces* **2016**, 3 (16), 1600074,

DOI:10.1002/admi.201600074

URL: http://onlinelibrary.wiley.com/doi/10.1002/admi.201600074

Ana M. S. Costa, Manuel Alatorre-Meda, Carmen Alvarez-Lorenzo, João F. Mano, Superhydrophobic Surfaces as a Tool for the Fabrication of Hierarchical Spherical Polymeric Carriers, *Small* **2015**,11 (30), pp. 3648-3652,

DOI: 10.1002/smll.201500192

URL: https://doi.org/10.1002/smll.201500192

Ana M. S. Costa, João F. Mano, Extremely strong and tough hydrogels as prospective candidates for tissue repair -A review, *European Polymer Journal* **2015**, 72, pp. 344-364,

DOI: doi:10.1016/j.eurpolymj.2015.07.053

URL: https://doi.org/10.1016/j.eurpolymj.2015.07.053

Ana M. S. Costa, João F. Mano, Highly robust hydrogels via a fast, simple and cytocompatible dual crosslinking-based process, *Chemical Communications* **2015**, 51 (86), pp. 15673-15676,

DOI: 10.1039/c5cc05564d

URL:http://pubs.rsc.org/en/Content/ArticleLanding/2015/CC/C5CC05564D#!divAbstract

Ana M. S. Costa, Manuel Alatorre-Meda, Nuno M. Oliveira, João F. Mano, Biocompatible Polymeric Microparticles Produced by a Simple Biomimetic Approach, *Langmuir* **2014**, 30 (16), pp. 4535–4539,

DOI: 10.1021/la500286v

URL: http://pubs.acs.org/doi/abs/10.1021/la500286v

A2- Not included in this thesis

Costa A.M.S., Rodrigues J. M. M., Pérez-Madrigal M.M., Mano J. F., Dove A., *In preparation*, 2019

Costa A.M.S., Freedman B., Mano J. F., Mooney D., *In preparation*, 2019

A3 – Conference Proceedings

Costa R. R., Mano J. F., Costa A. M. S., Caridade S. G., Saloplastic Membranes as Green Devices for Soft Tissue Regeneration, **Tissue Engineering** Part A, Vol. 21, Issue S1, pp. S159, doi:10.1089/ten.tea.2015.5000.abstracts, 2015

Costa A. M. S., Mano J. F., Highly Robust Chitosan Hydrogels via a Fast, Simple and Biocompatible Dual Crosslinking-based Process, **Tissue Engineering** Part A, Vol. 21, pp. 359, doi:10.1089/ten.tea.2015.5000.abstracts, 2015

A4 – International and national conferences

A4.1 – Oral communications

Costa, A. M. S., João F. Mano, **Jornadas CICECO 2018**, Aveiro, Portugal (June 2018); Rising Science Communicator Award

Costa, A. M. S., João F. Mano, Hydrogels: synthesis and applications, **Jornadas do Departamento de Química**, Aveiro, Portugal (March 2018);

A4.2 – Poster communications

Costa A. M. S., Mano J. F., Core-shell structured polymeric particles through a solvent-free strategy, **Jornadas CICECO 2019**, Aveiro, Portugal (June 2019);

Rodrigues J. M. M., Costa A. M. S., Mano J. F., Laminarin-Catechol Injectable Hydrogels for Tissue Regeneration, **Jornadas CICECO 2019**, Aveiro, Portugal (June 2019);

Rodrigues J. M. M., Costa A. M. S., Mano J. F., Injectable Hydrogels with Self-healing for Tissue Regeneration, **Thermis EU 2019**, Rhodes, Greece (May 2019);

Costa A. M. S., Mano J. F., Polysaccharide-based Hydrogels for Biomedical Applicatons, **Ciência 2018**, Lisboa, Portugal (July 2018);

Costa A. M. S., Mano J. F., In air fabrication of polymeric capsules, **Jornadas CICECO 2018**, Aveiro, Portugal (June 2018);

Costa A. M. S., Mano J. F., Superamphiphobic surfaces as a tool to fabricate polymeric capsules, **International Symposium on Bioinspired Macromolecular Systems**, Aveiro, Portugal (November 2017);

Bjørge I. M., Costa A. M. S., A. Silva S., Vidal J. P., J. Nóbrega M., Mano J. F., Tuneable spheroidal hydrogel particles for cell and drug encapsulation, **International Symposium on Bioinspired Macromolecular Systems**, Aveiro, Portugal (November 2017);

Costa A. M. S., Mano J. F., In air fabrication of polymeric capsules, **5th International Symposium Frontiers in Polymer Science**, Seville, Spain (May 2017); Best Poster Presentation Award

Costa A. M. S., Azevedo Sara E., Mano J. F., Injectable, robust hydrogels towards cartilage repair, **European Chapter Meeting of the TERMIS 2016**, Uppsala, Sweden (July 2016);

Costa A. M. S., Azevedo S. E., Mano J. F., Injectable, robust hydrogels towards cartilage repair**, 5th PYCheMand 1nd EYCheM,** Guimarães, Portugal (April 2016);

Costa R. R., Mano J. F., Costa A. M. S., Caridade S. G., Saloplastic Membranes as Green Devices for Soft Tissue Regeneration, **4th TERMIS World Congress** 2015, Boston, USA (August 2015);

Costa A. M. S., Mano J. F., Highly Robust Chitosan Hydrogels via a Fast, Simple and Biocompatible Dual Crosslinking-based Process, **4th TERMIS World Congress** 2015, Boston, USA (August 2015);

Costa A. M. S., Alatorre-Meda M., Alvarez-Lorenzo C., Mano J. F., Fabrication of Hierarchical Polymeric Carriers for Drug Delivery and Cell Encapsulation using Superhydrophobic Surfaces, **TermStem 2014**, Porto, Portugal (October 2014).

B – Publications in international peer-reviewed journal resulting from collaborative work performed during the present PhD thesis

Jeanny S. Maciel, Sara Azevedo, Clara R. Correia, Ana M. S. Costa, Rui R. Costa, Francisco A. Magalhães, Aliny A. S. Monteiro, José Francisco G. Costa, Regina C. M de Paula,

Judith P. A. Feitosa, João F. Mano, Oxidized Cashew Gum Scaffolds for Tissue Engineering, *Macromolecular Materials and Engineering* **2019**, 304 (3), 1800574,

DOI: 10.1002/mame.201800574

URL: https://doi.org/10.1002/mame.201800574

Isabel M. Bjørge, Ana M. S. Costa, Ana S. Silva, João P. O. Vidal, J. Miguel Nóbrega, João F. Mano, Tuneable spheroidal hydrogel particles for cell and drug encapsulation, *Soft Matter* **2018**, 14, pp. 5622-5627,

DOI: 10.1039/C8SM00921J

URL: https://pubs.rsc.org/en/content/articlelanding/2018/sm/c8sm00921j#!divAbstract

Carla Ribeiro, João Borges, Ana M. S. Costa, Vítor M. Gaspar, Verónica De Zea Bermudez, João F. Mano, Preparation of Well-Dispersed Chitosan/Alginate Hollow Multilayered Microcapsules for Enhanced Cellular Internalization, *Molecules* **2018**, 23 (3), pp. 625-16,

DOI: 10.3390/molecules23030625

URL: https://www.mdpi.com/1420-3049/23/3/625

Álvaro J. Leite, Rui R.Costa, Ana M. S. Costa, Jeanny S. Maciel, José F. G. Costa, Regina C. M. de Paula, João F. Mano, The potential of cashew gum functionalization as building blocks for layer-by-layer films, *Carbohydrate Polymers* **2017**, 174, pp. 849-857,

DOI: 10.1016/j.carbpol.2017.06.055

URL: https://doi.org/10.1016/j.carbpol.2017.06.055

M. Fernandes, R. Leones, S. Pereira, Ana M. S. Costa, João F. Mano, M. M. Silva, E. Fortunato, V. de Zea Bermudez, R. Rego, Eco-friendly sol-gel derived sodium-based ormolytes for electrochromic devices, *Electrochimica Acta* **2017**, 232, pp. 484–494,

DOI: 10.1016/j.electacta.2017.02.098

URL: https://doi.org/10.1016/j.electacta.2017.02.098

R.R. Costa, Ana M. S. Costa, S. G. Caridade, João F. Mano, Compact Saloplastic Membranes of Natural Polysaccharides for Soft Tissue Engineering, *Chemistry of Materials* **2015**, 27 (21), pp. 7490-7502,

DOI: 10.1021/acs.chemmater.5b03648

URL: http://pubs.acs.org/doi/10.1021/acs.chemmater.5b03648

M. Fernandes, R. Leones, Ana M. S. Costa, M. M. Silva, S. Pereira, João F. Mano, E. Fortunato, R. Rego, V. De Zea Bermudez, Electrochromic devices incorporating biohybrid electrolytes doped with a lithium salt, anionic liquid or a mixture of both, *Electrochimica Acta* **2015**, 161, pp. 226-235,

DOI: doi:10.1016/j.electacta.2015.02.036

URL: https://doi.org/10.1016/j.electacta.2015.02.036

Thesis Outline

The present thesis explores various biomimetic strategies for the synthesis of novel hydrogel-based biomaterials with distinct macromolecular structures for a wide range of biomedical applications. In Section 1, the extracellular matrix (ECM) of tissues and the mussel byssus attachment system were used as an inspiration to create hydrogel devices by employing strategies of macromolecular design, which resulted in biomaterials with enhanced mechanical properties, self-healing and injectability. The processing of such biomaterials is required to successfully employ them for biomedical purposes. Accordingly, Section 2 contains a collection of experimental works inspired by the water-repellence ability of the Lotus leaf as well as by the complex hierarchical and compartmentalized structure of cells, with the aim of creating spherical shaped hydrogel devices with distinct macroscopic structures. A graphical overview of the information presented in each chapter of this thesis is shown below.

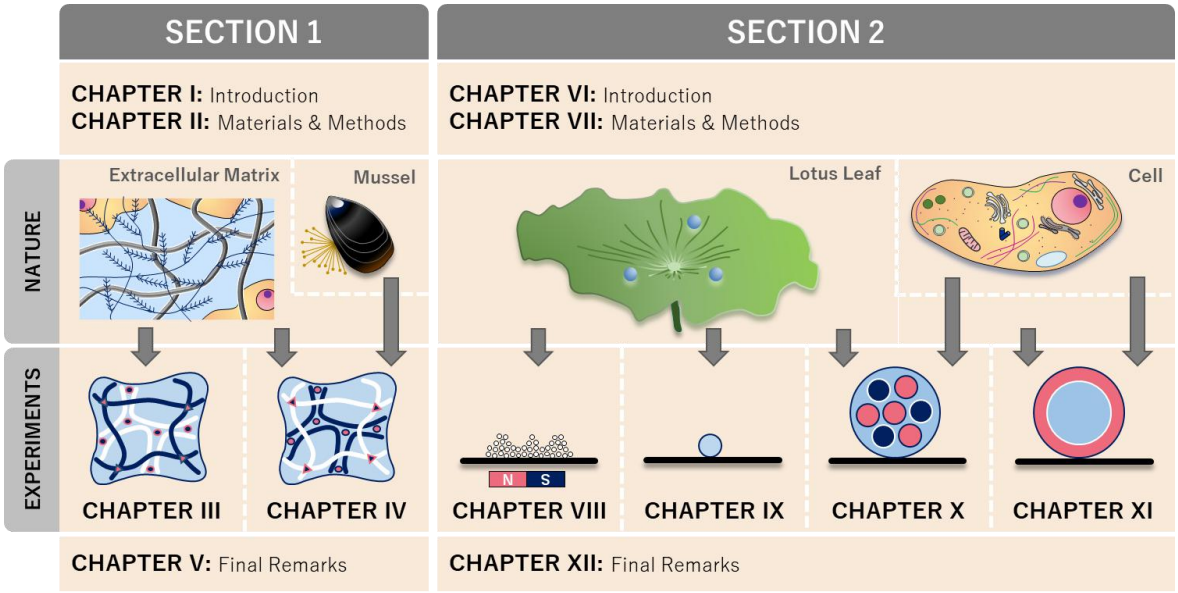

Hydrogels are 3D polymeric networks capable of absorbing high amounts of water like the ECM of tissues. However, there is an enormous gap in terms of mechanical properties

between body tissues and conventional hydrogel materials. Therefore, over the last years, material scientists and engineers have made several efforts to improve the mechanical performance of hydrogels.

Chapter I. contains an introductory summary of the main methodologies available in literature to improve the mechanical properties of conventional hydrogels, with a special emphasis on materials made of natural polymers.

From all the available methodologies, the Double-Network (DN) strategy, which consists in the combination of a fragile network with a ductile one, has been selected in this thesis to achieve extremely tough and yet extremely hydrated materials. The main aim of the experimental works described in Section 1 is to further develop the DN methodology to prepare, under physiological conditions, hydrogels made of a single biopolymer formulation for application in tissue-engineering of load-bearing tissues.

Chapter II. introduces the designed DN-based strategy, which combines chemical and physical crosslinking mechanisms, to obtain hydrogels with improved mechanical properties. The materials chosen to produce these highly hydrated polymeric networks as well as the characterization techniques employed in Chapter III and IV are also presented.

Chapter III. describes the experimental work performed to produce robust, tough and cytocompatible hydrogels made of a single polysaccharide through an adapted approach of the DN methodology. This is the first time that both polymer networks of the DN hydrogels are composed of the same macromolecule, differing only on the molecular weight and the crosslinking mechanism employed.

In **Chapter IV.**, the biomaterials described in Chapter III were further modified to achieve highly hydrated polymeric networks with more advantageous properties for biomedical purposes, namely self-healing and injectability, while retaining the enhanced mechanical properties already exhibited by the aforementioned materials. The described technology constitutes an advance over the conventional DN methodology as it overcomes some of its

drawbacks. First, the introduction of dynamic bonds, inspired by the mussel byssus attachment system, confers not only an increased toughness but also a self-healing ability, allowing to restore their initial mechanical properties upon unloading. Second, the proposed one-pot methodology potentiates their injectability, which may be relevant to fabricate hydrogels with specific shapes or to administer them through a minimal invasive manner. Third, the proved non-toxicity of the materials used in this study highlights the potential of the developed 3D structures for biomedical purposes.

Chapter V. presents a summary of the key findings of Chapters III and IV as well as future directions for these works.

Regarding Section 2, the overall aim is to use superamphiphobic (SA) surfaces, *i.e.* surfaces with high repellence to both water and organic liquids, as substrates to process natural-based hydrogels into spherical particles with distinct structures.

Chapter VI. provides the reader with the general background knowledge related with the use of liquid-repellent surfaces to create spherical polymeric particles.

Chapter VII. states the materials chosen and experimental procedures employed from Chapters VIII to XI.

Most of the available methodologies to fabricate bio-inspired artificial superantiwetting surfaces require (i) expensive equipment and materials, (ii) complex processes and/or harsh conditions, and (iii) are based on irreversible processes, meaning that it is impossible to recover the original substrate after employing the treatment; which are all major disadvantages for practical production and application of these surfaces.

In **Chapter VIII.**, a novel approach to create artificial SA surfaces was described by freely covering a solid substrate with specifically designed microcapsules containing magnetic particles. Owing to their responsiveness to an external magnetic field, both the fabricated microcapsules and the surface can be recovered. The potential usefulness of the developed

non-permanent SA surfaces was also assessed by producing solid hydrogel particles, marble particles and microfluidic channels.

Chapter IX. proposes a new strategy to produce spherical hydrogel microparticles based on the use of SA surfaces and a spraying mechanism. Compared to other methodologies, the sketched approach proved to be simple, fast, cost-effective, and totally biocompatible, allowing the production of polymeric microparticles under mild experimental conditions.

In **Chapter X.**, spherical multicompartmentalized devices with a hierarchical structure were obtained by assembling polymeric microparticles within macroscopic beads using SA surfaces as templates. The potential of the developed system as a cell or drug container was also assessed.

Chapter XI. investigates the possibility of using SA substrates to fabricate mono-sized, spherical hydrogel capsules with a liquefied core, wherein different objects such as biomolecules, cells or magnetic nanoparticles can be dispersed.

Chapter XII. compiles the final remarks and the future perspectives in the context of the experimental works described in Chapters IX to XI.

SECTION 1

Design of Double-network (DN) hydrogels using natural polysaccharides

Chapter I: Introduction

Extremely strong and tough hydrogels as prospective candidates for tissue repair – A review[1]

ABSTRACT

Ideal candidates for the repair of robust biological tissues should exhibit diverse features such as biocompatibility, strength, toughness, self-healing ability and a well-defined structure. Among the available biomaterials, hydrogels, as highly hydrated 3D-crosslinked polymeric networks, are promising for Tissue Engineering purposes as result of their high resemblance with native extracellular matrix. However, hydrogels often exhibit a poor mechanical behavior, hampering their use in load-bearing applications. During the last years, several efforts have been made to create new strategies and concepts to fabricate strong and tough hydrogels. Although it is already possible to shape the mechanical properties of artificial hydrogels to mimic bio-tissues, critical issues regarding, for instance, their biocompatibility and hierarchical structure are often neglected. Therefore, this review covers the structural and mechanical characteristics of the developed methodologies to toughen hydrogels, highlighting some pioneering efforts employed to combine the aforementioned properties in natural-based hydrogels.

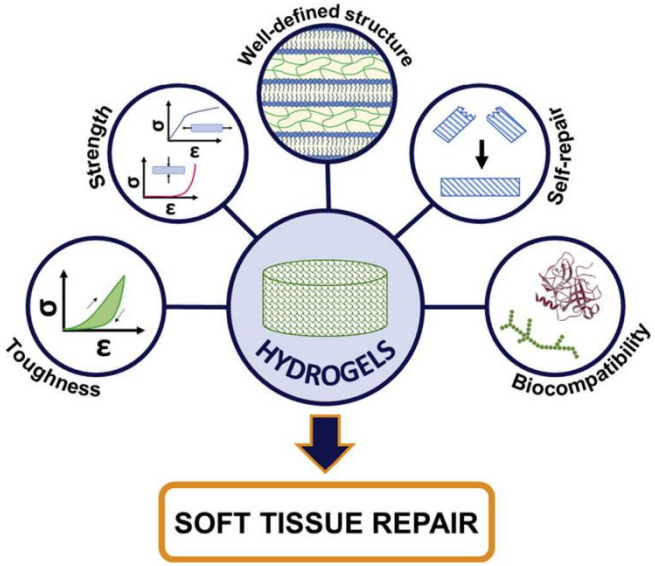

[1] Based on the publication: Ana M. S. Costa, João F. Mano, Extremely strong and tough hydrogels as prospective candidates for tissue repair -A review, *European Polymer Journal* **2015**, 72, pp. 344-364.

Contents

1. Introduction

Soft structural tissues such as cartilage, blood vessels and tendons are characterized by a high-water content, load-bearing ability (*i.e.* strength), fracture resistance (*i.e.* toughness) and softness (*i.e.* low modulus) [1]. For instance, cartilage, which contains about 75 wt% of water, can undertake a remarkable compressive stress of several MPa [2] without fracture, exhibits a toughness value of more than 1000 J m^{-2} and a nominal compressive modulus of 0.1–1.0 MPa [3]. This extraordinary mechanical behavior has been ascribed to a plethora of molecular and structural events occurring in biological tissues [4].

An optimal device for the repair of robust biological soft tissues either based on regeneration or replacement strategies should meet several criteria such as: (i) strength to sustain the applied forces, (ii) biocompatibility resorting, for instance, to natural polymers, (iii) a well-defined structure from the molecular to the macroscopic levels and (iv) recoverability to reversibly deform without fracture [1,5–8]. In the last years, many groups have been focusing their efforts in order to create these multifunctional systems combining the aforementioned properties [9]. One class of such materials are hydrogels, which consist of three-dimensional networks made from crosslinked hydrophilic polymer chains [10]. Owing to their outstanding characteristics such as water absorption and retention ability, biocompatibility and tunable physical, chemical and biological properties, these polymeric networks are excellent candidates

for a broad range of biomedical applications [11], which include scaffolds for Tissue Engineering (TE) [12–14], carriers for drug delivery [11,15–18], molecular filters in biological science [19–21], superabsorbent devices in disposable diapers [22] and valves for microfluidics [23–25]. Furthermore, when exposed to an environmental signal such as temperature and pH, some sensitive hydrogels can respond and translate this stimulus into a macroscopic event, allowing their application as sensors and/or actuators and smart drug release devices [9,26–32]. But, perhaps, the most interesting feature about these 3D networks is their high resemblance, in terms of structure and chemical properties, with the native extracellular matrix (ECM), highlighting their potential for TE [11,33–37]. However, their use in stress-bearing applications is often hindered since hydrogels, when highly swollen, often lack of mechanical properties such as strength, toughness, elongation and recoverability [20,38,39]. This poor mechanical performance is in high contrast with native structural hydrogels such as cartilage and may result in unintended failure *in vivo* [40]. Considering the former drawback, hydrogels were classified as mechanical weak materials, and hence, little attention was paid to them as artificial substitutes of load-bearing soft tissues. Nevertheless, in the last few years, new strategies and concepts have been developed to toughen hydrogels including double networks [41], topological [42] and nanocomposite hydrogels [43]; allowing the application of these 3D structures, for instance, as artificial substitutes of native tissues with structural properties similar to hydrogels such as skin [44], heart valves [45], spinal disks [46], cartilage [8], muscles and nerves [47,48].

In particular, natural-origin polymers are good candidates for biomedical applications as a result of their biocompatibility [49], low cost and easiness to process into hydrogels [50]. Although the chemical structure of synthetic polymers is easily controlled when comparing with natural polymers, they often lack of cell-signaling and cell-interactive motifs which are difficult to mimic in laboratory and are extremely important for the material integration with the surrounding tissues [51,52]. Several natural-based polymers have been investigated for this

purpose [53] including proteins such as collagen [54] and gelatin [55]; and polysaccharides such as cellulose [56], chitosan [57], hyaluronan [58] and chondroitin sulfate [59]. However, the brittleness of these hydrogels is in great contrast with the toughness of biological tissues, showing fracture energies of about 0.1–10 J m^{-2} [60,61], tensile moduli ranging from 10 to 10^4 Pa [62] and compressive fracture stresses lower than 1 MPa [63]. Consequently, many efforts have been done in order to apply the previously stated methods to create tough structures made of natural polymers for load-bearing biomedical applications.

From all the available materials in Nature, polymers are the main constitutes of living organisms and, remarkably, bio-tissues exhibit a huge variety of functionalities [4]. This diversity has been ascribed to the tissues well-defined and complex structure and, in this regard, the control over the hydrogel structure at all levels of hierarchy is also extremely important for the construction of bio-tissues substitutes [64–66].

Another critical point that should be addressed during the design of artificial structural biomaterials is the material self-healing ability, which contributes to the development of longer-lasting products. Self-repairing, which is the ability of materials to heal from their cracks, is found in biological materials such as in bones [67], wood [68] and skin [69]. This property is often achieved by a dynamic bond breaking/reforming upon deformation, which protects the material backbone from macroscopic fracture [4,70]. This Nature inspired feature can be mimicked by replacing irreversible covalent crosslinks by non-covalent ones, which often result in the overall increase of hydrogels' toughness [70]. Hydrogels with self-healing properties have been synthesized using different reversible interactions, for instance, electrostatic [71], hydrogen [72,73] and hydrophobic [74].

This review covers the recent advances done to produce artificial soft tissues with the previously stated characteristics. First, some pioneering works to fabricate hydrogels with enhanced mechanical properties will be described, highlighting the design concept employed and their network structure as well as the mechanism behind their outstanding toughness.

Although hydrogels synthesized through these strategies exhibit superior mechanical properties, in most cases, not enough attention was paid on the biocompatibility, self-healing and their macro/micro-structure. Therefore, this review will then focus on some natural-origin tough hydrogels produced employing the previous methodologies and their attempt to be applied as substitutes of biological tissues. Throughout this review, particular emphasis will be done on tough hydrogels devices with a well-defined architecture and self-healing properties.

2. Hydrogels with reinforced mechanical properties

Hydrogels are stable in aqueous solutions by virtue of crosslinking points, which can be formed either by a covalent or non-covalent mechanism, and thus, yielding chemical or physical hydrogels, respectively. While chemical hydrogels can be produced by radical polymerization, energy irradiation, chemical reactions between complementary groups and/or enzymatic crosslinking; physical networks are often the result of changes in environmental conditions such as temperature and pH, molecular entanglements and/or supramolecular interactions [75,76]. The advantages of physical hydrogels include the possibility to fabricate them under mild conditions and avoiding the use of organic solvents. By contrast, chemical hydrogels have often higher mechanical properties but need toxic crosslinkers and/or solvents [19]. Generally speaking, the mechanical properties of hydrogels arise mainly from two features: the intrinsic rigidity of the polymer chains and the crosslinking density [33]. Although their mechanical strength can be slightly enhanced by increasing the polymer concentration or the crosslinking density, single network hydrogels are often mechanically weak structures [77]. This inherent poor mechanical behavior is the result of various factors such as the (i) irregular distribution of crosslinking points per unit volume (crosslinking density), (ii) different polymer chains length between the crosslinking points (inter-crosslinking molecular weight) [78,79], (iii) high water content [80] and/or (iv) lack of energy-dissipation mechanisms to prevent the

macroscopic propagation of the crack [9]. Structure inhomogeneity, which is characterized by a random aggregation of crosslinking points, occurs typically during the hydrogel formation. This phenomenon is due to differences in reactivity between the monomer and the crosslinker since initially more densely crosslinked regions are formed, being later connected by large chains [81]. Moreover, when using crosslinking agents, it is difficult to ensure that the crosslinking process will occur at regularly separated positions, resulting in a broad distribution on the chains length. Accordingly, upon loading, the stress cannot be evenly distributed on the hydrogels chains and they start to break from the weakest link, reducing the overall mechanical properties [82,83]. Concerning the amount of water uptake, it is known that high water contents result in the reduction of the crosslinking density, which in turn, reduces the fracture energy as fewer chains are needed to be broken for the crack to propagate. Additionally, energy-dissipation mechanisms, for instance, through crystallization or viscoelasticity are also reduced by the separation of network chains in swollen hydrogels [84].

Therefore, substantial efforts have been done to design and fabricate robust hydrogel networks. While some of the research groups focus their work in creating homogeneous structures, others take advantage of their inherent heterogeneity to enhance the mechanical performance of conventional hydrogels. The careful synthesis of networks with a narrow inter-crosslinking molecular weight results in hydrogels with superior mechanical properties when comparing with their equivalent heterogeneous networks, because the applied load can be evenly distributed over all the chains of the hydrogel [85]. Contrarily, there are some studies suggesting that an optimization of the structural inhomogeneity rather than its removal, leads to a drastic improvement on the mechanical properties [19].

In this section, we will present some of the developed approaches to prepare tough and strong hydrogels. Although most of the concepts presented here are not suitable for cell encapsulation purposes due to their harsh processing conditions, these hydrogel systems exhibit enhanced mechanical behavior and, hence, the described methodologies could be

potentially adapted to fabricate artificial substitutes of load-bearing soft tissues. These outstanding mechanical properties are the result of the incorporation of several entities in the hydrogel structure, namely:

2.1. Functional end groups

2.1.1. Tetra-poly(ethylene)glycol (Tetra-PEG) Gel

Solving the inherent inhomogeneity of conventional hydrogels, Sakai *et al.* reported a method to fabricate strong and homogeneous polymeric networks by mixing two symmetrical tetrahedron-like macromonomers of the same size [82]. Each monomer consisted in a four-arm poly-ethylene glycol (PEG) macromer with a tetrahedron-like structure differing on the functional terminal group; either an amine or succinimidyl ester (Fig. 1.1, Tetra-PEG gel) [82]. A uniform 3D-network structure, with negligible topological defects such as entanglements [86], was obtained through the formation of amide bonds between the terminal groups when the stoichiometric ratio between the two macromonomers was unitary [87]. These gels exhibit a maximum compression stress and modulus of *ca.* 2.5 MPa and 40 kPa, respectively, by virtue of their extremely homogeneous and well-defined structure. Additionally, the Tetra-PEG hydrogels have the advantages of *in situ* gel formation and biocompatibility, which is of extreme importance for biomedical purposes [82].

2.1.2. Click chemistry-based (CCb) Gel

A similar concept to the previously stated was used to fabricate homogeneous hydrogels using click chemistry [88,89], specifically through the copper (I)-catalyzed formation of 1,2,3-triazoles from azides and terminal acetylenes [90]. Diacetylene- and tetraazide-functionalized PEG derivatives were mixed in presence of copper, which due to its chemical selectivity resulted in a uniformly crosslinked network with improved mechanical properties (Fig. 1.1, CCb Gel). Indeed, the obtained hydrogels were highly stretchable (*ca.* up to 1550%) with a tensile strength of *ca.* 2.39 MPa, which was also attributed to the well-defined architecture of these

hydrogels [91]. Moreover, the unreacted terminal groups can be used to incorporate different molecules into the hydrogel network without affecting its formation.

2.2. Sliding crosslinks

2.2.1. Topological (TP) Gel

A gel with a very elegant molecular design based on sliding crosslinks, named topological (TP) gel, was firstly presented by Okumura in 2001 [42]. TP hydrogels can be prepared from polyrotaxanes in which a long polymeric chain is sparsely populated with numerous cyclic molecules caged by large, bulky end groups [92]. Flexible, transparent and superabsorbent gels were produced by incorporating α -cyclodextrins (α -CD) along the chains of a high molecular weight PEG polymer followed by the covalent crosslinking of pairs of α-CDs through the action of cyanuric chloride (Fig. 1.1, TP Gel) [42]. One of the interesting features about these hydrogels is related with the absence of crosslinking points on the polymeric chains as they are, instead, topological interlocked by a figure-of-eight crosslinkers. As result of the former feature and contrarily to fixed chemical or physical crosslinked hydrogels [93], the cyclic molecules are able to slide along the polymeric chain with the aim of equalizing the applied tension (pulley effect) [94]. This unique structure allows these hydrogels to bear extensions up to 20 times their original length without fracture as the gel elasticity is exclusively dependent on the chain's topology [95].

2.3. Nanostructures

2.3.1. Nanocomposite (NC) Gel

Another approach is based on the incorporation of nanostructures into the main hydrogel network. One example is the nanocomposite (NC) hydrogel which is composed of polymeric chains (organic part) and clay, a natural mineral silicate, nanoplatelets (inorganic part) [96]. This hybrid structure is simply produced by first exfoliating inorganic clays followed by their

uniform dispersion in an aqueous solution. Specific organic monomers are used to fix the clays nanosheets in this dispersed state and subsequently, the *in situ* free radical polymerization is thermally initiated above the clay surface. The clay nanosheets act as multifunctional crosslinkers since the end groups of the polymer chains can adsorb strongly on the surface of the nanosheets by ionic and coordination interactions. In fact, several individual chains can attach to a single inorganic substrate. Therefore, a transparent, robust, 3D structure composed of flexible polymeric chains connected with different inorganic clay sheets is obtained. For example, the NC hydrogel composed of inorganic synthetic hectorite ($[Mg_{5.34}Li_{0.66}Si_8O_{20}(OH)_4]Na_{0.66}$) clay slab connected by N-isopropyl acrylamide (NIPAM) polymeric chains using potassium peroxodisulfate (KPS) as radical initiator is highly stretchable (*ca.* higher than 1000%) and exhibit a high elastic recoverability (*ca.* 98% of the total deformation), illustrating its overall robustness (Fig. 1.1, NC gel) [43]. The crack propagation is severely hampered as every single chain connecting different clay sheets needs to be broken, resulting in highly tough materials. Furthermore, NC hydrogels properties also include excellent swelling ability (*ca.* 500 times) and enhanced stimuli sensitivity as the polymer chains are not molecularly restricted by crosslinking points contrarily to what happen with chemical hydrogels [97]. Moreover, the high structure uniformity of these hydrogels is proved by their transparence, which is in high contrast with the conventional hydrogels' opacity. NC hydrogels drawbacks include (i) the relative low amount of inorganic clay that can be used to produce these hydrogels (typically lower than 12 wt%) as consequence of the nanoplatelets aggregation, which, in turn, leads to limited mechanical properties, and (ii) their lack of self-healing ability.

2.3.2. Layered nanocomposite (L-NC) Gel

One strategy to solve the first problem is based on mimicking the nacre micro- and nanostructure, which curiously constitutes also an inorganic/organic nanocomposite [66]. Indeed, nacre outstanding elastic modulus, strength and toughness emerge from its well-

ordered brick-and-mortar arrangement into organic and inorganic layers [42]. A layered NC (L-NC) was developed by incorporating the clay platelets (Laponite XLG) in a NIPAM monomer solution containing an initiator. The nanoplatelets were assembled into a lamellar structure by vacuum filtration. After UV irradiation, the *in situ* radical polymerization of NIPAM was initiated, forming the L-NC hydrogel [98]. The superior mechanical properties of the L-NC hydrogels compared with the other NC structures, further proved the importance of designing well-defined microstructures to obtain robust hydrogels.

2.3.3. Dendritic nanocomposite (D-NC) Gel

Due to the poor self-healing ability of NC hydrogels, a new supramolecular approach was developed, combining clay nanosheets, dendritic macromolecules and sodium polyacrylate (ASAP) under mild conditions [99]. The dendritic macromolecules work as ‘‘molecular glue’’ of the nanosheets and are composed of PEG chains containing two dendrons units with terminal guanidinium ions [100]. To fabricate these hydrogels, the clay nanosheets were also exfoliated and dispersed homogeneously in water possibly due to the repulsion between their positive-charged edge parts and anionic ASAP. Then, the oxyanions presented on the clay nanosheets react with the dendrons, yielding a strong hydrogel with self-healing ability. Remarkably, when freshly cut surfaces of these hydrogels were placed in contact, they were able to connect to each other, showing their capability to recover after structure damage. While the nanosheets are responsible for the obtained high strength values since they are the main component of this 3D network, the self-healing process is a consequence of the non-covalent attachment of the guanidinium ions to the exfoliated nanosheets [99].

2.4. Microparticles

2.4.1. Macromolecular microspheres composite (MMC) Gel

Similar to the NC hydrogels, macromolecular microspheres composite (MMC) networks also allow the control over the crosslinking density and the inter-crosslinking distance.

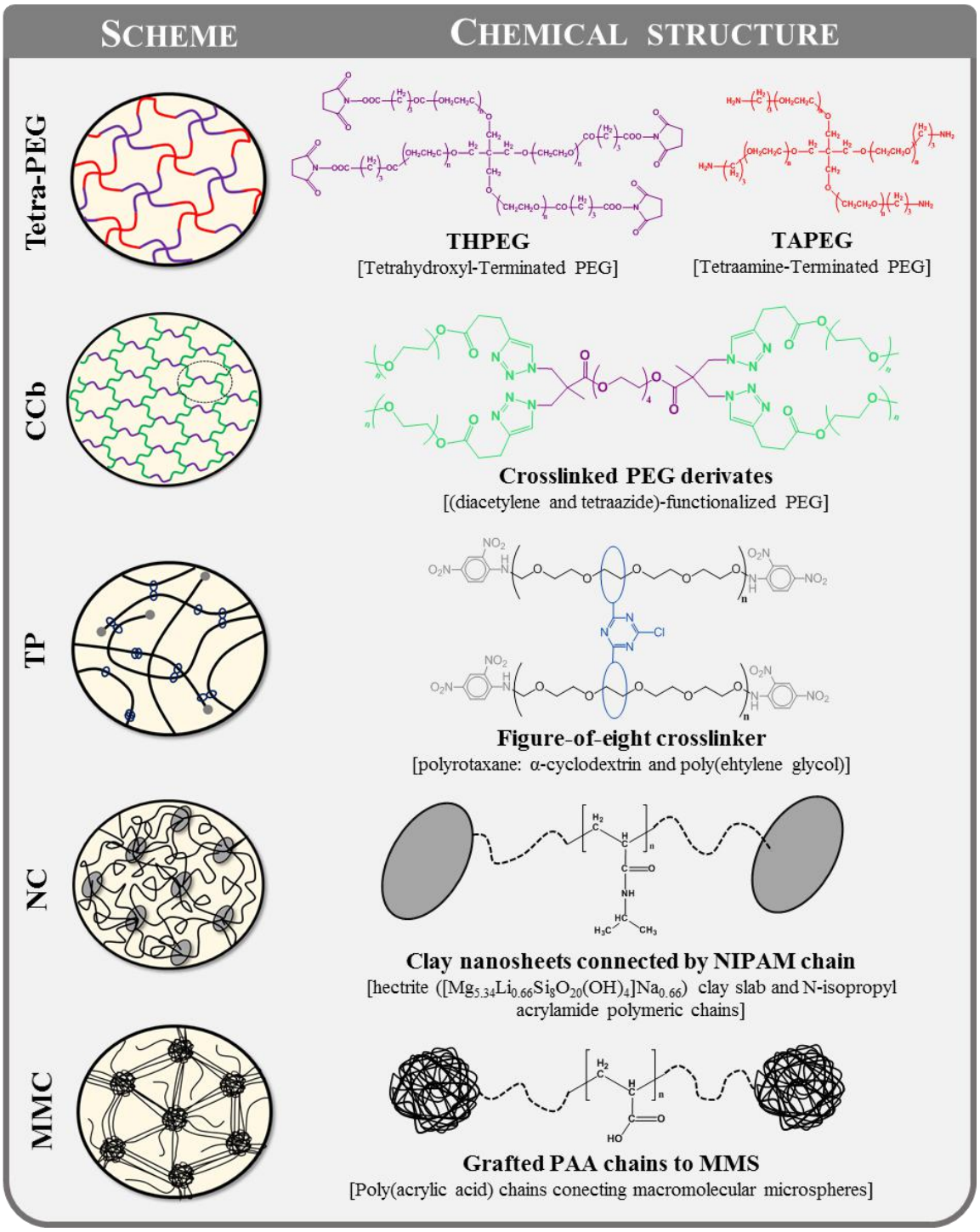

Figure 1.1 (Part A)- Schematic representation and chemical structure of the different strategies described to create strong and tough hydrogels devices, namely: Tetra-poly(ethylene) glycol (Tetra-PEG) gel, click chemistry-based (CCb) gel, topological (TP) gel, nanocomposite (NC) gel, macromolecular microspheres composite (MMC) gel, ionically crosslinked triblock copolymer (ITC) gel, hydrophobic interactions-based (HIb) gel, polyampholytes (PA) gel, lamellar bilayer (Lb) gel and double-network (DN) gel.

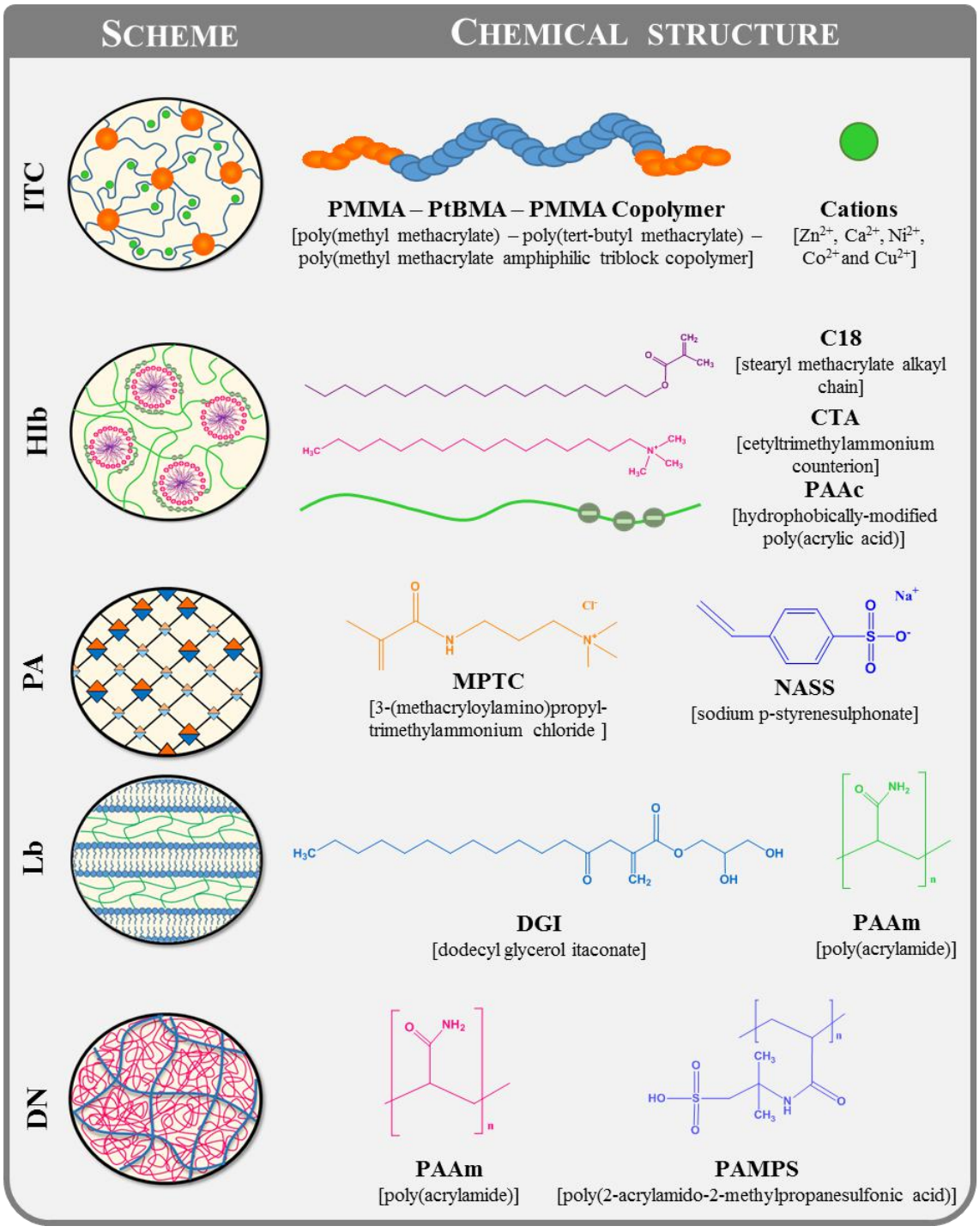

Figure 1.1 (Part B)- Schematic representation and chemical structure of the different strategies described to create strong and tough hydrogels devices, namely: Tetra-poly(ethylene) glycol (Tetra-PEG) gel, click chemistry-based (CCb) gel, topological (TP) gel, nanocomposite (NC) gel, macromolecular microspheres composite (MMC) gel, ionically crosslinked triblock copolymer (ITC) gel, hydrophobic interactions-based (HIb) gel, polyampholytes (PA) gel, lamellar bilayer (Lb) gel and double-network (DN) gel.

However, MMC hydrogels do not require an inorganic counterpart, being instead formed by covalent attachment of network chains to microparticles.

MMC hydrogels were designed by reacting surface activated macromolecular microspheres with polymeric monomers as shown by Huang *et al.* [101]. After the irradiation with ^{60}Co c-rays in the presence of oxygen, peroxides were formed on the surface of macromolecular microspheres, which are composed of styrene and butyl acrylate monomers. These groups under heat form free radicals which act as both crosslinkers (responsible for the covalent grafting of poly(acrylic acid) (PAA) monomers on the MMS) and initiators (responsible for starting PAA homopolymerization). This method results in a tough hydrogel due to its well-defined structure, consisting of MMS particles connected by PAA long chains, which can sustain the external stresses cooperatively (Fig. 1.1, MMC). Moreover, inter- and intramolecular hydrogen bonds can also occur between PAA chains, working as an energy dissipation mechanism [102]. In fact, MMC hydrogel (89 wt% water content) sustained a compressive stress of 10.2 MPa for a strain of 97.9%. After loading, the hydrogel structure elastically recovered its original shape for strains higher than 90%. It is worth to notice that by decreasing the water content, a higher compressive stress (78.6 MPa at 99.3% strain) was obtained but the hydrogels were permanently deformed. Moreover, their use as cell encapsulation vehicles could be hindered owing to the need for c-rays irradiation to form the peroxides [101].

2.5. Supramolecular interactions

2.5.1. Ionically crosslinked triblock copolymer (ITC) Gel

In this technique developed by Henderson *et al.* [103], a amphiphilic triblock copolymer consisting of a midblock made of poly(tert-butyl methacrylate) (PtBMA) and end blocks of poly(methyl methacrylate) (PMMA) was physically crosslinked through both (i) ionic crosslinks between the polyelectrolyte mildblocks and (ii) glass spherical domains on PMMA end blocks

(Fig. 1.1, ITC). Briefly, this copolymer was dissolved in dimethyl sulfoxide and then subjected to a vapor phase solvent exchange process to create the spherical aggregates. The ionic crosslinks were obtained by immersing the physically crosslinked hydrogels into a buffered cationic solution. Tough (1.4 MJ m^{-2}) and strong (*ca.* 1 MPa) ITC hydrogels were obtained by the reversible association/dissociation of the ionic crosslinks bridging the PMMA glass domains [103].

2.5.2. Hydrophobic interactions-based (HIb) Gel

The presence of hydrophobic interactions can also serve as a dissipation mechanism since after the unloading, they are able to re-assemble, leading to the hydrogel recovery [104]. Hydrophobic interactions can be achieved by introducing hydrophobic sequences within a hydrophilic polymeric network via micellar organization [105]. Combining self-healing, obtained by the presence of supramolecular bonds, with good mechanical properties is non-trivial as these bonds are relatively weak when comparing with covalent ones. Acknowledging this shortcoming, Gulyuz *et al.* proposed a new strategy using hydrophobically modified PAA polyelectrolyte with oppositely charged cetyltrimethylammonium (CTA) surfactant. These 3D structures were produced via micellar copolymerization of hydrophilic AA with hydrophobic stearyl methacrylate by free radical polymerization in CTAB aqueous solution containing NaBr (Fig. 1.1, HIb) [106]. The attained supramolecular hydrogels exhibited a strength as high as 1.7 MPa and elongation at break of 900%. Remarkably, these HIb hydrogels were able to heal either by heating or by surfactant treatment of the damage areas, recovering almost their initial strength (up to 1.5 MPa) and elongation (up to 600%) [106].

2.5.3. Polyampholytes (PA) Gel

PA gels belong to the physical hydrogels category as they are formed via non-covalent bonds between different charged monomers [107]. This supramolecular structure has multiple ionic bonds with a high disparity of strengths since the polymerization occurs randomly. The

strong bonds act as permanent crosslinkers which are responsible for maintaining the original shape, whereas the weak bonds break upon loading enhancing both their fracture energy as well as their self-healing ability via bond re-formation upon unloading. Sun *et al.* obtained a PA gel structure (water content of 50–70 wt%) after mixing a anionic monomer, 3-(methacryloylamino)propyl-trimethylammonium chloride with a cationic monomer, sodium p-styrenesulphonate, in a aqueous solution containing a photoinitiator and NaCl followed by UV-irradiation (Fig. 1.1, PA) [107]. In order to prevent both phase separation and polymer collapse to a globule state, the electrostatic attractions between the polymer chains were kept near the charge balance [108,109]. The obtained hydrogels exhibit enhanced fracture stress and strain up to 1.8 MPa and 750%, respectively, a high toughness as shown by a fracture energy of 4000 J m^{-2} and a complete recovery after loading up to 600%. Moreover, these hydrogels were also proved to have excellent biocompatibility using macrophages [107]. Although PA structure only possess supramolecular bonds, they are mechanically tough contrarily to other self-healing hydrogels previously developed [99,110]. This toughness was associated with the presence of a heterogeneous structure composed of randomly distributed strong and weak non-covalent bonds.

2.5.4. Lamellar bilayer (Lb) Gel

Haque *et al.* reported a tough and anisotropic hydrophilic matrix containing multiple lipid bilayers with unidirectional alignment [111]. These rigid hydrophobic bilayers were composed of a polymerizable surfactant, dodecyl glyceryl itaconate (DGI) whereas the ductile polymeric network was made of polyacrylamide (PAAm) polymer (Fig. 1.1, Lb). The processing method consisted in the self-assembly of DGI monomers into stacked bilayers followed by the free radical polymerization of acrylamide (AAm) in presence of N, N-methylenebis(acylamide) crosslinker and a photoinitiator. The lamellar structure was formed by applying a shear stress to the former precursor solution [112], resulting in an architecture composed of alternating polymer and lipid layers (water content higher than 90%) with a tensile fracture stress of 600

kPa parallel to the lipid bilayers direction. Additionally, these hydrogels exhibit a high toughness, self-recovery and fatigue resistance. The previous characteristics arise from the presence of lamellar bilayers, which upon deformation consume a large amount of energy by dissociating themselves before the complete hydrogel fracture. The former fact together with their lipid-like movements are the main reasons behind the Lb hydrogels superior mechanical properties [111].

2.6. Second network

2.6.1. Double network (DN) Gel

DN hydrogels were first introduced by Gong *et al.* in 2003 [41], being the result of combining two polymeric networks with contrasting physical structures and properties [113]. It is worth noting that contrarily to interpenetrating networks (IPNs), which are also composed by two polymeric structures, the mechanical properties of the combined networks of DN hydrogels are much higher than the ones of the two independent structures, showing a synergistic effect [41]. They are usually composed of a stiff and densely crosslinked structure (first brittle network) and a ductile and loosely crosslinked structure (soft second network). To effectively improve the mechanical properties, the mass ratio of the second to the first network must be very high (usually 7–20 times that of the first network) in order to get strong DN hydrogels [41,114]. These structures are often synthesized via a two-step sequential free radical polymerization process: (1) the first step involves the formation of a highly crosslinked rigid gel and (2) the second forms a loosely crosslinked network inside the first gel structure. The first structure is often a polyelectrolyte in order to ensure both a high swelling rate and the effective entanglement of the second network within this first structure. This concept was proved to be general and independent of specific chemical interactions between the two networks [107,115].

To date, several tough hydrogels with different macromolecular designs based on DN methodology have been reported such as void-DN gels [116], inverse DN gels [117], liquid crystalline DN gels [118], microgel-reinforced hydrogels [119] and ultra-thin DN gels [120].

One of these tough hydrogels pairs consists of poly (2-acrylamido-2-methylpropanesulfonic acid) (PAMPS) as the first network and PAAm as the second structure. The obtained DN hydrogels (*ca.* 90% water content) exhibit a tensile fracture stress of 2 MPa, hardness with elastic modulus of 0.3 MPa and tearing energy of several thousands of J m^{-2}, which are comparable to or even higher than that of cartilage [114,121]. Regarding their ability to sustain a compressive stress, they can hold a stress of 17.2 MPa for a strain of *ca.* 92%, which is much higher than that of their individual networks: PAMS gel break at 0.4 MPa for strain of 41% and PAA gel at 0.8 MPa for 84%. Upon deformation, the brittle network breaks into small clusters that efficiently disperse the stress around the crack tip into the surrounding damage zone, and thus imparts toughness to the DN gels. On the other side, the second ductile network extends extensively and, thereby, sustaining large deformations. In other words, the first network contributes to an increase on the elastic modulus, whereas the second structure is responsible for the increase on strain [114,115,122].

Remarkably, the high-level of inhomogeneities of strong DN hydrogels is the origin of their superior toughness, which is also revealed in other tough biological tissues for instance, in bone, whose heterogeneous porous structure is known to reduce the stress concentrations [19].

3. Natural-origin tough hydrogels

Among all the polymers that can be used to create hydrogels, natural-origin polymers offer several advantages including their non-toxicity, biocompatibility, the presence of unique biological and chemical features and easiness to fabricate into hydrogels [53]. In fact, some of these polymers are components of native ECM, being responsible for different cell regulation

processes spanning from migration to differentiation, and hence, suggesting their potential performance as soft tissues analogues [123,124]. Furthermore, versatile chemical structures can be obtained by modifying the high number of functional groups present along their backbone, resulting in materials with improved characteristics for a specific application while retaining crucial biological features [125]. From the commercial point of view, natural-origin materials are often inexpensive as they are readily available from renewable sources [50–52].

Despite these extraordinary attributes, conventional natural-based hydrogels exhibit low strength, hindering their use in several load-bearing applications [126]. Therefore, the strategies described in the former section were employed to create biopolymer-based hydrogels with enhanced mechanical properties. Such hydrogel systems combine high toughness and strength, obtained by employing the previous described methodologies, with the biocompatibility of natural polymers, whose association was only recently achieved. Moreover, their potential for biomedical applications will be also addressed.

3.1. Bacterial-cellulose and Gelatin

Extracted from bacteria, bacterial cellulose (BC) consists in a hydrophobic stratified structure composed of alternating dense and sparse ultrafine fiber layers [127]. Its structure (water content of *ca.* 90%) yields unique mechanical properties such as anisotropy, which is associated to its high tensile modulus (*ca.* 3 MPa) in the fiber-layer direction and its low compressive modulus (*ca.* 0.007 MPa) perpendicular to the stratified layer. Despite its high mechanical properties, the structure of the BC hydrogel does not recover after compression as result of hydrogen-bond formation between the cellulose fibers (Fig. 1.2I, BC). In order to solve this drawback, gelatin was incorporated in the BC network, resulting in a BC/gelatin DN hydrogel. Gelatin, a polypeptide derived from the denaturation of collagen, is mechanically brittle (compression stress of *ca.* 0.14 MPa and a compressive modulus of *ca.* 0.007 MPa), but it can sustain several repeated compression cycles without fracture (Fig. 1.2I, Gelatin). To

synthesize the DN gel, BC was immersed in an aqueous solution containing gelatin that was further crosslinked using N-(3-dimethy-laminopropyl)-N-ethylcarbodiimede hydrochloride. The combinatorial effect of these two mechanically contrasting structures (hard BC network and soft gelatin structure) resulted in a 3D network able to simultaneously bear a compression stress of *ca.* 3.7 MPa and recover its original shape after a second compressive deformation up to 30% of strain (Fig. 1.2I, BC/gelatin and 1.2IIa). Regarding their tensile properties, BC/gelatin hydrogel exhibit an impressive elastic modulus and stress of *ca.* 23 MPa and *ca.* 3 MPa, respectively (Fig. 1.2IIb). Other polysaccharides such as alginate, gellan-gum and carrageenan were also used to produce DN networks in combination with BC [128]. The resultant mechanical properties of these DN networks are comparable with that of the cartilage, however, the ultimate stress of the BC/gelatin DN hydrogels dramatically decreased after 6 weeks implantation into the subcutaneous tissue of rabbit [129]. The former fact severally hinders their potential application as an artificial substitute of load-bearing soft tissues. Additionally, due to the use of toxic crosslinkers, this device may not be a good candidate for cell encapsulation purposes.

3.2. Gellan-gum and Gelatin

The synthetic conditions for DN formation are often incompatible with cell viability due to the use of toxic solvents or/and crosslinkers as well as harsh processing conditions. With the aim of encapsulating cells, DN hydrogels composed of a stiff gellan gum methacrylate (GGMA) and a soft gelatin methacrylamide (GelMA) structures were synthesized [130]. GG is an anionic polysaccharide extracted from the *Sphingomonas elodea* [131], being composed of a tetrasaccharide repeating unit of β -D-glucose; β -D-glucuronic acid and α -L-rhamnose. This biopolymer can form a gel network by changing their chains conformation from disordered coils to double helices upon cooling, or through ionic crosslinks in the presence of mono- or divalent cations [132,133].

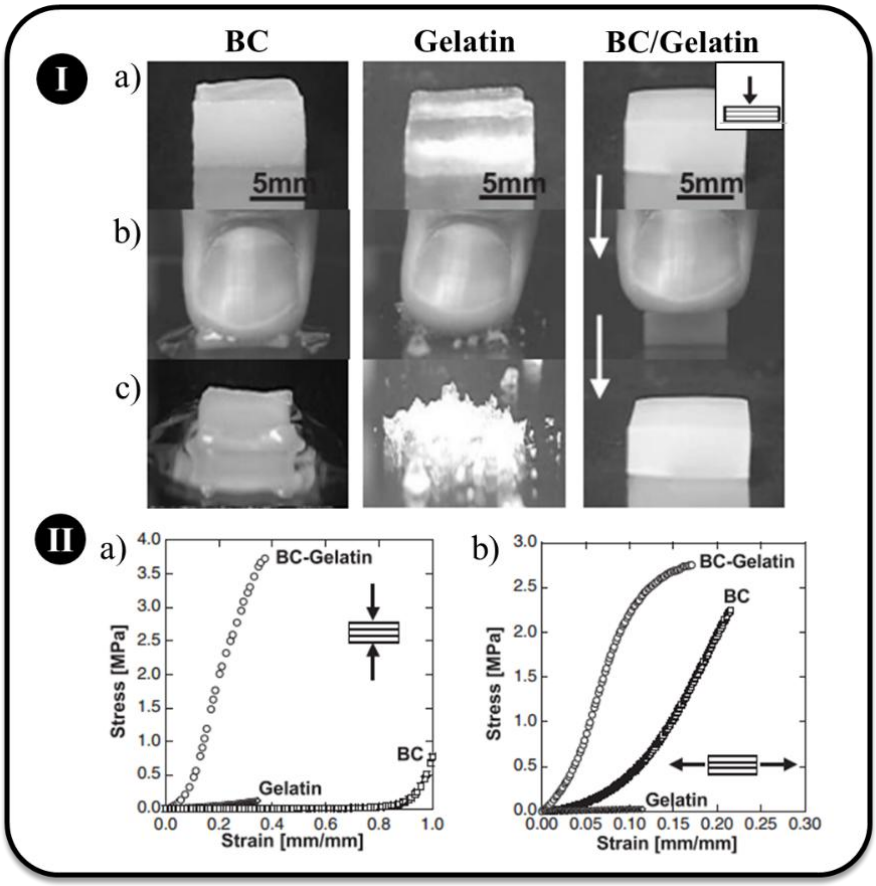

Figure 1.2 - I. Photographs depicting the bacterial cellulose (BC), gelatin and BC/gelatin hydrogels before compression (a); during the compression (b); and after compression (c). **II.** Typical compressive (a) and tensile (b) stress–strain curves of the three kinds of hydrogels. The compression and tensile assays were performed perpendicular to and parallel to the stratified direction of DN hydrogels, respectively. Adapted with permission [128] Copyright 2004, Wiley- VCH.

The GGMA/GelMA DN hydrogels were produced through a two-step photocrosslinking process by immersing GGMA hydrogel, which was obtained after UV-exposure for 120 s in presence of a photoinitiator, in a GelMA precursor solution. After the GelMA diffusion into the first network, a second photocrosslinking process was performed to yield the second network. The resulting DN hydrogels reached a maximum compressive failure stress of *ca.* 6.9 MPa for a failure strain of 81%. This remarkable behavior may be explained by the presence of the stiff GGMA network which is responsible for sustaining the applied stress while the soft GelMA network dissipates the crack energy avoiding the hydrogel macroscopic breakdown [134].

Moreover, NIH-3T3 fibroblasts were successfully encapsulated within the GGMA/GelMA DN hydrogel by suspending these cells in the GGMA precursor solution, which was then crosslinked by UV-light exposure [130]. Afterwards, the cell loaded GGMA hydrogels were placed inside a GelMA precursor solution followed by a second photocrosslinking process. After 3 days of cell incubation at physiological conditions, it was possible to verify that most of the cells survive within the DN hydrogel matrix as shown by Live/Dead assay images (Fig. 1.3l), proving the cell-compatibility character of the developed strategy to engineer tough hydrogels for biomedical purposes [130].

Irrespective of the high toughness and strength of the previous DN hydrogels, they do not recover after a loading/unloading cycle as result of the irreversible covalent-based crosslinking (permanent damage). Bakarich *et al.* designed and fabricated a tough hydrogel with the ability to recover from large strain by mixing hot solutions of GG with AAm monomers, which were then crosslinked through the addition of Ca^{2+} and N,N-methylenebisacrylamide (MBAAm), respectively, in the presence of N,N,N',N'-tetramethylethylenediamine and KPS [135]. The resultant GG/PAAm hydrogels (water content higher than 95%) were composed by an ionically crosslinked GG matrix and a covalently crosslinked PAAm network, which can withstand *ca.* 216 kPa in compression (2 and 13 times more stress than the corresponding GG and PAAm single networks, respectively). Although the presence of weak ionic crosslinks results in this low compressive strength value, these reversible interactions allow the hydrogel elastic recovery under mild conditions [136]. In addition, GG/PAAm hydrogels were subjected to several load/unload compression cycles. The results showed that these networks can recover 53 ± 4% of their initial mechanical properties after the first compressive cycle, and 90 ± 9% after the subsequent cycles, which is much better than the conventional DN hydrogels [114].

Recently, the previous process was further polished to attain strong and self-healing hydrogels by using a one-pot synthesis method [137]. To this end, hot aqueous solution of GG

was combined with gelatin and, subsequently, crosslinked by the action of Ca^{2+} and genipin, non-cytotoxic crosslinker [138], respectively. These structures containing both ionic (between GG polymer and Ca^{2+} ions) and covalent (between gelatin and genipin) crosslinking mechanisms exhibited a maximum fracture stress of 1.0 MPa and 0.62 MPa in compression and tension, respectively (Fig. 1.3IIa). To assess their recover ability, GG/gelatin DN hydrogels were compressed until a stress of 150 kPa and, then, allowed to rest in both air or immersed in simulated body fluid (SBF) (Fig. 1.3IIb and IIc). The results revealed that by placing the hydrogels in SBF for time intervals higher than 10 min leads to a recovery of the initial mechanical properties, especially regarding the hysteresis (95 ± 2%), suggesting that these gels were not permanently damaged by the first loading/unloading cycle [137].

In addition, the MMC concept has also employed to create microgel-reinforced GGMA/GelMA hydrogels [139], showing better mechanical and biological properties over the DN hydrogels using the same biopolymers [130]. Briefly, GGMA microgels were produced by water-in-oil emulsion, and then exposed to UV-radiation for 120 s. The resulting GGMA hydrogels were incorporated in GelMA matrix after a second photocrosslinking process for 180 s (Fig. 1.3III). Regarding their mechanical properties, MMC hydrogels were able to withstand a maximum strength of *ca.* 3.2 MPa, which was higher than the corresponding GGMA/GelMA DN structure (*ca.* 1.5 MPa). This behavior was explained by the higher GGMA concentration on MMC gels, enhancing their strength. Contrarily, on DN hydrogels the ratio of GGMA to GelMA is critical to attain the optimized mechanical properties and hence, this component should be prepared at relatively low polymer concentration. Additionally, the GGMA microgels protected the GelMA matrix from fracture by allowing the crack grow in their structures, which due to the microgels dispersion on the GelMA structure avoids the macroscopic propagation of the crack [119].

Concerning the biological properties, higher viability rates were observed in MMC hydrogels since the cells were encapsulated in GelMA matrix instead of GGMA. Indeed, gelatin is recognized as a great material for cell encapsulation owing to the presence of many adhesion

sites on its backbone [140]. Interestingly, the GelMA precursor solution containing GGMA microgels can be possibly injected followed by *in situ* photocrosslinking, after the assessment of the light penetration ability [139].

3.3. Chitin

Chitin is the second most available polymer in Nature being mainly obtained from crustaceans [141]. This biopolymer presents some interesting features for biomedical applications such as biocompatibility, antibacterial character and nontoxicity.

Due to its inherently poor mechanical behavior, chitin have been mixed with poly (vinyl alcohol) (PVA), a synthetic and biocompatible polymer [142], with the aim of creating a tough hydrogel structure [143]. These hydrogels were obtained by first dissolving chitin in NaOH/urea aqueous solution containing the PVA polymer followed by crosslinking with epichlorohydrin (ECH). To form PVA crystals and physically crosslink this synthetic material, a freezing-thawing method was employed [142,144]. The resultant chitin/PVA hydrogel composite is the result of two crosslinking mechanisms, namely (1) a chemical (between chitin and ECH) and (2) a physical (via hydrogen bonds between PVA and chitin chains). Additionally, PVA intermolecular interactions can lead to the formation of crystallites which, in turn, can ensure a higher stability of the hydrogel. Interestingly, the morphology of the obtained hydrogels containing 25% of PVA was found to be very similar to the one of the jellyfish (Fig. 1.4I shows a non-ordered Chitin/PVA structure while Fig. 1.4II displays an ordered layered structure) [144]. The obtained ordered and layered porous structure, in which the hydrophilic PVA crystals are tightly immobilized on the chitin backbone matrix through the presence of hydrogen bonds, was ascribed to the performed freezing/thawing cycles. Moreover, during the former procedure a microphase separation between the formed crystalline ice and PVA crystals can also explain the obtained ordered structure.

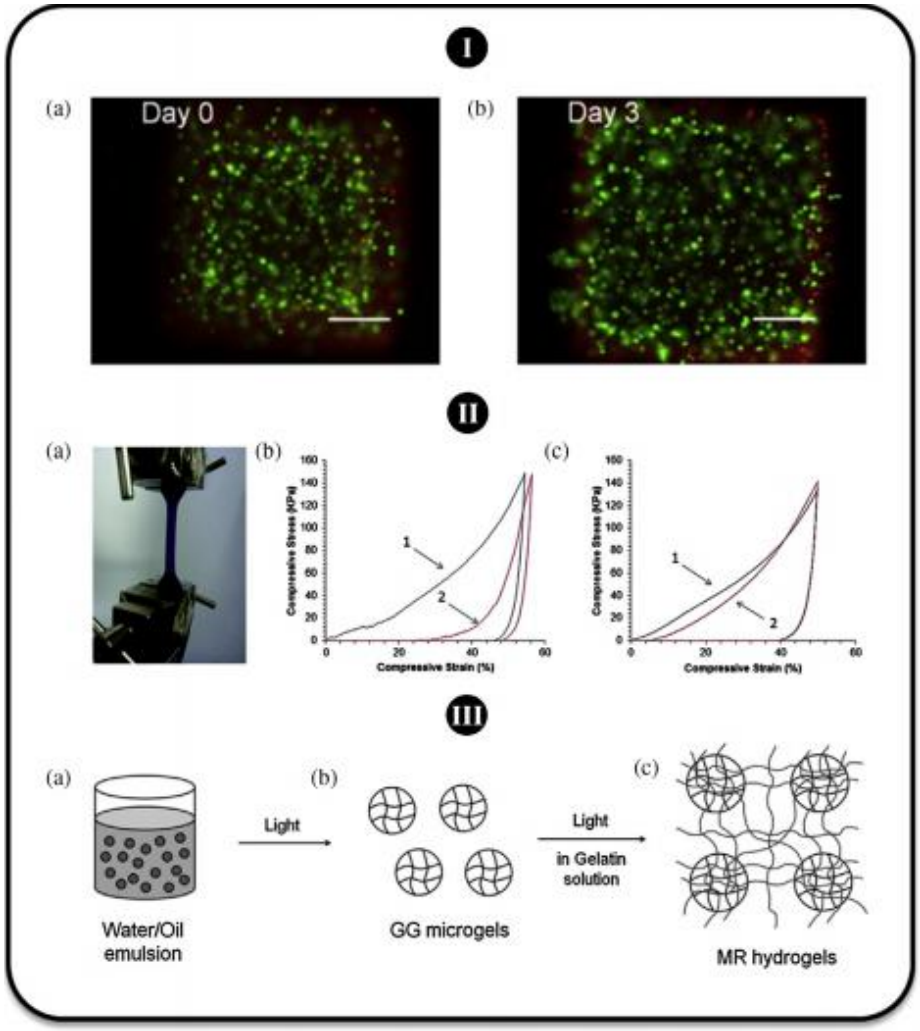

Figure 1.3 - I. Live/dead images of the gellan gum methacrylate/gelatin methacrylamide (GGMA/GelMA) DN hydrogels containing NIH-3T3 fibroblasts, which are labeled with calcein (viable cells, green) and propidium iodide (non-viable cells, red), after 0 days (a) and 3 days (b) of cell culture. The scale bar stands for 200 μm. Adapted with permission [130]. Copyright 2012, Elsevier. **II.** DN hydrogels combining a calcium crosslinked gellan gum network with a genipin crosslinked gelatin. (a) Image of the obtained GG/Gel structure being subjected to a tensile assay. Load–unload compression curves obtained by fixing the maximum stress at 150 kPa. The first sample (represented by 1) was deformed while the other sample (represented by 2) corresponds to the second cycle applied after allowing the sample to rest in air (b) or in SBF (c) for 10 min between cycles. Adapted with permission [137] Copyright 2012, Royal Society of Chemistry. **III.** Schematics of the purposed strategy to create GG microgel-reinforced gelatin hydrogels by first producing the GG microgel by oil in water emulsion (a). Afterwards, the obtained particles were photocrosslinked upon UV-light irradiation (b). Finally, GG crosslinked microgel were transferred to Gel solution followed by their polymerization (c). Adapted with permission [139] Copyright 2014, Royal Society of Chemistry.

In fact, these hydrogels with a jelly-fish like architecture were found to result in higher mechanical properties (compressive strength of 2.1 MPa and strain at break of 80%, Fig. 1.4III) than other hybrid gels containing different amounts of PVA polymer and even when comparing with pure chitin. The former fact has been related with the effective dispersion of the stress by multilayered structures, and hence, higher external stresses are needed in order to break this well-defined structure [145].

Additionally, these chitin/PVA hydrogels were proved to be cytocompatible after both L929 fibroblasts and MDKC cells seeding on its surface [143]. The combination of the aforementioned characteristics, namely their cytocompatibility, high mechanical properties and well-defined structure, highlights chitin/PVA hydrogel potential as an artificial substitute of load-bearing soft tissues. However, their use for cell encapsulation purposes may be compromised by the need for toxic reagents and harsh processing conditions, such as the freezing–thawing cycles.

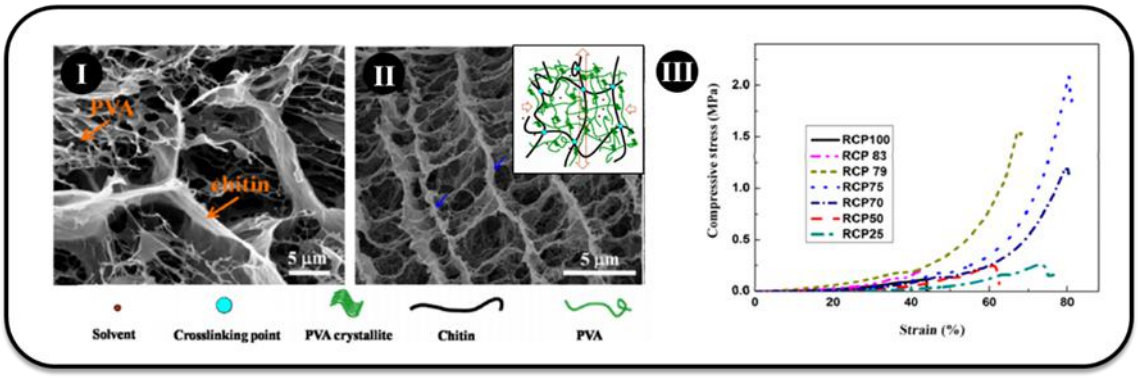

Figure 1.4 - Photographs depicting scanning electron microscopy images of the cross-sections for the resultant chitin/poly (vinyl alcohol) (RCP) hydrogels, namely the RCP83 **(I)** and RCP75 **(II)**, where it is possible to observe a jellyfish-like structure in the case of RCP75. The inset corresponds to the schematic representation of the chemical/physical crosslinking RCP75 structure. **III.** Typical compressive stress–strain curve of the RCP for different weight percentages of chitin (from 0% to 100 wt%) by fixing the total polymer concentration in about 6 wt%. Adapted with permission [143] Copyright 2014, American Chemical Society.

3.4. Alginate

One of the most used biomaterials is alginate due to its gelling properties in mild conditions [146]. This neutral polysaccharide is mainly obtained from brown algae and is composed of (1-4)-linked β -D-mannuronic acid and α -L-guluronic acid residues [33,147]. These monomers are organized in blocks rich in mannuronic acid, blocks rich in guluronic acid units and blocks rich in both units. The gelling process occurs through interactions between the carboxylic acid moieties and bivalent counter ions such as calcium [136,148]. Sun *et al.* developed a highly stretchable hybrid hydrogel composed of two crosslinked polymer networks: an ionically crosslinked alginate through the presence of calcium ions and a covalently crosslinked PAAm using MBAAm as crosslinker. The introduction of a non-covalent crosslinking mechanism allowed this hydrogel to recover upon unloading, which is not possible in conventional DN hydrogels. During deformation, the alginate network dissipates energy by unzipping its ionic crosslinks while the PAAm structure preserve its mechanical integrity. After unloading, the reversible ionic bonds can be reformed. These hybrid hydrogels with *ca.* 90% of water in their composition presented a tensile fracture stress, elongation and energy of 156 kPa, 20 times their initial length, and 9000 J m^{-2}, respectively. This outstanding fracture energy is much higher than the one of conventional hydrogels and have been ascribed to the energy dissipation occurring upon the unzip of the alginate chains [71]. *In vivo* results obtained upon implantation of these structures into dorsal subcutaneous pockets in rats suggested a minimal inflammatory response by the absence of macrophages and lymphocytes infiltration after 8 weeks, highlighting their potential for biomedical applications [149].

Although the alginate/PAAm hydrogels exhibited an outstanding toughness, they have a relatively low stiffness, which is mainly due to the alginate low concentration (further increase is hindered by the high viscosity of the final solution) and crosslinking density (calcium sulfate crosslinker has poor solubility in water). Realizing this difficulty, Li *et al.* introduced a hybrid alginate/PAAm hydrogel with both high stiffness and toughness by increasing both of the

aforementioned characteristics. While the alginate concentration was increased using alginate with different molecular weights, the crosslinking density was improved through the combination of calcium sulfate and calcium chloride (Fig. 1.5Ia) [150]. The results suggested that by increasing the amount of low molecular weight alginate while fixing the total alginate concentration, the stiffness remained constant (*ca.* 1 MPa) whereas the toughness increased, reaching the remarkable fracture energy of *ca.* 16 kJ m^{-2} (Fig. 1.5Ib). This phenomenon was related with the decrease of strength upon increasing the fraction of short chains, resulting in the growing of the region near the crack tip where the energy is dissipated, which, in turn, increases the toughness [150].

Alginate containing phenylboronic acid (PBA) was combined with PVA to yield a supramolecular hydrogel with both shape memory and self-healing ability (Fig. 1.5IIa) [151]. On the one hand, the shape memory properties were conferred by the presence of ionic crosslinks between alginate and Ca^{2+} ions, which can retain the temporary shape (100%), and then, recover to the permanent shape by extracting these cations using Na_2CO_3 (recovery ratio of *ca.* 100%) or EDTA (recovery ratio of *ca.* 92%) (Fig. 1.5IIb). On the other hand, the presence of supramolecular bonds through the reversible PBA-diol ester bond interaction between PBA groups of alginate-PBA and the PVA hydroxyl groups, is responsible for the self-recovery ability. This recoverability was demonstrated by connecting freshly cut pieces of this hydrogel as shown in Fig. 1.5IIc [151].

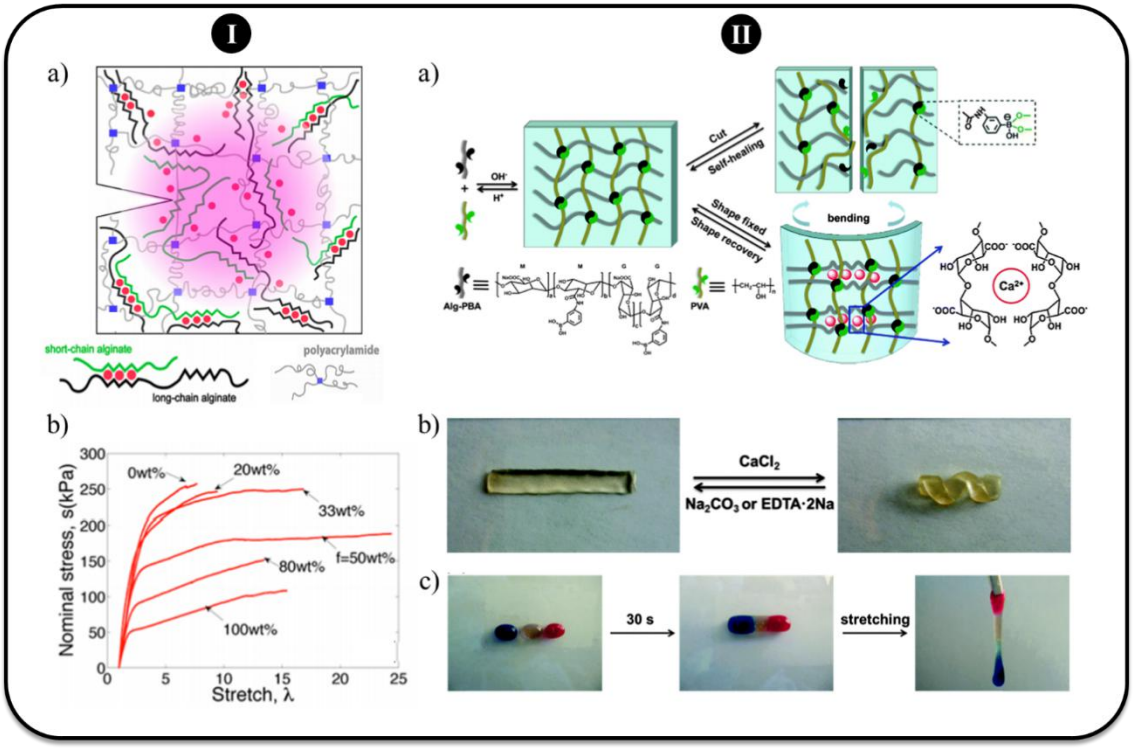

Figure 1.5 - I. (a) Schematic representation of the alginate/PAAm structure composed by covalently crosslinked PAAm through MBAAm and Ca-mediated ionically crosslinked alginate network made of both short and long chains. (b) Tensile stress–strain curves for different fractions of short-alginate chains. Adapted with permission [150] Copyright 2014, Royal Society of Chemistry. **II.** (a) Schematic representation of the alginate-PBA/poly(vinyl acid) supramolecular structure consisting of ionic crosslinks between alginate chains and Ca^{2+} ions and PBA-diol ester bonds between alginate-PBA and hydroxyl groups of PVA. (b) Photographs displaying the alginate-PBA/poly (vinyl acid) shape memory ability by using calcium chloride ($CaCl_2$) to fix the temporary shape and Na_2CO_3 or EDTA to recover the permanent one. (c) Photographs displaying the ability of the hydrogel to self-heal after cutting it into three pieces. After 30 s, the former pieces fused together as shown by the absence of fracture after stretching. Adapted with permission [151] Copyright 2014, American Chemical Society.

3.5. Agar

Agar, a polysaccharide extracted from red seaweeds, is able to form a hydrogel network by a thermoreversible sol–gel transition upon cooling to 30–40°C [152]. A one-pot methodology was introduced by Chen *et al.* to replace the conventional time-consuming DN multi-step polymerization process through the simultaneous mixing of agar, AAm monomers, initiators and chemical crosslinkers at 90– 95°C followed by cooling the precursor solution to physically

crosslink agar. The second PAAm structure is formed within the agarose structure after UV-light irradiation. Agar/PAAm DN hydrogels were tough with a compression modulus, stress and strain of 123 kPa, 38 MPa and 98%, respectively.

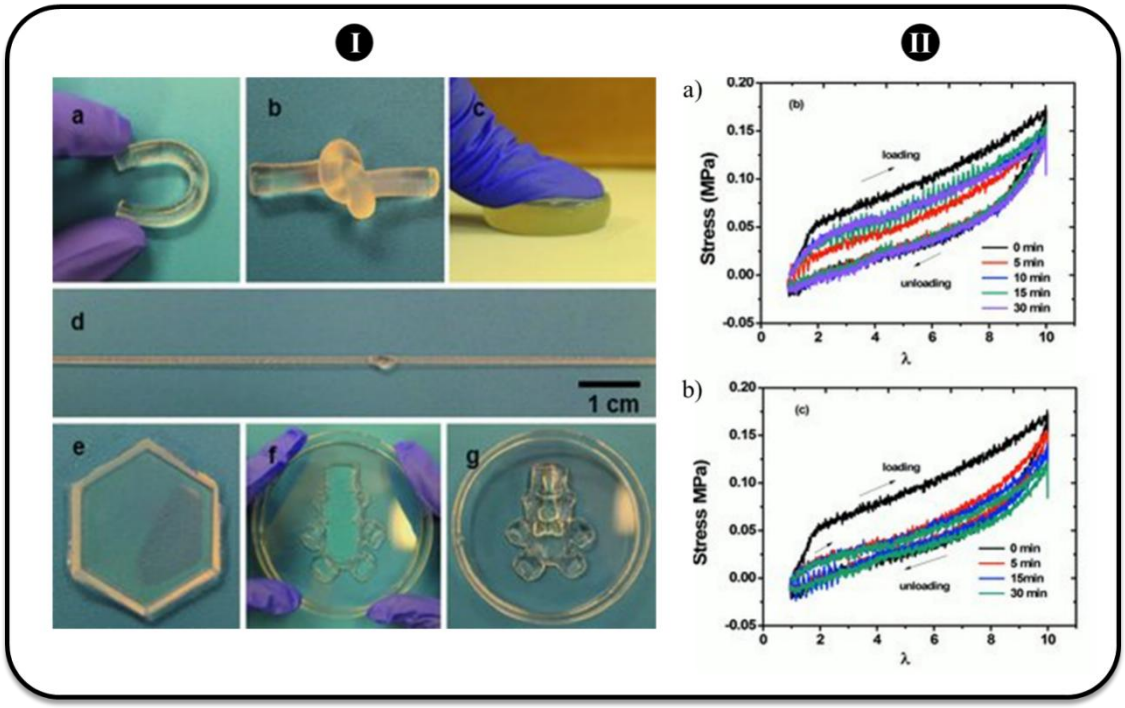

Figure 1.6 - I. Photographs depicting the agar/poly(acrylamide) (PAAm) hydrogels ability to withstand different types of deformation: bending (a); knotting (b); compression (c); knotting and stretching; and to adapt to different shapes: hexagon (e); teddy-bear during compression (f); and teddy-bear gel after unload (g). **II.** Load/unload cycle's recovery of Agar/PAM DN hydrogels stored at 100 °C and at 50 °C as function of time. Adapted with permission [153] Copyright 2013, WILEY-VCH.

Moreover, these DN hydrogels were able to recover their initial shape after being subjected to several types of deformation such as bending (Fig. 1.6Ia), knotting (Fig. 1.6Ib), compression (Fig. 1.6Ic) and elongation (Fig. 1.6Id), and also showed the ability to be synthesized with any shape (Fig. 1.6Ie–g).

Interestingly, the structure of agar/PAAm hydrogels can be recovered taking advantage of the agar thermoreversible nature as observed by the hysteresis loop recovery after 10 min at 100°C (above the agar melting point; Fig. 1.6IIa), which has not observed at 50°C (below the

agar melting point; Fig. 1.6IIb). Therefore, these hydrogels combining superior mechanical properties and recoverability are prospective candidates as load bearing artificial soft tissues analogues. However, these agar/PAAM hydrogels may not be suitable for cell encapsulation purposes due to the presence of toxic AAm monomers.

3.6. Carrageenan

Tough and recoverable hydrogels were produced from carrageenan using DN-based method [154]. Carrageenan, a partially sulfated polysaccharide obtained from red seaweeds, is composed by β-D-galactose and 3,6-anhydro-α-D-galactose units, linked by α-(1,3) and β-(1,4) glycosidic unions [51]. According with the degree of sulfation, three kinds of carrageenan can be obtained, namely, kappa-carrageenan (KC) with one sulfate per disaccharide, iota-carrageenan (IC) with two sulfates per disaccharide and lambda-carrageenan (LC) which is highly sulfated [51]. KC and IC polymers form hydrogels through ionic crosslinks between cations and double helix units, which are formed by changing the temperature. These two derivatives of carrageenan biopolymer were used to produce KC/PAAm DN hydrogels and IC/PAAm DN by mixing KC or IC polymers with AAm monomer in water containing KPS and MBAAm at 70°C followed by cooling down to 25°C. Consequently, this hydrogel combines an ionic carrageenan network with a covalent PAAm network, which resulted in a strong and tough structure at both compression (*ca.* 9.9 MPa and 4.0 MPa for KC and IC, respectively) and tension (*ca.* 75 kPa and 107 kPa for KC and IC, respectively) (Fig. 1.7Ia and Ib).

The improved mechanical properties of IC/PAAm DN hydrogels (compression, elongation, bending, knotting) can be observed in Fig. 1.7IIa–e. While KC/PAAm DN hydrogels presented a higher modulus (40.8 kPa), the IC is tougher (fracture energy of 9500 J m^{-2}). A quick recover ability was easily observed by forcing the hydrogel to pass through a buttonhole (Fig. 1.7II). This mechanical behavior is the result of the presence of ionic bonds, which are firstly broken upon loading, bridging the main PAAm backbone structure, which, in turn, is responsible for

maintaining the hydrogel structure. Interestingly, these DN hydrogels were able to heal from their cracks at mild temperatures, by the reestablishment of the broken supramolecular bonds. As described for the Agar/PAAm hydrogels, the presence of AAm monomers may hamper their use as cell-laden devices.

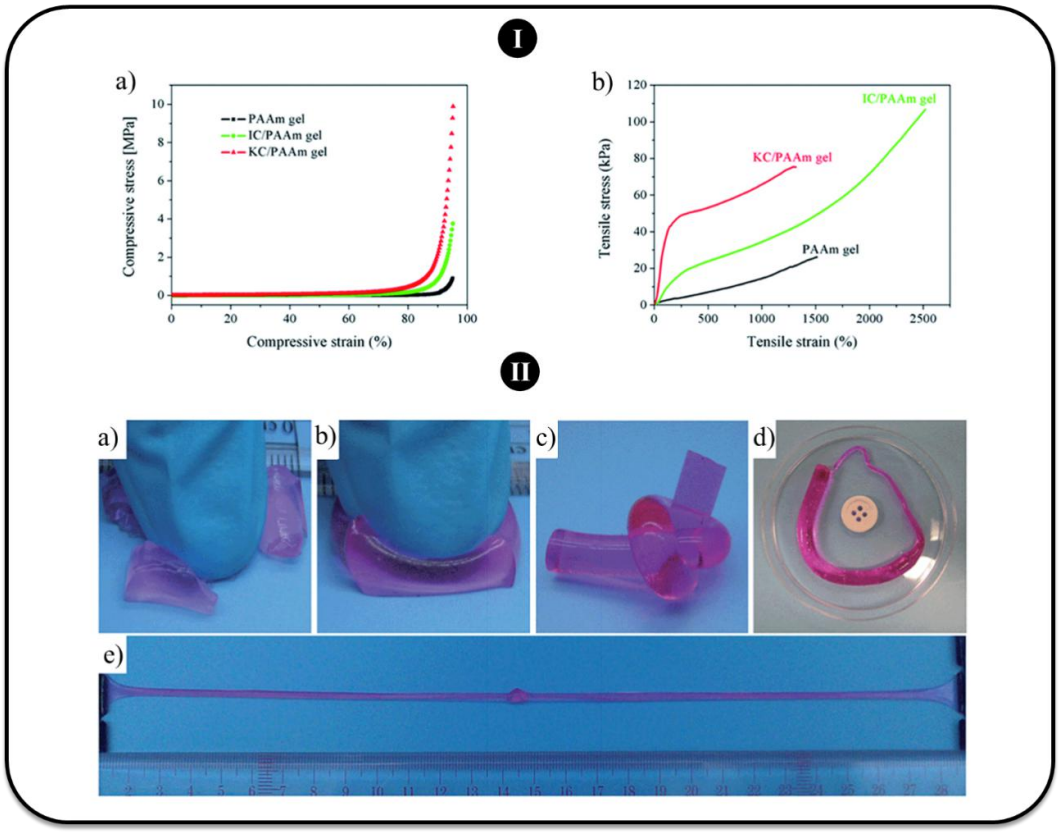

Figure 1.7 - I. Typical compression (a) and tensile (b) stress–strain curves of PAAm, IC/PAAm DN hydrogel and KC/PAAm DN hydrogel. **II.** Photographs displaying the mechanical brittle IC hydrogel (a), which broke under a modest compression. Contrarily, IC/PAAm DN hydrogel were able to sustain compression (b), (c) knotting, (d) skinning through a narrow hole, (e) knotting and stretching. Adapted with permission [154] Copyright 2014, Royal Society of Chemistry.

3.7. Hyaluronan

Hyaluronan (HA) is a natural occurring glycosaminoglycan, being abundant in connective, epithelial and neural tissues. Its structure has D-glucuronic acid and N-acetyl-D-glucosamine units linked together via alternating β -(1,4)-and β -(1,3) glycosidic bonds [155]. As this polysaccharide is part of the ECM, it is promisor for applications where one intends to mimic

this microenvironment [156]. Interpenetrated networks containing HA have been proposed [157] but efforts have been recently done to develop hydrogels with improved mechanical behavior based on the DN strategy.

A first network made of methacrylate HA (PHA), a photocrosslinkable derivative of HA polymer, was prepared by UV irradiation for 2 h in presence of a photoinitiator. Then, the resulting covalently crosslinked structure was immersed in a solution containing N, N-dimethylacrylamide (DAAm) monomers. After reaching the equilibrium, the second polymeric network was formed by UV exposure for 2 h in presence of MBAAm crosslinker and a photoinitiator, yielding a PHA/PDAAm DN hydrogel. Even though these hydrogels are mostly composed of water (more than 90%), the mechanical assays revealed a fracture stress as high as 5.2 MPa for a strain of 87.1% and compressive moduli of 0.1 MPa, which is much higher than that of pure PHA hydrogel (fracture stress, strain and compressive modulus of 0.29 MPa, 56.1% and 0.045 MPa, respectively). These properties resulted from the combination of a stiff but brittle HA network and one soft but ductile PDAAm network. These DN-based hydrogels can effectively dissipate the stress imposed during compression by either deforming the network conformation and/or sliding the physical entanglements points along the polymer chains. Additionally, these robust hydrogels were shown to be non-cytotoxic and resistant to fibroblast cells degradation after 2 months of cell culture [158]. The previous characteristics combined with the superior mechanical behavior allow their potential application as replacers of load-bearing tissues.

3.8. Chondroitin sulfate

Other biopolymer that is also found in the ECM of biological tissues, is chondroitin sulfate, being responsible for providing ECM strength. Chondroitin sulfate constitutes a sulfated polysaccharide made of both N-acetylgalactosamine and glucuronic acid sugars. Recently, a novel method was developed to produce tough DN gel combining a neutral and

biocompatible polymer with any polyelectrolyte biopolymer [159]. In this work, chondroitin sulfate proteoglycans, chondroitin sulfate and sodium hyaluronate were used as molecular stents and were combined with a neutral PDAAm polymer. To this end, the biopolymer was added to an aqueous solution containing the neutral monomer followed by its polymerization into a first PDAAm network. Since the biopolymer (polyelectrolyte) is physically trapped within the first polymer network, this structure is able to swell allowing the incorporation of a second neutral monomer needed to create a tough DN hydrogel. As can be observed in Fig. 1.8, only the incorporation of biopolymers in the first neutral structure do not contribute to the increase of the overall mechanical properties (Fig. 1.8Ia); however, the incorporation of a second matrix within the first one resulted in hydrogels with extraordinary mechanical properties (Fig. 1.8Ib). Moreover, the potential of using biopolymers to increase the biological activity was assessed by seeding HCAES above the DN hydrogels with or without biopolymers. The results revealed a cell spherical-like shape on the sample without molecular stents (Fig. 1.8IIa) whereas cells showed their typical spindle shape in the presence of the biopolymer (Fig. 1.8IIb).

The described strategy combines the strength and toughness of DN hydrogels with the bioactivity of biopolymers, enhancing their potential as soft tissues analogues. Moreover, this methodology is general in the sense that allows the introduction of any biopolymers without chemical modification and any neutral polymer [159].

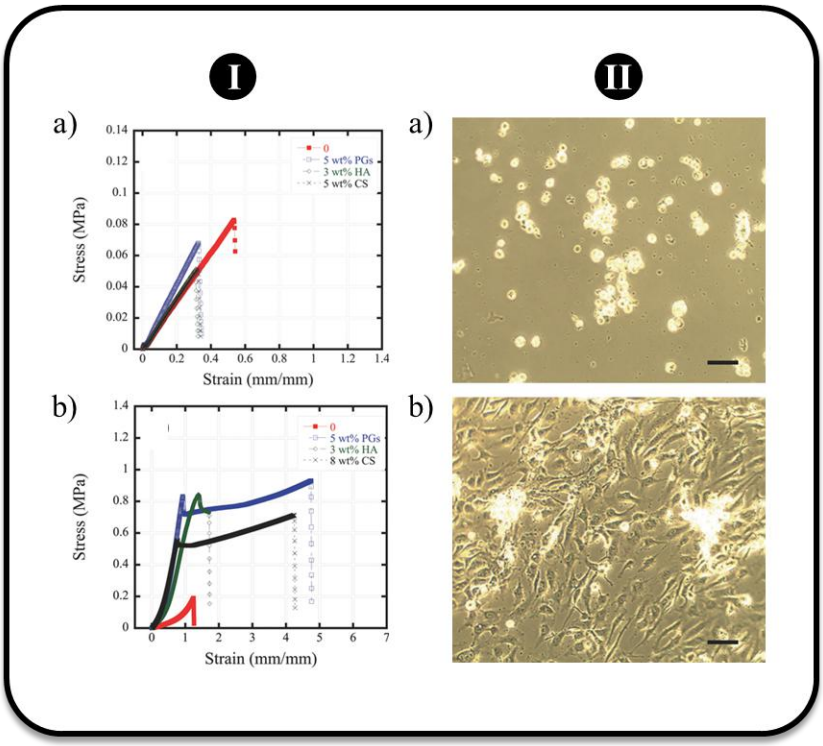

Figure 1.8 - I. Tensile stress–strain curves of single-network gels (a) and DN gels (b) without biopolymers (red) and with chondroitin sulfate proteoglycans (PGs, blue), sodium hyaluronate (HA, green) or chondroitin sulfate (CS, black). **II.** Photographs obtained by phase-contrast microscopy depicting human coronary artery endothelial cells (HCAEs) seeded on double-network hydrogels without (a) and with (b) PGs after 5 days in culture. Scale bar corresponds to 100 μm. Adapted with permission [159] Copyright 2013, Wiley-VCH.

4. Final remarks and future trends

As result of the high prevalence of degenerative diseases commonly suffered by old people, and the frequent occurrence of injuries in athletes, tissue repair has been highlighted as a hot research topic for some years now [160]. Early procedures for the treatment of these lesions explored the transplantation of organs or tissues to the site of injury; however, this practice presents collateral effects such as the possible damage of the donor site, disease transmission and recipient rejection as well as shortage of donors [161,162]. Consequently, new alternatives to grafts and artificial hard and dry substitutes are nowadays explored for repairing soft tissues, for instance, the promising TE technique. Generally speaking, TE

approaches aim at developing materials that can induce and guide cell proliferation, differentiation, and new tissue formation at the site of tissue injury or defect [126]. Accordingly, recapitulating the characteristics found in native ECM such as solutes permeability, high strength, large deformation, biocompatibility and bioactivity is likely to be the most favorable strategy to create scaffold based TE [37,163]. Notably, hydrogels provide a highly hydrated microenvironment similar to the native ECM, and hence, they have been pointed as prospective candidates for tissue repair [33,164]. As compared with other class of materials such as metals and ceramics, hydrogels exhibit the lowest rigidity, which is comparable with the one found in native soft tissues [10]. This softness constitutes a crucial aspect to consider when designing a biomaterial to mimic the ECM since it minimizes the irritation of the surrounding tissues [39]. However, regarding the toughness and strength, a large difference between natural tissues and biomaterials arises [165] as conventional hydrogels are often brittle with fracture energies lower than 10 J m^{-2}, which are far from the 1000 J m^{-2} of cartilage [166]. Recent advances in gel science were made through the development of a plethora of approaches to create customizable 3D polymeric network with superior mechanical properties. These strategies are based on the incorporation of different entities into a hydrogel structure, for instance, NC and MMC hydrogels have multifunctional crosslinkers to effectively diminish the structural inhomogeneity [43,101]; TP hydrogels present sliding crosslinks whose position on the polymeric network can be adjusted to cooperatively sustain the strain [42]; Tetra-PEG, CCb, PA hydrogels are the result of combining different monomers with different functional groups to create strong structures [82,91,107]; LB hydrogels have lamellar bilayers to provide high toughness and self-healing ability [111]; DN hydrogels are based on the introduction of a second polymeric matrix which consequently increase the fracture stress and toughness [41]. Therefore, the brittleness of conventional hydrogels can be suppressed by changing their network structure, which consists in randomly interconnected chains made from single polymers. Homogeneous hydrogels prevent the crack progression through the decrease of the

strand length distribution, and consequently, the stress can be equally sustained by all the strands. Contrarily, heterogeneous hydrogels with enhanced mechanical preformance suggest that heterogeneity is desirable considering that their toughening method depends on multiple random fractures. Moreover, the toughness of a material can be severely enhanced by introducing energy-dissipation methods. Several recent works have replaced the irreversible covalent bonds by supramolecular ones, for instance, hydrophobic associations [74,104,106], ionic crosslinks [103,107] and hydrogen bonds [73].

All of these methods constitute new concepts which can be applied to create strong, tough and endurable devices. The choice of the most suitable strategy will rely on the required properties for a specific application. For instance, if high elongations and low stiffness are needed (>8 times the original length) homogeneous hydrogels could be used such as TP gels. Besides the previous characteristics, DN hydrogels possesses also a high toughness, which may also be a requisite for a particular purpose. However, if stiffness is crucial, L-NC should be preferentially selected at the expense of lower strength values. Furthermore, a combination of the different strategies should also be envisaged as this would result in hydrogels with improved mechanical properties [167–169].

A recent theme that has attracted much attention in the biomaterials field is the fabrication of tough hydrogels for many load-bearing biomedical applications [113]. In this sense, biocompatibility is fundamental and can be achieved through the construction of biopolymer-based hydrogels [126]. Taking advantage of the previously stated methodologies to synthesize strong and tough hydrogels, researchers have engineered a variety of systems to meet the complex biological and mechanical requirements of TE. Undoubtedly, among all the methods, the DN approach affords the highest versatility in terms of composition and resulting properties, and therefore, it has been extensively employed by combining, for instance, bacterial-cellulose with gelatin, alginate, carrageenan or gellan-gum [128]; gellan-gum derivatives with gelatin [137,139] or poly(acrylamide) [135,139]; chitin with poly(vinyl alcohol)

[143]; alginate derivatives with poly(vinyl alcohol) [151] or poly(acrylamide) [71,150]; agar with poly(acrylamide) [153]; carrageenan with poly(acrylamide) [154]; acid hyaluronic derivatives with poly(dimethylacrylamide) [167]; and chondroitin sulfate with poly(acrylamide) [159], resulting in structures with improved strength and toughness which is of outmost importance for tissue repair. More hydrogels systems were already developed combining other natural-origin materials [140,170].

Hydrogel scientists may also use some hints found in Nature occurring hydrogels to design structural materials with superior mechanical properties [171]. Some animals like jellyfish and sea cucumber are examples of 3D networks with high water content, which exhibit a high tensile and compressive modulus [143,172]. These exceptional features found in biological tissues are mainly due to the presence of a sophisticated architecture from more than one type of molecule [173]. In particular, ECM can be conceived as a crosslinked matrix with a well-ordered structure on various length scales made of proteins such as collagen or elastin intertwined with high molecular weight molecules such as some polysaccharides (including hyaluronic acid and chondroitin sulfate) [174]. Having this in mind, the control of the hydrogel microstructure would potentially yield artificial substitutes of native tissues with outstanding mechanical performances [172,175]. In this review some of the attempted approaches to recapture the ECM structure were described, showing impressive mechanical properties when comparing with non-order structures made of the same materials [98,111,143]. These unique microstructures are able to effectively distribute the applied load over a wide area, slowing down the crack propagation and therefore, avoid the material fracture [145]. However, the reconstruction of the bio-tissues structure is extremely daunting [163]. Realizing this difficulty, Wang *et al.* proposed a peculiar way of preserving this natural feature by incorporating PAAm or PAA polymers into a fresh jellyfish (JF) gel, which is mainly composed of collagen and water (*ca.* 99 wt% after salt extraction) with layered structure [145]. Interestingly, only the native JF gel structure was able to withstand 1.16 MPa in compression

and 21.3 kPa in tension, which are severely higher when comparing with conventional hydrogels. The incorporation of the PAAm and PAA polymers into the jellyfish gel resulted in hydrogels with strengths much higher than those of JF and the corresponding PAAm or PAA structures [145], proving the importance of a well-defined microstructure to obtain hydrogels with superior mechanical properties. In addition, this defined organization may have beneficial biological features, for instance, by promoting cell infiltration and neovascularization [176,177]. This knowledge opens a new venue for the creation of materials with diverse functions simply by replacing non-ordered structure by a well-developed microstructure, instead of selecting a new material.

Although this review mainly focuses on the hydrogel's mechanical properties and biocompatibility, other aspects should also be considered to achieve the ultimate goal of TE. Besides providing an initial support for cell adhesion and proliferation, 3D artificial matrices should reproduce relevant native biochemical and biophysical microenvironments to pave a way toward the engineering of functional tissues [177]. Several studies demonstrated that the incorporation of bioclues (*e.g.* cell-binding motifs) and/or biological factors (*e.g.* growth factors) are crucial to ensure the cell viability and proliferation inasmuch as they constitute instructive microenvironment molecules to improve the cell/matrix interaction [52,176,178,179].

One research area, less studied in the past few years, is the design and construction of tough hydrogels with controlled degradation behavior. This degradability could be virtually introduced by labile bonds either on the polymer backbone or on the crosslinkers used to create the hydrogels, which can be later enzymatical or chemically broken under physiological conditions. Moreover, this degradation should be tailored, and the degradation products should be non-cytotoxic [76].

More recent approaches are also exploring non-invasive and patient-friendly procedures involving the targeted administration of therapeutic molecules, such as growth factors, within materials mimicking the mechanical and biological conditions of the site to be treated [180]. In

this sense, loaded injectable polymeric precursors able to self-assemble or crosslink into strong and biocompatible 3D networks after their injection, should also be developed.

Therefore, it is anticipated that hydrogels with high toughness, strength, recoverability, a well-defined architecture, biocompatibility and bioactivity will certainly enhance the applicability of these polymeric networks in the biomedical field [120,181]. However, the current state of research in this area is mainly focused on the improvement of the physicochemical properties of hydrogels and less on recapturing all the native ECM environment, and hence, must go further to significantly improve the applications of hydrogels in diverse areas.

The concepts and techniques summarized in this review to enhance the mechanical properties of conventional hydrogels are very promising for load-bearing applications. In particular, advanced strategies that combine simultaneously superior mechanical properties and biocompatibility of hydrogels are expected to expand the range of application to the Tissue Engineering field. We believe that this review will serve as guide in future development of natural-origin hydrogels for biomedical applications, especially as cell-laden analogues of load-bearing soft tissues and ECM artificial substitutes.

Acknowledgements

This work was funded by FCT (Fundação para a Ciência e a Tecnologia) through the PhD grant SFRH/BD/101748/2014, by the European Union's Seventh Framework Programme (FP7/2007-2013) under grant agreement no. REGPOT-CT2012-316331-POLARIS, by FEDER through the Competitive Factors Operation Program – COMPETE and by national funds through FCT in the scope of project PTDC/CTM-BIO/1814/2012.

References

[1] Y.C. Fung, Biomechanics: Mechanical Properties of Living Tissues, *Springer*, New York, **1993**.

[2] A.J. Kerin, M.R. Wisnom, M.A. Adams, The compressive strength of articular cartilage, *Proc. Inst. Mech. Eng. H* **1998**, 212 (4), 273–280.

[3] N.K. Simha, C.S. Carlson, J.L. Lewis, Evaluation of fracture toughness of cartilage by micropenetration, *J. Mater. Sci. Mater. Med.* **2004**, 15 (5), 631–639.

[4] P. Fratzl, Biomimetic materials research: what can we really learn from nature's structural materials?, *J Roy. Soc. Interface* **2007**, 4 (15) 637–642.

[5] J.L. Drury, D.J. Mooney, Hydrogels for tissue engineering: scaffold design variables and applications, *Biomaterials* **2003**, 24 (24), 4337–4351.

[6] H. Bodugoz-Senturk et al, Poly (vinyl alcohol)-acrylamide hydrogels as load-bearing cartilage substitute, *Biomaterials* **2009**, 30 (4), 589–596.

[7] F.T. Moutos, L.E. Freed, F. Guilak, A biomimetic three-dimensional woven composite scaffold for functional tissue engineering of cartilage, *Nat. Mater.* **2007**, 6 (2), 162–167.

[8] D.J. Huey, J.C. Hu, K.A. Athanasiou, Unlike bone, cartilage regeneration remains elusive, *Science* **2012**, 338 (6109), 917–921.

[9] J. Gong, Y. Osada, Soft and wet materials: from hydrogels to biotissues, in: M. Cloitre (Ed.), High Solid Dispersions, *Springer*, Berlin, Heidelberg, **2010**, 203–246.

[10] N.A. Peppas et al, Hydrogels in pharmaceutical formulations, *Eur. J. Pharm. Biopharm.* **2000**, 50 (1), 27–46.

[11] A.S. Hoffman, Hydrogels for biomedical applications, *Adv. Drug Deliv. Rev.* **2002**, 54 (1), 3–12.

[12] B.V. Slaughter et al, Hydrogels in regenerative medicine, *Adv. Mater.* **2009**, 21 (32–33), 3307–3329.

[13] H. Park et al, Shear-reversibly crosslinked alginate hydrogels for tissue engineering, *Macromol. Biosci.* **2009**, 9 (9), 895–901.

[14] C.L. Salgado, M.B. Oliveira, J.F. Mano, Combinatorial cell-3D biomaterials cytocompatibility screening for tissue engineering using bioinspired superhydrophobic substrates, *Integr. Biol.: Quant. Biosci. Nano Macro* **2012**, 4 (3), 318–327.

[15] W.B. Liechty et al, Polymers for drug delivery systems, *Annu. Rev. Chem. Biomol. Eng.* **2010**, 1, 149–173.

[16] T. Vermonden, R. Censi, W.E. Hennink, Hydrogels for protein delivery, *Chem. Rev.* **2012**, 112 (5), 2853–2888.

[17] Y. Qiu, K. Park, Environment-sensitive hydrogels for drug delivery, *Adv. Drug Deliv. Rev.* **2001**, 53 (3), 321–339.

[18] R. Langer, Drug delivery and targeting, *Nature* **1998**, 392 (6679 Suppl), 5–10.

[19] Y. Tanaka, J.P. Gong, Y. Osada, Novel hydrogels with excellent mechanical performance, *Prog. Polym. Sci.* **2005**, 30 (1), 1–9.

[20] P. Calvert, Hydrogels for soft machines, *Adv. Mater.* **2009**, 21 (7), 743–756.

[21] P.C. Thomas, B.H. Cipriano, S.R. Raghavan, Nanoparticle-crosslinked hydrogels as a class of efficient materials for separation and ion exchange, *Soft Matter* **2011**, 7 (18), 8192–8197.

[22] A.B. Imran, T. Seki, Y. Takeoka, Recent advances in hydrogels in terms of fast stimuli responsiveness and superior mechanical performance, *Polym. J.* **2010**, 42 (11), 839–851.

[23] D.J. Beebe et al, Functional hydrogel structures for autonomous flow control inside microfluidic channels, *Nature* **2000**, 404 (6778), 588–590.

[24] D. Kim, D.J. Beebe, Hydrogel-based reconfigurable components for microfluidic devices, *Lab Chip* **2007**, 7 (2), 193–198.

[25] H.-C. Chiu et al, Polymer vesicles containing small vesicles within interior aqueous compartments and pH-responsive transmembrane channels, *Angew. Chem. Int. Ed.* **2008**, 47 (10), 1875–1878.

[26] D. Buenger, F. Topuz, J. Groll, Hydrogels in sensing applications, *Prog. Polym. Sci.* **2012**, 37 (12), 1678–1719.

[27] M. Zrínyi, J. Fehér, G. Filipcsei, Novel gel actuator containing TiO2 particles operated under static electric field, *Macromolecules* **2000**, 33 (16), 5751– 5753.

[28] H. Okuzaki, T. Kunugi, Adsorption-induced bending of polypyrrole films and its application to a chemomechanical rotor, *J. Polym. Sci., Part B: Polym. Phys.* **1996**, 34 (10), 1747–1749.

[29] Y. Osada, H. Okuzaki, H. Hori, A polymer gel with electrically driven motility, *Nature* **1992**, 355 (6357), 242–244.

[30] H.J. Schneider, K. Kato, R.M. Strongin, Chemomechanical polymers as sensors and actuators for biological and medicinal applications, *Sensors (Basel)* **2007**, 7 (8), 1578–1611.

[31] J.F. Mano, Stimuli-responsive polymeric systems for biomedical applications, *Adv. Eng. Mater.* **2008**, 10 (6), 515–527.

[32] M. Prabaharan, J.F. Mano, Stimuli-responsive hydrogels based on polysaccharides incorporated with thermo-responsive polymers as novel biomaterials, *Macromol. Biosci.* **2006**, 6 (12), 991–1008.

[33] K.Y. Lee, D.J. Mooney, Hydrogels for tissue engineering, *Chem. Rev.* **2001**, 101 (7), 1869–1879.

[34] M.M. Stevens, A. Khademhosseini, Emerging materials for tissue engineering and regenerative medicine: themed issue for Soft Matter and Journal of Materials Chemistry, **Soft Matter 2010**, 6 (20), 4962–4962.

[35] J. Patterson, M.M. Martino, J.A. Hubbell, Biomimetic materials in tissue engineering, *Mater. Today* **2010**, 13 (1–2), 14–22.

[36] D.E. Discher, D.J. Mooney, P.W. Zandstra, Growth factors, matrices, and forces combine and control stem cells, *Science* **2009**, 324 (5935), 1673–1677.

[37] J.F. Mano, Designing biomaterials for tissue engineering based on the deconstruction of the native cellular environment, *Mater. Lett.* **2015**, 141, 198–202.

[38] M. Shibayama, Spatial inhomogeneity and dynamic fluctuations of polymer gels, *Macromol. Chem. Phys.* **1998**, 199 (1), 1–30.

[39] N.A. Peppas et al, Physicochemical foundations and structural design of hydrogels in medicine and biology, *Annu. Rev. Biomed. Eng.* **2000**, 2, 9–29.

[40] R.M. Hernández et al, Microcapsules and microcarriers for *in situ* cell delivery, *Adv. Drug Deliv. Rev.* **2010**, 62 (7–8), 711–730.

[41] J.P. Gong et al, Double-network hydrogels with extremely high mechanical strength, *Adv. Mater.* **2003**, 15 (14), 1155–1158.

[42] Y. Okumura, K. Ito, The polyrotaxane gel: a topological gel by figure-of-eight cross-links, *Adv. Mater.* **2001**, 13 (7), 485–487.

[43] K. Haraguchi, T. Takehisa, Nanocomposite hydrogels: a unique organic–inorganic network structure with extraordinary mechanical, optical, and swelling/de-swelling properties, *Adv. Mater.* **2002**, 14 (16), 1120–1124.

[44] N. Boucard et al, The use of physical hydrogels of chitosan for skin regeneration following third-degree burns, *Biomaterials* **2007**, 28 (24), 3478–3488.

[45] R. Sodian et al, Fabrication of a trileaflet heart valve scaffold from a polyhydroxyalkanoate biopolyester for use in tissue engineering, *Tissue Eng.* **2000**, 6 (2) 183–188.

[46] C.M. Bono, S.R. Garfin, History and evolution of disc replacement, *Spine J.* **2004**, 4 (6 Suppl), 145s–150s.

[47] H. Lee, C. Xia, N.X. Fang, First jump of microgel; actuation speed enhancement by elastic instability, *Soft Matter* **2010**, 6 (18), 4342–4345.

[48] C. Keplinger et al, Stretchable, transparent, ionic conductors, *Science* **2013**, 341 (6149), 984–987.

[49] S.S. Silva, J.F. Mano, R.L. Reis, Potential applications of natural origin polymer-based systems in soft tissue regeneration, *Crit. Rev. Biotechnol.* **2010**, 30 (3), 200–221.

[50] H.F. Ko, C. Sfeir, P.N. Kumta, Novel synthesis strategies for natural polymer and composite biomaterials as potential scaffolds for tissue engineering, *Philos. Trans. A Math. Phys. Eng. Sci.* **1917**, 2010 (368), 1981–1997.

[51] T. Coviello et al, Polysaccharide hydrogels for modified release formulations, *J. Control. Release* **2007**, 119 (1), 5–24.

[52] C.A. Custódio, R.L. Reis, J.F. Mano, Engineering biomolecular microenvironments for cell instructive biomaterials, *Adv. Healthcare Mater.* **2014**, 3 (6), 797–810.

[53] J.F. Mano et al, Natural origin biodegradable systems in tissue engineering and regenerative medicine: present status and some moving trends, *J. R. Soc. Interface* **2007**, 4 (17), 999–1030.

[54] E.Y. Egawa et al, Enhanced proliferation of neural stem cells in a collagen hydrogel incorporating engineered epidermal growth factor, *Biomaterials* **2011**, 32 (21), 4737–4743.

[55] Y. Liu, M.B. Chan-Park, A biomimetic hydrogel based on methacrylated dextran-graft-lysine and gelatin for 3D smooth muscle cell culture, *Biomaterials* **2010**, 31 (6), 1158–1170.

[56] M. He et al, Fast contact of solid–liquid interface created high strength multi-layered cellulose hydrogels with controllable size, *ACS Appl. Mater. Interfaces* **2014**, 6 (3), 1872–1878.

[57] A.M. Costa et al, Biocompatible polymeric microparticles produced by a simple biomimetic approach, *Langmuir* **2014**, 30 (16), 4535–4539.

[58] X. Zheng Shu et al, *In situ* crosslinkable hyaluronan hydrogels for tissue engineering, *Biomaterials* **2004**, 25 (7–8), 1339–1348.

[59] Q. Li et al, Photocrosslinkable polysaccharides based on chondroitin sulfate, *J. Biomed. Mater. Res. A* **2004**, 68 (1), 28–33.

[60] G.J. Lake, A.G. Thomas, The Strength of Highly Elastic Materials, *Proc. R. Soc. Lond. A* **1967**, 300, 108–119.

[61] D. Bonn et al, Delayed fracture of an inhomogeneous soft solid, *Science* **1998**, 280 (5361), 265–267.

[62] Y.D. Park, N. Tirelli, J.A. Hubbell, Photopolymerized hyaluronic acid-based hydrogels and interpenetrating networks, *Biomaterials* **2003**, 24 (6), 893– 900.

[63] J.A. Burdick et al, Controlled degradation and mechanical behavior of photopolymerized hyaluronic acid networks, *Biomacromolecules* **2005**, 6 (1), 386–391.

[64] J. Hawkes, The structure of fish skin, *Cell Tissue Res.* **1974**, 149 (2), 159–172.

[65] M.P. Rao et al, Laminar ceramics that exhibit a threshold strength, *Science* **1999**, 286 (5437), 102–105.

[66] G.M. Luz, J.F. Mano, Mineralized structures in nature: examples and inspirations for the design of new composite materials and biomaterials, *Compos. Sci. Technol.* **2010**, 70 (13), 1777–1788.

[67] J.B. Thompson et al, Bone indentation recovery time correlates with bond reforming time, *Nature* **2001**, 414 (6865), 773–776.

[68] J. Keckes et al, Cell-wall recovery after irreversible deformation of wood, *Nat. Mater.* **2003**, 2 (12), 810–813.

[69] V. Amendola, M. Meneghetti, Self-healing at the nanoscale, *Nanoscale* **2009**, 1 (1), 74–88.

[70] G.E. Fantner et al, Sacrificial bonds and hidden length: unraveling molecular mesostructures in tough materials, *Biophys. J.* **2006**, 90 (4), 1411–1418.

[71] J.-Y. Sun et al, Highly stretchable and tough hydrogels, *Nature* **2012**, 489 (7414), 133–136.

[72] P.J. Skrzeszewska et al, Fracture and self-healing in a well-defined self-assembled polymer network, *Macromolecules* **2010**, 43 (7), 3542–3548.

[73] J. Cui, A.D. Campo, Multivalent H-bonds for self-healing hydrogels, *Chem. Commun.* **2012**, 48 (74), 9302–9304.

[74] S. Abdurrahmanoglu, V. Can, O. Okay, Design of high-toughness polyacrylamide hydrogels by hydrophobic modification, *Polymer* **2009**, 50 (23), 5449–5455.

[75] A. Clark, S. Ross-Murphy, Structural and mechanical properties of biopolymer gels, in: Biopolymers, *Springer*, Berlin, Heidelberg, **1987**, 57–192.

[76] W.E. Hennink, C.F. van Nostrum, Novel crosslinking methods to design hydrogels, *Adv. Drug Deliv. Rev.* **2002**, 54 (1), 13–36.

[77] M. Shibayama, Universality and specificity of polymer gels viewed by scattering methods, *Bull. Chem. Soc. Jpn.* **2006**, 79 (12), 1799–1819.

[78] T.-P. Hsu, D.S. Ma, C. Cohen, Effects of inhomogeneities in polyacrylamide gels on thermodynamic and transport properties, *Polymer* **1983**, 24 (10), 1273–1278.

[79] C.H. Lee et al, Characterization of heterogeneous polyacrylamide hydrogels by tracking of single quantum dots, *Macromolecules* **2014**, 47 (2), 741–749.

[80] W.-C. Lin et al, Large strain and fracture properties of poly(dimethylacrylamide)/silica hybrid hydrogels, *Macromolecules* **2010**, 43 (5), 2554–2563.

[81] H. Furukawa et al, Swelling-induced modulation of static and dynamic fluctuations in polyacrylamide gels observed by scanning microscopic light scattering, *Phys. Rev. E* **2003**, 68 (3), 031406.

[82] T. Sakai et al, Design and fabrication of a high-strength hydrogel with ideally homogeneous network structure from tetrahedron-like macromonomers, *Macromolecules* **2008**, 41 (14), 5379–5384.

[83] B. Fei et al, Hydrogel of biodegradable cellulose derivatives. I. Radiation-induced crosslinking of CMC, *J. Appl. Polym. Sci.* **2000**, 78 (2), 278–283.

[84] S. Naficy et al, Progress toward robust polymer hydrogels, *Aust. J. Chem.* **2011**, 64 (8), 1007–1025.

[85] E. Nedkov, S. Tsvetkova, Effect of gamma irradiation on the crystalline structure of ultra high molecular weight poly(ethylene oxide), *Radiat. Phys. Chem.* **1994**, 43 (4), 397–401.

[86] Y. Akagi et al, Evaluation of topological defects in tetra-PEG gels, *Macromolecules* **2009**, 43 (1), 488–493.

[87] T. Matsunaga et al, Structure characterization of tetra-PEG gel by small-angle neutron scattering, *Macromolecules* **2009**, 42 (4), 1344–1351.

[88] D.A. Ossipov, J. Hilborn, Poly(vinyl alcohol)-based hydrogels formed by ‘‘click chemistry’’, *Macromolecules* **2006**, 39 (5), 1709–1718.

[89] V. Crescenzi et al, Novel hydrogels via click chemistry: synthesis and potential biomedical applications, *Biomacromolecules* **2007**, 8 (6), 1844–1850.

[90] V.V. Rostovtsev et al, A stepwise Huisgen cycloaddition process: copper(I)-catalyzed regioselective ‘‘ligation’’ of azides and terminal alkynes, *Angew. Chem. Int. Ed.* **2002**, 41 (14), 2596–2599.

[91] M. Malkoch et al, Synthesis of well-defined hydrogel networks using click chemistry, *Chem. Commun.* **2006**, 26, 2774–2776.

[92] S.A. Nepogodiev, J.F. Stoddart, Cyclodextrin-based catenanes and rotaxanes, *Chem. Rev.* **1998**, 98 (5), 1959–1976.

[93] T. Koga, F. Tanaka, Elastic properties of polymer networks with sliding junctions, *Eur. Phys. J. E* **2005**, 17 (2), 225–229.

[94] T. Karino et al, SANS studies on deformation mechanism of slide-ring gel, *Macromolecules* **2005**, 38 (14), 6161–6167.

[95] K. Ito, Novel cross-linking concept of polymer network: synthesis, structure, and properties of slide-ring gels with freely movable junctions, *Polym. J.* **2007**, 39 (6), 489–499.

[96] K. Haraguchi, Nanocomposite hydrogels, *Curr. Opin. Solid State Mater. Sci.* **2007**, 11 (3–4), 47–54.

[97] K. Haraguchi, K. Murata, T. Takehisa, Stimuli-responsive properties of nanocomposite gels comprising (2-methoxyethylacrylate-co-N, Ndimethylacrylamide) copolymer-clay networks, *Macromol. Symp.* **2013**, 329 (1), 150–161.

[98] J. Wang et al, A strong bio-inspired layered PNIPAM–clay nanocomposite hydrogel, *Angew. Chem. Int. Ed.* **2012**, 51 (19), 4676–4680.

[99] Q. Wang et al, High-water-content mouldable hydrogels by mixing clay and a dendritic molecular binder, *Nature* **2010**, 463 (7279), 339–343.

[100] H. Ihre, O.L. Padilla De Jesús, J.M.J. Fréchet, Fast and convenient divergent synthesis of aliphatic ester dendrimers by anhydride coupling, *J. Am. Chem. Soc.* **2001**, 123 (25), 5908–5917.

[101] T. Huang et al, A novel hydrogel with high mechanical strength: a macromolecular microsphere composite hydrogel, *Adv. Mater.* **2007**, 19 (12), 1622–1626.

[102] N. Tanaka, H. Kitano, N. Ise, Raman spectroscopic study of hydrogen bonding in aqueous carboxylic acid solutions. 3. Polyacrylic acid, *Macromolecules* **1991**, 24 (10), 3017–3019.

[103] K.J. Henderson et al, Ionically cross-linked triblock copolymer hydrogels with high strength, *Macromolecules* **2010**, 43 (14), 6193–6201.

[104] D.C. Tuncaboylu et al, Tough and self-healing hydrogels formed via hydrophobic interactions, *Macromolecules* **2011**, 44 (12), 4997–5005.

[105] M. Shibayama, T. Tanaka, Volume phase transition and related phenomena of polymer gels, in: K. Dušek (Ed.), Responsive Gels: Volume Transitions I, *Springer*, Berlin, Heidelberg, **1993**, 1–62.

[106] U. Gulyuz, O. Okay, Self-healing poly(acrylic acid) hydrogels with shape memory behavior of high mechanical strength, *Macromolecules* **2014**, 47 (19), 6889–6899.

[107] T.L. Sun et al, Physical hydrogels composed of polyampholytes demonstrate high toughness and viscoelasticity, *Nat. Mater.* **2013**, 12 (10), 932–937.

[108] P.G. Higgs, J.F. Joanny, Theory of polyampholyte solutions, *J. Chem. Phys.* **1991**, 94 (2), 1543–1554.

[109] S. Kudaibergenov, Recent advances in the study of synthetic polyampholytes in solutions, in: Polymer Latexes – Epoxide Resins – Polyampholytes, *Springer*, Berlin, Heidelberg, **1999**, 115–197.

[110] F.M. Chen, M. Zhang, Z.F. Wu, Toward delivery of multiple growth factors in tissue engineering, *Biomaterials* **2010**, 31 (24), 6279–6308.

[111] M.A. Haque et al, Lamellar bilayers as reversible sacrificial bonds to toughen hydrogel: hysteresis, self-recovery, fatigue resistance, and crack blunting, *Macromolecules* **2011**, 44 (22), 8916–8924.

[112] M.A. Haque et al, Unidirectional alignment of lamellar bilayer in hydrogel: one-dimensional swelling, anisotropic modulus, and stress/strain tunable structural color, *Adv. Mater.* **2010**, 22 (45), 5110–5114.

[113] M.A. Haque, T. Kurokawa, J.P. Gong, Super tough double network hydrogels and their application as biomaterials, *Polymer* **2012**, 53 (9), 1805–1822.

[114] J.P. Gong, Why are double network hydrogels so tough?, *Soft Matter* **2010**, 6 (12), 2583–2590

[115] T. Nakajima et al, Characterization of internal fracture process of double network hydrogels under uniaxial elongation, *Soft Matter* **2013**, 9 (6), 1955–1966.

[116] T. Nakajima et al, Effect of void structure on the toughness of double network hydrogels, *J. Polym. Sci., Part B: Polym. Phys.* **2011**, 49 (17), 1246–1254.

[117] D. Myung et al, Design and fabrication of an artificial cornea based on a photolithographically patterned hydrogel construct, *Biomed. Microdev.* **2007**, 9 (6), 911–922.

[118] W. Yang, H. Furukawa, J.P. Gong, Highly extensible double-network gels with self-assembling anisotropic structure, *Adv. Mater.* **2008**, 20 (23), 4499–4503.

[119] J. Hu et al, Microgel-reinforced hydrogel films with high mechanical strength and their visible mesoscale fracture structure, *Macromolecules* **2011**, 44 (19), 7775–7781.

[120] Y.M. Chen et al, Cultivation of endothelial cells on adhesive protein-free synthetic polymer gels, *Biomaterials* **2005**, 26 (22), 4588–4596.

[121] T. Nakajima et al, True chemical structure of double network hydrogels, *Macromolecules* **2009**, 42 (6), 2184–2189.

[122] Y.H. Na et al, Necking phenomenon of double-network gels, *Macromolecules* **2006**, 39 (14), 4641–4645.

[123] P.B. Malafaya, G.A. Silva, R.L. Reis, Natural-origin polymers as carriers and scaffolds for biomolecules and cell delivery in tissue engineering applications, *Adv. Drug Deliv. Rev.* **2007**, 59 (4–5), 207–233.

[124] T.J. Klein et al, Long-term effects of hydrogel properties on human chondrocyte behavior, *Soft Matter* **2010**, 6 (20), 5175–5183.

[125] J. Velema, D. Kaplan, Biopolymer-based biomaterials as scaffolds for tissue engineering, *Adv. Biochem. Eng. Biotechnol.* **2006**, 102, 187–238.

[126] B. Balakrishnan, R. Banerjee, Biopolymer-based hydrogels for cartilage tissue engineering, *Chem. Rev.* **2011**, 111 (8), 4453–4474.

[127] S. Hestrin, M. Schramm, Synthesis of cellulose by Acetobacter xylinum. 2. Preparation of freeze-dried cells capable of polymerizing glucose to cellulose, *Biochem. J.* **1954**, 58 (2), 345–352.

[128] A. Nakayama et al, High mechanical strength double-network hydrogel with bacterial cellulose, *Adv. Funct. Mater.* **2004**, 14 (11), 1124–1128.

[129] C. Azuma et al, Biodegradation of high-toughness double network hydrogels as potential materials for artificial cartilage, *J. Biomed. Mater. Res. A* **2007**, 81 (2), 373–380.

[130] H. Shin, B.D. Olsen, A. Khademhosseini, The mechanical properties and cytotoxicity of cell-laden double-network hydrogels based on photocrosslinkable gelatin and gellan gum biomacromolecules, *Biomaterials* **2012**, 33 (11), 3143–3152.

[131] I. Giavasis, L.M. Harvey, B. McNeil, Gellan gum, *Crit. Rev. Biotechnol.* **2000**, 20 (3), 177-211.

[132] H. Grasdalen, O. Smidsrød, Gelation of gellan gum, *Carbohydr. Polym.* **1987**, 7 (5), 371–393.

[133] E.R. Morris, K. Nishinari, M. Rinaudo, Gelation of gellan – a review, *Food Hydrocolloids* **2012**, 28 (2), 373–411.

[134] Y.-H. Na et al, Structural characteristics of double network gels with extremely high mechanical strength, *Macromolecules* **2004**, 37 (14), 5370–5374.

[135] S.E. Bakarich et al, Recovery from applied strain in interpenetrating polymer network hydrogels with ionic and covalent cross-links, *Soft Matter* **2012**, 8 (39), 9985–9988.

[136] X. Zhao et al, Stress-relaxation behavior in gels with ionic and covalent crosslinks, *J. Appl. Phys.* **2010**, 107 (6).

[137] D.M. Kirchmajer, M.I.H. Panhuis, Robust biopolymer based ionic-covalent entanglement hydrogels with reversible mechanical behaviour, *J. Mater. Chem. B* **2014**, 2 (29), 4694–4702.

[138] C.-C. Tsai et al, In vitro evaluation of the genotoxicity of a naturally occurring crosslinking agent (genipin) for biologic tissue fixation, *J. Biomed. Mater. Res.* **2000**, 52 (1), 58–65.

[139] H. Shin, B.D. Olsen, A. Khademhosseini, Gellan gum microgel-reinforced cell-laden gelatin hydrogels, *J. Mater. Chem. B* **2014**, 2 (17), 2508–2516.

[140] J.W. Nichol et al, Cell-laden microengineered gelatin methacrylate hydrogels, *Biomaterials* **2010**, 31 (21), 5536–5544.

[141] M. Rinaudo, Chitin and chitosan: properties and applications, *Prog. Polym. Sci.* **2006**, 31 (7), 603–632.

[142] C. Hassan, N. Peppas, Structure and applications of poly(vinyl alcohol) hydrogels produced by conventional crosslinking or by freezing/thawing methods, in: Biopolymers PVA Hydrogels, Anionic Polymerisation Nanocomposites, *Springer*, Berlin, Heidelberg, **2000**, 37–65.

[143] M. He et al, Construction of chitin/PVA composite hydrogels with jellyfish gel-like structure and their biocompatibility, *Biomacromolecules* **2014**, 15 (9), 3358–3365.

[144] R. Ricciardi et al, X-ray diffraction analysis of poly(vinyl alcohol) hydrogels, obtained by freezing and thawing techniques, *Macromolecules* **2004**, 37 (5), 1921–1927.

[145] X. Wang, H. Wang, H.R. Brown, Jellyfish gel and its hybrid hydrogels with high mechanical strength, *Soft Matter* **2011**, 7 (1), 211–219.

[146] A.D. Augst, H.J. Kong, D.J. Mooney, Alginate hydrogels as biomaterials, *Macromol. Biosci.* **2006**, 6 (8), 623–633.

[147] J.A. Rowley, G. Madlambayan, D.J. Mooney, Alginate hydrogels as synthetic extracellular matrix materials, *Biomaterials* **1999**, 20 (1), 45–53.

[148] K.I. Draget, O. Smidsrød, G. Skjåk-Bræk, Alginates from algae, in: Biopolymers Online, *Wiley-VCH Verlag GmbH & Co. KGaA*, **2005**.

[149] M.C. Darnell et al, Performance and biocompatibility of extremely tough alginate/polyacrylamide hydrogels, *Biomaterials* **2013**, 34 (33), 8042–8048.

[150] J. Li et al, Hybrid hydrogels with extremely high stiffness and toughness, *ACS Macro Lett.* **2014**, 3 (6), 520–523.

[151] H. Meng et al, Self-healable macro-/microscopic shape memory hydrogels based on supramolecular interactions, *Chem. Commun.* **2014**, 50 (82), 12277–12280.

[152] V. Normand et al, New insight into agarose gel mechanical properties, *Biomacromolecules* **2000**, 1 (4), 730–738.

[153] Q. Chen et al, A robust, one-pot synthesis of highly mechanical and recoverable double network hydrogels using thermoreversible sol–gel polysaccharide, *Adv. Mater.* **2013**, 25 (30), 4171–4176.

[154] X. Lu et al, Super-tough and thermo-healable hydrogel – promising for shape-memory absorbent fiber, *J. Mater. Chem. B* **2014**, 2 (43), 7631–7638.

[155] J.R.E. Fraser, T.C. Laurent, U.B.G. Laurent, Hyaluronan: its nature, distribution, functions and turnover, *J. Intern. Med.* **1997**, 242 (1), 27–33.

[156] X.Z. Shu et al, Disulfide-crosslinked hyaluronan-gelatin hydrogel films: a covalent mimic of the extracellular matrix for in vitro cell growth, *Biomaterials* **2003**, 24 (21), 3825–3834.

[157] J.R. Santos, N.M. Alves, J.F. Mano, New thermo-responsive hydrogels based on poly (N-isopropylacrylamide)/hyaluronic acid semi-interpenetrated polymer networks: swelling properties and drug release studies, *J. Bioactive Comp. Polym.* **2010**, 25 (2), 169–184.

[158] L. Weng et al, Mechanically strong double network photocrosslinked hydrogels from N,N-dimethylacrylamide and glycidyl methacrylated hyaluronan, *Biomaterials* **2008**, 29 (14), 2153–2163.

[159] Y. Zhao et al, Proteoglycans and glycosaminoglycans improve toughness of biocompatible double network hydrogels, *Adv. Mater.* **2014**, 26 (3), 436– 442.

[160] D. Puppi et al, Polymeric materials for bone and cartilage repair, *Prog. Polym. Sci.* **2010**, 35 (4), 403–440.

[161] J.S. Temenoff, A.G. Mikos, Review: tissue engineering for regeneration of articular cartilage, *Biomaterials* **2000**, 21 (5), 431–440.

[162] E.B. Hunziker, Articular cartilage repair: are the intrinsic biological constraints undermining this process insuperable?, *Osteoarth Cartil.* **1999**, 7 (1), 15–28.

[163] X. Jia, K.L. Kiick, Hybrid multicomponent hydrogels for tissue engineering, *Macromol. Biosci.* **2009**, 9 (2), 140–156.

[164] N.M. Alves et al, Controlling cell behavior through the design of polymer surfaces, *Small* **2010**, 6 (20), 2208–2220.

[165] J. Elisseeff et al, Advances in skeletal tissue engineering with hydrogels, *Orthod. Craniofac. Res.* **2005**, 8 (3), 150–161.

[166] M.V. Chin-Purcell, J.L. Lewis, Fracture of articular cartilage, *J. Biomech. Eng.* **1996**, 118 (4), 545–556.

[167] K. Harrass et al, Mechanically strong hydrogels with reversible behaviour under cyclic compression with MPa loading, *Soft Matter* **2013**, 9 (10), 2869–2877.

[168] G. Gao et al, Tough nanocomposite double network hydrogels reinforced with clay nanorods through covalent bonding and reversible chain adsorption, *J. Mater. Chem. B* **2014**, 2 (11), 1539–1548.

[169] J. Shen, N. Li, M. Ye, Preparation and characterization of dual-sensitive double network hydrogels with clay as a physical crosslinker, *Appl. Clay Sci.* **2015**, 103, 40–45.

[170] A.R. Fajardo et al, Dual-network hydrogels based on chemically and physically crosslinked chitosan/chondroitin sulfate, *React. Funct. Polym.* **2013**, 73 (12), 1662–1671.

[171] C. Sanchez, H. Arribart, M.M. Giraud Guille, Biomimetism and bioinspiration as tools for the design of innovative materials and systems, *Nat. Mater.* **2005**, 4 (4), 277–288.

[172] T. Miyazaki et al, Hydrogels with crystalline or liquid crystalline structure, *Macromol. Rapid Commun.* **2002**, 23 (8), 447–455.

[173] Z.L. Wu, J.P. Gong, Hydrogels with self-assembling ordered structures and their functions, *NPG Asia Mater.* **2011**, 3, 57–64.

[174] B.J. DeKosky et al, Hierarchically designed agarose and poly(ethylene glycol) interpenetrating network hydrogels for cartilage tissue engineering, *Tissue Eng. Part C Methods* **2010**, 16 (6), 1533–1542.

[175] A. Sidorenko et al, Reversible switching of hydrogel-actuated nanostructures into complex micropatterns, *Science* **2007**, 315 (5811), 487–490.

[176] M.P. Lutolf, J.A. Hubbell, Synthetic biomaterials as instructive extracellular microenvironments for morphogenesis in tissue engineering, *Nat. Biotechnol.* **2005**, 23 (1), 47–55.

[177] N. Zagris, Extracellular matrix in development of the early embryo, *Micron* **2001**, 32 (4), 427–438.

[178] D. Gullberg, P. Ekblom, Extracellular matrix and its receptors during development, *Int. J. Dev. Biol.* **1995**, 39 (5), 845–854.

[179] B.K. Mann et al, Smooth muscle cell growth in photopolymerized hydrogels with cell adhesive and proteolytically degradable domains: synthetic ECM analogs for tissue engineering, *Biomaterials* **2001**, 22 (22), 3045–3051.

[180] X. Jia et al, Hyaluronic acid-based microgels and microgel networks for vocal fold regeneration, *Biomacromolecules* **2006**, 7 (12), 3336–3344.

[181] K. Yasuda et al, Biomechanical properties of high-toughness double network hydrogels, *Biomaterials* **2005**, 26 (21), 4468–4475.

Chapter II: Materials & Methods

This chapter presents an overview of the materials and techniques employed in Chapters III and IV, as well as the reasons for their selection. Some general theoretical concepts will be also discussed herein. The materials used in this thesis were purchased from specialized commercial distributors and some of them were chemically modified to be suitable for a specific purpose. All the materials, experimental procedures and equipment suppliers can be found in more detail in the experimental subsection of each chapter.

1. Design of Double-network (DN) hydrogels using natural polysaccharides

Hydrogels are water-insoluble three-dimensional networks arising from the crosslinking of water-soluble polymers. The crosslinking mechanism can be either based on covalent or non-covalent interactions between the polymer chains [1,2]. These highly hydrated networks are used for a broad range of applications including in Tissue Engineering, mainly because of their high resemblance with body tissues in terms of composition and physical structure. However, conventional hydrogels usually exhibit low mechanical performance [3]. Since the pioneering study of Gong [4], the DN technology has been employed to enhance the mechanical properties of hydrogels (for more details about this technique and other strategies to improve the mechanical behavior of hydrogels, please consult Chapter I).

Moreover, when intended for biomedical purposes, it is also essential to ensure the safety of the materials used. In this sense, polysaccharides are potential material candidates as a result of their typical biocompatibility, structural similarity to glycosaminoglycans of the native extracellular matrix and the possibility to be processed under mild conditions [5]. From the commercial point of view, natural-origin polymers are often inexpensive as they are readily available from renewable sources [3].

1.1. Chitosan (CHI) polysaccharide

CHI is a linear polysaccharide composed of randomly distributed D-glucosamine and N-acetyl-D-glucosamine units linked through $\beta(1\rightarrow4)$ glycosidic bonds (Figure 2.1) [6]. This cationic copolymer is mainly obtained through deacetylation of chitin, a polysaccharide typically found in the exoskeleton of crustaceans, by enzymatic hydrolysis in the presence of chitin deacetylase or under alkaline conditions [7]. If the obtained deacetylation degree is higher than 50%, the resultant polymer is denominated as chitosan [8]. Contrarily to chitin, CHI is soluble in diluted acidic solutions by virtue of electrostatic repulsions between the protonated amine groups on D-glucosamine repeat unit (pKa value of *ca.* 6.5) [6].

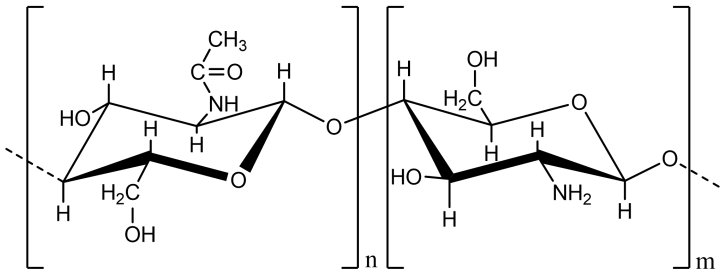

Figure 2.1 - Molecular structure of CHI.

CHI has been widely used for biomedical purposes owing to its well-established biocompatibility, biodegradability, non-toxicity and possibility to interact with other biomolecules such as proteins [7]. But, perhaps, the most appealing property of CHI is the possibility to be functionalized with desired moieties under mild conditions. This fact is the result of the high number of reactive amine groups on its backbone, which can be used to incorporate a plethora of functionalities such as the ability to crosslink upon UV-irradiation or the possibility of establishing coordination bonds with metal ions. This wide range of chemical structures is extremely relevant for the purpose of the works described in Chapter III and IV, which consists on enhancing the mechanical properties of polysaccharide-based hydrogels by

combining chemical and physical crosslinking mechanisms (Figure 2.2). Therefore, CHI was the selected material to produce these DN hydrogels.

In Chapter III, CHI was modified into its photocrosslinkable derivative, namely MACHI, to allow the formation of a covalent-crosslinked structure upon UV-irradiation in the presence of a photoinitiator. On the other side, the physical network was obtained through ionic interactions between the positively charged amine groups of CHI and the negatively charged tripolyphosphate (TPP) ions, a non-toxic polyanion (Figure 2.2; Chapter III and Figure 2.3A) [9].

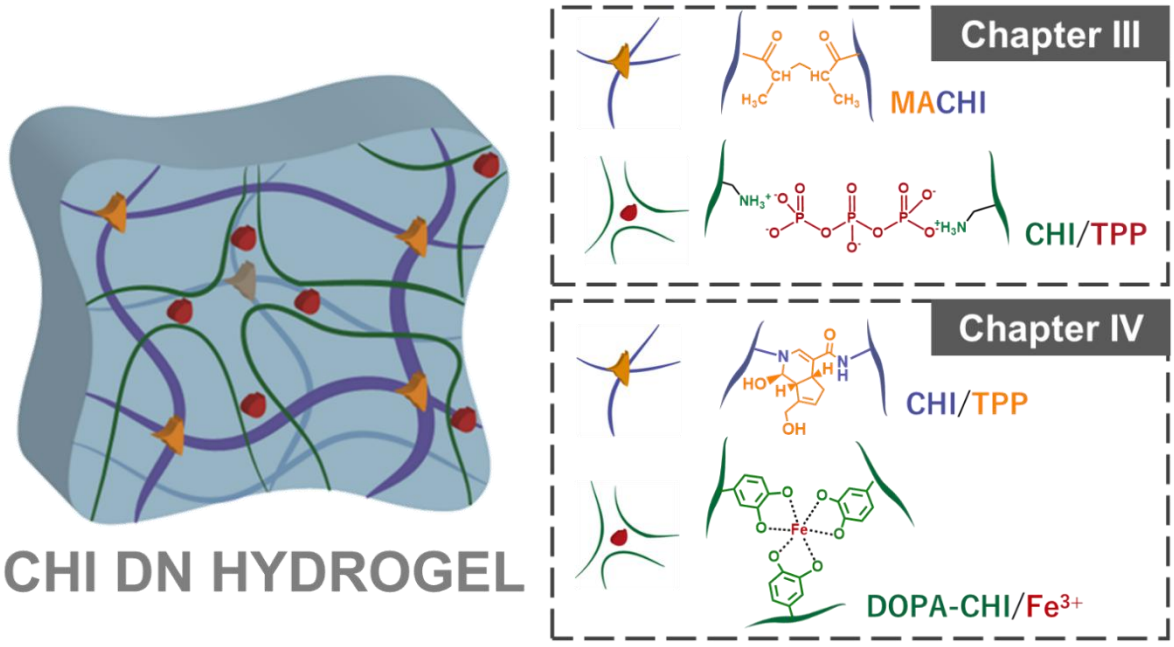

Figure 2.2 - Graphical overview of the research presented in the Chapters III and IV. CHI hydrogels with enhanced mechanical properties were fabricated by employing a DN strategy combining covalent (labeled in yellow) and non-covalent (labeled in red) crosslinking mechanisms. In Chapter III, the covalent network was formed upon UV-irradiation of the MACHI derivative, and the non-covalent network was the result of ionic interactions between the positively charged amine groups on CHI and negatively charged TPP ions. In Chapter IV, GP was used as crosslinker of the amine groups on CHI to create a covalent network whereas Fe^{3+} ions formed coordination bonds with DOPA moieties present in DOPA-CHI derivative, yielding a non-covalent network.

In Chapter IV, other crosslinking strategies were employed to obtain hydrogels with additional properties, namely self-healing and injectability. Therefore, genipin (GP) was used

as a crosslinker agent of the CHI amine groups to yield a covalently crosslinked network. GP is a natural chemical crosslinker obtained from the enzymatic hydrolysis of geniposide, found in fruits of *Genipa Americana* and *Gardenia jasminoides* (Figure 2.3 B) [10]. The main advantage of using this crosslinker is its low toxicity when comparing with other molecules such as glutaraldehyde [11]. In the same Chapter, the physical network resulted from coordination bonds between iron ions (Figure 2.3C) and a CHI derivative containing 3,4-dihydroxy-L-phenylalanine (DOPA) moieties (DOPA-CHI).

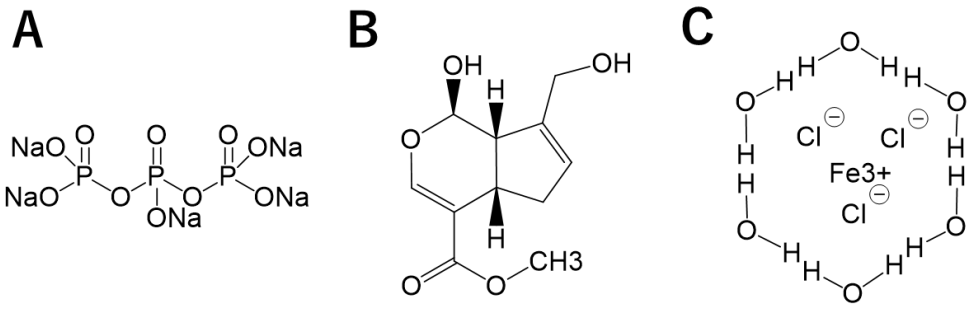

Figure 2.3 - Molecular structure of the crosslinker agents used in Chapter III and IV, namely sodium tripolyphosphate **(A)**, GP **(B)** and iron (III) chloride hexahydrate **(C)**.

Besides the need for two different crosslinking methodologies, it is also essential to have polymers with contrasting features in order to achieve superior mechanical performance using a DN-based strategy. In both Chapters, this contrast was attained by using CHI polymers with different molecular weights. To this end, a CHI polymer with low-molecular weight and from a medical grade was modified into its MACHI and DOPA-CHI derivatives to be used in Chapter III and IV, respectively. Additionally, a CHI polymer with a medium molecular weight was used in both Chapters to obtain the second polymeric network, after being purified to remove all the impurities arising from the deacetylation process of chitin. Importantly, the batches used during the execution of all the experiments were kept the same, in order to avoid batch-to-batch variability.

Chitosan purification procedure: The method was adapted from the literature [12] and takes advantage of the pH-mediated conformational transition of CHI, which is soluble below pH 6.4 and precipitates above it. Briefly, a 1% (w/v) CHI solution in 1% (v/v) acetic acid was vacuum filtered twice using filters with a cutoff of 20-25 µm to remove insoluble impurities. The filtered CHI was then precipitated using 1M sodium hydroxide solution, which was added dropwise until reaching a pH value of 8. Afterwards, the white precipitated chitosan was repeatedly rinsed with distilled water until no changes in the pH of the residual waters were detected (pH ≈ 7). Finally, CHI was rinsed with absolute ethanol, vacuum-filtered and stored at -80 °C before being lyophilized.

1.1.1. Synthesis of the low molecular weight-methacrylamide chitosan (LMW-MACHI)

Procedure: Low molecular weight-chitosan (LMW-CHI) was modified into LMW-MACHI by incorporating methacrylic moieties on its backbone [13]. Briefly, LMW-CHI (3% (w/v)) was dissolved in 2% (v/v) acetic acid overnight at room temperature (RT) with constant stirring. Once dissolved, methacrylic anhydride (at 1 molar equivalents per chitosan repeat unit) was added dropwise and left in incubation for 5h at RT in dark. The mixture was, then, dialyzed against distilled water for 5 days, changing the water twice a day. Finally, the LMW-MACHI solution was freeze-dried and stored at -20 °C until use.

Characterization: ^{1}H–Nuclear Magnetic Resonance (^{1}H-NMR) was used to infer about the correct LMW-MACHI methacrylation and to estimate both the substitution (SD) and crosslinking (CD) degrees.

1.1.2. Synthesis of the DOPA functionalized chitosan (DOPA-CHI)

Procedure: DOPA-CHI was synthesized by standard 1-ethyl-3-(3-dimethylaminopropyl) carbodiimide (EDC)/ N-hydroxysuccinimide (NHS) coupling chemistry [14]. To this end, DOPA

(9.69 mmol, 2 equiv.) was dissolved in 400 mL 0.5 % trifluoroacetic acid under stirring followed by the mixture degassing with nitrogen gas for 20 min at RT. Next, LMW-CHI (4.84 mmol, 1 equiv.) and NHS (29.1 mmol, 6 equiv.) were added to the DOPA solution and the pH adjusted to 5.5 using a 2M NaOH solution to prevent the catechol oxidation and increase the EDC/NHS coupling efficiency. After 15 min, EDC (29.1 mmol, 6 equiv.) was added to the DOPA/CHI/NHS reaction to activate the carboxylic groups on DOPA molecules for direct conjugation to the primary amines of CHI through the formation of amide bonds. NHS is required to form a semi-stable ester since the EDC-ester formed by the reaction between DOPA and CHI is unstable in aqueous media. The mixture was left to react under stirring and N_2 atmosphere in a light protected flask at RT. After 20h, the solution was dialyzed against 4 mM HCl for 6 days under stirring and the dialysis solvent was changed once a day. The purified solution was dried by rotary evaporation and grinded to yield a light-brown powder.

Characterization: UV-Vis spectroscopy was used to determine the grafting density of DOPA-CHI using a DOPA-standard. This CHI derivative was previously characterized by ^{1}H-NMR and Fourier Transformed Infrared Spectroscopy (FTIR). Moreover, its pKa value was determined by potentiometric titration [14].

2. Fabrication of CHI DN hydrogels with enhanced mechanical behavior

2.1. CHI DN hydrogels of Chapter III

CHI DN hydrogels were synthesized by first dissolving medium molecular weight chitosan (MMW-CHI) in a 2% (v/v) acetic acid solution followed by its neutralization (pH 6.4) using a weak base, β-glycerophosphate (β-GP) to obtain a pH value close to the physiological one. The former solution was mixed with LMW-MACHI polymer and a photoinitiator (0.25% (w/v)). The photoinitiator used in this work was the 2-hydroxy-4′ -(2-hydroxyethoxy)-2-methylpropiophenone (I2959), which is a radical photoinitiator widely used

for the UV curing of unsaturated monomers and prepolymers. This compound cytocompatibility was previously proved (Figure 2.4) [15]. The total polymer concentration was set on 2% (w/v) corresponding to, under optimized conditions, a 1:1 ratio of LMW-MACHI/MMW-CHI polymer. This polymeric precursor solution was poured into polydimethylsiloxane (PDMS) molds in order to obtain cylindric-shaped samples with a diameter of 6 mm and height of 4 mm and, then, harden into a hydrogel by employing two different crosslinking processes. In a first step, the LMW-MACHI polymer was photocrosslinked through the reaction between its methacrylic groups upon UV-light exposure (365 nm, 11.4 mW/cm^2) in the presence of a photoinitiator. In the second step, the MMW-CHI polymer was ionically crosslinked by immersing the previous photocrosslinked hydrogel in a 2% (w/v) TPP aqueous solution to prepare the soft and ductile structure. Then, the hydrogels were rinsed in deionized water to remove any TPP ion excess.

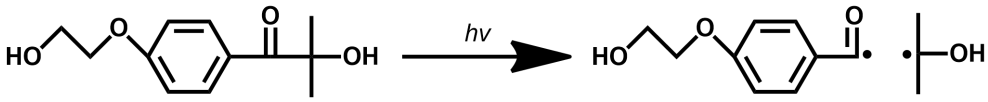

Figure 2.4 - Chemical structure of the I2959 photoinitiator.

2.2. CHI DN hydrogels of Chapter IV

A solution of MMW-CHI was prepared by dissolving 10 mg of purified MMW-CHI in 418.3 µL of 1% (v/v) acetic acid, which was further neutralized using a weak base, β-GP, to reach a pH near to the physiological one. Afterwards, the polymer total concentration was fixed at 10% (w/v) and MMW-CHI was mixed with DOPA-CHI in a mass ratio of 1:9. Once dissolved, different amounts of GP, 0.1% (w/v) or 0.5% (w/v) were added to the resultant solution in order to crosslink the primary backbone amines of CHI. The pH value of this polymeric precursor solution was adjusted to 7 by adding NaOH (1M). The precursor solution was transferred into a PDMS mold with a diameter of 5 mm and height of 4 mm. Afterwards, Fe^{3+} ions (0.1 M) were

added to each well to achieve a Fe^{3+}:catechol ratio of 1:3 followed by their properly mixing to ensure the hydrogel homogeneity.

3. Characterization of the designed CHI DN hydrogels

3.1. Mechanical characterization

The mechanical characterization was carried out on the basis of compression tests employing a Universal Mechanical Testing Machine equipped with a load cell of 1 kN. To this end, both uniaxial and cyclic compression assays were conducted on as-prepared cylindrical hydrogels specimens at RT. The sample was set on the lower plate and compressed by moving the upper plate at a compression rate of 1 mm per min. It is noted that a pre-load was applied to ensure the correct contact between the hydrogel and the equipment plates.

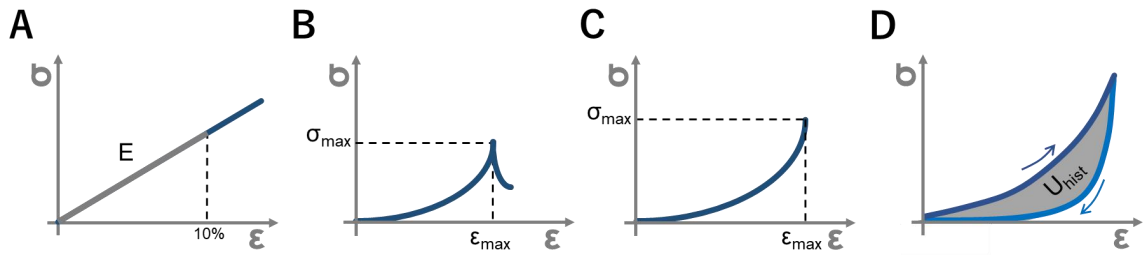

Figure 2.5 - Determination of the compressive modulus, E, **(A)**; fracture stress, σ max, and strain, ε max, corresponding to either the stress or strain point at which the hydrogel broke **(B)**, or the maximum stress/strain value reached **(C)**, respectively; and the energy dissipated during a loading-unloading cycle, U_{hist}, **(D)** from the stress-strain curves.

The nominal stress was obtained by dividing the compressive load by the initial (uncompressed) area of the specimen. From the obtained stress-strain curves, several parameters were determined including: (i) compressive modulus (E – Figure 2.5A), which corresponds to the average slope of the stress-strain curve in the initial linear region from 0 to 10% of strain; (ii) fracture stress (σ max) and strain (ε max), which can be either the stress or

strain point at which the hydrogel broke (Figure 2.5B), or the maximum stress/strain value reached since some of the developed hydrogels did not fracture for a strain lower than 90% (Figure 2.5C); (iii) hysteresis or energy dissipated during a loading-unloading cycle (U_{hist}; Figure 2.5D), which was estimated from the area between the loading and unloading curves up to a strain $x\%$ according to the equation 1.

$$U_{hist} = \int_{0\%}^{x\%} \sigma_{loading} d\mathcal{E} - \int_{0\%}^{x\%} \sigma_{unloading} d\mathcal{E} \quad (1)$$

3.2. Probing the self-healing behavior

Autonomous self-healing is defined as the ability of material to automatically heal from a damage, meaning that its broken parts can be brought into contact to restore its initial shape [16]. For the CHI DN hydrogels developed in Chapter IV, its self-healing ability was evaluated.

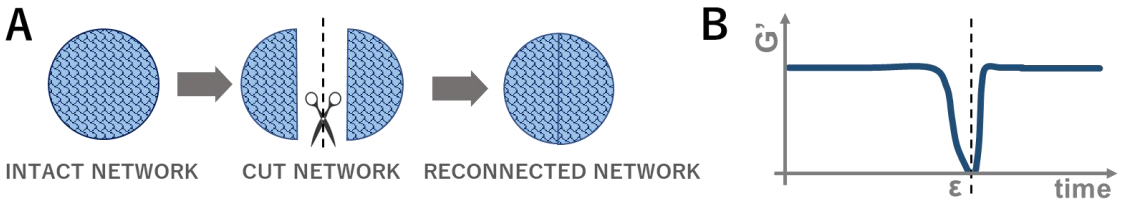

Figure 2.6 - Testing for autonomous self-healing ability of hydrogels by qualitative **(A)** and quantitative methods **(B)**.

To qualitatively assess this property, each hydrogel was macroscopically broken in half and after that the two pieces were placed together (Figure 2.6A). The hydrogel's self-healing ability was inspected by visually noting changes occurring at the interface [17]. Additionally, it was performed a dynamic oscillatory rheology assay using a parallel plate geometry. This assay allowed to quantify the hydrogel ability to recover from internal damage and the subsequent restoration of the mechanical viscoelastic properties at 37 °C (Figure 2.6B). Briefly, each gel was strained from 0.1% to 500% at a frequency of 1 Hz until fracture. Once the high strain was

removed, the recovery was verified by monitoring the storage modulus (G'; represents the elastic response of the material) as a function of time at 1 Hz and a strain rate of 1%. This time-course experiment can be used to reveal the lifetime of the reversible interactions [18].

3.3. Morphology evaluation of the CHI DN hydrogels

DN hydrogels were analyzed in terms of their morphology and elemental chemical composition resorting to a Scanning Electron Microscope (SEM) and an Energy-Dispersive X-Ray Spectroscopy (EDS), respectively. Briefly, hydrogel samples were first dehydrated by immersing them in solutions with an increased concentration of absolute ethanol, namely 20, 40, 60, 70, 80, 90, 95 and 100% and, then, dried using supercritical carbon dioxide dryer. To this end, the samples were loaded in a high-pressure vessel heated at 37 °C and pressurized to 80 bar. In order to ensure the complete removal of the solvent, a carbon dioxide stream was passed through the vessel at constant rate for 1 h. To prepare the samples for SEM analysis, the CHI DN hydrogels were fractured in liquid nitrogen to reveal the cross-sectional surface followed by their sputter-coating with gold or platinum. The images were acquired in high vacuum by tracking the signal of secondary electrons, and employing an accelerating voltage of 10 kV and a working distance of 10 mm. On the other side, the EDS profile was obtained from non-coated samples after drawing a line in the middle section of the CHI DN hydrogel.

3.4. Water content and uptake by the CHI DN hydrogels

Water uptake studies were performed on as-prepared cylindrical hydrogels. The samples were first weighed (m_i) and, then, immersed in distilled water (pH = 6.9) at 37°C. At predefined time points, the hydrogels were removed from water, blotted with tissue paper to remove the excess of water, and weighed again (m_f). The swelling percentage (S) was calculated according to the following equation (2):

$$S(\%) = \frac{m_f - m_i}{m_i} \times 100 \quad (2)$$

Moreover, the amount of water contained in the as-prepared CHI DN hydrogels was assessed using the equation (3):

$$Water\ content\ (\%) = \frac{m_i - md}{mi} \times 100 \quad (3)$$

,in which the (m_i) weight corresponds to the initial as-prepared weight of the hydrogel and (m_d) to the dry sample weight, which was obtained by freeze-drying the sample until a constant weight was reached.

4. *In vitro* biological performance analysis of the CHI DN hydrogels

The *in vitro* evaluation of the cellular response upon contact with biomaterials is the first step to estimate the potential of developed materials for biomedical purposes. In Chapter III and IV, cells were either encapsulated inside the produced CHI DN hydrogels or seeded on the material's surface, respectively.

4.1. Cells lines

In Chapter III, fibroblasts from an immortalized mouse lung fibroblast cell line (L929, European Collection of Cell Cultures) were routinely cultured in 150 cm^2 tissue culture flasks using a complete α-MEM medium supplemented with 3.7 gL^{-1} sodium bicarbonate, 10% FBS and 1% penicillin-streptomycin (pH 7.4) at 37 °C in a humidified air atmosphere of 5% CO_2. The culture medium was exchanged every 3 days. Upon reaching 90% of confluence, the culture medium was replaced by freshly prepared phosphate buffer saline (PBS) and cells were chemically detached from the tissue culture flasks using 0.05% Tryple Express solution for 5 min at 37°C in a humidified air atmosphere of 5% CO_2. To inactivate the Tryple Express effect, fresh medium was added and the cells were centrifuged at 1200 rpm for 5 min. Afterwards, the medium was decanted followed by the cells re-suspension in the optimized polymeric

precursor solution (this solution was prepared by mixing LMW-MACHI with MMW-CHI in ratio of 1:1 - final polymer concentration of 2% (w/v) -, 0.25% w/v I2959 and β-GF enough to neutralize the acetic acid needed to dissolve the MMW-CHI and set the pH to 6.4) at density of 1×10^6 cells per mL of this polymer solution. CHI DN hydrogels with cells-enclosed were, then, produced using the method previously described in Section 2.1 of Chapter II and placed in 24-well tissue culture plates at 37°C with a humidified air atmosphere of 5% CO_2.

In Chapter IV, chondrocytes from a mouse teratocarcinoma cell line (ATDC5, European Collection of Cell Cultures) were grown in 150 cm^2 tissue culture flasks using a Dulbecco's Modified Eagle's Medium (DMEM) F-12 medium supplemented with 10% FBS, 3.7 gL^{-1} sodium bicarbonate and 1% penicillin-streptomycin (pH 7.4) at 37 °C in a humidified air atmosphere of 5% CO_2. The culture medium was exchanged every 3 days. ATDC5 cell line is a well characterized chondrogenic cell line, being considered an excellent model to investigate molecular mechanisms of chondrogenesis *in vitro* [19]. Upon reaching 90% of confluence, the culture medium was removed and replaced by fresh-prepared PBS. Afterwards, cells were chemically detached from the tissue culture flasks using a 0.05% Tryple Express solution for 8 min at 37 °C in a humidified air atmosphere of 5% CO_2. After that, fresh medium was added, and the cells were centrifuged at 1200 rpm for 5 min. Then, the medium was decanted followed by the cells re-suspension in culture medium at cell density of 1×10^6 cells/mL. One day earlier, DN hydrogels (0.5% (w/v) of GP) were prepared in cylindrical PDMS molds following the previously described protocol in Section 2.2 of Chapter II. The obtained hydrogels were placed into non-treated and sterile 6-well plates and, then, 100 µL of the previous cell suspension was pipetted above the hydrogel samples.

4.2. Live/Dead assay

This assay is typically performed to evaluate the cell viability and uses two dyes, calcein-AM (membrane permeant dye), which is hydrolyzed into calcein (green fluorescent dye) by

estereases on viable cells, and propidium iodide (PI, red fluorescent dye), which in turn binds to DNA of only disrupted cells due to its membrane impermeant character. Therefore, the viable cells appear stained in green whereas the disrupted cells are labeled in red. After 24h, the culture medium was replaced by 1 mL of fresh-prepared culture medium containing 2 µL of calcein-AM and 1 µL of PI and the samples were incubated at 37°C for 10 min protected from light. To remove excess of dye, the samples were washed three times with PBS and immediately after visualized using a fluorescence microscope. The cell viability rate was determined by the ratio between the number of living cells and the total number of cells in the microscopy images.

4.3. MTS assays

MTS colorimetric assay was performed to quantify the cell metabolic activity [20] and is based on the bioreduction of 3-(4,5-dimethylthiazol-2-yl)-5-(3-carboxymethoxyphenyl)-2-(4-sulphofenyl)-2H-tetrazolium (MTS) compound in brown formazan products, directly soluble in cell culture medium, by mitochondrial dehydrogenase enzymes present in viable cells. To implement this methodology, the hydrogels were transferred to new wells and rinsed once with PBS. Serum and phenol red-free cell culture medium was mixed with MTS salt in a medium/reagent ratio of 5:1 and the resultant mixture was added to each well. Each condition was tested in triplicates. Furthermore, negative (well with seeded cells and no material added) and positive (latex rubber) controls were prepared. The plate was protected from light since the MTS reagent is light-sensitive. After this, the plate was incubated at 37 °C, during 3h in a humidified 5% CO_2 atmosphere. In the end of the incubation time, 100 µl of the resultant solution in each well were transferred to a new 96-well plate and the absorbance was recorded in the spectrophotometer at 490 nm [21].

5. Additional techniques employed to characterize the CHI DN hydrogels

Other procedures were followed to evaluate several issues that required clarification in the course of the experiments. Although they will be discussed in more detail in Chapter III and IV, some examples are presented below:

1. Zeta potential was used to measure the charge density of the main components involved on CHI DN hydrogel fabrication process. This parameter is extremely important to predict the ability of CHI to interact with TPP ions via electrostatic interactions;

2. Images were acquired using a stereomicroscope to figure out the time needed for the TPP ions to diffuse into the center of CHI hydrogels. Taking advantage of the loss of hydrogel transparency as result of the formation of ionic crosslinks;

3. Swelling assays were also performed using other solvents rather than water, namely PBS and culture medium (α-MEM, pH = 7.4) and 0.01 M PBS (pH = 7.4) at 37°C to better simulate the physiological conditions;

4. Fourier Transformed Infrared Spectroscopy (FTIR) was selected to characterize the chemical structure of the CHI DN hydrogels prepared in Chapter IV and to prove the successful GP-mediated crosslinking;

5. It was explored the possibility of using the CHI DN hydrogels described in Chapter IV as an injectable system and, hence, avoiding the drawbacks of highly invasive implantation techniques.

References

[1] A. S. Hoffman, Hydrogels for biomedical applications. *Adv. Drug Deliv. Rev.* **2012**, 64, 18–23.
[2] Y. S. Zhang, A. Khademhosseini, Advances in engineering hydrogels. *Science* **2017**, 356.
[3] A. M. S. Costa, J. F. Mano, Extremely strong and tough hydrogels as prospective candidates for tissue repair -A review, *Eur. Polym. J.* **2015**, 72, 344-364.
[4] J. P. Gong et al, Double-network hydrogels with extremely high mechanical strength, *Adv. Mater.* **2003**, 15 (14), 1155–1158.

[5] J. F. Mano et al, Natural origin biodegradable systems in tissue engineering and regenerative medicine: present status and some moving trends, *J. R. Soc. Interface* **2007**, 4 (17), 999–1030.
[6] M. N. V. Ravi Kumar, A review of chitin and chitosan application, *React. Funct. Polym.* **2000**, 46, 1–27.
[7] M. Rinaudo, Chitin and chitosan: Properties and applications, *Prog. Polym. Sci.* **2006**, 31, 603-632.
[8] Dash M., Chiellini F., Ottenbrite R. M., and Chiellini E., Chitosan—A versatile semi-synthetic polymer in biomedical applications, *Prog. Polym. Sci.* **2011**, 36, 981-1014.
[9] Mi F. L., Shyu S. S., Wong T. B., Jang S.-F., Lee S.-T. and Lu K.-T., Chitosan-polyelectrolyte complexation for the preparation of gel beads and controlled release of anticancer drug. II. Effect of pH-dependent ionic crosslinking or interpolymer complex using tripolyphosphate or polyphosphate as reagent, *J. Appl. Polym. Sci.* **1999**, 74, 1093–107.
[10] Butler MF, Ng Y-F, Pudney PDA. Mechanism and kinetics of the crosslinking reaction between biopolymers containing primary amine groups and genipin. *J. Polym. Sci. part A* **2003**, 41, 3941-53.
[11] Manickam B, Sreedharan R, Elumalai M. 'Genipin' - the natural water soluble cross-linking agent and its importance in the modified drug delivery systems: an overview. *Curr Drug Deliv.* **2014**, 11, 139-45.
[12] Signini R., and Campana Filho S. P., On the preparation and characterization of chitosan hydrochloride, *Polymer Bulletin* **1999**, 42, 159-166.
[13] L. M. Y. Yu, K. Kazazian, M. S. Shoichet, Peptide surface modification of methacrylamide chitosan for neural tissue engineering applications, *J. Biomed. Mater. Res., part A* **2007**, 82A, 243-255.
[14] M. Krogsgaard, M. R. Hansen, H. Birkedal, Metals & polymers in the mix: fine-tuning the mechanical properties & color of self-healing mussel-inspired hydrogels, *J. Mater. Chem. B* **2014**, 2, 8292.
[15] Stephanie J. Bryant, Charles R. Nuttelman, Kristi S. Anseth, Cytocompatibility of UV and visible light photoinitiating systems on cultured NIH/3T3 fibroblasts in vitro, *J. Biomater. Appl.* **2000**, 439.
[16] M. D. Hager, P. Greil, C. Leyens, S. van der Zwaag, U. S. Schubert, Self-healing materials, *Adv. Mater.* **2010**, 22, 5424.
[17] C. C. Deng, W. L. A. Brooks, K. A. Abboud, B. S. Sumerlin, Boronic Acid-Based Hydrogels Undergo Self-Healing at Neutral and Acidic pH, *ACS Macro Lett.* **2015**, 4, 220.
[18] Y.-G. Jia, X. X. Zhu, Self-Healing Supramolecular Hydrogel Made of Polymers Bearing Cholic Acid and β-Cyclodextrin Pendants, *Chem. Mater.* **2015**, 27, 387.
[19] Y. Yao, Y. Wang, ATDC5: an excellent in vitro model cell line for skeletal development, *J. Cell. Biochem.* **2013**, 114, 1223.

[20] T. L. Riss, R. A. Moravec, A. L. Niles, S. Duellman, H. A. Benink, T. J. Worzella, L. Minor, Cell Viability Assays, Assay Guid. Man. **2004**.
[21] A. J. Salgado, O. P. Coutinho, R. L. Reis, Novel starch-based scaffolds for bone tissue engineering: cytotoxicity, cell culture, and protein expression, *Tissue Eng.* **2004**, 10, 465-474.

Chapter III: Results & Discussion

Highly robust hydrogels via a fast, simple and cytocompatible dual crosslinking-based process[2]

ABSTRACT

A highly robust hydrogel device made from a single biopolymer formulation is reported. Owing to the presence of covalent and non-covalent crosslinks, these engineered systems were able to (i) sustain a compressive strength of *ca.* 20 MPa, (ii) quickly recover upon unloading, and (iii) encapsulate cells with high viability rates. Such multifunctional devices could potentially be used for the repair of load-bearing soft tissues or as an encapsulation platform for a variety of biological applications, such as disease modeling for drug screening and therapies in a more realistic mechanical environment.

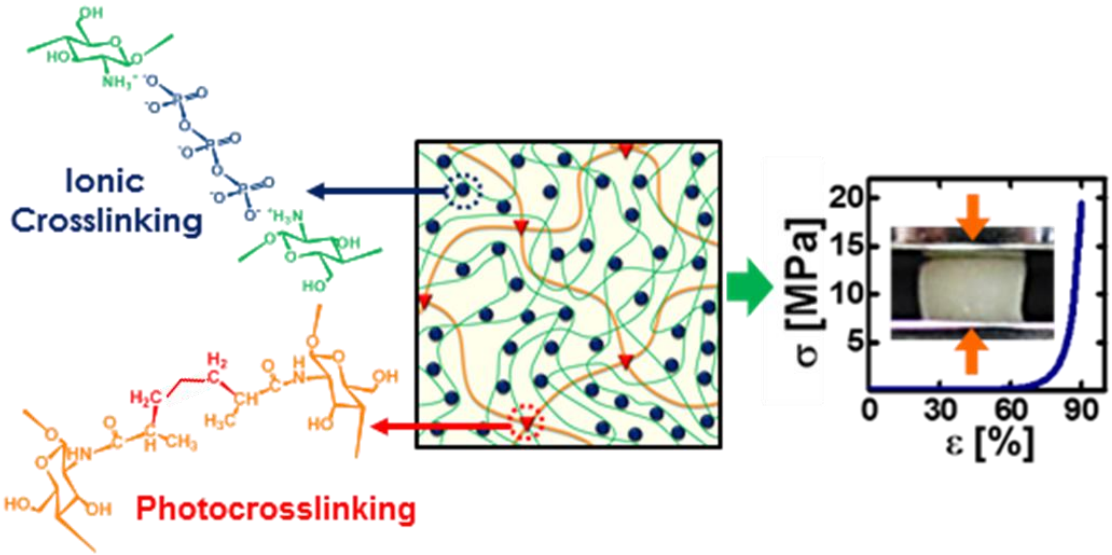

[2] Based on the publication: Ana M. S. Costa, João F. Mano, Highly robust hydrogels via a fast, simple and cytocompatible dual crosslinking-based process, *Chemical Communications* **2015**, 51 (86), pp. 15673-15676.

1. Introduction

Hydrogels, as highly hydrated 3D polymeric networks, have been widely used for many medical applications including scaffolds for tissue engineering [1], carriers for drug delivery [2] and sensors for biomedical purposes [3]. Generally, swollen hydrogels are soft and compatible with the majority of living tissues, highlighting their potential use as analogues of the native extracellular matrix (ECM). [1b,4] However, their high-water content along with intrinsic structural inhomogeneity and lack of efficient energy dissipation mechanisms often yields hydrogels with a poor mechanical performance. [5] Recognizing the aforementioned drawback, several researchers have been focusing their work on the design of innovative and distinctive hydrogel with exceptional mechanical properties [6], as the case of the double-network (DN) methodology, which is quickly becoming an essential tool in materials science field [7]. Beneath their outstanding mechanical behavior is the specific combination of two crosslinked networks with contrasting properties, namely, a highly crosslinked brittle matrix and a loosely crosslinked ductile network. While the brittle network contributes to an increase in the elastic modulus, the ductile structure is responsible for the increase in strain [7b]. In fact, under optimized conditions, most of the DN gels have water contents higher than 90 wt% and are stiff, with an elastic modulus of 0.1–1.0 MPa, strong, as proved by a failure compressive stress of 20–60 MPa, and tough, possessing a tearing fracture energy of 100–4400 J m^{-2} [7b,8]. This excellent mechanical performance is comparable to and even exceeds some soft load-bearing tissues. For instance, cartilage typically exhibits a compressive strength of *ca.* 35.7 MPa, while the tendon possesses a tensile strength of *ca.* 23.65–78.52 MPa [10].

Traditionally, DN hydrogels are covalently crosslinked networks produced by a two-step sequential free radical polymerization process [7]. This methodology presents some drawbacks: (i) it is time-consuming, as it involves a swelling/diffusion step which can take several days; (ii) it has limited reproducibility, due to the difficulty of controlling the exact molar ratio of both structures; (iii) it yields hydrogels with low recoverability, as its high toughness depends on the

irreversible damage of the brittle network; and (iv) it requires harsh processing conditions, hampering their use as cell-laden devices [7a,8c,11].

The ECM of load-bearing soft tissues is characterized by a well-defined and complex hierarchical architecture which is responsible for its high mechanical strength [12]. One example of such structures is the one of the tendons, which is composed of 3D assemblies of fibrillar structures with different levels of organization. Remarkably, despite this complex organization, tendon is mainly composed of a single material [13].

Inspired by the native ECM of living tissues, we demonstrate the possibility to fabricate strong chitosan (CHI) hydrogels from a single polymeric precursor formulation and under physiological conditions. CHI is of particular interest for biomedical purposes as it exhibits a plethora of desirable physicochemical and biological properties including biocompatibility, biodegradability, adhesiveness and versatility in both modification and fabrication [14]. These systems were produced through a DN-based methodology combining chemical and physical crosslinking mechanisms. Contrary to chemical crosslinks, physical crosslinks are able to reversibly associate/dissociate in response to an applied load, resulting in hydrogels with high toughness as well as with the ability to recover their mechanical properties upon bond reformation [15,16]. Although this combination of strong and weak crosslinks was already applied in other hydrogel devices [15,11a,11e,17], this is the first time that both polymer networks are composed of the same macromolecule, in this case CHI, differing only on the molecular weight and the crosslinking mechanism employed. Additionally, with the present technology, both polymer components are mixed together in a single hydrogel precursor solution, which solves the aforementioned drawbacks of the current DN strategies with the additional advantage of enabling cell encapsulation with high viability rates.

2. Materials & Methods

2.1 Materials

Medium molecular weight chitosan (MMW-CHI, 200-800 cP), methacrylic anhydride (MA, ≥92%), sodium tripolyphosphate (TPP, 85%), β-glycerolphosphate disodium salt hydrate BioUltra (β-GF, ≥ 99.0%), 2-hydroxy-4'-(2-hydroxyethoxy)-2-methylpropiophenone (I2959, 98%), dialysis tubing cellulose membrane (MWCO 14,000) and phosphate buffer saline (PBS) were from Sigma-Aldrich (U.S.A.). Low molecular weight chitosan 95/20 (LMW-CHI, 16-30 mPa.s) was from Heppe Medical Chitosan GmbH (Germany). Acetic acid (Glacial) and sodium bicarbonate were supplied from VWR (Belgium). Deuterium oxide (D_2O) was purchased from Laborspirit (Portugal). TrypLE Express, fetal bovine serum (FBS), penicillin/streptomycin solution, calcein-AM, propidium iodide (PI) and complete α-MEM culture medium were from Alfagene (Portugal). All materials were used as received. Unless otherwise stated, water purified in an 18 MΩ cm MilliQ Plus water system was used throughout.

2.2. Low molecular weight-methacrylamide chitosan (LMW-MACHI) polymer synthesis and characterization

LMW-CHI was modified into its photocrosslinkable derivative, LMW-MACHI, by incorporating methacrylic groups on its backbone [18]. Briefly, LMW-CHI (3% (w/v)) was dissolved in 2% (v/v) acetic acid overnight at RT with constant stirring. Once dissolved, MA (at 1 molar equivalents per chitosan repeat unit) was added dropwise and left in incubation for 5h at RT in dark. The mixture was, then, dialyzed against distilled water for 5 days, changing the water twice a day. Finally, the LMW-MACHI solution was freeze-dried and stored at -20 ºC until use. ^{1}H–Nuclear Magnetic Resonance (^{1}H-NMR, Bruker Avance III, 300 MHz) was used to infer about the correct LMW-CHI methacrylation and to estimate both the substitution (SD) and crosslinking (CD) degrees. To this end, 20 mg of LMW-MACHI were dissolved in 1 mL of

deuterium oxide containing 0.25 w/v % I2959 and placed inside a 5 mm diameter NMR test tube (Sigma-Aldrich). On the one hand, the SD was determined by the ratio between the average value of the area of the peaks at 5.7 and 5.4 ppm [19], and the area at 3.0 ppm (H2 (GluN, glucosamine)) [20]. On the other side, to determine the CD degree, the LMW-MACHI solution was dispensed inside NMR tubes and, then, photocrosslinked using UV-light (365 nm, 11.4 mW/cm^2) for different exposition times ranging from 30 to 900 s. As a result of the UV-light exposure, the photoinitiator (I2959) forms free radicals needed, which initiate the polymerization process between the pendant vinyl groups of the LMW-MACHI. As the reaction proceeds, these vinyl groups are consumed. Accordingly, the crosslinking degree was determined as the decrease in the area under the curve of the peaks corresponding to the two protons adjacent to C=C double bond (located at 5.7 and 5.4 ppm) relative to the H2 peak at 3 ppm (GluN) [21]. Chemical shifts were expressed in ppm (δ units). Data was processed using the MestReNova software (MestreLab, Spain).

2.3. Production and characterization of CHI DN hydrogels

CHI DN hydrogels were synthesized by first dissolving MMW-CHI in a 2% (v/v) acetic acid solution followed by its neutralization (pH 6.4) using a weak base, β-GF. Afterwards, the former solution was mixed with LMW-MACHI polymer and a cytocompatible photoinitiator, I2959 (0.25% (w/v)). Different amounts of both CHI derivatives were tested to determine the optimal polymer ratio in terms of the resultant mechanical properties. The total polymer concentration was kept constant in 2% (w/v). The polymeric precursor solution was prepared and poured into cylindrical PDMS molds with a diameter of 6 mm and height of 4 mm and, then, harden into a hydrogel by employing two different crosslinking processes. In a first step, the LMW-MACHI polymer was photocrosslinked through the reaction between its methacrylic groups, which occurs upon UV-light exposure (365 nm, 11.4 mW/cm^2) in the presence of I2959. Various UV-light exposure times were tested in order to assess the minimum value which

allowed both high mechanical properties and cell encapsulation with high viability rates. In the second step, the MMW-CHI polymer was ionically crosslinked by immersing the photocrosslinked hydrogel in a 2% (w/v) TPP aqueous solution to prepare the soft and ductile structure. Then, the hydrogels were rinsed in deionized water to remove any TPP ion excess and ensure a homogeneous structure.

The mechanical characterization was carried out on the basis of compression tests employing a Universal Mechanical Testing Machine (INSTRON 5540) equipped with a load cell of 1 kN. To this end, both unidirectional and cyclic compression assays were performed at room temperature on as-prepared cylindrical hydrated hydrogels specimens with a diameter of 6 mm and height of 4 mm. Afterwards, the sample was set on the lower plate and compressed by moving the upper plate at a compression rate of 1 mm per min. It is noted that a pre-load of 0.1 N was applied to ensure the correct contact of hydrogel with the equipment plates. An exception was made for the LMW-MACHI and MMW-CHI single-network hydrogels were a pre-load of 0.01N was used instead. The nominal stress was obtained by dividing the compressive load by the initial (uncompressed) cross-sectional area of the specimen. From the obtained stress-strain curves, several parameters were determined including compressive modulus (*i.e.* the average slope of the stress-strain curve in the initial linear region from 0 to 10% strain), fracture stress and strain (*i.e.* the stress or strain point at which the hydrogel broke, or the maximum stress/strain value reached since some of the developed hydrogels did not fracture up to a strain of 90%) and energy dissipation (*i.e.* the area between the loading and unloading curves). All these tests allowed assessing the resulting mechanical properties of CHI DN hydrogels as well as to elect the optimal synthesis parameters.

2.4. Cells Encapsulation in the CHI DN hydrogels

Fibroblasts from an immortalized mouse lung fibroblast cell line (L929, European Collection of Cell Cultures) were grown in 150 cm^2 tissue culture flasks using a complete α-

MEM medium supplemented with 3.7 gL^{-1} sodium bicarbonate, 10% FBS and 1% penicillin-streptomycin (pH 7.4) at 37 ºC in a humidified air atmosphere of 5% CO_2. The culture medium was exchanged every 3 days.

Upon reaching 90% of confluence, culture medium was replaced by PBS and L929 cells were chemically detached from the tissue culture flasks using 0.05% Tryple Express solution for 5 min at 37ºC in a humidified air atmosphere of 5% CO_2. To inactivate the Tryple Express effect, fresh medium was added and the cells were centrifuged at 1200 rpm for 5 min. Afterwards, the medium was decanted followed by the cells re-suspension in the optimized polymeric precursor solution (this solution was prepared by mixing LMW-MACHI with MMW-CHI in ratio of 1:1 - final polymer concentration of 2% (w/v) -, 0.25% w/v I2959 and β-GF enough to neutralize the acetic acid needed to dissolve the MMW-CHI and set the pH to 6.4) at density of 1×10^6 cells per mL of this polymer solution. CHI DN hydrogels with cells-enclosed were, then, produced using the method previously described and placed in 24-well tissue culture plates at 37ºC with a humidified air atmosphere of 5% CO_2.

To evaluate the effect of the developed methodology to fabricate strong CHI DN hydrogels on the cell viability, the LIVE/DEAD assay was performed. Briefly, the culture medium was replaced by 1 mL of PBS containing 2 µL of calcein-AM and 1 µL of PI and the samples were incubated at 37ºC for 10 min. To remove excess of dye, the samples were washed three times with PBS and immediately after visualized using a confocal microscope (TCS SP8, Leica) with an excitation and emission wavelengths of 494 and 535 nm and 517 and 617 nm for calcein-AM and PI, respectively.

3. Results and Discussion

For the fabrication of strong DN hydrogels, two CHI derivatives, namely LMW-MACHI and MMW-CHI, were mixed with a photoinitiator (I2959) (SI.3; Section S3.1) and a weak base, β-glycerolphosphate. Afterwards, a dual-crosslinking process was performed by (1) UV-light

exposure of the methacrylic groups on LMW-MACHI, forming a covalently crosslinked network (Scheme 3.1c(i)) and (2) immersing the resultant hydrogel in a solution containing negatively-charged tripolyphosphate (TPP) ions to ionically crosslink MMW-CHI through their positively-charged amine groups (Scheme 3.1c(ii)). Both crosslinking times were kept in the minimum value which allowed the attaining of strong hydrogels without ultimately compromise cell viability (SI.3; Section S3.2 and S3.3). The resultant hydrogels had a homogeneous composition and morphology (SI.3; Section S3.4). It is worth noting that the described strategy is simple, relatively fast and occurs under physiological conditions.

Figure 3.1 displays the compressive mechanical behavior of the resultant hydrogels. LMW-MACHI single network broke into small fragments upon reaching a strain value of *ca.* 60%, as easily observed by comparing Fig. 3.1A and B. In contrast, the CHI DN hydrogels did not fracture after a strain of *ca.* 90% (Fig. 3.1C and D). In fact, under optimized conditions, CHI DN structures exhibited an outstanding compressive strength of *ca.* 19.481 MPa, which is several orders of magnitude higher than those of their precursors: 0.094 MPa and 0.100 MPa for LMW-MACHI and MMW-CHI, respectively (SI.3; Movies S3.1 and S3.2, and Fig. 3.1E). This synergistic effect on their mechanical properties highlights their DN-based character, contrary to interpenetrating networks (IPN), whose mechanical behavior results from the linear combination of their individual network properties [22]. To assess the influence of each crosslinked network on the overall mechanical properties of the CHI DN hydrogels, different amounts of each polymer were mixed together, keeping the total polymer amount fixed.

By observing Fig. 3.1F, it can be noted that hydrogels with lower amounts of MMW-CHI polymer, namely 0 and 25%, fractured at strains lower than 60%, however, for the same strain value, these same hydrogels exhibited higher strengths, compared to hydrogels with 50, 75 and 100% MMW-CHI contents, indicating that the LMW-MACHI network can significantly improve the mechanical strength of the CHI DN hydrogels. The initial compressive modulus and fracture stress of each hydrogel are summarized in Fig. 3.1G. Upon increasing the amount of

MMW-CHI from 25% to 50% of the total polymer mass, the strength increases drastically from *ca.* 0.1 MPa to *ca.* 19.5 MPa.

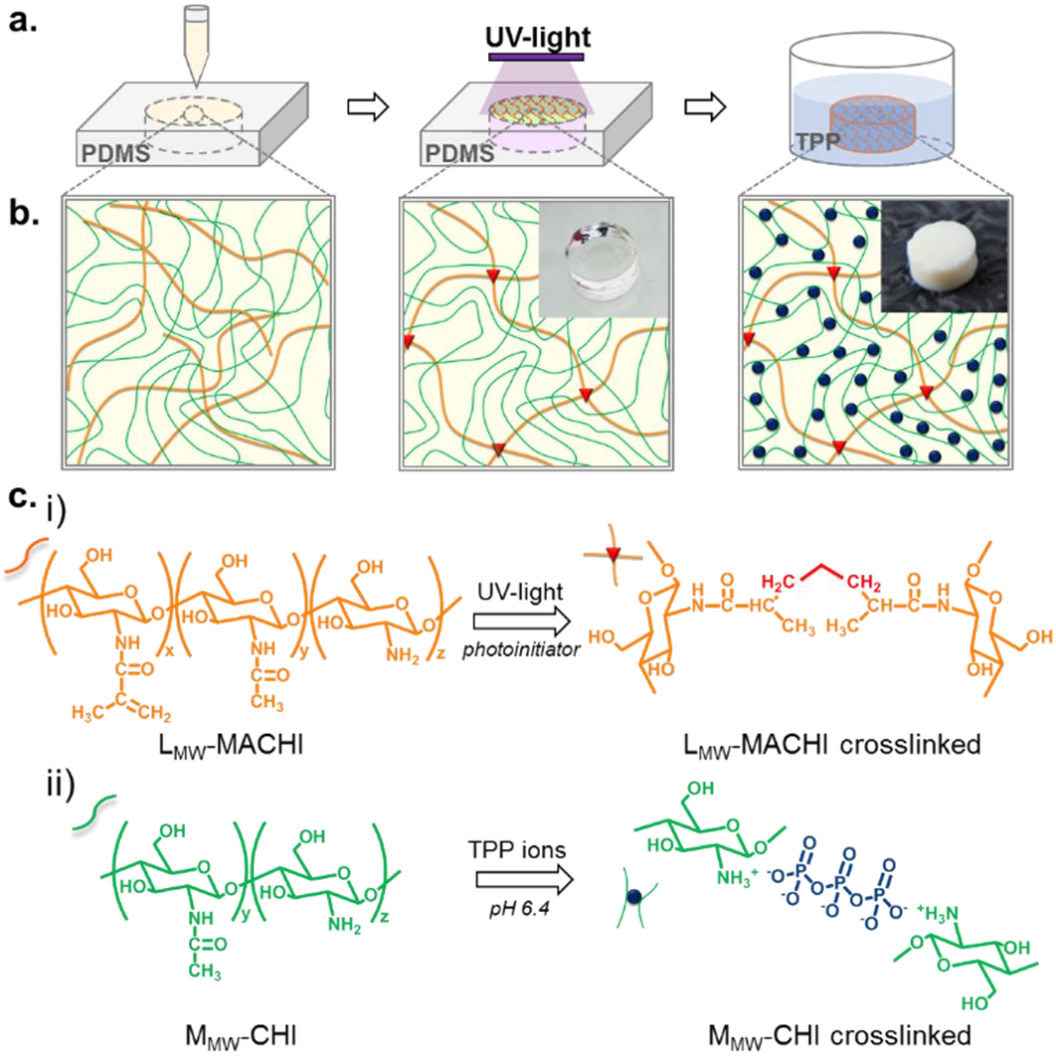

Scheme 3.1 - (a) CHI DN hydrogels fabrication process. First, the polymeric precursor solution containing both polymers (LMW-MACHI and MMW-CHI) is poured into a PDMS mold. Upon UV-light exposure, covalent crosslinks (red triangles) are formed between the methacrylic groups on the LMW-MACHI. Afterwards, the MMW-CHI polymer is ionically crosslinked through the action of TPP ions (blue circles). **(b)** Schematic representation of the hydrogel structure after each crosslinking step as well as their appearance. **(c)** Chemical structures of the LMW-MACHI (i) and MMW-CHI (ii) polymers as well as their respective crosslinked form.

On the other side, the elastic modulus decreased considerably from *ca.* 44.3 kPa to 4.7 kPa for an increase of the MMW-CHI from 50% to 75% of the total polymer mass. An optimal balance of the mechanical properties was obtained for the 1:1 ratio of both structures, yielding CHI DN hydrogels with an improved mechanical performance.

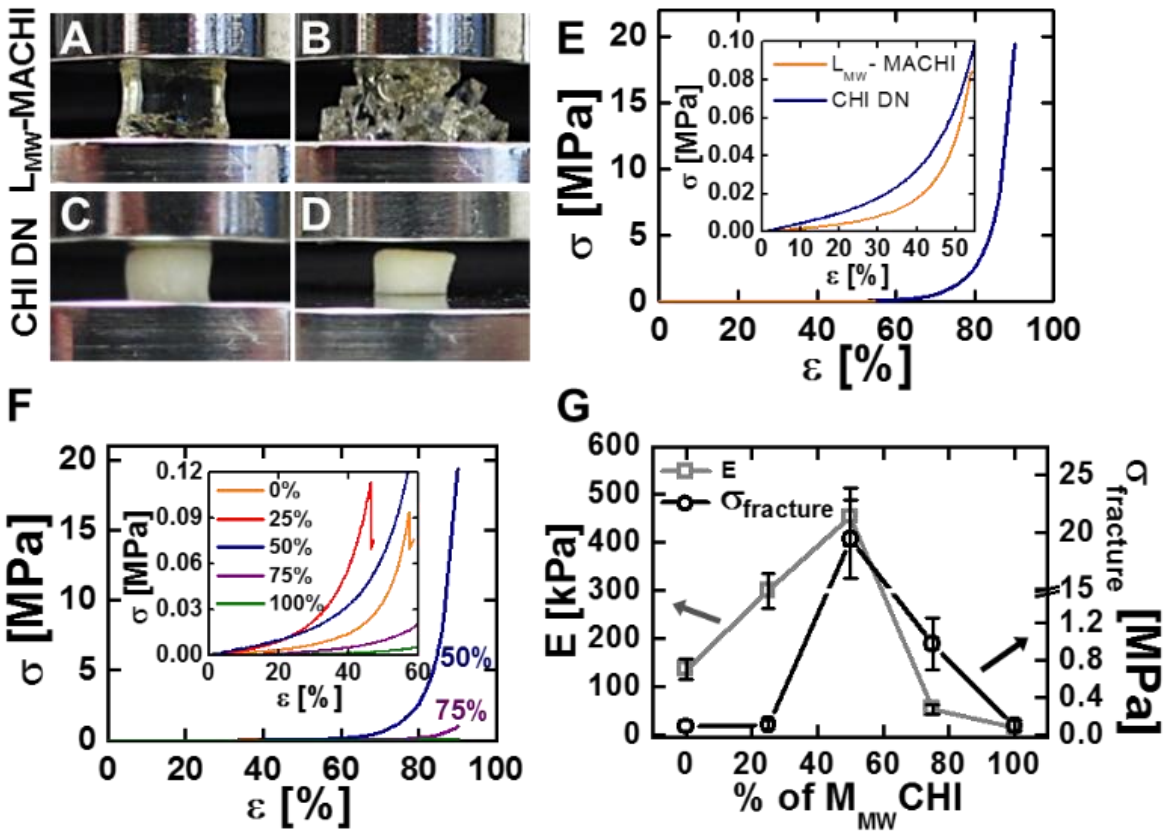

Figure 3.1 - Photographs showing the LMW-MACHI (**A** and **B**) and CHI DN (**C** and **D**) hydrogels before (**A** and **C**) and after (**B** and **D**) a ε = 90%, respectively. (**E**) Representative compressive stress–strain curve of LMW-MACHI and CHI DN hydrogels. (**F**) Compressive curves obtained by keeping the total polymer mass constant and changing the ratio of both structures. The percentage values are in relation to the MMW-CHI polymer. (**G**) Compressive modulus and fracture stress as a function of % of MMW-CHI in the hydrogel final structure.

Interestingly, these properties are even higher than other DN hydrogels composed of natural-origin polymers [11d,23]. Taking into account all of these results, it is suggested that the LMW-MACHI network is responsible for providing the hydrogel strength and the MMW-CHI

the high strain values, contributing to the simultaneous elastic and tough behavior of CHI DN hydrogels.

Moreover, the effective energy dissipation of the CHI DN hydrogel was proved by the presence of a pronounced hysteresis in the loading and unloading curves, being directly related to the toughness of the material (Fig. 3.2). Indeed, the energy dissipated during a first cycle of compression was much higher for the CHI DN hydrogels than for hydrogels of the two extreme compositions (*ca.* 10 times for LMW-MACHI and 55 times for MMW-CHI) for the same strain value (Fig. 3.2A and SI; Section S3.5). Then, CHI DN hydrogels were subjected to five successive compression cycles up to a maximum strain of 50%, as shown in Fig. 3.2B. The results suggest a decrease of the hysteresis and compressive strength values, being more pronounced from the first cycle to the second cycle since the curves of the subsequent cycles almost overlapped. In order to assess if the initial mechanical properties could be recovered, the samples were allowed to rest after a first compression cycle under mild conditions. Fig. 3.2C suggests different recovery rates depending on the time of recuperation. Nevertheless, these hydrogels were able to recover almost completely their initial mechanical properties if the second loading is delayed by 2 hours (Fig. 3.2D), which is of outmost importance for repairing structural soft tissues that are continuously subjected to stresses. Based on previous studies [11a,11e,17b,24], the high level of hysteresis with low permanent deformation is possibly the result of combining strong and weak crosslinks. In a single covalently or ionically crosslinked network, the polymer chains in direct contact with the applied load sustain it until one of the chains break or an ionic bond is disrupted, respectively. Afterwards, the crack is able to run throughout the hydrogel, resulting in low toughness as the fracture occurs in a localized injured area. Contrarily, in DN hydrogels containing strong and weak crosslinks, the damage zone is much larger, allowing for the accumulation of more damage before the macroscopic crack propagation. In this case, the weak ionic bonds are first disrupted and, as the stress increases, the neighbor ionic bonds are also dissociated in order to cooperatively

sustain the load. Consequently, the spread of the stress and the damage zones are larger. In short, the LMW-MACHI is responsible for preserving the initial hydrogel shape once the ionic crosslinks are broken, while the MMW-CHI dissipates the energy over a wider region and protects the LMW-MACHI structure from fracturing. If the load is released, the MMW-CHI hydrogel structure is able to recover through bond reformation, explaining the low permanent deformation. Although CHI polymer was already used to produce other strong hydrogels devices [25], these mechanical properties were never observed in hydrogels only made of the same macromolecule.

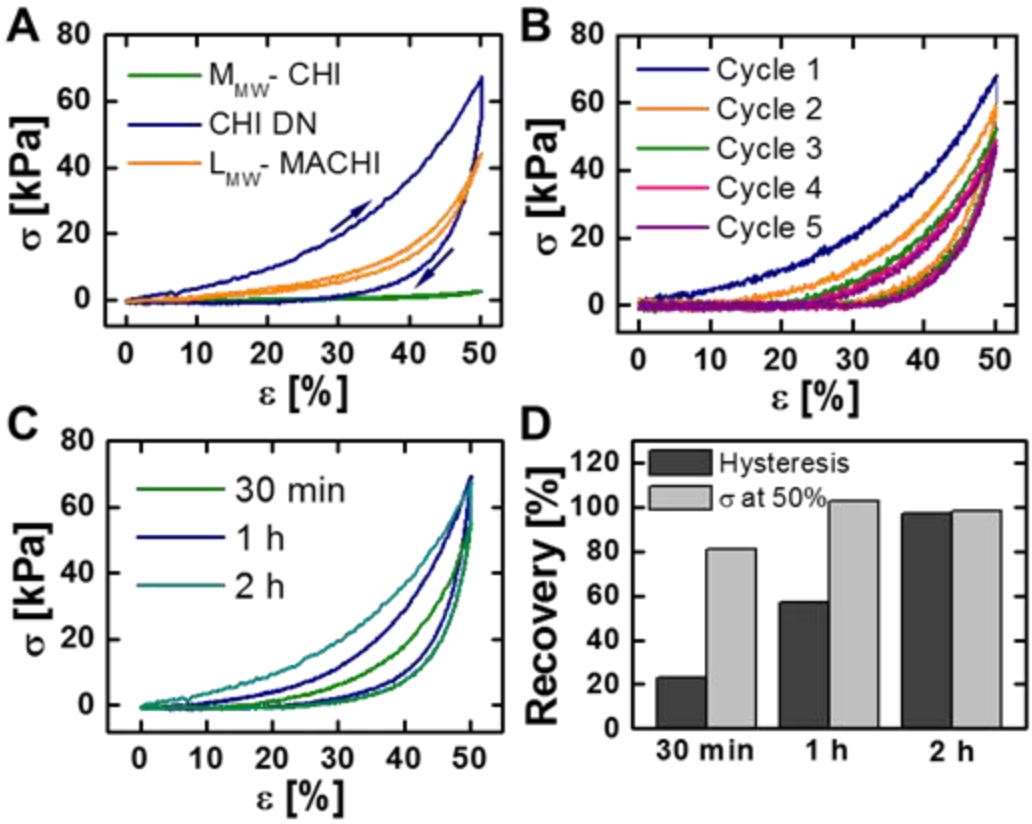

Figure 3.2 - (A) Representative load/unload compressive stress–strain curves of CHI DN, LMW-MACHI and MMW-CHI hydrogels up to ε = 50%. **(B)** Five successive loading/unloading cycles of CHI DN hydrogels. **(C)** 2nd loading cycle after the CHI DN sample rested for 30 min, 1 h and 2 h after a 1st compression cycle. **(D)** Recovery rate [%] of CHI DN hydrogels in function of the time of recuperation at RT.

Moreover, two other interesting features about these hydrogels were also observed. First, contrary to conventional DN hydrogels, these networks showed a de-swelling effect in water, PBS and culture medium (SI.3; Section S3.6). This behavior was already observed in other systems [26], being ascribed to the release of water from the hydrogel structure either due to the presence of (1) hydrophobic methacrylic groups on LMW-MACHI or (2) higher ion concentration in the enclosing medium. This property is relevant as swelling severely weakens the hydrogels, compromising their behavior *in vivo*. [25,27] Second, it was found that to create hydrogels with improved mechanical properties, it is necessary to combine two polymeric networks with distinct features, in this case different molecular weights, and use two different crosslinking processes. This fact was proved since the production of strong hydrogels was prevented by employing both crosslinking processes on the LMW-MACHI network (SI.3; Section S3.7).

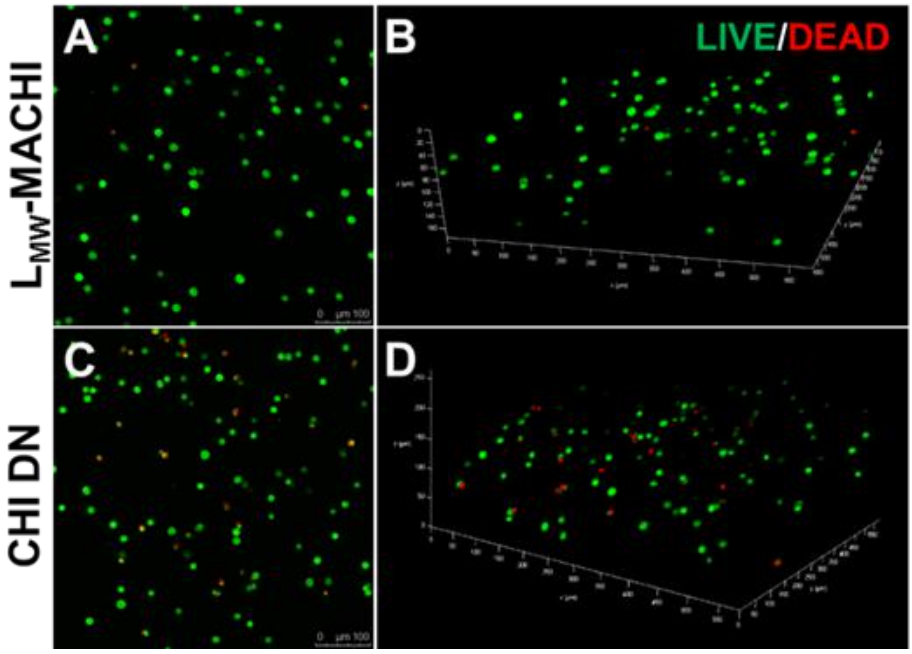

Figure 3.3 - 2D and 3D LIVE/DEAD confocal images of L929 cells encapsulated within LMW-MACHI (**A** and **B**) and on CHI DN hydrogels (**C** and **D**), respectively. Viable cells appear in green whereas dead cells are stained in red. Scale bar corresponds to 100 μm.

To further explore the biomedical or biological interest of the developed systems, L929 cells were mixed with the polymeric precursor solution to assess the ability of the hydrogels to efficiently encapsulate cells. Fig. 3.3 shows that cells were uniformly distributed within the CHI DN hydrogels, exhibiting high viability rates (*ca.* 80%) after 24 h of incubation under physiological conditions. These values are comparable with the ones obtained for the LMW-MACHI hydrogels (*ca.* 95%) and for other DN hydrogels [23a], proving the cytocompatible character of the developed strategy and emphasizing its potential to create cell-laden artificial substitutes of native soft-tissues.

4. Conclusion

This is the first report of single polysaccharide DN hydrogel with the ability to (i) withstand an impressive compressive stress in the same order of magnitude as the ones found in native load-bearing soft tissues, (ii) fast recover their mechanical properties upon unloading, and (iii) encapsulate cells with high viability rates. Such multifunctional devices could potentially be used for the repair of load-bearing soft tissues or as an encapsulation platform for a variety of biological applications, such as disease modeling for drug screening and therapies in a more realistic mechanical environment.

Acknowledgements

This work was funded by FCT through PhD grant SFRH/BD/101748/2014, the European Union's Seventh Framework Programme (FP7/2007-2013) under grant agreement no. REGPOT-CT2012-316331-POLARIS, by FEDER through the Competitive Factors Operation Program – COMPETE and by national funds through FCT in the scope of project PTDC/CTM-BIO/1814/2012.

Supplementary information (SI.3)

S3.1. I2959 photoinitiator structure and properties

The photoinitiator used in this work was the 2-hydroxy-4′ -(2-hydroxyethoxy)-2-methylpropiophenone (I2959), which is a radical photoinitiator widely used for the UV curing of unsaturated monomers and prepolymers (Figure S3.1). This compound cytocompatibility was already assessed in several publications [28].

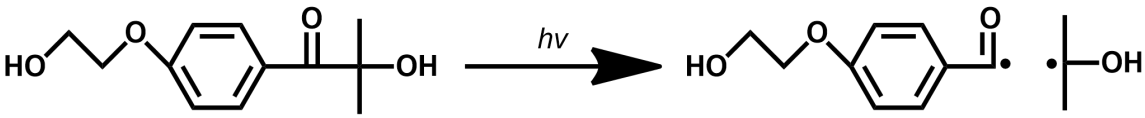

Figure S3.1 - Chemical structure of the I2959 photoinitiator.

S3.2. Optimization of the crosslinking mechanism of the LMW-MACHI network

LMW-CHI was successfully modified into its photocrosslinkable derivative, LMW-MACHI, through its reaction with MA. Figure S3.2A depicts ^{1}H-NMR spectra of LMW-MACHI polymer as a function of the UV-light exposure time using D_2O as a solvent. Two new chemical shifts appeared because of the chemical modification of LMW-CHI at 5.7 and 5.4 ppm corresponding to the protons of the double bond (C=C, Figure S3.2A Ha and Hb). The SD was calculated by dividing the average value of the area of the peaks at 5.7 and at 5.4 ppm by the area at 3.0 ppm (Figure S3.2A H2), which corresponds to the anomeric proton, and was found to be *ca.* 21%. These results confirm the successful incorporation of methacrylic groups into the LMW-CHI molecular backbone structure, which are needed for the photocrosslinking process.

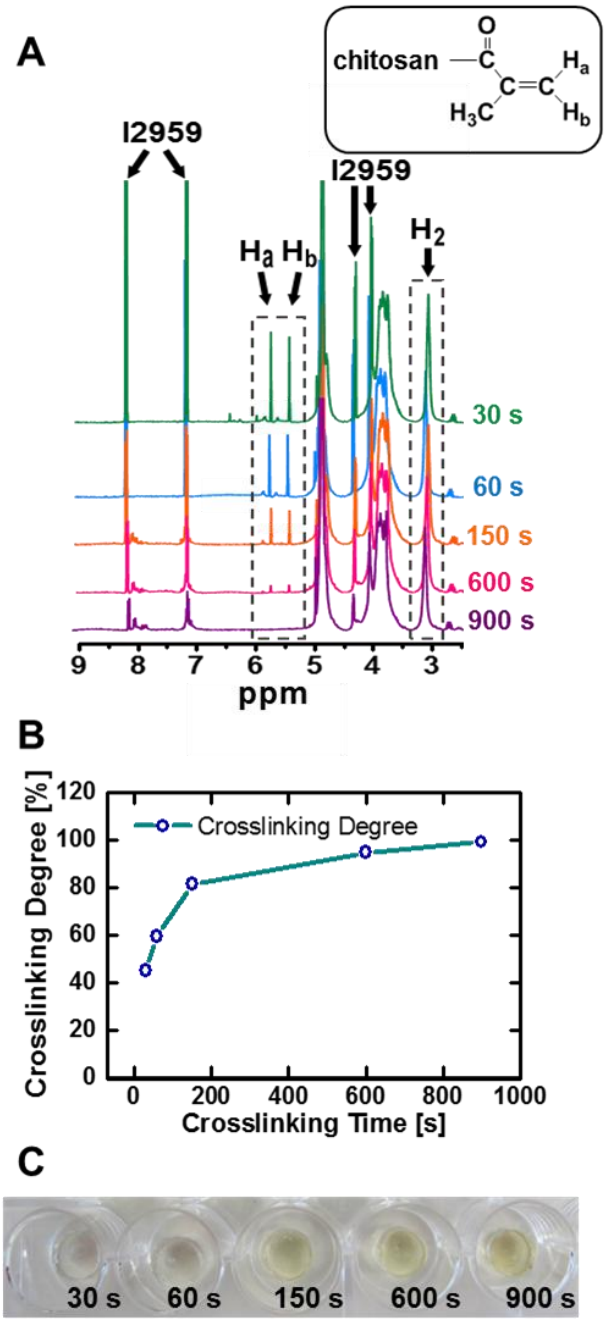

Figure S3.2 - (A) ^{1}H NMR spectra of LMW-MACHI after different crosslinking times. The box on top of the graphs shows the chemical structure of LMW-MACHI. **(B)** Variation of the crosslinking degree (defined as % of reacted methacrylic groups) as a function of the UV-light exposure time. **(C)** Visual inspection of the obtained hydrogels after different UV-light exposure times using an optical stereomicroscope (TR500, VWR, USA) equipped with a digital camera (G12 Olympus, Canon, Japan).

The NMR spectra were also used to infer about the CD of the LMW-MACHI using different UV-light exposure times. During the photocrosslinking process, the peaks at 5.4 and 5.7 are consumed as can be observed in Figure S3.2A. Therefore, the obtained CD was defined as % of reacted methacrylic groups and are summarized on Figure S3.2B. As expected, an increase on the CD was obtained with the increase on the UV-light irradiation time. Taking into account the aforementioned outcomes, a crosslinking time of 150 s was selected for further studies as after this value the crosslinking degree remained almost constant. Moreover, since the final purpose of this device is to encapsulate cells, shorter crosslinking times are of extreme importance to not compromise cell viability.

Freeze-dried LMW-MACHI polymer (0.2 g) was first dissolved in 10 mL of distilled water containing 0.25% (w/v) of I2959. Then, the previous solution was transferred into PDMS molds (diameter 6 mm and height 4 mm) to covalently crosslink LMW-MACHI polymer upon UV-light (365 nm, 11.4 mW/cm^2) exposure. Figure S3.2C displays the resultant hydrogels after different UV-light exposure times using an optical stereomicroscope.

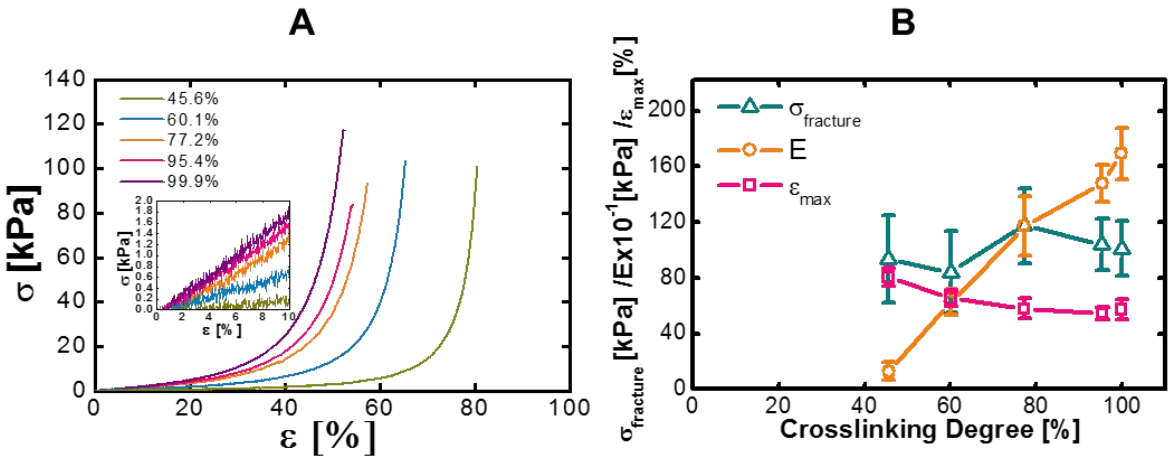

Figure S3.3 - (A) Representative compressive stress-strain curves of LMW-MACHI with different crosslinking degrees. The inset represents a zoom of the region used to determine the compressive modulus (E, from 0-10% of strain). **(B)** Variation of fracture stress (σ fracture), maximum strain (ε max) and E as a function of the crosslinking degree of LMW-CHI polymer.

The effect of the LMW-MACHI crosslinking density on the mechanical properties was assessed by varying the time of crosslinking from 30 s to 900 s. The nominal elastic modulus (E), fracture stress (σmax) and strain (εmax) were determined in compression using a Universal Mechanical Testing Equipment (Model 5543, INSTRON) equipped with BLUEHILL software. Figure S3.3A illustrates the increase of the E with the increase of the crosslinking time. On the other side, for higher crosslinking times the fracture strain is lower. Regarding the σmax, the results suggest that independently of the UV-light irradiation time the maximum stress sustained by the MACHII hydrogels was *ca.* 0.1 MPa (Figure S3.3B). These results corroborate with other photocrosslinked hydrogels from natural-origin polymers. [19b, 29]

S3.3. Optimization of the ionic crosslinking of the MMW-CHI network

MMW-CHI was dissolved in acetic acid (2% (v/v), pH = 4.0) followed by the addition of a weak base, β-GF, to achieve a pH equal to 6.4. The resultant solution was transferred to a dialysis membrane and placed into a TPP (2% (w/v)) aqueous solution, resulting in the formation of ionic crosslinks between the positively charged amine groups present on the MMW-CHI backbone and the negatively charged TPP ions. Afterwards, the dialysis membranes were sliced to yield cylindric-shaped hydrogels with a diameter of 6 mm and a height of 4 mm using a biopsy punch.

To figure out the time needed for the TPP ions to diffuse into the center of CHI hydrogels, optical images were periodically collected using an optical stereomicroscope (Figure S3.4A). As result of the formation of ionic crosslinks, the hydrogel structure loses its transparency as easily observed in Figure S3.4B. These results suggest that after 60 min the TPP ions reach the center of the hydrogel as proved by a homogeneous structure (Figure S3.4B) and the increase on the overall amount of phosphorus in hydrogel network (Figure S3.4C). The presence of phosphorus in the initial structure (time of 0 min) can be explained by the presence of β-GF in

the polymer precursor solution. This increase on the amount of phosphorus is easily seen on Figure S3.4D.

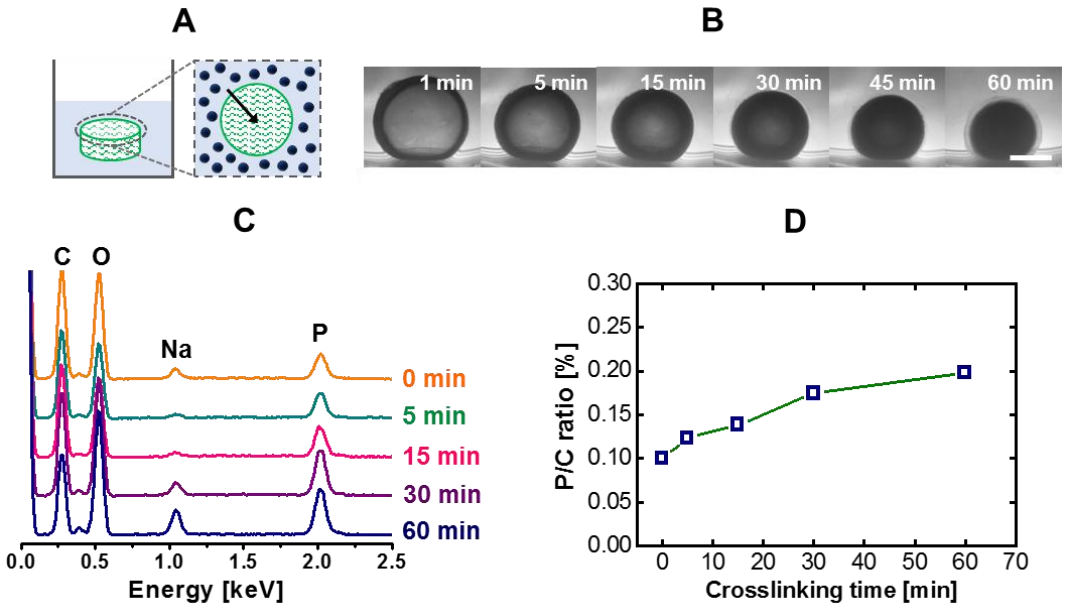

Figure S3.4 - (A) Schematics of the TPP ions diffusion (blue circles) into the center of CHI DN hydrogels after their immersing in an aqueous solution containing these negatively-charged ions. **(B)** Visual inspection of the previous process using an optical stereomicroscope (TR500, VWR, USA) equipped with a digital camera (G12 Olympus, Canon, Japan). The CHI DN hydrogels were cylindrical with 6 mm diameter and 4 mm height. The scale bar corresponds to 3 mm. **(C)** EDS profiles obtained by fixing the analysis area and for different incubation times. **(D)** Phosphorus (P)/Carbon (C) ratio [%] in function of the incubation time in the TPP solution.

Above 3 % (w/v), it is difficult to dissolve MMW-CHI in acetic acid and for concentrations lower than 1 % (w/v) is challenging to obtain a hydrogel structure. Therefore, two MMW-CHI concentrations, 2 and 3 % (w/v), were tested and the results suggest that both CHI networks were able to withstand fracture strains of 90%, however they differ on the fracture stress: 2 % (w/v) MMW-CHI reach values of *ca.* 100 kPa while 3% (w/v) MMW-CHI reach *ca.* 350 kPa (Figure S3.5). Moreover, the compressive modulus increased from 3.6 ± 2 to 5.2 ± 2 kPa when the MMW-CHI concentration was increased from 2% to 3% (w/v). This enhancement on the mechanical properties for higher polymer concentrations was already observed in other

hydrogel systems and have been ascribed to the increased viscosity of the solution with higher polymer concentration. [30] Although the 3% (w/v) MMW-CHI network showed improved mechanical performance, its viscosity was too high. Therefore, the lower MMW-CHI polymer concentration was used in further studies.

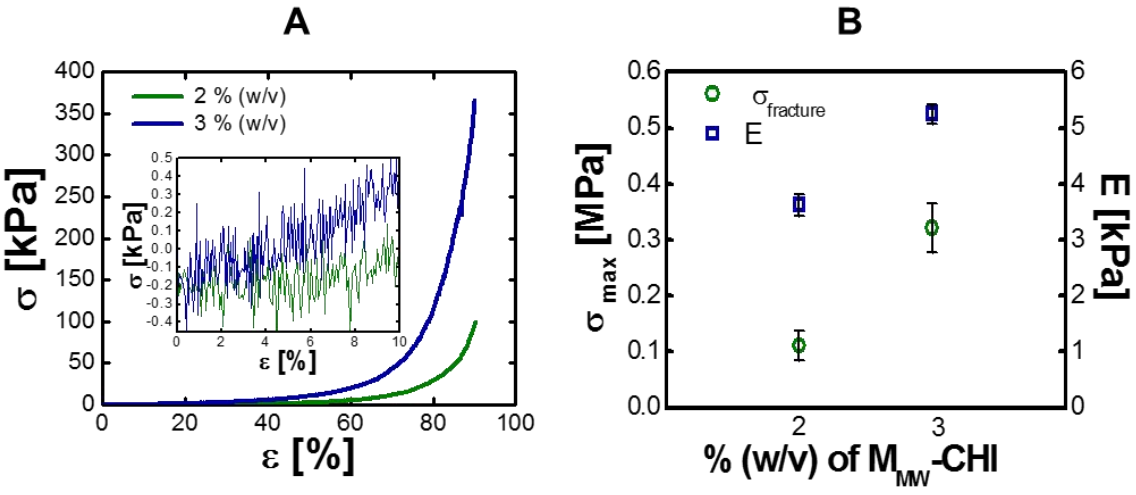

Figure S3.5 - (A) Typical compressive stress-strain curves of MMW-CHI using two different polymer concentrations, namely, 2% and 3% (w/v). The inset represents a zoom of the region used to determine the compressive modulus (E, from 0-10% of strain). **(B)** Variation of both maximum stress (σ max) and E in function of the MMW-CHI polymer concentration. It is worth notice that both structures were able to withstand a compressive strain of at least 90%.

S3.4. Study of the morphology of the CHI DN hydrogels

The CHI DN hydrogels were characterized for their morphology and elemental composition by Scanning Electron Microscopy (SEM, JSM-6010LV, JEOL, Japan) and Energy-Dispersive X-ray Spectroscopy (EDS), respectively. Briefly, the CHI DN hydrogels were first dehydrated by immersing them in solutions with an increased amount of ethanol: 20, 50, 70, 90, 95 and 100% and, then, dried using supercritical carbon dioxide (Thar SFE1000-F, Thar Instruments)[31]. To this end, the samples were loaded in a high-pressure vessel heated at 37 ºC and pressurized to 80 bar. In order to ensure the complete removal of the organic solvent, a carbon dioxide stream was passed through the vessel at constant rate for 1 h.

To prepare the samples for SEM analysis, the CHI DN hydrogels were fractured in liquid nitrogen to reveal the cross-sectional surface followed by their sputter-coating with gold. The images were acquired in high-vacuum by tracking the signal of secondary electrons, and employing an accelerating voltage of 10 kV and a working distance of 10 mm. On the other side, the EDS profile was obtained on a non-coated sample after drawing a line in the middle section of the CHI DN hydrogel.

It can be easily observed in Figure S3.6, that the CHI DN hydrogel presents both a homogeneous structure (A) and composition (B).

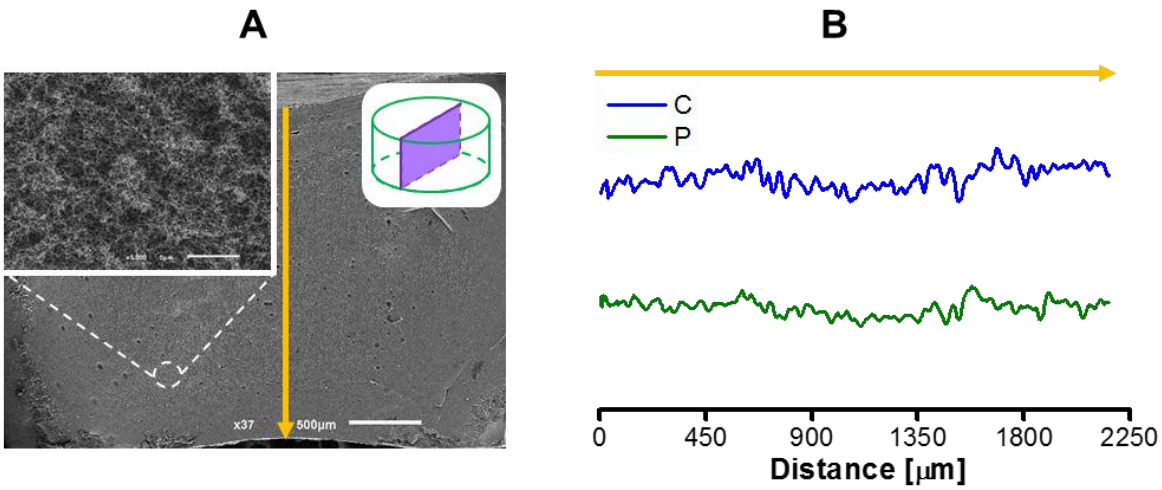

Figure S3.6 - (A) SEM image of the CHI DN hydrogel cross-section after 1h of immersing in a TPP solution and successive washes to remove the excess of ions. The scale bar corresponds to 500 µm. The inset displays a zoom in of a certain region of the former SEM image. The scale bar corresponds to 5 µm. **(B)** Carbon (C) and phosphorus (P) distribution on CHI DN hydrogels along a line (represented with a yellow arrow).

S3.5. Study of the ability of the three types of hydrogels, LMW-MACHI, MMW-CHI and CHI DN hydrogels, to efficiently dissipate energy

All three types of CHI hydrogels produced on this work, namely CHI DN, LMW-CHI and MMW-CHI, were subjected to five consecutive loading/unloading cycles at 50% of strain to assess their ability to dissipate energy as shown in Figure S3.7. The first compressive cycle

was performed on an as-prepared sample that has not been previously deformed and between cycles the sample was not allowed to rest. The dissipated energy during a cycle (U_{hist}) was estimated from the area between the loading and unloading curves following the equation 1:

$$U_{hist} = \int_{0\%}^{50\%} \sigma_{loading} d\varepsilon - \int_{0\%}^{50\%} \sigma_{unloading} d\varepsilon \quad (1)$$

The U_{hist} value of the first compressive cycle is 743 ± 68 kJ m^{-3}, 71 ± 9 kJ m^{-3} and 13 ± 1 kJ m^{-3} for the CHI DN, LMW-MACHI and MMW-CHI hydrogels.

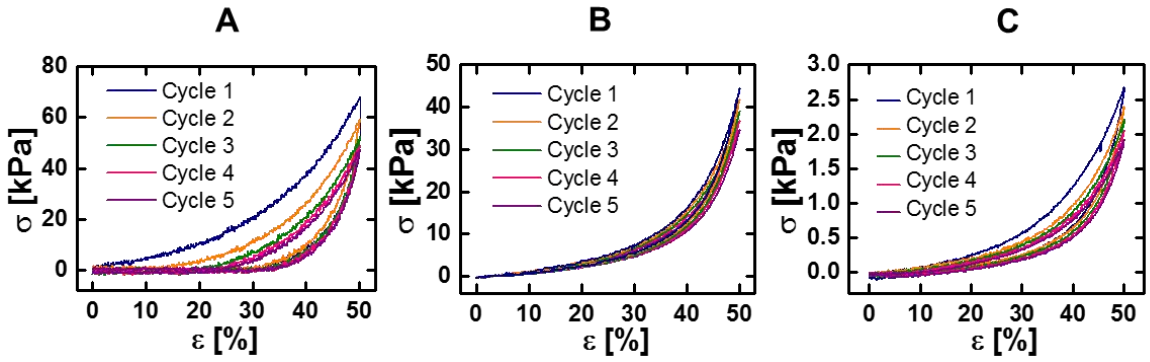

Figure S3.7 - Representative cyclic strain/stress curves of CHI DN hydrogels **(A)**, LMW-MACHI hydrogels **(B)** and MMW-CHI **(C)** hydrogels after applying five successive compression cycles.

S3.6. Study of the water uptake by the CHI hydrogels with different amounts of MMW-CHI polymer

The amount of water contained in the CHI DN hydrogels was defined as the weight ratio of swollen to dry sample. Dry hydrogels were obtained by drying in vacuum until a constant weight was reached. The CHI DN hydrogels with optimized mechanical properties exhibit a water content of *ca.* 93 ± 2 %.

Moreover, water uptake studies were performed on as-prepared CHI hydrogels with different amounts of MMW-CHI polymer. Briefly, hydrogels were first weighed ($W_{initial}$) and,

then, immersed in different liquid environments, namely distilled water (pH = 6.9), culture medium (α-MEM, pH = 7.4) and 0.01 M PBS (pH = 7.4) at 37°C. After 24 h, the hydrogels were removed from the respective solution, blotted with tissue for removal of the excess of water, and weighed ($W_{equilibrium}$) again. The water uptake (*WU*) was measured through the following equation (2):

$$WU\ [\%] = (W_{equilibrium} - W_{initial})/W_{equilibrium} \times 100 \quad (2)$$

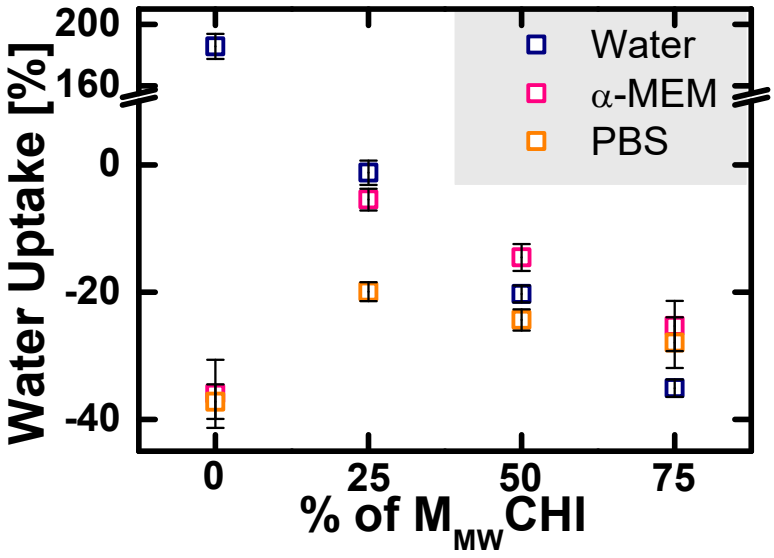

Figure S3.8 - Water uptake by as-prepared CHI hydrogels as a function of the % of the amount of MMW-CHI polymer in the final hydrogel structure using three different media: water, α-MEM and PBS at 37°C.

The hydrogels were produced and immediately transferred to the three different solutions tested. With the exception of LMW-MACHI network (0% of MMW-CHI polymer), when the obtained hydrogels were immersed in the previous solutions their mass decreased as suggested on Figure S3.8. This fact can be ascribed to the presence of water in the hydrogel network, which may be expelled to reach the osmotic equilibrium. Additionally, this decrease

on hydrogel weight can also be attributed to the release of non-bonded ions present on the hydrogel initial structure. For the solutions containing ions, the high degree of water release from the CHI hydrogels may be explained by the formation of a more crosslinked network. This crosslinking mechanism results from the presence of ions in solution, which may lead to the establishment of new junction zones.

S3.7. Study the effect of the MMW-CHI polymer on the CHI DN hydrogel mechanical properties

The methacrylation process of the LMW-MACHI polymer was not complete (see section 2 for further information), meaning that this polymer bears free amino groups. Having this in mind, one could think about synthesizing CHI DN hydrogels by employing the two crosslinking mechanisms to only LMW-MACHI polymer as this polymer has both positive amino groups to react with the TPP negative ions and methacrylic groups to create the covalent crosslinks. Therefore, the charge density of the main components involved on CHI DN hydrogel fabrication process was obtained by measuring their zeta potential (Zetasizer, Malvern, United Kingdom). Figure S3.9A shows that the LMW-MACHI solution exhibits a less positive potential when comparing with the one of the MMW-CHI; additionally, the TPP solution presented a negative charge. For this reason, both CHI derivatives are able to react with TPP ions, but it is expected that MMW-CHI polymer will be more reactive than LMW-MACHI.

Figure S3.9B shows the typical compressive curves of LMW-CHI hydrogels obtained using only a photocrosslinking mechanism (line in orange) and by combining the photocrosslinking mechanism with an ionic one (line in purple). Although the dual-crosslinked LMW-MACHI hydrogels have higher compressive modulus (*ca.* 35.0 ± 83 kPa) when comparing with the equivalent photocrosslinked structure (*ca.* 11.8 ± 36 kPa), their fracture stress and strain (*ca.* 41 ± 13 kPa and 28 ± 5 %) are much lower than the ones obtained using the DN-based methodology (*ca.* 19 ± 3 MPa and 90%). These results suggest that the

improved mechanical behavior of the CHI DN hydrogels is the result of combining two CHI derivatives with contrasting molecular weights as well as two distinct crosslinks.

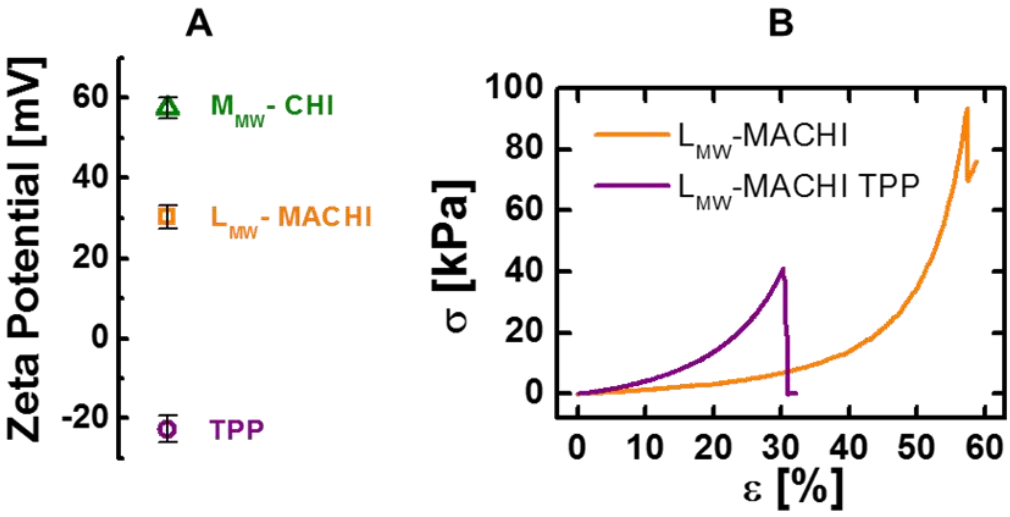

Figure S3.9 - (A) Zeta potential of the LMW-MACHI, TPP and MMW-CHI solutions. Error bars correspond to the S.D. of 5 replicates. **(B)** Representative compressive stress-strain curves of LMW-MACHI hydrogel before and after 1h of incubation in a TPP aqueous solution.

Movie S3.1. Compression assay until ε =50% performed on the LMW-MACHI hydrogels and **Movie S3.2.** Compression assay until ε =50% performed on the CHI DN hydrogels are online available using DOI: 10.1039/c5cc05564d.

References

[1] a) C. R. Nuttelman, M. A. Rice, A. E. Rydholm, C. N. Salinas, D. N. Shah, K. S. Anseth, Macromolecular Monomers for the Synthesis of Hydrogel Niches and Their Application in Cell Encapsulation and Tissue Engineering, *Prog. Polym. Sci.* **2008**, 33, 167; b) K. Y. Lee, D. J. Mooney, Hydrogels for tissue engineering, *Chem Rev.* **2001**, 101, 1869; c) C. L. Salgado, M. B. Oliveira, J. F. Mano, Combinatorial cell-3D biomaterials cytocompatibility screening for tissue engineering using bioinspired superhydrophobic substrates, *Integr. Biol.* **2012**, 4, 318.

[2] a) A. S. Hoffman, Hydrogels for biomedical applications, *Adv. Drug Deliver. Rev.* **2002**, 54, 3; b) M. B. Oliveira, J. F. Mano, On-chip assessment of the protein-release profile from 3D hydrogel arrays, *Anal. Chem*. **2013**, 85, 2391.
[3] D. Buenger, F. Topuz, J. Groll, Hydrogels in sensing applications, *Prog. Polym. Sci.* **2012**, 37, 1678.
[4] N. A. Peppas, Y. Huang, M. Torres-Lugo, J. H. Ward, J. Zhang, Physicochemical foundations and structural design of hydrogels in medicine and biology, *Annu. Rev. Biomed. Eng.* **2000**, 2, 9.
[5] P. Calvert, Hydrogels for Soft Machines, *Adv. Mater.* **2009**, 21, 743.
[6] A. M. S. Costa, J. F. Mano, Extremely strong and tough hydrogels as prospective candidates for tissue repair -A review, *Eur. Polym. J.* **2015**, 72, 344-364.
[7] a) J. P. Gong, Y. Katsuyama, T. Kurokawa, Y. Osada, Double - Network Hydrogels with Extremely High Mechanical Strength, *Adv. Mater.* **2003**, 15, 1155; b) J. P. Gong, Why are double network hydrogels so tough?, *Soft Matter* **2010**, 6, 2583.
[8] a) H. Tsukeshiba, M. Huang, Y.-H. Na, T. Kurokawa, R. Kuwabara, Y. Tanaka, H. Furukawa, Y. Osada, J. P. Gong, Effect of polymer entanglement on the toughening of double network hydrogels, *J. Phys. Chem. Part B* **2005**, 109, 16304; b) A. Argun, V. Can, U. Altun, O. Okay, Nonionic Double and Triple Network Hydrogels of High Mechanical Strength, *Macromolecules* **2014**, 47, 6430; c) M. A. Haque, T. Kurokawa, J. P. Gong, Super tough double network hydrogels and their application as biomaterials, *Polymer* **2012**, 53, 1805.
[9] a) N. K. Simha, C. S. Carlson, J. L. Lewis, Evaluation of fracture toughness of cartilage by micropenetration, *J. Mater. Sci.-Mater.* **2004**, 15, 631; b) A. J. Kerin, M. R. Wisnom, M. A. Adams, The compressive strength of articular cartilage, *Proc. Inst. Mech. Eng. H J. Eng. Med.* **1998**, 212, 273.
[10] Y. Chen, K. Dong, Z. Liu, F. Xu, Double network hydrogel with high mechanical strength: Performance, progress and future perspective, *Sci. China Technol. Sci.* **2012**, 55, 2241.
[11] a) Q. Chen, L. Zhu, C. Zhao, Q. Wang, J. Zheng, A robust, one-pot synthesis of highly mechanical and recoverable double network hydrogels using thermoreversible sol-gel polysaccharide, *Adv. Mater.* **2013**, 25, 4171; b) R. E. Webber, C. Creton, H. R. Brown, J. P. Gong, Large Strain Hysteresis and Mullins Effect of Tough Double-Network Hydrogels, *Macromolecules* **2007**, 40, 2919; c) K. Harrass, R. Kruger, M. Moller, K. Albrecht, J. Groll, Mechanically strong hydrogels with reversible behaviour under cyclic compression with MPa loading, *Soft Matter* **2013**, 9, 2869; d) L. Weng, A. Gouldstone, Y. Wu, W. Chen, Mechanically strong double network photocrosslinked hydrogels from N,N-dimethylacrylamide and glycidyl methacrylated hyaluronan, *Biomaterials* **2008**, 29, 2153; e) J.-Y. Sun, X. Zhao, W. R. K. Illeperuma, O. Chaudhuri, K. H. Oh, D. J. Mooney, J. J. Vlassak, Z. Suo, Highly stretchable and tough hydrogels, *Nature* **2012**, 489, 133; f) Y. Zhao, T. Nakajima, J. J. Yang, T. Kurokawa, J. Liu, J. Lu, S. Mizumoto, K. Sugahara, N. Kitamura, K. Yasuda, A. U. D. Daniels, J. P. Gong, Proteoglycans and Glycosaminoglycans Improve Toughness of Biocompatible Double Network Hydrogels, *Adv. Mater.* **2013**, 26, 436; g) J. Saito, H. Furukawa, T. Kurokawa, R. Kuwabara, S.

Kuroda, J. Hu, Y. Tanaka, J. P. Gong, N. Kitamura, K. Yasuda, Robust bonding and one-step facile synthesis of tough hydrogels with desirable shape by virtue of the double network structure, *Polym. Chem.* **2011**, 2, 575.

[12] a) P. Fratzl, Biomimetic materials research: what can we really learn from nature's structural materials?, *J. R. Soc. Interface* **2007**, 4, 637; b) Z. L. Wu, J. P. Gong, Hydrogels with self-assembling ordered structures and their functions, *NPG Asia Mater* **2011**, 3, 57.

[13] V. Ottani, D. Martini, M. Franchi, A. Ruggeri, M. Raspanti, Hierarchical structures in fibrillar collagens, *Micron* **2002**, 33, 587.

[14] a) F. L. Mi, Y. C. Tan, H. F. Liang, H. W. Sung, In vivo biocompatibility and degradability of a novel injectable-chitosan-based implant, *Biomaterials* **2002**, 23, 181; b) I. A. Sogias, A. C. Williams, V. V. Khutoryanskiy, Why is chitosan mucoadhesive?, *Biomacromolecules* **2008**, 9, 1837; c) A. Di Martino, M. Sittinger, M. V. Risbud, Chitosan: a versatile biopolymer for orthopaedic tissue-engineering, *Biomaterials* **2005**, 26, 5983.

[15] M. A. Haque, T. Kurokawa, G. Kamita, J. P. Gong, Lamellar Bilayers as Reversible Sacrificial Bonds To Toughen Hydrogel: Hysteresis, Self-Recovery, Fatigue Resistance, and Crack Blunting, *Macromolecules* **2011**, 44, 8916.

[16] Q. Chen, L. Zhu, H. Chen, H. Yan, L. Huang, J. Yang, J. Zheng, A Novel Design Strategy for Fully Physically Linked Double, *Adv. Funct. Mater.* **2015**, 25, 1598.

[17] a) D. M. Kirchmajer, M. i. h. Panhuis, Robust biopolymer based ionic–covalent entanglement hydrogels with reversible mechanical behavior, *J. Mater. Chem. Part B* **2014**, 2, 4694; b) S. E. Bakarich, G. C. Pidcock, P. Balding, L. Stevens, P. Calvert, M. in het Panhuis, Recovery from applied strain in interpenetrating polymer network hydrogels with ionic and covalent cross-links, *Soft Matter* **2012**, 8, 9985.

[18] L. M. Y. Yu, K. Kazazian, M. S. Shoichet, Peptide surface modification of methacrylamide chitosan for neural tissue engineering applications, *J. Biomed. Mater. Res., part A* **2007**, 82A, 243.

[19] a) S. H. Kim, C. C. Chu, Synthesis and characterization of dextran-methacrylate hydrogels and structural study by SEM, J. *Biomed. Mater. Res.* **2000**, 49, 517; b) O. Jeon, K. H. Bouhadir, J. M. Mansour, E. Alsberg, Photocrosslinked alginate hydrogels with tunable biodegradation rates and mechanical properties, *Biomaterials* **2009**, 30, 2724.

[20] E. Fernandez-Megia, R. Novoa-Carballal, E. Quiñoá, R. Riguera, Optimal routine conditions for the determination of the degree of acetylation of chitosan by 1H-NMR, *Carbohydr. Polym.* **2005**, 61, 155.

[21] A. M. Costa, M. Alatorre-Meda, N. M. Oliveira, J. F. Mano, Biocompatible Polymeric Microparticles Produced by a Simple Biomimetic Approach, *Langmuir* **2014**, 30, 4535.

[22] Y. D. Park, N. Tirelli, J. A. Hubbell, Photopolymerized hyaluronic acid-based hydrogels and interpenetrating networks, *Biomaterials* **2003**, 24, 893.

[23] a) H. Shin, B. D. Olsen, A. Khademhosseini, The mechanical properties and cytotoxicity of cell-laden double-network hydrogels based on photocrosslinkable gelatin and gellan gum

biomacromolecules, *Biomaterials* **2012**, 33, 3143; b) A. Nakayama, A. Kakugo, J. P. Gong, Y. Osada, M. Takai, T. Erata, S. Kawano, High Mechanical Strength Double - Network Hydrogel with Bacterial Cellulose, *Adv. Funct. Mater.* **2004**, 14, 1124.

[24] (a) D. M. Kirchmajer and M. i. h. Panhuis, Robust biopolymer based ionic–covalent entanglement hydrogels with reversible mechanical behavior, *J. Mater. Chem. B* **2014**, 2, 4694; (b) S. E. Bakarich, G. C. Pidcock, P. Balding, L. Stevens, P. Calvert and M. in het Panhuis, Recovery from applied strain in interpenetrating polymer network hydrogels with ionic and covalent cross-links, *Soft Matter* **2012**, 8, 9985.

[25] V. X. Truong, M. P. Ablett, S. M. Richardson, J. A. Hoyland, A. P. Dove, Simultaneous orthogonal dual-click approach to tough, in-situ-forming hydrogels for cell encapsulation, *J. Am. Chem. Soc.* **2015**, 137, 1618.

[26] a) D. F. Coutinho, S. V. Sant, H. Shin, J. T. Oliveira, M. E. Gomes, N. M. Neves, A. Khademhosseini, R. L. Reis, Modified Gellan Gum hydrogels with tunable physical and mechanical properties, *Biomaterials* **2010**, 31, 7494; b) Q. Li, J. Wang, S. Shahani, D. D. Sun, B. Sharma, J. H. Elisseeff, K. W. Leong, Biodegradable and photocrosslinkable polyphosphoester hydrogel, *Biomaterials* **2006**, 27, 1027.

[27] T. Nakajima, T. Kurokawa, S. Ahmed, W.-l. Wu, J. P. Gong, Characterization of internal fracture process of double network hydrogels under uniaxial elongation, *Soft Matter* **2013**, 9, 1955.

[28] Stephanie J. Bryant, Charles R. Nuttelman, Kristi S. Anseth, Cytocompatibility of UV and visible light photoinitiating systems on cultured NIH/3T3 fibroblasts in vitro, *J. Biomater. Appl.* **2000**, 439.

[29] J. W. Nichol, S. T. Koshy, H. Bae, C. M. Hwang, S. Yamanlar, A. Khademhosseini, Cell-laden microengineered gelatin methacrylate hydrogels, *Biomaterials* **2010**, 31, 5536-5544.

[30] N. Annabi, S. M. Mithieux, P. Zorlutuna, G. Camci-Unal, A. S. Weiss, A. Khademhosseini, Engineered cell-laden human protein-based elastomer, *Biomaterials* **2013**, 34, 5496-5505.

[31] S. S. Silva, A. Motta, M. T. Rodrigues, A. F. M. Pinheiro, M. E. Gomes, J. F. Mano, R. L. Reis, C. Migliaresi, Novel genipin-cross-linked chitosan/silk fibroin sponges for cartilage engineering strategies, *Biomacromolecules* **2008**, 9, 2764-2774.

Chapter IV: Results & Discussion

Bioinspired Ultratough Hydrogel with Fast Recovery, Self-Healing, Injectability and Cytocompatibility[3]

ABSTRACT

Inspired by the mussel byssus attachment system, a highly hydrated polymeric structure was designed to combine, for the first time, a set of interesting features for load-bearing purposes. These characteristics include a (i) compressive strength in the MPa range, (ii) toughness and ability to recover it upon successive cyclic loads, (iii) ability to quick self-heal upon rupture, (iv) the possibility to be administered through minimal invasive techniques such as by injection, (v) swelling ratio adjusted to space-filling applications and (vi) cytocompatibility. Owing to these characteristics and the mild conditions employed during the fabrication process, the reported self-healable, ultratough and strong hydrogel is a prospective candidate for a wide range of applications including the biomedical field.

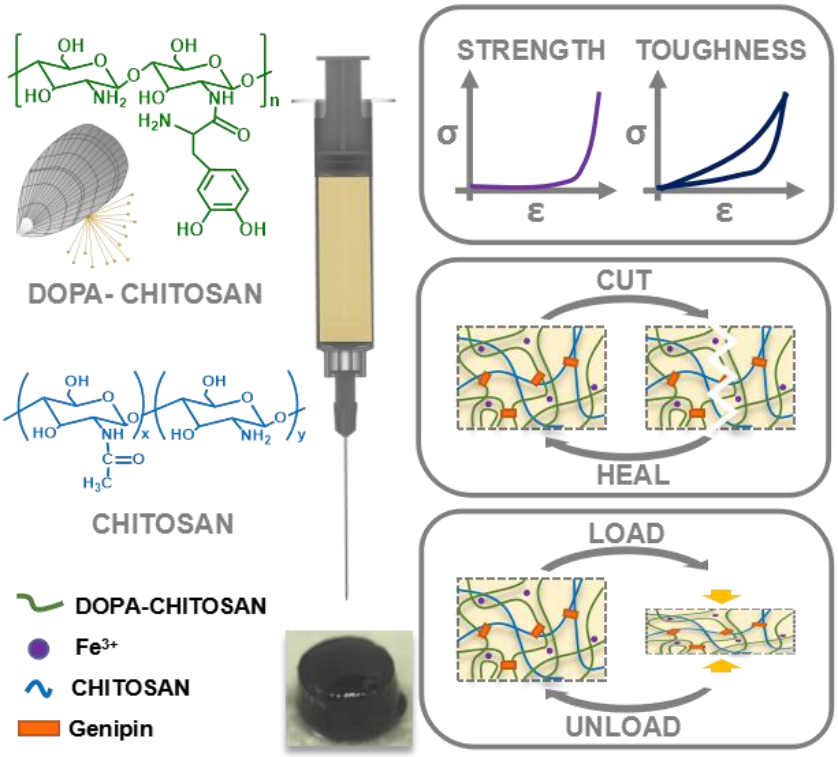

[3] Based on the publication: Sara Azevedo#, Ana M. S. Costa#, Amanda Andersen, Insung S. Choi, Henrik Birkedal, João F. Mano, (#authors contributed equally), Bioinspired Ultratough Hydrogel with Fast Recovery, Self-Healing, Injectability and Cytocompatibility, *Advanced Materials* **2017**, 29 (28), pp. 1700759.

1. Introduction

Highly robust hydrogels are emerging to enhance the mechanical performance of conventional hydrogels and, thus, extending their application field as regenerative medicine [1], waste treatment [2], superabsorbents [3] and electronic [4] devices. For example, the double network (DN) concept, which consists in the combination of a fragile network with a ductile one, has been applied to achieve extremely tough and yet extremely hydrated materials [5]. In conventional chemically crosslinked DN hydrogels, their outstanding toughness has been ascribed to the internal fracture of the fragile network. Thus, owing to this permanent bond breakage, they are unable to efficiently recover their initial toughness upon unloading, meaning that the integrity of the material is irreversibly lost [5,6]. By contrast, hydrogels with self-healing behavior have improved lifetime and safety, which are of outmost importance for load-bearing applications. These characteristics are the result of their ability to repair themselves after fracture, allowing the recovery of the original material function [7]. Several strategies have been devised to engineering hydrogels with self-healing either by applying the concept of constitutional dynamic chemistry, which uses reversible covalent or non-covalent bonds, or by introducing microcapsules filled with a resin, which upon fracture is able to polymerize the crack using an adjuvant catalyst [8,9]. However, self-healing hydrogels often exhibit a poor mechanical behavior, as consequence of the weaker and reversible nature of their dynamic interactions [6]. Therefore, significant efforts have been done to fabricate hydrogels with both high mechanical strength and self-healing [9]. Despite the good mechanical performance of some of these hydrogels, they still exhibit some drawbacks, namely (i) the healing process do not occur in an autonomous manner, often requiring harsh healing conditions such as high temperatures, (ii) the healing is typically not complete, meaning that the mechanical properties of the healed samples are usually lower than the ones of the virgin samples, (iii) the time required to ensure the complete healing of the material is often very long, ranging from a couple of hours to several days and (iv) some uncertainties about the biocompatibility of both

the healing process and the polymers used to fabricate the hydrogel devices still prevail [9]. The aforementioned aspects acquire a special importance when hydrogels are intended for biomedical purposes as it is crucial to ensure (i) the proper performance *in vivo* of the chosen material, (ii) the good biocompatibility and favorable cell interactions, which can be achieved by resorting to natural-origin materials, (iii) the mild fabrication methods and conditions employed to allow, for example, the encapsulation of cells and proteins, and (iv) that the developed system can be administrated through minimal invasive methods, for instance, by injection [10]. Therefore, the motivation for this work was the absence of a simple, fast and cytocompatible methodology to prepare both highly robust, with strength values in MPa order, and self-healable natural-based hydrogels with potential to be injected into the body. To this end, chitosan (CHI), a widely used polysaccharide obtained by deacetylation of chitin, was functionalized with catechol groups forming the DOPA-CHI derivative [11]. This conjugate was inspired by the presence of proteins rich in DOPA (3,4-dihydroxiphenylalanine) aminoacids bearing catechol groups on the mussels byssus, enabling the attachment of these organisms to a wide range of surfaces through covalent and/or non-covalent bonds [12]. In this work, to enhance the mechanical performance of the developed hydrogels, either a double crosslinked (DC) or a DN strategy were employed. In both strategies, two crosslinking mechanisms were applied, namely (i) a covalent process using genipin (GP) as a cytocompatible chemical crosslinker of CHI free amine groups and (ii) a non-covalent one through coordination bonds between the catechol groups present in DOPA-CHI and Fe^{3+} ions. In the case of DC hydrogels, DOPA-CHI with a modification degree of 5.1% (SI.4, Section S4.1) was mixed with GP followed by the addition of the required amount of Fe^{3+} ions to create complexes with the catechol groups (Scheme 4.1). By contrast, DN hydrogels were produced by incorporating also a small portion of medium molecular weight CHI (MMW-CHI) in the former hydrogel precursor solution containing DOPA-CHI, GP and Fe^{3+} ions (SI.4, Section 4.2 and 4.3). All the hydrogel formulations tested in this work were summarized on Table S4.1 of the SI.4. It is worth noting

that in both cases, Fe^{3+}-catechol coordination bonds and GP-mediated crosslinks between different chains of DOPA-CHI are present (Scheme 4.1a and 4.1b). In DN hydrogels, which contain also MMW-CHI, GP can further establish crosslinks between two chains of MMW-CHI polymer (Scheme 4.1d) or a chain of MMW-CHI and one of DOPA-CHI (Scheme 4.1c).

The described technology constitutes an advance over the conventional DN methodology as it overcomes some of its current drawbacks. First, the introduction of dynamic bonds confers not only an increased toughness but also a self-healing ability, allowing to restore the initial mechanical properties in few minutes. Second, the proposed one-pot methodology potentiates their injectability, which may be relevant to fabricate hydrogels with specific shapes or to administer them through a minimal invasive manner. Third, the proved non-toxicity of the materials used in this study: CHI [11,13], GP [14], and Fe^{3+} [15], highlights the potential of the developed 3D structures for biomedical purposes. Moreover, other authors [16] tested the GP-mediated crosslinking *in vivo* and did not detect any adverse response, being a good indicator of the promising character of the developed hydrogel system to be implanted. It is worth noticing that both polymeric networks of the produced healable hydrogels are based on a natural-occurring biopolymer, CHI, which is an innovative feature with respect to recent works where only one of the networks was biopolymer-based such as κ-carrageenan, agar and xanthan gum, whereas polyacrylamide, polyethylene glycol, polyacrylic acid or polyurethane, among others, were employed for the second one [1]. Finally, enhanced mechanical properties are ensured by both introducing an energy dissipation mechanism and adjusting the pH value. From acidic to basic conditions, the stoichiometry of the complex bond changes from mono- to tris-complexes, via the deprotonation of the catechol hydroxyls, leading to an increased polymer crosslinking and mechanical strength [17]. Thereby, the pH of the precursor solution was adjusted to almost 7.0 (physiological pH) given that the pKa of the conjugate acid (protonated amines) is approximately 6.7 [18].

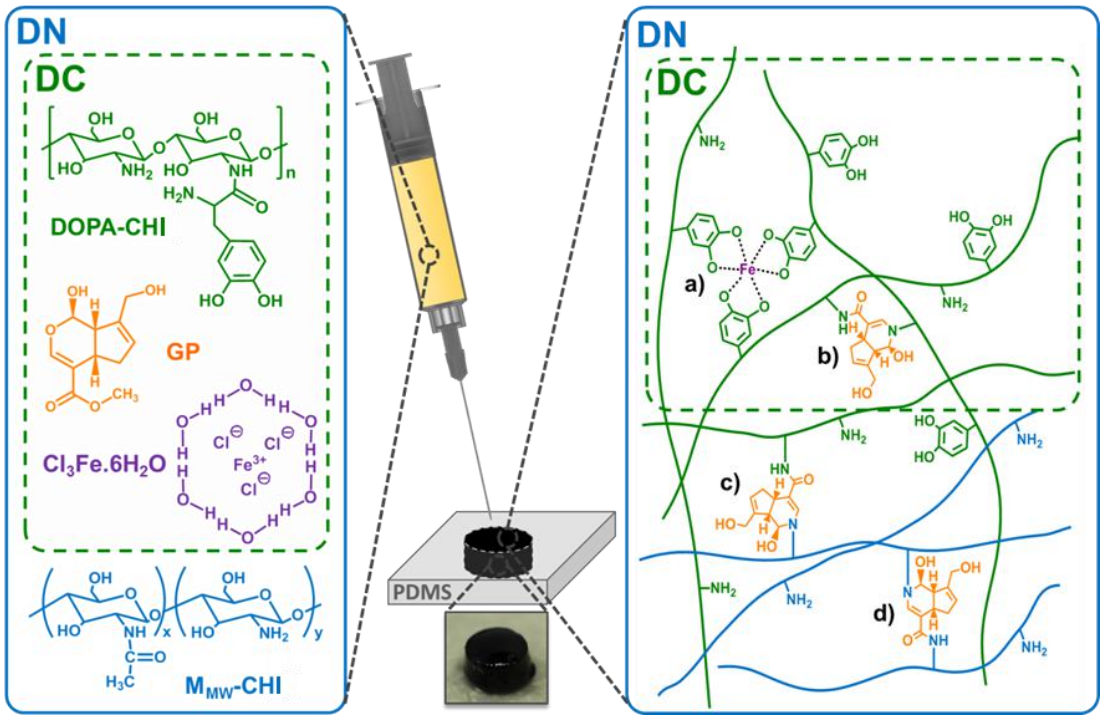

Scheme 4.1 - Schematic representation of the method developed to fabricate the DC and DN hydrogels. Besides the DOPA-CHI, GP and Fe^{3+} ions, DN hydrogels are also composed of MMW-CHI. The inset depicts a picture of the obtained hydrogels (DC and DN showed a similar appearance). Two crosslinking processes were employed to produce hydrogels, namely a covalent crosslinking using GP and a physical crosslinking through coordination bonds in presence of Fe^{3+} ions. Therefore, DC hydrogels can be composed of bis- and tris-complexes Fe:DOPA-CHI (**a**) or/and covalent bonds between two DOPA-CHI chains (**b**). Additionally, DN hydrogel can also establish covalent bonds between a chain of DOPA-CHI and a chain of MMW-CHI (**c**) or/and between two chains of MMW-CHI (**d**).

2. Materials & Methods

2.1. Materials

Medium molecular weight chitosan (MMW-CHI, MW 190-310 kDa, 83.2% deacetylated), DOPA (3,4-dihydroxy-L-phenylalanine), CHI (chitosan oligosaccharide lactate, MW 4-6 kDa, >90% deacetylated), TFA (trifluoroacetic acid, 99%), NHS (N-hydroxysuccinimide) and EDC (N-(3-dimethylaminopropyl)-N'-ethylcarbodiimide hydrochloride) were purchased from Sigma Aldrich (Saint Louis, MO). Spectra dialysis membranes with a MWCO of 3.5 kDa were supplied

from Spectrum Labs. Sodium hydroxide (NaOH, pellets) was purchased from Fischer Chemical (Leicestershire, England). Acetic acid glacial solvent (CH_3COOH) was purchased from VWR Chemicals (Leuven, Belgium). β-glycerolphosphate disodium salt pentahydrate (β-GP) and iron(III) chloride hexahydrate ($Cl_3Fe.6H_2O$) were supplied from Sigma Aldrich (Saint Louis, MO). Genipin (GP, purification of 98%) was purchased from Wako Chemicals GmbH (Neuss, Germany). Tryple express, fetal bovine serum (FBS), penicillin/streptomycin solution, calcein-AM, propidium iodide (PI), CellTiter 96® AQueous One Solution Reagent, and both D-MEM F-12 and DMEM without phenol culture mediums were from Alfagene (Portugal). Water purified in an 18MΩ cm MilliQ Plus water system was used throughout.

2.2. Synthesis of the DOPA functionalized chitosan (DOPA-CHI)

DOPA-CHI was produced by standard EDC/NHS coupling chemistry [18]. To this end, DOPA (9.69 mmol, 2 equiv.) was dissolved in 400 mL 0.5 % trifluoroacetic acid (TFA) under stirring followed by the mixture degassing with nitrogen gas for 20 min at room temperature (RT). Next, CHI (4.84 mmol, 1 equiv.) and NHS (29.1 mmol, 6 equiv.) was added to the reaction mixture in which it was dissolved, and the pH of the solution was carefully adjusted to 5.5 using a 2M NaOH solution. After 15 min, EDC (29.1 mmol, 6 equiv.) was added to the DOPA/CHI/NHS reaction. The solution was left to react under stirring and N_2 atmosphere, in a light protected flask at ambient temperature. After 20h, the solution was transferred to dialysis bags and dialyzed against 4 mM HCl for 6 days under stirring, while the dialysis solvent was changed once a day. The purified solution was dried by rotary evaporation and grinded to yield a light-brown powder.

2.3. Preparation of double crosslinked (DC) hydrogels

GP was mixed with DOPA-CHI (10% (w/v) in water) in order to reach a final concentration of 0.1% (w/v) or 0.5% (w/v). The pH of the former precursor solution was

adjusted to 7 by adding, drop by drop, a NaOH solution (1M). The final solution was poured into a polydimethylsiloxane (PDMS) mold in order to obtain cylindric-shaped samples with a diameter of 5 mm and height of 4 mm. Afterwards, Fe^{3+} ions (0.1 M) were added to each well to achieve a Fe^{3+}:catechol ratio of 1:3 followed by their properly mixing to ensure the hydrogel homogeneity.

2.4. Preparation of double network (DN) hydrogels

The DN hydrogels were produced in a similar manner to the previously described for the DC hydrogels. Briefly, a solution of MMW-CHI was prepared by dissolving 10 mg of purified MMW-CHI in 418.3 µL of 1% (v/v) acetic acid, which was further neutralized using a weak base, β-GP, to reach a pH close to the physiological one. Previously, MMW-CHI was purified, as described in the literature [19]. Afterwards, the polymer total concentration was fixed at 10% (w/v) as in the case of the DC hydrogels and MMW-CHI was mixed with DOPA-CHI in a ratio of 1:9. Once dissolved, different amounts of GP, 0.1% (w/v) or 0.5% (w/v) were added to the resultant solution, whose pH was adjusted to 7 by adding NaOH (1M). The precursor solution was transferred to the PDMS molds and Fe^{3+} ions were added in a 1:3 molar ratio. It is worth noting that a strong base is essential to promote the coordination bonds between Fe^{3+} ions and the DOPA moieties present on the DOPA-CHI backbone. Hydrogels without GP (SFe) or Fe^{3+} ions were used as controls. SC and SN hydrogels correspond to the GP controls (without Fe^{3+} ions) for DC and DN hydrogels, respectively. All hydrogels were placed at 37 ºC to accelerate the covalent crosslinking through GP during both 2 h and 24 h. The formation of characteristic dark blue/green coloration from GP was verified after 2 h of incubation at 37 ºC [20]. To prevent water evaporation, all the samples were covered with mineral oil.

2.5. Mechanical characterization of the produced hydrogels

The mechanical properties of the resultant hydrogels were tested using a Universal Mechanical Testing Equipment (INSTRON 5540). This equipment is equipped with a load cell of 1 kN at a speed of 1 mm/min. Both uniaxial and cyclic compressive tests were conducted on cylindrical samples at RT after applying a pre-load of 0.01 N. As the GP-mediated crosslinking degree was proved to be dependent of time, the mechanical properties were analyzed 2 h and 24 h after hydrogel production.

The nominal stress was obtained by dividing the compressive load by the initial area of the specimen. Compressive modulus (E), fracture stress (σ max) and strain (ε max) were calculated from stress-strain curves. Compressive modulus corresponds to the average slope of the stress-strain curve in the initial linear region, from 0% to 10%. Fracture stress and strain can be either the stress/strain point at which the hydrogel broke completely, or the maximum stress/strain reached since some of the hydrogels did not fracture until a strain of 90%. Cyclic assays until ε =30% were used to evaluate the ability of the one-day produced hydrogels to dissipate energy (hysteresis). Moreover, the time needed for the hydrogels to recover the initial hysteresis after the first compression cycle until ε =30% was also assessed.

The dissipated energy during a cycle (U_{hist}) was estimated from the area between the loading/unloading curves following the equation (1):

$$U_{hist} = \int_{0\%}^{30\%} \sigma_{loading} d\mathcal{E} - \int_{0\%}^{30\%} \sigma_{unloading} d\mathcal{E} \quad \textbf{(1)}$$

To ensure the complete crosslinking with GP, the self-healing ability was assessed 24h after producing the hydrogels. To qualitatively assess the self-healing ability, each gel was cleaved, and the pieces were brought into contact. Quantitatively, it was performed a dynamic oscillatory rheology assay. The rheological measurements were collected using a Kinexus Pro Rheometer at 37 ºC with a stainless-steel parallel plate geometry. Briefly, each gel was

strained from 0.1% to 500% until failure at a frequency of 1Hz. The recovery was verified by monitoring the storage modulus (G'), immediately after the fracture, as a function of time at 1 Hz and a strain rate of 1%.

2.6. Design of an injectable device for *in situ* gelation

Under clinical conditions, it is desirable that designed materials can be placed into the body through a minimally invasive strategy. Therefore, we developed an injectable device, which envisaged the *in-situ* administration of the developed DN hydrogel system. The device consists of a double-syringe with a mounted double-needle system connected by a narrow channel. One of the syringes contains the precursor solution of the hydrogel (MMW-CHI, DOPA-CHI and GP) and another with the iron ions. The mixture of each syringe content occurs only at the tip, during the injection.

2.7. Cell seeding on surface of the SFe, SN and DN hydrogels

Chondrocytes from a mouse teratocarcinoma cell line (ATDC5, European Collection of Cell Cultures) were grown in 150 cm^2 tissue culture flasks using a DMEM F-12 medium supplemented with 10% FBS, 3.7 gL^{-1} sodium bicarbonate and 1% penicillin-streptomycin (pH 7.4) at 37 °C in a humidified air atmosphere of 5% CO_2. The culture medium was exchanged every 3 days. ATDC5 cell line is a well characterized chondrogenic cell line, being considered an excellent model to investigate molecular mechanisms of chondrogenesis *in vitro* [21]. Briefly, upon reaching 90% of confluence, the culture medium was removed and replaced by fresh-prepared PBS. Afterwards, the cells were chemically detached from the tissue culture flasks using a 0.05% Tryple Express solution for 8 min at 37 C in a humidified air atmosphere of 5% CO_2. After that, fresh medium was added and the cells were centrifuged at 1200 rpm for 5 min. Afterwards, the medium was decanted followed by the cells re-suspension in culture medium

at cell density of 1×10^6 cells/mL per well. All the procedure was developed under sterile conditions.

One day earlier, DN and SN hydrogels (0.5% (w/v) of GP) as well as SFe hydrogels were prepared in cylindrical PDMS molds (diameter of 5 mm and height of 1.5 mm) following the previously described protocol. The obtained hydrogels were placed into non-treated and sterile 6-well plates and, then, 100 µL of the cell suspension was pipetted above them. After 2 h incubation period, fresh culture medium was added. During 7 days of cell culture, D-MEM was exchanged every two days. After this time, two type of assays were performed.

LIVE/DEAD cell staining was applied to evaluate the cell viability. This technique uses two dyes: calcein-AM, which is a membrane permeant dye and marks the viable cells (green fluorescent dye), and PI (propidium iodide), which binds to DNA of disrupted cells, identifying dead cells (red fluorescent dye). To this end, 1 mL of culture medium containing 2µL of calcein-AM and 1µL of PI was added to the hydrogel samples at 37 ºC and protected from light. After 10 min, to remove excess dye, hydrogels were washed three times with medium and immediately visualized in a fluorescence microscope (ApoTome.2, Zeiss) with red and green filters. The cell viability rate was determined by the ratio between the number of living cells and the total number of cells in the microscopy images.

MTS assay was performed to quantify the cell metabolic activity [22] and is based on the reduction of tetrazolium reagents in formazan products, directly soluble in cell culture medium, by the viable cells. MTS reagent is one of the tetrazolium reagents and is commercially available as CellTiter 96® AQueous One Solution Reagent. To implement this method, the hydrogels were transferred to new wells and rinsed one time with PBS. Meanwhile, the CellTiter 96® AQueous One Solution Reagent was thawed. Next, serum-free cell culture medium without phenol red (DMEM without phenol) was mixed with CellTiter 96® AQueous One Solution Reagent in a medium/reagent ratio of 5:1 and the resultant mixture was added to each well. Each condition was tested in triplicates. Furthermore, negative (well with seeded

cells) and positive (latex rubber) controls were prepared. The plate was protected from light since the MTS reagent is light-sensitive. After this, the plate was incubated at 37 °C, during 3h in a humidified 5% CO_2 atmosphere. In the end of the incubation time, 100 µl of the resultant solution in each well were transferred to a new 96-well plate and the absorbance at 490 nm was recorded in the spectrophotometer (Synergy, BioTek) [23].

2.8. Statistical Analysis

The statistical significance of the obtained data was assessed using One-Way ANOVA (OriginPro software) with Tukey's post hoc test. The homogeneity of variances and the normality distribution criteria were verified using Levene test and Shapiro-Wilk test, respectively. Non-parametric tests were employed in case the data did not follow the previous criteria, namely the Brown-Forsythe (homogeneity of variances criterium) test and Kolmogorov–Smirnov test (normality distribution criterium). A statistically significant difference was defined as $p \leq 0.05$ and the results are presented as mean ± standard deviation. All the experiments were repeated three times and carried out in at least three independent samples.

3. Results and Discussion

The mechanical properties of the resultant hydrogels were assessed by performing a uniaxial compression assay (SI.4, Section S4.4) and the results are displayed in Figure 4.1. DOPA-CHI hydrogels only crosslinked with GP (SC 0.5%) exhibited a brittle behavior, characteristic of the resultant covalent bonds, which means that this network is not able to withstand large deformations and breaks at $\varepsilon = 47.83 \pm 2.07\%$ ($E = 16.60 \pm 2.10$ kPa). By contrast, DOPA-CHI hydrogels crosslinked only through Fe^{3+} ions (SFe) did not break at strains as high as 90% ($E = 1.64 \pm 0.67$ kPa), suggesting their soft and ductile behavior. DC hydrogels (DC 0.5%) exhibited a maximum compressive strength of 1.05 ± 0.19 MPa, without fracturing until 90% of deformation ($E = 28.50 \pm 2.09$ kPa). This behavior is commonly found in

interpenetrating polymer networks (IPN), which explore the linear combination of the mechanical properties of both individual networks [5].

Remarkably, when we replaced just 10% of the total DOPA-CHI polymer used by MMW-CHI, some curious effects on the overall mechanical properties were noticed. Indeed, the resultant DN structures did not fracture and reached a compressive strength of approximately 2.46 ± 0.34 MPa exceeding the DC counterpart by more than a factor of two. Moreover, the compressive modulus of DN 0.5% hydrogels was also about twice the modulus of DC 0.5% (49.60 ± 9.01 kPa vs. 28.50 ± 2.09 kPa). The improved mechanical properties suggest a synergistic effect between the individual networks, typical of the DN concept [5]. Once again, the mechanical properties of DN hydrogels were significantly higher than the corresponding control crosslinked only through covalent bonds (SN 0.5%), whose rupture occurs at 73.33 ± 11.55 kPa (ε = 44.54 ± 1.28 %). The former behavior can be observed in Figure 4.1B since the DN 0.5% hydrogel remained intact after being compressed at ε = 50%, while the SN 0.5% hydrogel was broken into small fragments. Several factors were found to influence the hydrogels mechanical behavior such as the GP crosslinking time or the amount of GP added during the fabrication process. Overall, the compressive modulus and maximum compressive strength increased when the gelation time increased from 2 h (day 0) to 24 h (day 1), as expected since the GP crosslinking is a gradual process (Figure 4.1C and 4.1D) (for more details about the GP-mediated crosslinking please check SI, Section 4). On the other side, the increase of the GP amount led to a generic enhancement of the mechanical properties, in terms of both compressive strength and modulus (Figure 4.1C and 4.1D).

Cyclic compressive assays were conducted to evaluate the ability of the DN hydrogel to efficiently dissipate energy (Figure 4.1E and 4.1F). DN hydrogels exhibited an evident hysteresis between the loading/unloading curves, revealing the presence of an effective dissipation mechanism. By contrast, the DC hydrogel as well as the SFe and SN controls had 3-4 times lower hysteresis values than the DN hydrogel. SC hydrogels store energy without

dissipation, exhibiting an elastic behavior characteristic of covalently crosslinked gels. Afterwards, the ability of the resultant hydrogels to recover the initial dissipated energy was assessed by first subjecting them to a compression cycle up to ε = 30%, followed by a second cycle after 1 h or 24 h. Figure 4.1F suggests that DC and SN hydrogels could recover the initial mechanical properties if the second loading was delayed by 1 h, whereas the DN and SFe hydrogels only equal the initial energy dissipated after 24 h. The high toughness levels observed in DN hydrogels were previously ascribed to the combination of a covalent crosslinked network with a non-covalent one [5, 24]. Upon loading, the coordination interactions between the polymer chains are first dissociated, allowing the effective energy dissipation and preventing the disruption of the covalent structure. Thus, this progressive Fe^{3+}-DOPA detachment avoids the catastrophic crack propagation, allowing the recovery of the initial shape [24]. Interestingly, owing to the dynamic nature of the coordination bonds in DN hydrogels they can be reestablished when the external load is removed, and recover all or part of the original mechanical properties, highlighting their efficiency as an energy dissipating mechanism. By contrast, SFe, SC and SN hydrogels sustain the applied load only until the coordination bonds or covalent crosslinks are disrupted, resulting in lower toughness values than the DN hydrogel since the crack propagation volume is smaller [25]. (SI.4, Section 4.5).

Afterwards, the self-healing behavior of the developed hydrogels was evaluated by both qualitative and quantitative methods (Figure 4.2 and SI, Section 6). One-day prepared gels were cleaved in half with a blade and the pieces were immediately brought into contact. Five minutes after this procedure, the SN hydrogel still showed the fracture plane, whereas the DN had completely recovered since it did not exhibit any signs of the cut (Figure 4.2A). This ability was imparted by the reversible nature of the created coordination bonds, as already described by other authors [26]. In contrast to other healing mechanisms [27], this recovery occurs rapidly, under mild conditions and autonomously without the demand for any external stimulus to trigger the healing process.

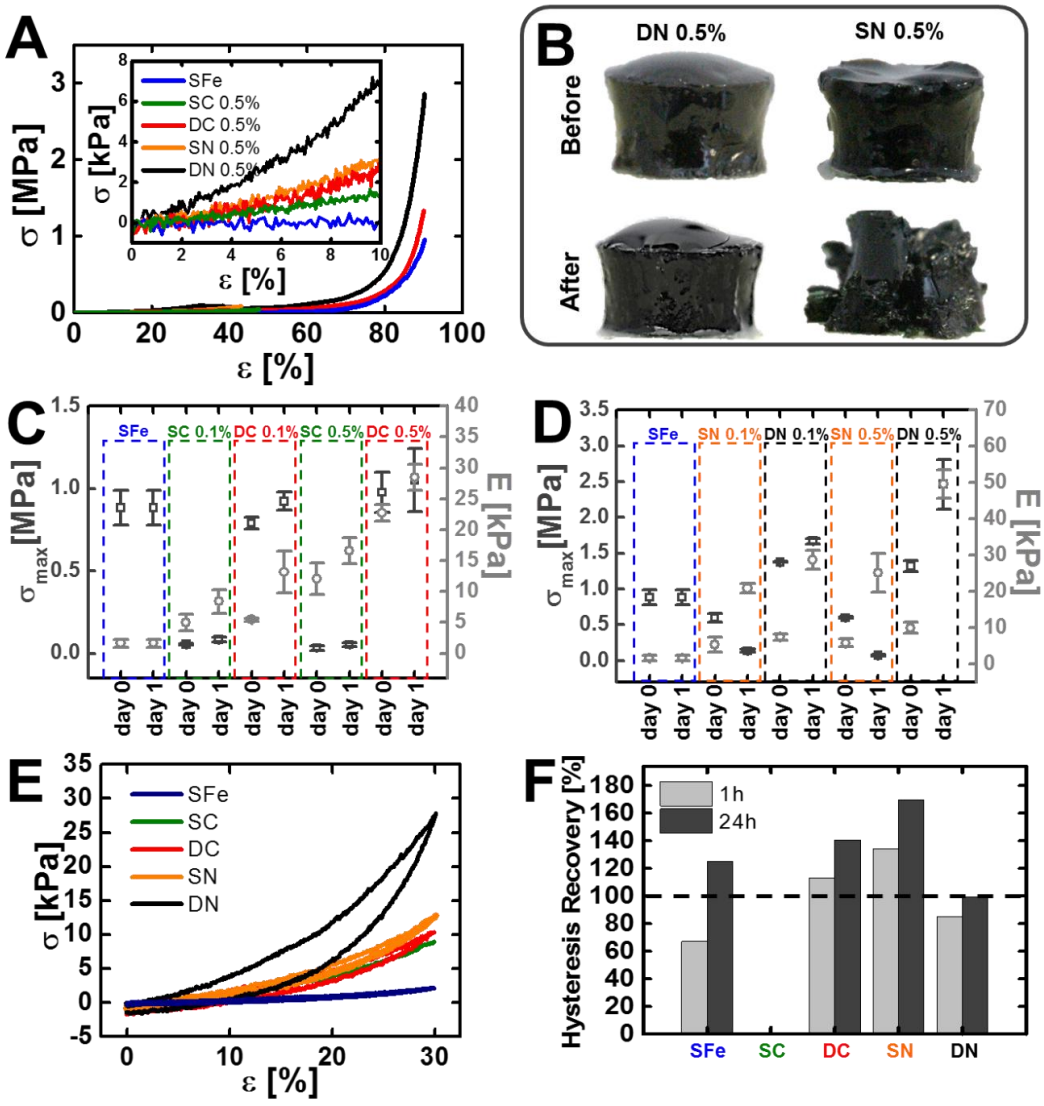

Figure 4.1 - **(A)** Representative compressive stress-strain curves of one-day prepared hydrogels at a fixed GP concentration of 0.5% (w/v). **(B)** Images of the SN 0.5% and DN 0.5% hydrogels before and after compression until 50% of the initial height. Maximum compressive stress, σmax, and modulus, E, of DC hydrogels and their controls **(C)** and DN hydrogels and their controls **(D)** at 37° C after 2 h (day 0) and 24 h (day 1). **(E)** Representative compressive cyclic stress-strain curves of SFe, SC, DC, SN and DN hydrogels. **(F)** Hysteresis recovery [%] for the SFe, SC, DC, SN and DN hydrogels after resting for 1 h and 24 h at mild conditions.

To investigate in more detail the self-healing ability, a dynamic oscillatory rheometer was used to determine the recovery rate (Figure 4.2B). A strain amplitude sweep was applied to break the hydrogel followed by an oscillatory time sweep to monitor the recovery. The results

showed that the DC hydrogel could recover the initial storage modulus (G') in 8 min, whereas the DN hydrogel recovered its G' after 15 min. Nevertheless, neither SC nor the SN that have only covalent bonds fully recovered their moduli - 3.93 kPa and 10.71 kPa after failure vs 6.33 kPa and 17.66 kPa before failure, respectively. SFe hydrogel crosslinked only with Fe^{3+} recovered its modulus of 2.85 kPa instantaneously as already reported by others [18]. These results are due to the dynamic nature of the DOPA:Fe interactions, a hydrogel with these bonds is able to autonomous and immediately reestablish its original mechanical properties after fracture. However, the introduction of covalent crosslinks in DC and DN hydrogels, reduces the mobility of the DOPA-CHI chains within the hydrogel, delaying the recovery process. The presence of the MMW-CHI chains in DN hydrogel causes an even slower healing [28].

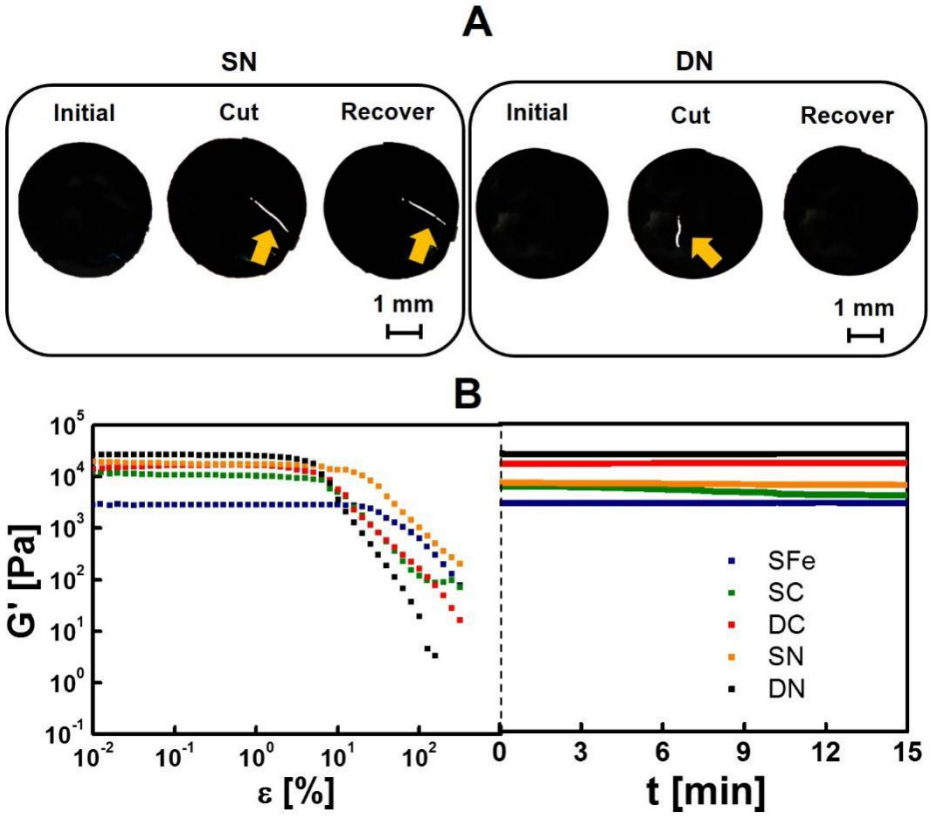

Figure 4.2 - (A) SN and DN hydrogels before (Initial) being cut with a blade (yellow arrow) and after resting for 5 min (Recover). **(B)** Dynamic oscillatory rheology was employed by shearing the samples at 1 Hz until reaching a 500% strain and, then, by monitoring the time recovery dependence at 1% strain and 1 Hz.

Considering all the characteristics previously described, namely the maximum compressive strength, stiffness and toughness, the DN 0.5% hydrogel is the most robust and tough hydrogel. The importance of materials with superior mechanical properties comes from the possibility to bear high loads and simultaneously ensure a mechanical harmonization with the surrounding soft tissues [14a].

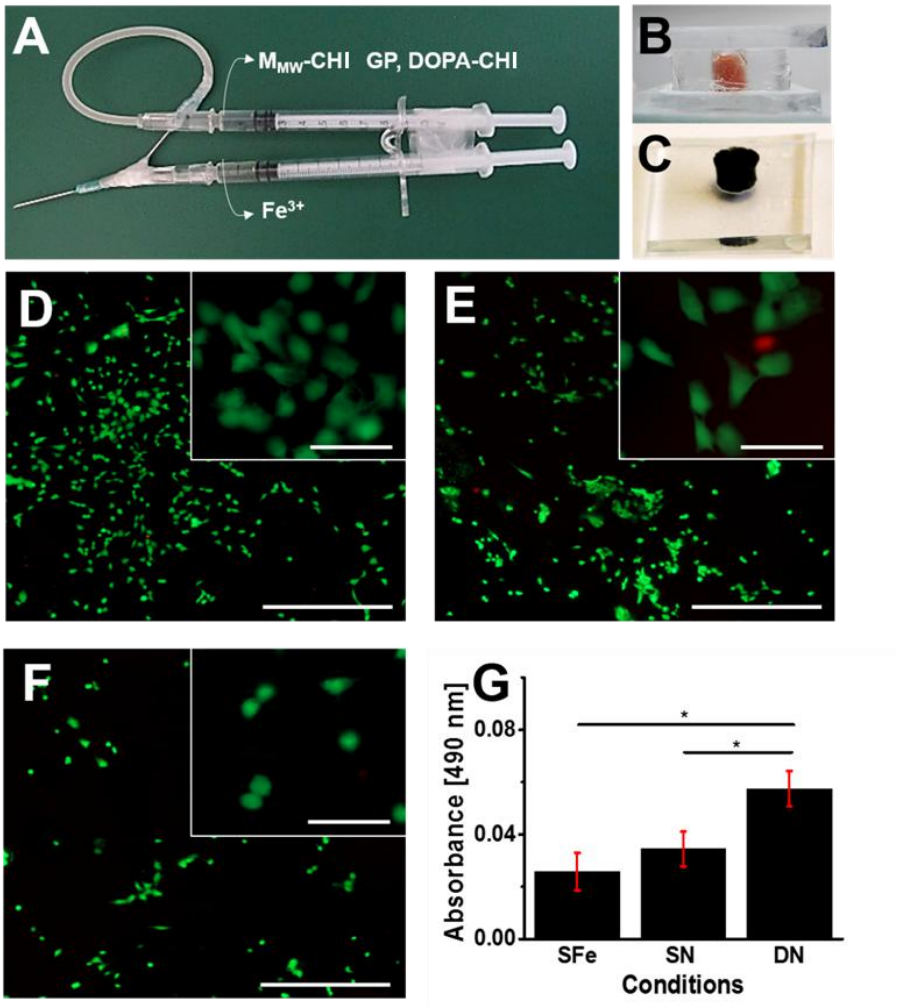

Figure 4.3 - (**A**) Double-syringe device engineered to combine the polymeric precursor solution with the Fe^{3+} ions. (**B**) DN hydrogel immediately after its injection into a PDMS mold and (**C**) after 2 h at 37 °C. LIVE/DEAD fluorescence images of ATDC5 cells seeded on top of (**D**) DN, (**E**) SN and (**F**) SFe hydrogels. Viable cells appear in green whereas dead cells are stained in red. The scale bar of the overview and the inset corresponds to 200 µm and 50 µm, respectively. (**G**) MTS assay results of SFe, SN and DN hydrogels using ATDC5 cell line.

The biomedical potential of DN 0.5% hydrogels was further explored by studying the possibility of using them as an injectable system and, hence, avoiding the drawbacks of highly invasive implantation techniques. The quick gelation within the syringe as result of the fast Fe^{3+}-mediated crosslinking was avoided by designing a double-channel syringe device, filling one channel with the precursor polymeric solution and the GP crosslinker, and the other with the Fe^{3+} ions (Movies S4.1 and S4.2 and Figure 4.3A). As previously described in literature [17,18], the Fe^{3+}-mediated crosslinking occurs in less than 8 seconds, making the gelation process faster and, hence, extremely relevant to achieve a fast *in situ* gelling and to prevent the earlier gel clearance from the defect [14b]. Moreover, it was found that the water uptake ability was lower for DN 0.5% hydrogels (62.65 ± 9.45%), which can further highlight its potential as an appropriate defect filling. (SI.4, Section 4.7).

The ability of the gels to interact with cells was assessed by seeding ATDC5 cells at the surface of one-day produced hydrogels. After seven days of incubation, the cell viability was higher for the DN hydrogels as proved by a higher number of living cells (around 91%) when comparing with SN (around 85%) and SFe (around 88%) conditions (Figure 4.3). The former results were supported by the MTS data, which follow the same trend (Figure 4.3G). Besides the mild processing conditions and the proved biocompatibility of the used polymer, this cytocompatibility may also be associated with the formation of a homogeneous structure with microscale features favorable to cell growth on DN hydrogels as visualized by SEM (SI.4, Section 4.8).

4. Conclusion

In summary, a set of innovative features were combined in a single DN hydrogel, namely (i) improved compressive strength and stiffness in the same order of magnitude as the ones found in native soft tissues, (ii) toughness and ability to recover it upon successive

compressive cyclic loads, (iii) self-healing behavior, (iv) injectability, (v) swelling adjusted to space-filling applications and (vi) cytocompatibility. Owing to their prominent character, such hydrogels may have applicability as regenerative medicine, waste treatment, superabsorbents and electronic devices.

Acknowledgements

This work was funded by FCT through the grant SFRH/BD/101748/2014, from the Danish Council for Independent Research | Technology and Production Sciences through grant 0602-02426B and from the Lundbeck Foundation through grant R180-2014-3468.

Supplementary information (SI.4)

S4.1. Characterization of DOPA functionalized chitosan (DOPA-CHI)

The grafting density was determined by UV-Vis spectroscopy using a DOPA-standard. To this end, the absorbance of aqueous solutions of the DOPA-CHI polymer was measured at 280 nm and the grafting density (g) was determined according to the equation (2):

$$g = \frac{n_{DOPA-side\,chain}}{n_{Monomer}} = \frac{M_{monomer}}{\frac{\varepsilon_{DOPA,B} \cdot L \cdot m_{total}}{A_B \cdot V} - M_{DOPA-side\,chain}} \quad (2)$$

The grafting density is related to the molar mass of the DOPA-CHI monomer ($M_{monomer}$) and DOPA group from side chain ($M_{DOPA-side\,chain}$), extinction coefficient of the B band of DOPA ($\varepsilon_{DOPA,B}$), path length of the cuvette used during UV-vis measurements (L), mass of the polymer in the stock solution (m_{total}), absorbance of the B band of DOPA (A_B) and volume of the stock solution (V). The absorption profile of the DOPA-CHI solutions ($g = 5\%$) was acquired to prove the incorporation of the catechol groups in the CHI backbone by the presence of two peaks (Figure S4.1). The data was obtained on a PerkinElmer Lambda 25 UV-Visible absorption spectrophotometer equipped with quartz cuvettes with 1 cm path length.

Regarding the tendency for catechol oxidation in a basic environment, no visible changes were verified over time. The metal redox activity (at low pH) can be considered negligible since the addition of iron ions occurs when the pH of the precursor solution was close to 7.

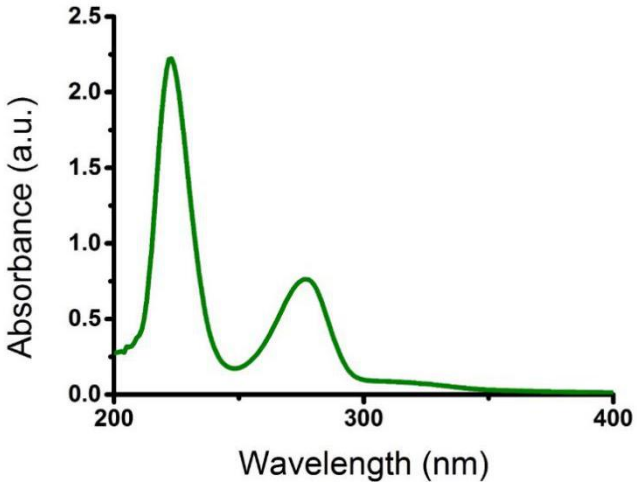

Figure S4.1 - Absorption profile of a 1.5 g/L solution of DOPA-CHI in H_2O. g = 5 %.

S4.2. Composition of all the formulations tested

All the hydrogel formulations tested in this work were summarized on Table S4.1.

Table S4.1 – Summary of all tested conditions, including the composition of each hydrogel formulation as well as the crosslinking mechanism employed.

	Composition				**Crosslinking Mechanism**	
	DOPA-CHI	*MMW-CHI*	*Fe^{3+}*	*GP*	*Covalent*	*Coordination*
SFe	✓		✓			✓
SC	✓			✓	✓	
DC	✓		✓	✓	✓	✓
SN	✓	✓		✓	✓	
DN	✓	✓	✓	✓	✓	✓

S4.3. Chemical characterization of the hydrogels – FTIR

Fourier Transformed Infrared Spectroscopy (FTIR) was performed with a Bruker Tensor-27 FTIR (resolution of 4 cm^{-1}) equipped with an Attenuated Total Reflection (ATR) accessory (Golden Gate Accessory, SPECAC). For each freeze-dried sample, 256 scans were collected.

FTIR assays were recorded from the M_{MW}-CHI, SFe hydrogel, SN hydrogel and DN hydrogel. As visualized in Figure S4.2, all spectra presented peaks at 897 and 1151 cm^{-1}, which have been assigned to the structure of CHI [29,30]. The other characteristic peak at around 1029 cm^{-1} is resulted from the C-O or/and C-N stretching.

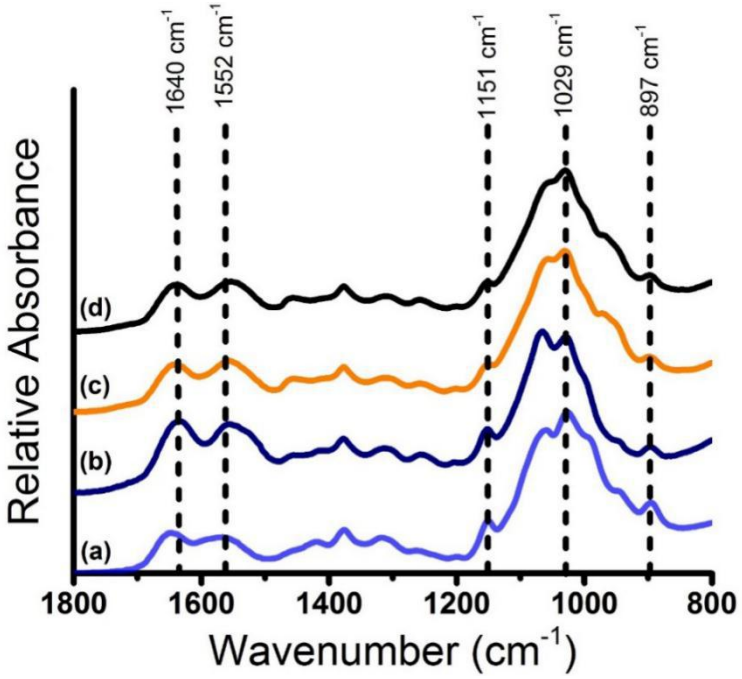

Figure S4.2 - FTIR spectra of (a) M_{MW}-CHI; (b) SFe hydrogel; (c) SN hydrogel and (d) DN hydrogel.

The crosslinking with GP can be confirmed by a band shifting of both peaks at 1552 cm^{-1} and 1640 cm^{-1}. The first peak moves slightly to lower wavenumbers and the second to higher, indicating the consumption of primary amine groups or the formation of secondary amide groups, respectively [31]. The DC hydrogel spectrum was not shown in Figure S4.2 due to its similarity with the spectrum of DN hydrogel.

S4.4. Mechanical characterization of the hydrogels – Uniaxial and Cyclic Assays

The mechanical properties of the hydrogel samples obtained using 0.5% GP and stored at 37 °C during 24 h are summarized in the Table S4.2.

Table S4.2 - Maximum compressive stress (σ_{max}), maximum compressive strain (ε_{max}) and modulus (E) of hydrogel samples with 0.5% GP.

Samples	σ_{max} **[MPa]**	ε_{max} **[%]**	E **[kPa]**
SFe	0.88 ± 0.11	> 90	1.64 ± 0.67
SC 0.5%	$5.33 \times 10^{-2} \pm 1.16 \times 10^{-2}$	47.83 ± 2.07	16.60 ± 2.10
DC 0.5%	1.05 ± 0.19	> 90	28.50 ± 2.09
SN 0.5%	$7.33 \times 10^{-2} \pm 1.16 \times 10^{-2}$	44.54 ± 1.28	25.20 ± 5.34
DN 0.5%	2.46 ± 0.34	> 90	49.60 ± 9.01

S4.5. Study of the energy dissipation in SFe, SC, DC and DN hydrogels

A possible explanation for the energy dissipation phenomenon observed after applying a compressive load in the produced hydrogels is illustrated in Figure S4.3.

In the control hydrogels, the applied load is only sustained by the chains near the zone were the fracture occurred, resulting in a low level of energy dissipation. Thus, the fracture can easily propagate within the hydrogel after the disruption of one catechol:Fe^{3+} bond (SFe hydrogel) or one of the polymer chains breaks (SC and SN hydrogels).

On the other hand, DC and DN hydrogels contain both covalent and non-covalent interactions, which cooperatively sustain the load to protect the overall structure. As result, in the case of DC hydrogels, the macroscopic propagation of the crack is delayed by a great energy dissipation over an extended area. Regarding the DN hydrogels, the presence of MMW-CHI allows an even more efficient energy transfer between the covalent network and the coordination crosslinks resulting in a synergy mechanism. As already reported for other DN systems [24a], it is believed that the disruption of catechol:Fe^{3+} bonds over a large area is the result of the energy transfer between the chemical and the physical networks. Consequently, the energy dissipation volume is the highest and the dissociation of neighbor catechol:Fe^{3+} bonds is extended and protects the covalent structure preventing the macroscopic failure of the hydrogel.

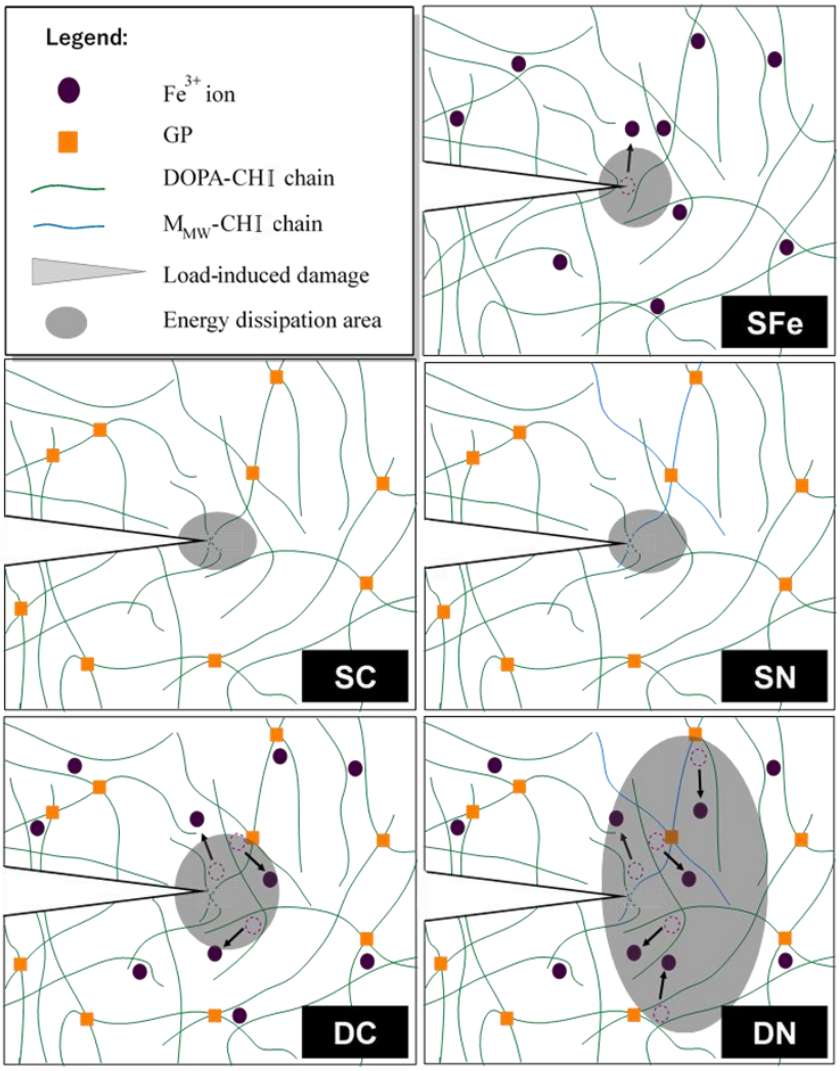

Figure S4.3 – Mechanisms of energy dissipation upon the formation of a damage. In the SFe hydrogel, only the coordination crosslinks crossing the fracture plan are unzipped and the iron crosslinks elsewhere remain intact. In the SC and SN hydrogels, the chains and crosslinks directly ahead of the crack are broken, whereas the remaining networks are undamaged. In the previous cases, the dissipation of energy occurs over a highly localized area. In the DC hydrogel, the crack propagation area is slightly enlarged by the presence of coordination crosslinks, which disassociate over a large zone, avoiding the rapid propagation of the crack. In the DN hydrogels, the efficient energy transfer between the MMW-CHI network and DOPA-CHI network, increases further the zone around the crack, where the DOPA-CHI chains were disentangled through the release of the Fe^{3+} ions.

S4.6. Evaluation of the self-healing ability of the produced hydrogels

Table S4.3 summarizes the results obtained using a rheometer to infer about the self-healing ability of the produced hydrogels.

The elastic modulus (*G'*) from the strain amplitude sweep test can be analyzed and a comparison between conditions can be established.

Table S4.3 - Rheological response of all the formulations tested in this work before and after the hydrogel rupture as well as the corresponding recovery time.

Samples	**G' [kPa]**		**Recovery time [min]**
	Before failure	*After failure*	
SFe	2.85	2.85	0
SC 0.5%	10.71	3.93	-
DC 0.5%	16.75	16.75	8
SN 0.5%	17.66	6.33	-
DN 0.5%	26.29	25.61	15

S4.7. Study of the water uptake by the hydrogels

Water uptake studies were performed on as-prepared cylindrical hydrogels after an incubation period of 24 h at 37 °C. Firstly, three specimens of each condition were weightd to determine the initial weight (m_i). Thereafter, gel samples were immersed in deionized water during 7 days at RT. At pre-defined time points, samples were removed from water, blotted with a paper filter to remove the excess surface water and weighed (m_f). The swelling percentage was determined according the equation (3):

$$\mathrm{SP}(\%) = \frac{m_f - m_i}{m_i} \times 100 \qquad (\mathbf{3})$$

The DN structure showed a lower water uptake of about 62.65 ± 9.45% comparing with the other conditions. In fact, the DN hydrogels are higher crosslinked networks, which hinders the entry of water into the structure. On the other hand, the water uptake of SFe hydrogels was higher (556.14 ± 72.80 %) since there is lower crosslinking density, facilitating further the swelling of the structure.

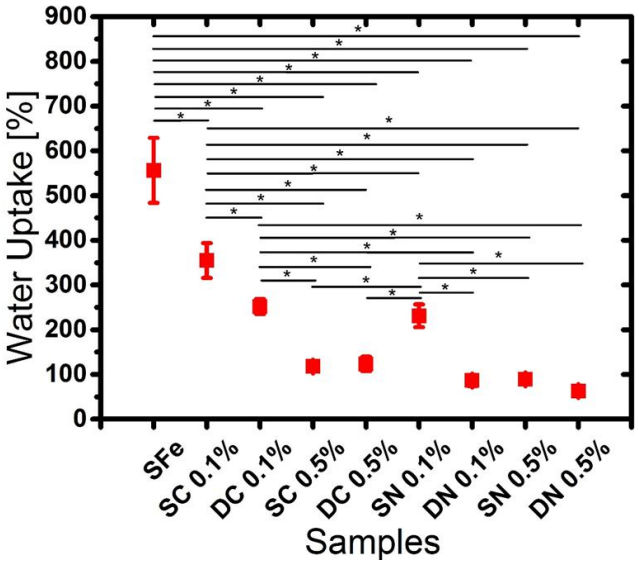

Figure S4.4 - Water uptake [%] by one-day prepared hydrogels corresponding to all the conditions tested under this study.

Moreover, the amount of water contained in the as-prepared hydrogels was also assessed using the equation (4):

$$Water\ content\ (\%) = \frac{Wet\ weight - Dry\ weight}{Wet\ weight} \times 100 \qquad (4)$$

, the wet sample weight corresponds to the initial weight of the hydrogel after 24 h at 37 °C. Dry sample weight was measured after freeze-drying each sample. All conditions exhibited a water content of *ca.* 86.09 ± 5.43 %.

S4.8. Study of the morphology of the SFe, DC and DN hydrogels

DN, DC and SFe hydrogels were analyzed in terms of their morphology and elemental chemical composition resorting to a Scanning Electron Microscope (SEM, JSM-6010LV, JEOL, Japan) and an Energy-Dispersive X-Ray Spectroscopy (EDS), respectively. Briefly, 24 h after production, the samples were dehydrated in solutions with increased concentrations of absolute ethanol, namely 20, 40, 60, 70, 80, 90, 95 and 100%. Subsequently, they were further subjected to a drying process on a critical point dryer (Autosamdri-815, Series A). The hydrogels were, then, cut in liquid nitrogen to reveal the cross-sectional surface. EDS profile was obtained over a line drawn in the middle section – see Figure S4.5 A2, B2 and C2. As expected, the chemical elements carbon (C), oxygen (O) and nitrogen (N) from the M_{MW}-CHI and DOPA-CHI, as well as iron (Fe) and chlorine (Cl) from $Cl_3Fe.6H_2O$ were found in all the spectra. Phosphate (P) could only be found in DN hydrogels since this hydrogel contains β-GP, which was used to neutralize the M_{MW}-CHI solution in the preparation of DN hydrogels.

For the SEM images, the hydrogels were exposed to platinum sputter-coating. The images were acquired in high vacuum using the signal of the secondary electrons, and employing an accelerating voltage of 10 kV and a working distance of 11 mm. As can be seen in Figure S4.5 A1, B1 and C1, all hydrogels presented a homogeneous morphology. In addition, DN hydrogels revealed associated globular like elements with sizes around 1 µm.

Movie S4.1. Injection of the precursor solution of the DN hydrogel inside a PDMS mold; and **Movie S4.2.** Removal of the DN hydrogel from the PDMS mold 2 h after its preparation are online available using DOI: 10.1002/adma.201700759.

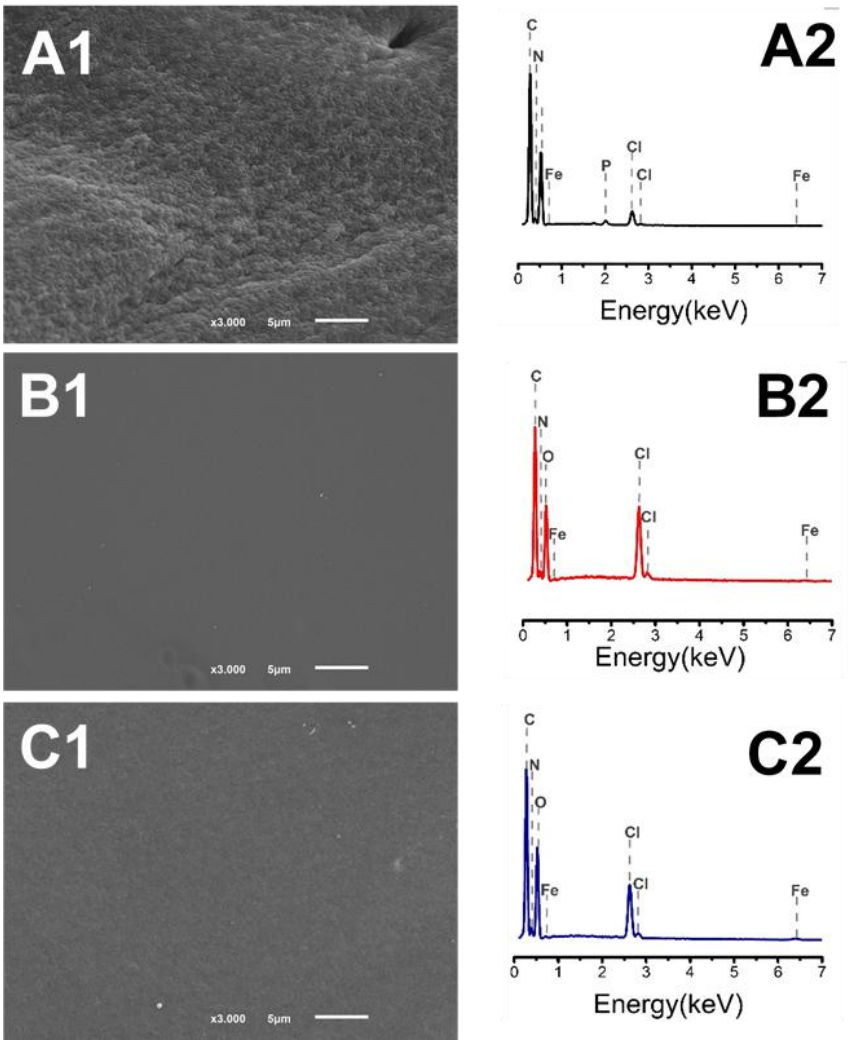

Figure S4.5 - SEM images (**A1**, **B1**, **C1**) and EDS profiles (**A2**, **B2**, **C2**) corresponding to the cross sections of the DN hydrogel (**A1**) (**A2**), DC hydrogel (**B1**) (**B2**) and SFe hydrogel (**C1**) (**C2**). The scale bar of the SEM images corresponds to 500 μm.

References

[1] a) N. Annabi, A. Tamayol, J. A. Uquillas, M. Akbari, L. E. Bertassoni, C. Cha, G. Camci-Unal, M. R. Dokmeci, N. A. Peppas, A. Khademhosseini, 25th anniversary article: Rational design and applications of hydrogels in regenerative medicine, *Adv. Mater.* **2014**, 26, 85; b) A. M. S. Costa, J. F. Mano, Extremely strong and tough hydrogels as prospective candidates for tissue repair–A review, *Eur. Polym. J.* **2015**, 72, 344.

[2] H. Jia, Z. Li, X. Wang, Z. Zheng, Facile functionalization of a tetrahedron-like PEG macromonomer-based fluorescent hydrogel with high strength and its heavy metal ion detection, *J. Mater. Chem. A* **2015**, 3, 1158.

[3] B. H. Cipriano, S. J. Banik, R. Sharma, D. Rumore, W. Hwang, R. M. Briber, S. R. Raghavan, Superabsorbent hydrogels that are robust and highly stretchable, *Macromolecules* **2014**, 47, 4445.

[4] S. Lin, H. Yuk, T. Zhang, G. A. Parada, H. Koo, C. Yu, X. Zhao, Stretchable hydrogel electronics and devices *Adv. Mater.* **2016**, 28, 4497.

[5] J. P. Gong, Y. Katsuyama, T. Kurokawa, Y. Osada, Double - network hydrogels with extremely high mechanical strength, *Adv. Mater.* **2003**, 15, 1155.

[6] D. L. Taylor, M. in het Panhuis, Self - healing hydrogels, *Adv. Mater.* **2016**, 28, 9060.

[7] Z. Wei, J. H. Yang, J. Zhou, F. Xu, M. Zrínyi, P. H. Dussault, Y. Osada, Y. M. Chen, Self-healing gels based on constitutional dynamic chemistry and their potential applications, *Chem. Soc. Rev.* **2014**, 43, 8114.

[8] S. R. White, N. R. Sottos, P. H. Geubelle, J. S. Moore, M. R. Kessler, S. R. Sriram, E. N. Brown, S. Viswanathan, Autonomic healing of polymer composites, *Nature* **2001**, 409, 794.

[9] a) X. Xing, L. Li, T. Wang, Y. Ding, G. Liu, G. Zhang, A self-healing polymeric material: from gel to plastic, *J. Mater. Chem. A* **2014**, 2, 11049; b) Q. Chen, L. Zhu, H. Chen, H. Yan, L. Huang, J. Yang, J. Zheng, A novel design strategy for fully physically linked double network hydrogels with tough, fatigue resistant, and self - healing properties, *Adv. Funct. Mater.* **2015**, 25, 1598; c) X. Li, Q. Yang, Y. Zhao, S. Long, J. Zheng, Dual physically crosslinked double network hydrogels with high toughness and self-healing properties, *Soft Matter* **2017**, 13, 911; d) S. Liu, L. Li, Recoverable and self-healing double network hydrogel based on κ-carrageenan, *ACS Appl. Mater. Interfaces* **2016**, 8, 29749; e) N. Yuan, L. Xu, H. Wang, Y. Fu, Z. Zhang, L. Liu, C. Wang, J. Zhao, J. Rong, Dual physically cross-linked double network hydrogels with high mechanical strength, fatigue resistance, notch-insensitivity, and self-healing properties. *ACS Appl. Mater. Interfaces* **2016**, 8, 34034.

[10] a) J. F. Mano, G. A. Silva, H. S. Azevedo, P. B. Malafaya, R. A. Sousa, S. S. Silva, L. F. Boesel, J. M. Oliveira, T. C. Santos, A. P. Marques, N. M. Neves, R. L. Reis, Natural origin biodegradable systems in tissue engineering and regenerative medicine: present status and some moving trends, *J. R. Soc. Interface* **2007**, 4, 999; b) L. Yu, J. Ding, Injectable hydrogels as unique biomedical materials, *Chem. Soc. Rev.* **2008**, 37, 1473.

[11] R. Cheung, T. Ng, J. Wong, W. Chan, Chitosan: an update on potential biomedical and pharmaceutical applications, *Mar. Drugs* **2015**, 13, 5156.

[12] J. Sedõ, J. Saiz-Poseu, F. Busqué, D. Ruiz-Molina, Catechol - based biomimetic functional materials, *Adv. Mater.* **2013**, 25, 653.

[13] T.-C. Tseng, L. Tao, F.-Y. Hsieh, Y. Wei, I.-M. Chiu, S. Hsu, An injectable, self - healing hydrogel to repair the central nervous system, *Adv. Mater.* **2015**, 27, 3518.

[14] a) C. Fan, J. Fu, W. Zhu, D.-A. Wang, A mussel-inspired double-crosslinked tissue adhesive intended for internal medical use, *Acta Biomater.* **2016**, 33, 51; b) J. Xu, S. Strandman, J. X. X. Zhu, J. Barralet, M. Cerruti, Genipin-crosslinked catechol-chitosan mucoadhesive hydrogels for buccal drug delivery, *Biomaterials* **2015**, 37, 395.

[15] A. M. Prodan, S. L. Iconaru, C. S. Ciobanu, M. C. Chifiriuc, M. Stoicea, D. Predoi, Magnetic Properties and Biological Activity Evaluation of Iron Oxide Nanoparticles, J. *Nanomater.* **2013**, 2013, 1.

[16] a) G. Fessel, J. Cadby, S. Wunderli, R. van Weeren, J. G. Snedeker, Dose-and time-dependent effects of genipin crosslinking on cell viability and tissue mechanics–toward clinical application for tendon repair, *Acta Biomater.* **2014**, 10, 1897; b) R. Muzzarelli, M. El Mehtedi, C. Bottegoni, A. Aquili, A. Gigante, Genipin-crosslinked chitosan gels and scaffolds for tissue engineering and regeneration of cartilage and boné, *Mar. Drugs* **2015**, 13, 7314.

[17] M. Krogsgaard, M. a. Behrens, J. S. Pedersen, H. Birkedal, Self-healing mussel-inspired multi-pH-responsive hydrogels, *Biomacromolecules* **2013**, 14, 297.

[18] M. Krogsgaard, M. R. Hansen, H. Birkedal, Metals & polymers in the mix: fine-tuning the mechanical properties & color of self-healing mussel-inspired hydrogels, *J. Mater. Chem. B* **2014**, 2, 8292.

[19] Signini R., and Campana Filho S. P., On the preparation and characterization of chitosan hydrochloride, *Polymer Bulletin* **1999**, 42, 159.

[20] M. J. Moura, M. M. Figueiredo, M. H. Gil, Rheological study of genipin cross-linked chitosan hydrogels, *Biomacromolecules* **2007**, 8, 3823.

[21] Y. Yao, Y. Wang, ATDC5: an excellent in vitro model cell line for skeletal development, *J. Cell. Biochem.* **2013**, 114, 1223.

[22] T. L. Riss, R. A. Moravec, A. L. Niles, S. Duellman, H. A. Benink, T. J. Worzella, L. Minor, Cell Viability Assays, Assay Guid. Man. **2004**.

[23] A. J. Salgado, O. P. Coutinho, R. L. Reis, Novel starch-based scaffolds for bone tissue engineering: cytotoxicity, cell culture, and protein expression, *Tissue Eng.* **2004**, 10, 465.

[24] a) J.-Y. Sun, X. Zhao, W. R. K. Illeperuma, O. Chaudhuri, K. H. Oh, D. J. Mooney, J. J. Vlassak, Z. Suo, Highly stretchable and tough hydrogels, *Nature* **2012**, 489, 133; b) Q. Chen, H. Chen, L. Zhu, J. Zheng, Fundamentals of double network hydrogels, *J. Mater. Chem. B* **2015**, 3, 3654.

[25] a) D. G. Barrett, D. E. Fullenkamp, L. He, N. Holten-Andersen, K. Y. C. Lee, P. B. Messersmith, pH - Based Regulation of Hydrogel Mechanical Properties Through Mussel - Inspired Chemistry and Processing, *Adv. Funct. Mater.* **2013**, 23, 1111. b) A. M. S. Costa, J. F. Mano, Highly robust hydrogels via a fast, simple and cytocompatible dual crosslinking-based process, *Chem. Commun.* **2015**, 51, 15673.

[26] a) U. Gulyuz, O. Okay, Self-healing poly (acrylic acid) hydrogels with shape memory behavior of high mechanical strength, *Macromolecules* **2014**, 47, 6809; b) Z. Wei, J. H. Yang, Z. Q. Liu, F. Xu, J. X. Zhou, M. Zrínyi, Y. Osada, Y. M. Chen, Novel biocompatible polysaccharide - based self - healing hydrogel, *Adv. Funct. Mater.* **2015**, 25, 1352; c) I. Jeon, J. Cui, W. R. K. Illeperuma, J. Aizenberg, J. J. Vlassak, Extremely stretchable and fast self - healing hydrogels, *Adv. Mater.* **2016**, 28, 4678.

[27] a) A. Argun, M. P. Algi, D. C. Tuncaboylu, O. Okay, Surfactant-induced healing of tough hydrogels formed via hydrophobic interactions, *Colloid Polym. Sci.* **2014**, 292, 511; b) S. Li, H.-Y. Lu, Y. Shen, C.-F. Chen, A Stimulus - Response and Self - Healing Supramolecular Polymer Gel Based on Host–Guest Interactions, *Macromol. Chem. Phys.* **2013**, 214, 1596.
[28] a) G. Li, H. Zhang, D. Fortin, H. Xia, Y. Zhao, Poly (vinyl alcohol)–poly (ethylene glycol) double-network hydrogel: a general approach to shape memory and self-healing functionalities, *Langmuir* **2015**, 31, 11709; b) M. Ahmadi, L.G.D Hawke, H. Goldansaz, E. van Ruymbeke, Dynamics of entangled linear supramolecular chains with sticky side groups: Influence of hindered fluctuations, *Macromol.* **2015**, 48, 7300.
[29] M. F. Butler, Y.-F. Ng, P. D. A. Pudney, Mechanism and kinetics of the crosslinking reaction between biopolymers containing primary amine groups and genipin, *J. Polym. Sci. Part A Polym. Chem*. **2003**, 41, 3941.
[30] F.-L. Mi, H.-W. Sung, S.-S. Shyu, C.-C. Su, C.-K. Peng, Synthesis and characterization of biodegradable TPP/genipin co-crosslinked chitosan gel beads, *Polymer (Guildf).* **2003**, 44, 6521.
[31] J. Kawadkar, M. K. Chauhan, Intra-articular delivery of genipin cross-linked chitosan microspheres of flurbiprofen: preparation, characterization, in vitro and in vivo studies, *Eur. J. Pharm. Biopharm.* **2012**, 81, 563.

Chapter V: Final Remarks

DN methodology was used to fabricate, for the first time, robust hydrogels from a single polymeric precursor formulation and under physiological conditions. The resultant engineered systems were described in Chapter III and combined a set of interesting features for load-bearing purposes. They were able to: (i) sustain a compressive strength in the MPa range as the ones found in native soft tissues, (ii) recover its original structure upon successive cyclic loads, and (iii) encapsulate cells with high viability rates. These highly hydrated DN networks were further improved in Chapter IV to also include the ability to: (iv) quick self-heal upon rupture and (iv) be administered through minimal invasive techniques such as by injection.

In this thesis, the conventional DN methodology was altered by combining chemical and physical crosslinking mechanisms using the same macromolecule to produce both polymer networks. Contrary to chemical crosslinks, physical crosslinks can reversibly associate/dissociate in response to an applied load, resulting in hydrogels with high toughness as well as with the ability to recover their mechanical properties via bond reformation. Additionally, with the present technology, both polymer components were mixed together in a single hydrogel precursor solution, resulting in a fast, simple and reproducible process with the additional advantage of enabling cell encapsulation with high viability rates.

1. General Conclusion of the main results of Chapter III and IV

In Chapter III, robust DN hydrogels were fabricated using two CHI derivatives, namely low molecular weight methacrylamide CHI (MACHI) and medium molecular weight CHI (CHI), and a dual-crosslinking process by: (1) UV-light exposure of the methacrylic groups on MACHI, forming a covalently crosslinked network and (2) immersing the resultant hydrogel in a solution containing negatively-charged tripolyphosphate (TPP) ions to ionically crosslink CHI through

their positively-charged amine groups (Figure 5.1, Chapter III). Under optimized conditions, the obtained CHI DN structures were able to withstand an outstanding compressive strength of *ca.* 19.5 MPa without fracture, which is several orders of magnitude higher than those of their individual networks. It was concluded that the MACHI network is responsible for providing the hydrogel strength, whereas the MMW-CHI structure its high deformation ability, contributing to the simultaneous elastic and tough behavior of these CHI DN hydrogels. Worth noticing, the resultant mechanical properties were the highest ever achieved for hydrogels made only of polysaccharides and even higher than other DN hydrogels partially composed of natural-origin polymers.

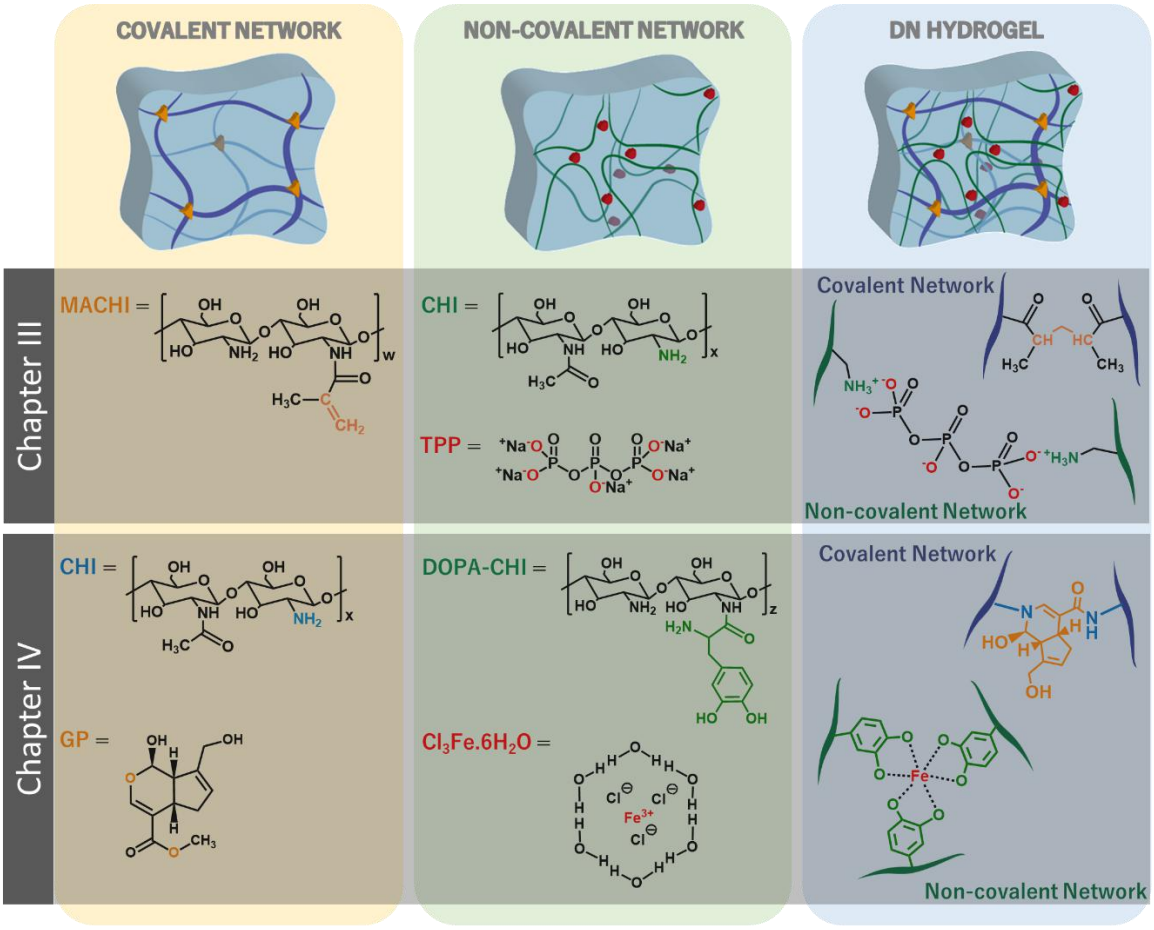

Figure 5.1 - Graphical overview of the designed CHI DN hydrogels reported in this thesis.

The effective energy dissipation of the developed CHI DN hydrogel was proved by the presence of a pronounced hysteresis in the loading and unloading curves, being directly related to the toughness of the material. These hydrogels were able to autonomously recover almost completely their initial mechanical properties upon a loading/unloading cycle up to 50%, which is of outmost importance for repairing structural soft tissues that are continuously subjected to stresses. Moreover, cells with high viability rates were uniformly distributed within the CHI DN hydrogels, proving the cytocompatible character of the developed strategy and emphasizing its potential to create cell-laden artificial substitutes of native soft-tissues.

Despite the extraordinary mechanical performance of the CHI DN hydrogels described in Chapter III, the resultant structures were not able to repair themselves after fracture similar to what happens with other DN-hydrogels described in literature. The self-healing ability is essential for load-bearing applications to not only prolong the material lifetime but also to increase its durability and safety by avoiding failures caused by the accumulation of cracks. Therefore, the motivation for the work presented in Chapter IV was to develop a simple, fast and cytocompatible methodology to prepare simultaneously highly robust, with strength values in MPa order, and self-healable natural-based hydrogels with potential to be injected into the body. Similarly to Chapter III, CHI polymer and a combination physical and chemical crosslinks was also employed to produce these DN hydrogels (Figure 5.1, Chapter IV). The differences were that the low molecular weight MACHI derivative was replaced by a low molecular weight DOPA-functionalized CHI and two different crosslinking mechanisms were used instead, namely (i) a covalent process using GP as a cytocompatible chemical crosslinker of MMW-CHI free amine groups and (ii) a non-covalent one through coordination bonds between the catechol groups present in DOPA-CHI and Fe^{3+} ions. Under optimized conditions, the resultant DN structures did not fracture for strain as high as 90% and reached a compressive strength of approximately 2.46 MPa exceeding their single-networks counterparts. Additionally, the introduction of coordination bonds conferred not only an increased toughness but also a self-

healing ability. Five minutes after cutting in half these DN CHI hydrogels, it was observed the recovery of its initial structure since no signs of the cut were noticed. In contrast with other healing mechanisms, this recovery occurs rapidly, under mild conditions and autonomously without the demand for any external and potential harmful stimulus to trigger the healing process. To investigate in more detail the self-healing ability, a dynamic oscillatory rheometer was used to determine the recovery rate. The results showed that the DN hydrogel recovered its initial storage modulus (G') after 15 min.

This one-pot methodology potentiates their injectability, which may be relevant to fabricate hydrogels with specific shapes or to administer them through a minimal invasive manner. As the Fe^{3+}-mediated crosslinking occurs in less than 8 seconds, it is expected a fast *in situ* gelling, which may prevent the earlier gel clearance from the defect. The developed hydrogels also showed a low degree of swelling, which is relevant as swelling severely weakens the hydrogels mechanical behavior and can compromise the surrounding tissues, highlighting its potential as an appropriate defect filling. Finally, its cytocompatibility character was proved, being ascribed to the mild processing conditions employed, the well-stated biocompatibility of the materials used and to the formation of a homogeneous structure with topological features favorable to cell growth.

Although the aim of both works was to develop a simple methodology to fabricate mechanically robust hydrogels under mild conditions, these studies allowed to answer more fundamental questions such as - which are the essential parameters to attain a DN hydrogel using the same polysaccharide in both polymeric networks and which is the role of each structure on the overall mechanical properties. It was concluded that it is necessary to combine, using an optimal ratio, two polymer derivatives with contrasting molecular weights, and to employ two distinct crosslinked networks: one based on physical interactions and other on chemical bonds.

2. Future perspectives on the use of natural-based DN hydrogels

The described experimental works provide a new methodology to produce highly robust hydrogels using a single polymeric precursor solution under mild conditions. It is envisioned that this one-pot methodology could be used to produce other DN-hydrogels made of other macromolecules and employing various crosslinking mechanisms.

2.1. Potential applications of the developed systems

Owing to their outstanding mechanical properties and their simple, fast and reproducible fabrication process, hydrogels devices like these ones could have a broad applicability not only for biomedical purposes but also, for example, as waste treatment, superabsorbent and electronic devices for agriculture and electronics.

Based on their cytocompatibility, injectability and self-healing ability, such multifunctional hydrogel devices could potentially be used for the repair of load-bearing soft structural tissues such as cartilage, skin, spinal disks, blood vessels, muscles and tendons. The importance of materials with superior mechanical properties for the repair of these body tissues comes from the possibility to withstand high loads and, simultaneously, ensure a mechanical harmonization with the surrounding tissues to encourage an optimal load distribution.

Moreover, due to the mild conditions employed during their synthesis, these materials could also be envisioned for other biomedical purposes, such as soft actuators, wound dressings or as an encapsulation platform for a variety of biological applications, such as disease modeling for drug screening and therapies in a more realistic mechanical environment.

2.2. Further biocompatibility assays

The previously described works focused on the materials design and mechanical characterization, but more assays will be needed before implementing them to repair load-

bearing soft tissues such as cartilage. In this thesis, the cytocompatibility of the obtained hydrogels was studied, but further biocompatibility assays must be performed to ensure the *in vivo* safety of the obtained biomaterials. After proving its totally biocompatible character, these materials could be used to repair defects of injured load-bearing tissues. Furthermore, tissue engineering approaches could also be employed by encapsulating, for example stem cells, and growth factors within the produced materials. This last strategy would be advantageous on the integration of the materials with the body tissues and on its associated repair efficiency.

2.3. Combination of other relevant features for the repair of load-bearing tissues

Further alterations on the developed CHI DN hydrogels will be needed to meet the required criteria for a specific purpose, for instance:

2.3.1. Enhanced cell-adhesion

To boost both the cell adhesion and proliferation, the incorporation of bioactive motifs such as RGD (Arginine-Glycine-Aspartic Acid), which is recognized by integrin receptors on cellular membrane, could be envisaged. However, obtaining peptides with high degrees of purification constitutes a very expensive and extremely daunting process. Therefore, natural polymers such as gelatin, which is derived from an ECM component, may be used as a cost-effective alternative since it contains ligands that engage receptors on cells.

2.3.2. Responsiveness to stimulus

Versatile chemical structures can be obtained by modifying the high number of functional groups present along the backbone of natural-origin polymers, resulting in materials with improved characteristics for a specific application while retaining their crucial biological features. For instance, when exposed to an environmental signal such as temperature and pH, some sensitive hydrogels can respond and translate this stimulus into a macroscopic event. These smart materials could be developed by functionalizing the resultant biomaterials with

specific functional groups to better mimic the native tissues or to be applied as sensors, actuators or smart drug release devices.

2.3.3. Body-tissue adhesiveness

Besides the material properties, the integration of biomaterials with the surrounding environment also needs to be consider in order to ensure their optimal performance. For instance, further studies on the ability of these DN hydrogels to adhere through permanent bonding or reversible attachment to other surfaces are required. Although the adhesive character of the produced hydrogels was not assessed in this thesis, it is expected that the dynamic phenolic ligands present on DOPA-CHI derivative and the charged polymer backbone could confer this additional feature, enabling the resultant hydrogel to adhere to the tissues surrounding the injury. Importantly, these moieties have also been pointed as promoters of underwater adhesion, which is relevant for biomedical applications that require a wet environment such as in the designing of artificial organs and underwater soft robotics. The overall bonding strength of hydrogels is dependent on both adhesive and cohesive individual strengths, which could be enhanced by functionalizing the materials with stronger adhesive functional groups or by introducing energy dissipation mechanisms, respectively. The typical poor adhesion of hydrogels in their fully swollen state is associated with the formation of a water film at its interface. Therefore, the hydrogel surface could also be modified to promote the water drainage between to two approaching surfaces by, for instance, creating a macroscale roughness.

2.3.4. Mechanical assays

Load-bearing body tissues are constantly subjected to consecutive, high-level loading-unloading processes through a large variety of mechanical stimulus, including compression, torsion, bending and elongation. In this thesis, the mechanical performance of the developed CHI DN hydrogels was studied by performing uniaxial and cyclic compressive assays. The

obtained results could be used to predict the behavior of the developed biomaterials as artificial substitutes of cartilage, for example. Future improvements could include assessing the behavior of these systems under other types of deformation such as tensile, which could allow their application to repair soft-tissues like tendon and blood vessels, which are continuously exposed to large tensile forces. Although the DN approach affords the highest versatility in terms of composition and resulting properties, a combination of different strategies such as the ones described in Chapter I should also be envisaged as this could result in hydrogels with improved mechanical and biological properties.

2.3.5. Mimicking the ECM complex structure

Body tissues exhibit a well-defined and complex structure, which has been associated with their outstanding mechanical properties. In this regard, the control over the material structure at all levels of hierarchy is also extremely important for the construction of bio-tissues substitutes. Having this in mind, by replacing the non-ordered, homogeneous structure of the obtained CHI DN hydrogels by a well-developed hierarchical structure could potentially yield artificial substitutes of the native tissues with outstanding mechanical performance. Moreover, this defined organization may have beneficial biological features such as the promotion of cell infiltration and neovascularization.

2.3.6. Biodegradability

Although the hypothesis of this work was proved, the control over the biomaterial's degradation needs to be evaluated in order to enable the use of these DN hydrogels for the repair of structural soft tissues. In fact, the study of the degradation behavior of tough DN hydrogels is still in its infancy. Regarding the CHI DN hydrogels developed, it is known that CHI can be both enzymatic and chemically degraded. The first process could be the result of the enzymatic action of lysozyme whereas the chemical degradation can occur, for instance, in the stomach due to an acid-catalyzed degradation process. It has already been reported other

mechanisms of CHI degradation through oxidation-reduction and free radical degradation, but they are unlikely to play a significant role in the *in vivo* degradation.

Besides these degradation mechanisms, the material degradability could be tuned by introducing labile bonds either on the polymer backbone or on the crosslinkers used to create the hydrogels, which could be later enzymatic or chemically broken under physiological conditions. Moreover, the non-cytotoxicity of the degradation products should also be studied.

SECTION 2

Superantiwetting Platforms to produce Spherical-Shaped Particles

Chapter VI: Introduction

Superantiwetting Platforms to produce Spherical-Shaped Particles

1. Introduction

During evolution, distinct biological systems were advanced to provide specific functions to organisms, allowing their adaptation to the surrounding environment and, ultimately, their survival [1]. Lotus leaf is the most well-known example of a water-repellent natural structure. This unique property is due to the presence of a hierarchical micro- and nanostructure, composed of branch-like nanostructures on the top of micropapillae, and a thin layer of an epicuticula wax, which contains non-polar methyl groups. This isotropic superhydrophobic (SH) surface allows the water droplets to easily roll off, carrying with them several contaminants [2]. Interestingly, butterfly wings are one example of an anisotropic SH surface as their self-cleaning mechanism, which is also mediated by the movement of droplets on their surface, can follow a preferential direction [3]. In the case of desert beetles, they use their structures with extreme wettability to collect water from the atmosphere and, consequently, to resist the extreme conditions of their environment [4].

Inspired by the spherical shape acquired by water droplets on the top of lotus leaves, our group developed a novel biomimetic strategy using SH surfaces as platforms to produce hydrogel spheres [5]. This particular shape is the most widely used geometry in the biomedical field to create cell and drugs containers [6]. The main advantage of using spherical objects is related with their mass-transport mechanism as they provide an optimal surface-to-volume ratio for the diffusion of molecules [7].

In this chapter, it will be discussed how surfaces with extreme wettabilities, namely SH and superamphiphobic (SA) surfaces, can be used to produce spherical polymeric particles.

2. Overview of the methodology to fabricate spherical-shaped particles above superantiwetting surfaces

This technique consists in dispensing a polymeric precursor solution onto a superantiwetting surface, in which the liquid droplet acquires a spherical shape. Afterwards, a crosslinking mechanism is applied to retain this shape and obtain a polymeric particle [8]. In order to implement this biomimetic strategy, one requires a: (1) a polymeric precursor solution, which may also contain other molecules such as bioactive agents and/or cells; (2) a dispensing mechanism, which typically consists in using a micropipette; (3) a surface with extreme wettability such as SH and SA surfaces; and (4) a crosslinking and/or an evaporation methodology to harden the polymeric precursor solution into a hydrogel and/or a solid polymeric particle, respectively (Figure 6.1).

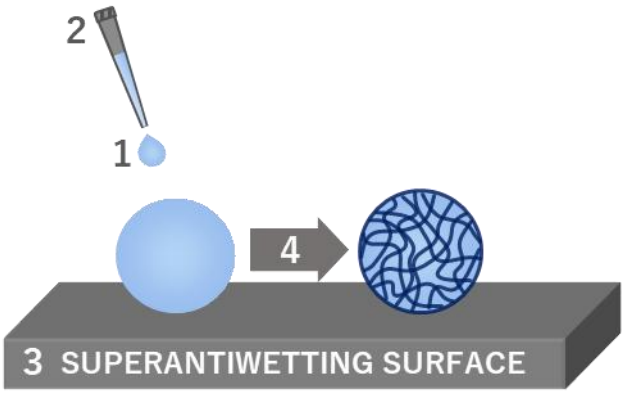

Figure 6.1 - Schematic representation of the strategy to fabricate spherical hydrogel or solid polymeric particles above a superantiwetting surface, which requires a: **1)** polymeric precursor solution; **2)** dispensing mechanism; **3)** liquid-repellent substrate; and **4)** crosslinking and/or evaporation process.

Comparing with the conventional technologies, the main advantages of using this innovative method to produce hydrogel particles are its: (i) highly cost-effectiveness due to the simplicity of the process, which does not require sophisticated and complex equipment; (ii) environmental-friendly nature as there are no waste residues or need for toxic organic solvents

or materials; (iii) encapsulation efficiency of ≈ 100% owing to the negligible contact area between the surface and the droplet as well as to the air-liquid interface in which the particles are produced, avoiding the use of a surrounding liquid medium from where the encapsulated molecules may diffuse and be lost; (iv) mild processing conditions, arising from the absence of extreme environmental settings such as high temperatures and mechanical stresses, which may hamper the encapsulation of sensitive molecules or living cells; (v) narrow particle size distribution due to the control over the volume of the polymeric precursor solution dispensed; (vi) absence of particle aggregation, which is the result of combining the high repellence of the substrates with individual crosslinking of the resultant polymeric droplets; and (vii) versatility, which allows the production of particles made from a wide range of materials and crosslinking mechanisms [5,8].

3. Designing principles for obtaining substrates with extreme wettability

Over the past decades, several methodologies have been purposed aiming in producing biomimetic surfaces with extreme wettability [9]. These works, which resulted from the intense and detailed analysis of some of the previously described natural structures, revealed that the superantiwetting ability is due to the cooperation between the: (i) surface roughness, typically a hierarchical topography with features at both micro- and nano levels and the (ii) surface chemistry, mainly obtained by a low surface energy [10]. This knowledge resulted in the design and production of novel superantiwetting surfaces such as SH and SA substrates.

3.1. Some useful theoretical principles related with wettability

Surface wettability characterizes what happens when a liquid droplet is brought into contact with a substrate [11]. Under static conditions, this parameter is evaluated by the apparent contact angle (CA, θ), which is the angle at which the liquid droplet joins the solid surface over the three-phase contact line (Figure 6.2, A). Based on the obtained value, if the

CA is lower than 90°, the surface is classified as wettable, which is typically associated with high values of surface energy ranging from 500 and 5000 mNm^{-1}. By contrast, if the CA is higher than 90°, the surface is called non-wettable and their associated low surface energy value may vary between 10 to 50 mNm^{-1} [12]. For the specific case, in which the liquid is water, the surface can be designated as superhydrophilic, hydrophilic, hydrophobic or superhydrophobic, according to the obtained CA value (Figure 6.2, C).

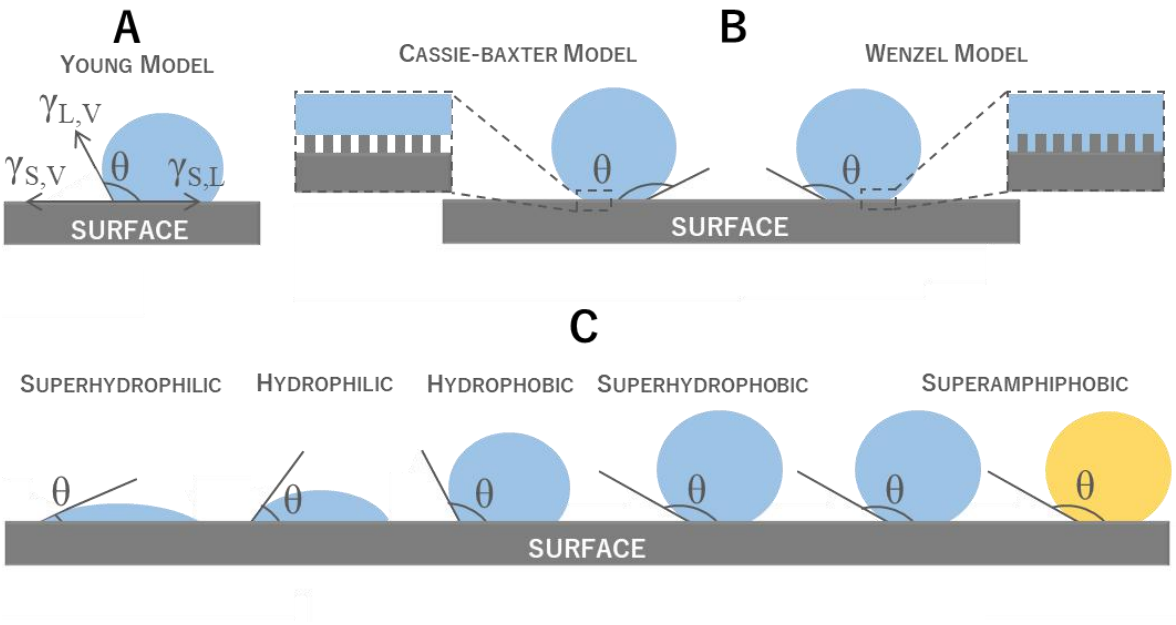

Figure 6.2 - A) The Young model relates the contact angle (θ) with the interfacial tensions: solid/liquid (S,L), liquid/vapor (L,V), solid/vapor (S,V) for an ideal smooth surface. **B)** Both Cassie-Baxter and Wenzel models take into consideration surface roughness. **C)** A surface can be denominated as superhydrophilic, hydrophilic, hydrophobic, superhydrophobic and superamphiphobic, if the θ is lower than 10°, lower than 90°, higher than 90°, higher than 150°, higher than 150° for both water (represented by a blue circle) and oil droplet (represented by a yellow circle), respectively.

Several models were proposed in order to characterize the surface wettability by determining the relation between various parameters, such as surface roughness and energy. One of these wetting models is the Young's model, which is valid for a sessile droplet deposited above an ideal flat, rigid and homogeneous surface, and is given by the following

equation, which relates the surface tensions (γ) between the three phases: solid (S), liquid (L) and vapor (V):

$$\cos\theta = \frac{\gamma_{S,V} - \gamma_{S,L}}{\gamma_{L,V}}$$

Wenzel's equation was proposed to predict the effect of the surface roughness on the CA value [13] and can be written as stated below:

$$\cos\theta_w = r\cos\theta$$

,where r corresponds to the roughness factor, which is a measure of how surface roughness affects a homogeneous surface, and θ_w is the apparent Wenzel contact angle.

It is worth noticing that the former model assumes that the liquid can penetrate into the surface asperities. By contrast, in the Cassie-Baxter model, air pockets are formed inside the surface grooves, hampering the water penetration (Figure 6.2B) [14]. Since the liquid droplet is resting on the top of the surface topographic features, the CA is described as:

$$\cos\theta_{CB} = r_f f\cos\theta + f - 1$$

,where r_f is the roughness ratio of the wet surface area, θ_{CB} is the apparent contact angle and f is the fraction of solid surface area wet by the liquid.

Moreover, it is possible to occur a wetting transition from the Cassie state to the Wenzel state, if the air pockets became thermodynamically instable and, consequently, filled with liquid. This phenomenon has been ascribed to the presence of a non-homogeneous distribution of the surface in terms of topography and chemical properties or external factors such as droplet impact [15].

3.2. SH Surfaces

Surfaces exhibiting water CA (WCA) values higher than 150º are commonly referred as superhydrophobic surfaces [16]. As previously referred, the desired wettability can be achieved by controlling the surface properties including its topography and chemical composition. In case of SH surfaces, it is well-accepted that the multiscale roughness at both micro- and nano levels is responsible for promoting higher WCA values as well as a more stable composite solid–liquid–air interface. On the one hand, the microstructures support the droplet in the Cassie wetting state through air entrapment within the valleys between the asperities while, on the other hand, the nanostructures prevent the valleys filling by small droplets and, hence, the droplet collapse into the Wenzel wetting state. For a low surface energy value, roughness significantly influences the wettability properties by increasing the CA value [17].

Considerable efforts have been devoted to the creation of bio-inspired artificial SH surfaces with special wettability, including electrospinning, plasma etching, layer-by-layer and lithography [9, 18].

3.3. SA surfaces

Surfaces that are simultaneously SH and superoleophobic are referred as superamphiphobic surfaces and are characterized by CA values higher than 150º for both water and oil-based liquids. SA surfaces are also typically designed by combining a low surface energy and a hierarchical roughness, in which the microstructures allow the resistance to the capillary waves whilst the nanostructures can prevent the valleys filling by small droplets [19]. The ability to repel also oil-based liquids has been associated with the additional presence of overhanging, inverted trapezoid and mushroom-like structures, for example [20]. Comparing with SH surfaces, superoleophobic surfaces are more difficult to obtain since organic liquids present lower surface tensions than water [21].

Taking together all these features, both SH and SA surfaces can be foreseen as platforms to produce spherical shaped objects owing to their extreme liquid repellence. The main advantage of using SA surfaces for this specific purpose is the possibility to broad the application spectrum to diverse technological applications such as agriculture, biotechnology, cosmetics, and electronics, where solvents different than water are often required.

4. Examples of spherical-shaped particles produced above SH surfaces

In 2010, Song *et al.* [5]. first reported a biomimetic methodology to fabricate hydrogel particles using SH substrates, in which liquid droplets acquire a spherical shape. To this end, polystyrene SH surfaces were employed as a template to obtain chitosan hydrogel particles crosslinked by genipin. This strategy was proven to be biologically friendly since drug and cell spherical reservoirs were successfully synthesized through the incorporating of bioactive agents and cells in an alginate precursor solution.

Following this publication, several works were presented in literature taking advantage of this bioinspired producing technique to obtain spherical hydrogel or solid polymeric particles under mild conditions by employing a crosslinking and/or solvent evaporation process, respectively. The most relevant and representative examples in biomedical field were summarized on Table 6.1. For instance, mili-sized smart and spherical-shaped hydrogel particles made of dextran-methacrylate (MA-DEXT)/poly(N-isopropylacrylamide) (PNIPAAm) were obtained above SH surfaces upon UV-mediated crosslinking. Owing to the incorporation of PNIPAAm during the beads formation, these obtained particles were able to respond to changes in temperature as proved by the possibility of tuning these particles' release profile by setting the temperature above or below the critical solution temperature of PNIPAAm [22].

Table 6.1 - Examples of spherical hydrogel and solid polymeric (after solvent evaporation) particles obtained using bioinspired SH surfaces with potential for biomedical purposes.

	Substrate	Particle			Applications	
		Material	*Cargo*	*Diameter*		
HYDROGEL	Polystyrene SH surface	Chitosan Alginate	Theophylline; albumin; L929 cells; Fe_3O_4 particles	1-3 mm	Tissue Engineering; Cell encapsulation; Drug delivery	[5]
	Polystyrene, aluminum and copper SH surfaces	Dextran PNIPAAm	Insulin Albumin	1-3 mm	Controlled Drug Release	[22]
	Copper SH surfaces	Dextran Alginate	Fluorescent dyes; L929 cells	1-3 mm	Drug and cell encapsulation	[23]
	Polystyrene SH surface	Chitosan	Fibroblasts: Dexamethasone	2.7 mm	Tissue Engineering	[24]
	Polystyrene SH surface	Collagen	Platelet Lysate; human adipose-derived stem cells	1.5-2.5 mm	Tissue Engineering	[25]
	Polystyrene SH surface	Alginate	Fibronectin; Mesenchymal Stem cells	2 mm	Bone regeneration	[26]
	Polystyrene SH surface	Dextran γ-CD	Dexamethasone	2 mm	Bone Regeneration	[27]
POLYMERIC PARTICLES	Polystyrene SH surface	Elastin-like recombiner	-	*≈ 1 mm*	Bone Regeneration	[28]
	Copper SH surface	Bioactive glass nanoparticles	-	≈ 1.3 mm	Bone regeneration	[29]
	Polystyrene SH surface	Chitosan Pectin	5-fluorouracil	≈ 0.6 mm	Oral Drug Delivery; Skin and colorectal tumors	[30]
	Polystyrene SH surface	Chitosan	Fe_3O_4 nanoparticles	≈ 1 mm	Bioreactors; Scaffolds	[31]

The possibility of using this biomimetic strategy to produce hydrogels devices containing living cells with high viability rates was also assessed, highlighting its potential for tissue

engineering purposes. For example, a collagen polymeric solution containing platelet lysates and human adipose-derived stem cells was deposited onto a SH surface to yield cell-laden particles for applications in skin regeneration [25]. Another example was the co-encapsulation of mesenchymal stem cells from brown marrow and fibronectin into alginate beads, which were envisioned as implantable systems for bone regeneration [26]. Besides water soluble cargos, hydrophobic drugs were also successfully loaded into MA-DEXT/γ-cyclodextrins particles produced above SH surfaces [27].

All the previously stated examples comprised a unique crosslinking step, in order to obtain more complex systems regarding their properties and structure, a new methodology based on multiple crosslinking steps was reported. For example, chitosan particles with enhanced mechanical properties were obtained by combining a first ionic crosslinking mechanism with a second temperature-mediated process [24]. Moreover, spherical and multilayered systems were also successfully produced onto SH surfaces through the deposition of successive layers of a polymeric precursor solution and employing the respective crosslinking steps. The obtained concentric multilayer particles allowed the tailoring of the molecules release profiles and, importantly, gathered the appropriate conditions to support viable cells [23]. Additionally, pectin-coated chitosan particles were also developed following the former strategy. The pectin coating prevented the premature leakage of the drug under the acidic conditions of stomach and, hence, ensuring the release of drugs in the intestine [30].

SH surfaces were also proved to be efficient in producing other complex spherical structures composed by elements organized at the micro/macro levels. For instance, magnetic responsive chitosan beads were prepared by incorporating magnetic nanoparticles in hydrogel precursor solution in order to spatial control the resultant hydrogels using a magnetic field [5, 31]. Moreover, bioactive-glass nanoparticles were assembled into spherical aggregates above SH surfaces. These macrospheres were obtained after evaporation of the liquid-phase and were validated for bone regeneration [29].

5. Conclusion

Inspired by extreme repellent structures found in nature, it is now well-accepted that both surface topography and surface chemistry play a key role to achieve this behavior. Having this in mind, different strategies were proposed to obtain artificial superantiwetting platforms, combining a hierarchical morphology with a low surface energy.

These unique properties of highly repellent surfaces have been explored to prepare spherical hydrogel and solid polymeric particles with high encapsulation efficiency, by dispensing droplets of aqueous-based polymeric solutions over SH surfaces. Afterwards, these droplets were hardened into hydrogel or solid polymeric particles through a crosslinking and/or evaporation step, respectively. Owing to its mild conditions and high encapsulation efficiency, this strategy was proven to be successful in the fabrication of a variety of functional natural-based systems with potential as drug and/or cell-laden carriers. Some examples of the obtained polymeric particles included spherical homogeneous hydrogel matrices, smart and responsive hydrogel networks, spherical solid polymeric particles and, more recently, multilayered hydrogel systems with potential for biomedical purposes.

Although the use of these platforms suppresses some of the disadvantages of the currently available methodologies to fabricate polymeric particles, some concerns still need to be clarified before the widespread application of this technology. First, in all the aforementioned experimental works, a micropipette was used to dispense the polymeric precursor solution onto a SH surface. Although this dispensing mechanism allows the precise control over the particle size, the minimum dispensed volume is limited to *ca.* 2 μL, resulting in the production of particles not smaller than 1 mm in diameter. Therefore, other dispensing strategies are required to obtain particles with sizes in the micrometer range using this bioinspired strategy and, hence, producing microcarriers suitable for drug delivery and tissue engineering.

Improvements on the automatization of this procedure are also required to extend the applicability of the present technology to biomedical research and industry. It is expected that SH surfaces with larger areas could be used to scale-up this procedure, which could be combined with mobile substrates and optimized processes to recover the particles from the superantiwetting substrates.

Additionally, SA surfaces could also be envisioned as supporting surfaces to fabricate hydrogel particles, which could possibly expand the spectrum of applications to, for example, agriculture and pharmaceutical industry, where solvent different than water are often required. Lastly, due to the simplicity of this technique, spherical polymeric systems with more complex architectures could potentially be produced above these liquid-repellent surfaces.

References

[1] a) Yan Y. Y., Gao N. and Barthlott W., Mimicking natural superhydrophobic surfaces and grasping the wetting process: a review on recent progress in preparing superhydrophobic surfaces, *Adv. Colloid Interface Sci.* **2011**, 169, 80; b) Yao X., Song Y. and Jiang L., Applications of bio-inspired special wettable surfaces, *Adv. Mater.* **2011**, 23, 719; c) Sun T., Feng L., Gao X., Jiang L., Bioinspired surfaces with special wettability, *Acc. Chem. Res.* **2005**, 38, 644; d) L. Wen, Y. Tian and L. Jiang, Bioinspired super-wettability from fundamental research to practical applications, *Angew. Chem., Int. Ed.*, **2015**, 54, 3387.
[2] a) Barthlott W. and Neinhuis C., Purity of the sacred lotus, or escape from contamination in biological surfaces, *Planta* **1997**, 202, 1. B) Gao L. and McCarthy T. J., The “lotus effect” explained: two reasons why two length scales of topography are important, *Langmuir* **2006**, 22, 2966.
[3] Zheng Y.M., Gao X.F., and Jiang L., Directional adhesion of superhydrophobic butterfly wings, *Soft Matter* **2007**, 3, 178.
[4] Parker A. R., Lawrence C. R., Water capture by a desert beetle, *Nature* **2001**, 414, 33.
[5] Song W., Lima A. C., Mano J. F., Bioinspired methodology to fabricate hydrogel spheres for multi-applications using superhydrophobic substrates, *Soft Matter* **2010**, 6, 5868.
[6] a) Orive G., Hernández R. M., Gascón A. R., Calafiore R., Chang T. M. S., De Vos P., Hortelano G., Hunkeler D., Lacík I., Shapiro A. M. and Pedraz J. L., Cell encapsulation: promise and progress, *Nat. Med.* **2003**, 9, 104; b) Custódio C. A., Santo V. E., Oliveira M. B., Gomes M. E., Reis R. L. and Mano J. F., Functionalized Microparticles Producing Scaffolds in Combination with Cells, *Adv. Funct. Mater.* **2014**, 24, 1391.

[7] Hernandez R.M., Orive G., Murua A., Pedraz J.L., Microcapsules and microcarriers for in situ cell delivery, *Adv. Drug Delivery Rev.* **2010**, 62, 711-730.
[8] Lima A. C., Sher P. and Mano J. F., Production methodologies of polymeric and hydrogel particles for drug delivery applications, *Expert Opin. Drug Deliv.* **2012**, 9, 231.
[9] a) X. Zhang, F. Shi, J. Niu, Y. Jiang, Z. Wang, Superhydrophobic surfaces: from structural control to functional application, *J. Mater. Chem.* **2008**, 18, 621; b) Celia E., Darmanin T., Taffin de Givenchy E., Amigoni S. and Guittard F., Recent advances in designing superhydrophobic surfaces, *J. Colloid Interface Sci.* **2013**, 402, 1.
[10] Feng L., Li S. H., Li Y. S., Li H. J., Zhang L. J., Zhai J., et al., Super-hydrophobic surfaces: From natural to artificial. *Adv Mater.* **2002**, 14, 1857.
[11] a) Verplanck N., Coffinier Y., Thomy V. and Boukherroub R., Wettability switching techniques on superhydrophobic surfaces, *Nanoscale Res. Lett.* **2007**, 2, 577; b) Genzer J. and Efimenko K., Recent developments in superhydrophobic surfaces and their relevance to marine fouling: a review, *Biofouling* **2006**, 22, 339.
[12] Bellanger H., Darmanin T., Taffin de Givenchy E. and Guittard F., Chemical and physical pathways for the preparation of superoleophobic surfaces and related wetting theories, *Chem. Rev.* **2014**, 114, 2694.
[13] Wenzel R. N., Surface roughness and contact angle, *J. Phys. Colloid Chem.* **1949**, 53 (9), 1466.
[14] Cassie A. B. D., Baxter S., Wettability of porous surfaces, *Trans. Faraday Soc.* **1944**, 40, 546.
[15] a) Cheng Z., Du M., Lai H., Zhang N. and Sun K., From petal effect to lotus effect: a facile solution immersion process for the fabrication of super-hydrophobic surfaces with controlled adhesion, *Nanoscale* **2013**, 5 , 2776; b) Luo C, Xiang M, Heng X. A Stable Intermediate Wetting State after a Water Drop Contacts the Bottom of a Microchannel or Is Placed on a Single Corner, *Langmuir* **2012**, 28, 9554.
[16] Lafuma A, Quere D. Superhydrophobic states. *Nat Mater.* **2003**, 2, 457.
[17] Öner D., McCarthy T. J., Ultrahydrophobic Surfaces. Effects of Topography Length Scales on Wettability, *Langmuir* **2000**, 16, 7777.
[18] Wang S., Liu K., Yao X., Jiang L., Bioinspired Surfaces with Superwettability: New Insight on Theory, Design, and Applications, *Chem. Rev.* **2015**, 115, 8230.
[19] Tuteja A., Choi W., Ma M., Mabry J. M., Mazzella S. A., Rutledge G. C., McKinley G.H. and Cohen R. E., Designing superoleophobic surfaces, *Science* **2007**, 318, 1618.
[20] a) Yong J. L., Chen F., Yang Q., Fang Y., Huo J. and Hou X., Femtosecond laser induced hierarchical ZnO superhydrophobic surfaces with switchable wettability, *Chem. Commun.* **2015**, 51, 9813; b) Nosonovsky M. and Bhushan B., Hierarchical roughness makes superhydrophobic states stable, *Microelectron. Eng.* **2007**, 84, 382-386; c) Yong J., Chen F., Yang Q.,Huo J., Hou X., Superoleophobic surfaces, *Chem. Soc. Rev.* **2017**,46, 4168.

[21] Butt H.-J., Semprebon C., Papadopoulos P., Vollmer D., Brinkmann M., Ciccotti M., Design principles for superamphiphobic surfaces, *Soft Matter* **2013**, 9, 418.
[22] Lima A. C., Song W., Blanco-Fernandez B., Alvarez-Lorenzo C. and Mano J. F., Synthesis of temperature-responsive dextran-MA/PNIPAAm particles for controlled drug delivery using superhydrophobic surfaces, *Pharm. Res.* **2011**, 28, 1294.
[23] Lima A. C., Custódio C. A., Alvarez-Lorenzo C. and Mano J. F., Biomimetic methodology to produce polymeric multilayered particles for biotechnological and biomedical applications, *Small* **2013**, 9, 2487.
[24] Lima A. C., Correia C. R., Oliveira M. B. and Mano J. F., Sequential ionic and thermogelation of chitosan spherical hydrogels prepared using superhydrophobic surfaces to immobilize cells and drugs, *J. Bioact. Compat. Polym.* **2013**, 29, 50.
[25] Lima A. C., Mano J. F., Concheiro A. and Alvarez-Lorenzo C., Fast and mild strategy, using superhydrophobic surfaces, to produce collagen/platelet lysates gel beads for skin regeneration, *Stem Cell Rev. Rep.* **2015**, 11, 161.
[26] Lima A. C., Batista P., Valente T. A. M., Silva A. S., Correia I. J. and Mano J. F., Novel methodology based on biomimetic superhydrophobic substrates to immobilize cells and proteins in hydrogel spheres for applications in bone regeneration, *Tissue Eng. Part B* **2013**, 19, 1175.
[27] Lima A. C., Puga A. M., Mano J. F., Concheiro A. and Alvarez-Lorenzo C., Free and copolymerized g-cyclodextrins regulate the performance of dexamethasone-loaded dextran microspheres for bone regeneration, *J. Mater. Chem. B* **2014**, 2, 4943.
[28] Oliveira M. B., Song W., Martín L., Oliveira S. M., Caridade S. G., Alonso M. Rodriguez-Cabello J. C. and Mano J. F., Development of an injectable system based on elastin-like recombinamer particles for tissue engineering applications, *Soft Matter* **2011**, 7, 6426.
[29] Luz G. M. and Mano J. F., A nanotectonics approach to produce hierarchically organized bioactive glass nanoparticles-based macrospheres, *Nanoscale* **2012**, 4, 6293.
[30] Puga A. M., Lima A. C., Mano J. F., Concheiro A. and Alvarez-Lorenzo C., Pectin-coated chitosan microgels crosslinked on superhydrophobic surfaces for 5-fluorouracil encapsulation, *Carbohydr. Polym.* **2013**, 98, 331.
[31] Song W., Oliveira M. B., Sher P., Gil S., Nóbrega J. M. and Mano J. F., Bioinspired methodology for preparing magnetic responsive chitosan beads to be integrated in a tubular bioreactor for biomedical applications, *Biomed. Mater.* **2013**, 8, 045008.

Chapter VII: Materials & Methods

Most of the current available technologies to fabricate hydrogel spheres require a liquid-liquid interface, meaning that the polymeric particles are obtained under wet-conditions. For example, hydrogel particles are typically produced by precipitation/crosslinking in a coagulation bath, in which the liquid polymeric precursor solution hardens into its hydrogel form upon immersion in another insoluble liquid solution containing the crosslinking agent.

Inspired by the rolling of water droplets on lotus leaves, it was hypothesized that by dispensing a polymeric precursor solution on the top of substrates with extreme wettability, followed by a crosslinking step, it would be possible to obtain almost spherical particles. This biomimetic methodology was first reported in 2010 by *Song et al.* [1] and, in this thesis, was further extended to produce hydrogel micro- and macroparticles with distinct structures.

The aim of this Chapter is to present, in a more comprehensive manner, the details concerning both the materials and methodologies used in Chapters VIII to XI, as well as the reasons for their selection. The materials used in this thesis were purchased from specialized commercial distributors and some were chemically modified to be suitable for a specific purpose. All the experimental procedures and, materials and equipment suppliers can be found in more detail in the experimental subsection of each chapter.

As referred in Chapter VI, to successfully use superantiwetting surfaces to produce spherical hydrogel particles, it is required a: **(1)** polymeric precursor solution; **(2)** superantiwetting surface; and a **(3)** fabrication methodology combining dispensing and crosslinking mechanisms.

1. Polymeric precursor solution

Natural polymers were selected to develop the different hydrogels spheres described in this thesis. The main advantages of using natural polymers are: (i) their similar structure with

ECM of many tissues; (ii) their typical biocompatibility, non-toxicity and low immunogenicity; (iii) their typically high availability from renewable sources; and (iv) their ability to be easily processed under mild conditions. All these properties make these macromolecules suitable for creating hydrogel devices for biomedical purposes [2].

1.1. Alginate (ALG)

ALG, a polysaccharide mainly obtained from brown algae, is a linear anionic copolymer composed of consecutive blocks of (1-4)-linked β-D-mannuronic acid (M-blocks) or its C-5 epimer α-L-guluronic acid (G-blocks) monomers or alternating M and G-residues (M-G blocks) (Figure 7.1). This natural polymer tends to be negatively charged at a pH around 7.4 (the physiological pH) since its pKa value is of 3.4 and 3.7 for M and G acids, respectively [3]. Therefore, ALG can yield gels when the carboxylic acid groups present on its backbone encounter divalent cations such as calcium ions. These interactions occur between G-blocks of adjacent ALG chains during gelling, creating an egg-box-like structure [4].

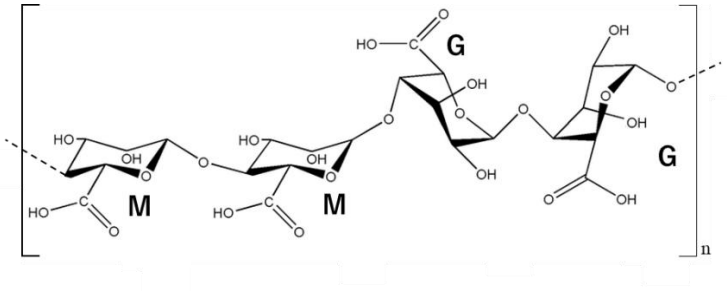

Figure 7.1 - Structure of ALG polymer.

A unique characteristic of calcium-mediated crosslinking of ALG is the ability to reverse this gelling process, meaning that it is possible to return to ALG non-crosslinked form (liquid state) by simply adding Ca^{2+} chelators such as EDTA [5]. ALG was selected due to its biocompatibility as well as for its ability to reversibly form hydrogels at mild conditions, making it a great candidate for the liquid core of the hydrogel capsules developed in Chapter XI. ALG

was also used in Chapter VIII and Chapter X to validate the possibility of fabricating microspheres above the newly developed SA surfaces and to produce hydrogel spheres with a hierarchical architecture on the top of a SA surface, respectively.

1.2. Chitosan (CHI)

CHI, a polycationic biopolymer widely used in the biomedical field, is attractive because of its biocompatibility and chemical versatility [6]. In Chapter IX, MACHI derivative was used to produce, for the first time, hydrogel microparticles above SA surfaces. In Chapter XI, this modified polysaccharide was the selected biomaterial to produce the polymeric shell of the liquified hydrogel spheres described in this chapter.

The experimental procedure followed to synthesize this derivative and its main characteristics have already been described in Chapter III.

Characterization: ^{1}H–Nuclear Magnetic Resonance (^{1}H-NMR) was used to infer about the correct MACHI methacrylation and to estimate both the substitution and crosslinking degrees. Fourier Transform InfraRed Spectroscopy (FTIR) was also used to infer about the correct CHI methacrylation.

1.3. Dextran (DEXT)

DEXT polysaccharide is produced from sucrose via the action of dextransucrase enzyme, which is found in some bacteria strains such as *Leuconostoc mesenteroides.* Its structure consists of α (1-6)-linked D-glucose monomers with branches from α (1-3) linkages [7]. DEXT is biocompatible and biodegradable by the action of dextranase produced by some anaerobic Gram-negative intestinal bacteria [8]. Worth notice, DEXT contains many chemically reactive hydroxyl groups, which can be used for functionalization, and hence, extend its applicability. In Chapter X, DEXT was functionalized with methacrylic groups (MA-DEXT) through its reaction with glycidyl methacrylate (GMA) in the presence of dimethyl sulfoxide (DMSO), a polar aprotic

solvent, and dimethylamine pyridine (DMAP), a base which act as a catalyst for the coupling reaction between GMA and DEXT [9]. During this process, the hydroxyl groups of DEXT are ionized as a consequence of the alkaline pH, allowing the direct attachment of methacrylate esters to the 2- and 3- hydroxyl groups of the DEXT chain, in proportion of 1:1 [10]. Although it is expected that this functionalization occurs mainly by transesterification, the epoxide ring-opening mechanism cannot be discarded [11]. This modification was performed in Chapter X to enable the formation of hydrogel microspheres upon UV-light exposure. Photocrosslinking process is advantageous to produce spherical hydrogel particles above superantiwetting surfaces since it only requires the dispensing of the polymeric precursor solution and, hence, there is no need for another dispensing mechanism to release the crosslinker agent.

MA-DEXT polymer synthesis: MA-DEXT was synthesized as already described in literature [11] by mixing DMAP catalyst (0.5 g) with a dextran solution (0.1 g/mL, 25 mL) in DMSO. Once dissolved, GMA (2.45 mL, 0.4 eq per hydroxyl group in the glucose unit) was added followed by the degassing of the previous solution with N_2 for 5 minutes. After a 48h incubation period, the DMAP was neutralized with HCl 1M and the solution was dialyzed (MWCO 12400 Da) against water over 4 days and freeze-dried.

Characterization: ^{1}H–Nuclear Magnetic Resonance (^{1}H-NMR) was used to infer about the correct methacrylation and to estimate the substitution degree.

1.4. Gelatin (GEL)

This natural polymer is obtained from the partial hydrolysis of collagen, the main structural protein of the ECM of various body connective tissues. GEL is well-known for its biocompatibility, biodegradability and non-immunogenicity as well as for exhibiting cell-adhesive motifs all along its backbone [12]. This polysaccharide has a very interesting temperature-responsive behavior. At low temperatures typically below 4ºC, this polymer is in gel state. By contrast, for higher temperature values, GEL becomes a liquid solution [13].

Taking advantage of this feature, GEL was used to produce the liquid core of the hydrogel capsules described in Chapter XI.

2. Superantiwetting surfaces

In Chapter VIII, a new methodology to design SA surfaces was reported by simply depositing polyamide capsules coated with a perfluorinated hydrocarbon precursor, 1H,1H,2H,2H-perfluorodecyltriethoxysilane (PFDTS), and entrapping magnetic particles above a solid substrate (Figure 7.2; Chapter VIII). To this end, microspheres entrapping magnetic microparticles were synthesized by a previously reported one-step process [14, 15]. The former methodology is based on an activated anionic polymerization in suspension of caprolactam using a hydrocarbon solvent. These capsules were used to produce SA surfaces since it was noticed that by placing them above a solid substrate, a hierarchical structure like the one of lotus leaf was formed. Moreover, the presence of magnetic microparticles within these particles allows for controlling their arrangement and temporal fixation through an external magnetic field. This former feature is important to permit the complete recuperation of both substrate and polyamide capsules without any loss after elimination of the magnetic field. Afterwards, two approaches were employed to lower the surface energy of the resultant particles, which is crucial to obtain a SA surface, either (i) by immersing the particles in a PFDTS solution in deionized water for 48 h or (ii) by chemical vapor deposition (CVD) of a PFDTS solution inside a desiccator for 48 h.

Moreover, stable and robust membranes made of the previously described microcapsules were produced by spreading 500 µL of a particle suspension (20% (w/v) in water) above a glass substrate and, then, heated in a furnace for 30 min at 150 °C to obtain a sintered membrane. The samples were cooled to RT and washed with ethanol in an ultrasound bath for 15 min to remove non-attached microspheres. Next, the washed substrates were immersed in a PFDTS solution at 1% (v/v) in deionized water for 48 h and dried in air.

The potential of such superantiwetting substrates in the fabrication of highly versatile water/oil repellent surfaces, to produce liquid marbles, microfluidic channels and patterns or as templates for microspheres fabrication was assessed.

In Chapter IX to XI, SA surfaces were used as substrates to produce spherical hydrogel particles and were prepared using a CVD method described elsewhere with subtle variations [16]. From all the available methodologies reported in literature, this strategy was selected due to: (i) the high contact angle values obtained, particularly *ca.* 165º and 161º for water and diiodomethane, respectively; and (ii) the ability to maintain its superamphiphobic properties after abrasion. These features are particularly relevant when using these substrates to create hydrogel spherical particles in the micrometer range. On the one side, the high CA values are essential to ensure a minimal surface contact between the deposited droplet and the SA substrate and, consequently, avoid any shape distortions. On the other side, since these superantiwetting platforms were combined with a spraying mechanism, this abrasion resistance is required to prevent the potential damage of the SA coating after spraying.

Fabrication Process: Briefly, a glass support was held above the flame of a paraffin candle in order to form a soot layer. Afterwards, the soot coated substrates were exposed to CVD of tetraethyl orthosilicate (4 mL) in the presence of ammonia (4 mL) for 24 h in a desiccator, followed by the calcination of the hybrid carbon/silica network at 550 ºC for 2 h. Finally, the hydrophilic silica shell was coated with PFDTS (150 µL) by CVD for 3 days.

Characterization: All the obtained SA surfaces were characterized for their morphology, elemental composition, topography and water contact angle (WCA) by Scanning Electron Microscopy (SEM), EDS, both Atomic Force Microscopy (AFM) and Profilometry, and static WCA measurements, respectively.

3. General overview of the fabrication methodologies described in Chapters IX to XI to produce spherical multistructured particles

In Chapters IX to XI, different methodologies were designed to obtain spherical-shaped hydrogel particles. A graphical overview of each of the developed strategies is displayed in Figure 7.2 (a more detailed description of the experimental methodologies employed can be found in each corresponding chapter).

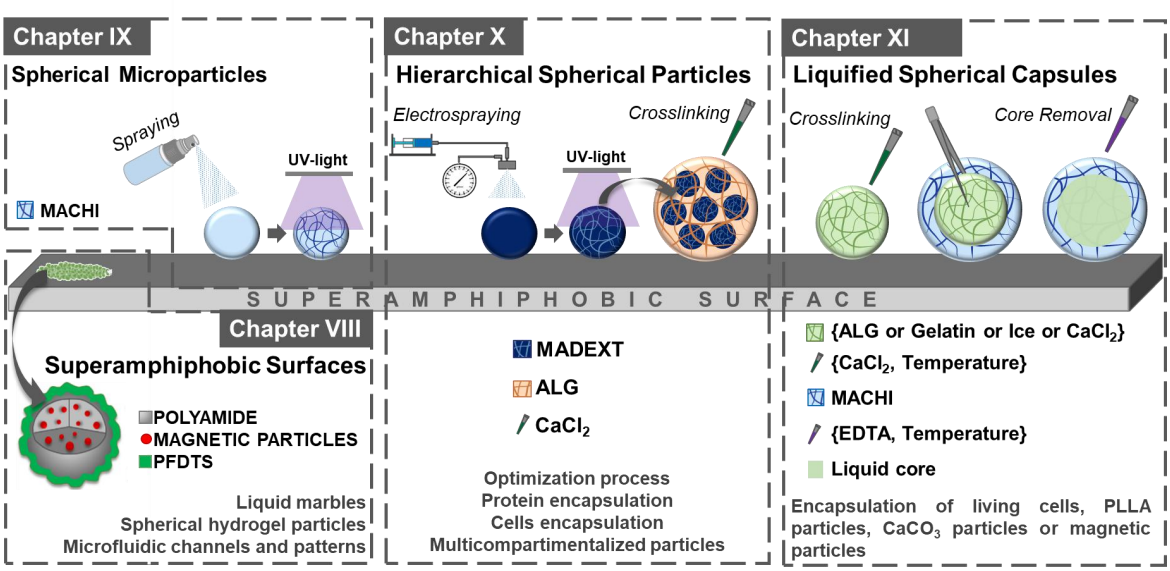

Figure 7.2 - Graphical overview of the research presented from the Chapters VIII and XI. In this thesis, a new methodology to develop SA surfaces was developed and was described in Chapter VIII. Moreover, spherical microparticles, hierarchical particles and liquified capsules were fabricated above SA surfaces and were described in Chapter IX, X, XI, respectively.

In Chapter IX, spherical hydrogel microparticles were produced, for the first time, on top of SA surfaces. To this end, a MACHI precursor solution was sprayed over a SA surface followed by the UV-mediated crosslinking of this polymer to yield hydrogel spheres with nominal sizes in the micrometer range (Figure 7.2; Chapter IX).

In Chapter X, hierarchical polymeric assemblies of microparticles within macroscopic beads were produced above SA surfaces (Figure 7.2; Chapter X). First, an electrospraying

system was used to better control the size of the obtained microspheres by tuning the flow rate of the polymeric precursor solution and the pressure inside the nozzle. MA-DEXT polymer was selected to produce the polymeric subcompartments. The potential of the developed strategy to yield cell/drug microcarriers was also assessed by entrapping L929 cells or bovine serum albumin (BSA) during the MA-DEXT microparticles fabrication process, respectively. The hierarchical particles were obtained by the incorporation of cell/BSA-loaded MA-DEXT microparticles into ALG macroscopic beads over a SA surface which were, subsequently, crosslinked by calcium-mediated (Ca^{2+}) ionic gelation. Moreover, the possibility of packing several small compartments loaded with different molecules into larger polymeric containers was also evaluated.

In Chapter XI, capsules with a liquefied core were fabricated via the assembly of polymeric droplets induced by SA surfaces (Figure 7.2; Chapter XI). MACHI polymer was used to produce the polymeric shell while a wealth variety of template cores were tested. The cores were made of either ALG, $CaCl_2$, gelatin or ice and were selected owing to the ALG reversible crosslinking mechanism in presence of EDTA, a Ca^{2+}-mediated interfacial gelation of ALG, and the temperature responsiveness of both gelatin and ice, respectively. Moreover, hierarchical systems were fabricated by incorporating different objects, namely calcium carbonate ($CaCO_3$), polylactic acid (PLLA) or magnetic particles (Fe_4O_3) particles, inside the core during the synthesis process.

References

[1] W. Song, A. C. Lima, J. F. Mano, Bioinspired methodology to fabricate hydrogel spheres for multi-applications using superhydrophobic substrates, *Soft Matter* **2010**, 6, 5868.
[2] S.S. Silva, J.F. Mano, R.L. Reis, Potential applications of natural origin polymer-based systems in soft tissue regeneration, *Crit. Rev. Biotechnol.* **2010**, 30 (3), 200.
[3] K.Y. Lee, D.J. Mooney, Hydrogels for tissue engineering, *Chem. Rev.* **2001**, 101 (7), 1869–1879.

[4] I. Braccini and S. Pérez, Molecular Basis of Ca2+-Induced Gelation in Alginates and Pectins: The Egg-Box Model Revisited, *Biomacromolecules* **2001**, 2, 1089.
[5] K.I. Draget, O. Smidsrød, G. Skjåk-Bræk, Alginates from algae, in: Biopolymers Online, *Wiley-VCH Verlag GmbH & Co. KGaA*, **2005**.
[6] N. M. Alves, J. F. Mano, Chitosan derivatives obtained by chemical modifications for biomedical and environmental applications, *Int. J. Biol. Macromol.* **2008**, 43 (5), 401.
[7] M. Naessens, A. Cerdobbel, W. Soetaert, E. J. Vandamme, Leuconostoc dextransucrase and dextran: production, properties and applications. *J Chem Technol Biotechnol* **2005**, 80, 845.
[8] V. R. Sinha and R. Kumria, Polysaccharides in colon-specific drug delivery, *Int. J. Pharm.* **2001**, 224, 19.
[9] V. N. E. van Dijk-Wolthius, O. Franssen, H. Talsma, M. J. van Steenbergen, J. J. Kettenes-van den Bosch and W. E. Henninkt, Synthesis, Characterization, and Polymerization of Glycidyl Methacrylate Derivatized Dextran, *Macromolecules* **1995**, 28, 6317.
[10] A. C. Lima, W. Song, B. Blanco-Fernandez, C. Alvarez-Lorenzo and J. F. Mano, Synthesis of temperature-responsive dextran-MA/PNIPAAm particles for controlled drug delivery using superhydrophobic surfaces, *Pharm. Res.* **2011**, 28, 1294.
[11] S. H. Kim, C. C. Chu, Synthesis and characterization of dextran-methacrylate hydrogels and structural study by SEM, *J. Biomed. Mater. Res.* **2000**, 49, 517.
[12] F. Bode, M. A. da Silva, A. F. Drake, S. B. Ross-Murphy and C. A. Dreiss, Enzymatically cross-linked tilapia gelatin hydrogels: physical, chemical, and hybrid networks, *Biomacromolecules* **2011**, 12, 3741.
[13] A. Duconseille, T. Astruc, N. Quintana, F. Meersman and V. Sante-Lhoutellier, Gelatin structure and composition linked to hard capsule dissolution: A review, *Food Hydrocolloid.* **2015**, 43, 360.
[14] F. M. Oliveira, N. Dencheva, P. Martins, S. Lanceros-Méndez, Z. Denchev, Reactive microencapsulation of carbon allotropes in polyamide shell-core structures and their transformation in hybrid composites with tailored electrical properties, *Express Polym. Lett.* **2016**, 10, 160.
[15] N. Dencheva, Z. Denchev, S. Lanceros-Méndez, T. A. Ezquerra, One - Step In Situ Synthesis of Polyamide Microcapsules With Inorganic Payload and Their Transformation into Responsive Thermoplastic Composite Materials, *Mat. Eng.* **2015**, 301, 119.
[16] X. Deng, L. Mammen, H.-J. Butt, D. Vollmer, Candle Soot as a Template for a Transparent Robust Superamphiphobic Coating, *Science* **2012**, 335, 67.

Chapter VIII: Results & Discussion

Moldable Superhydrophobic Surfaces[4]

ABSTRACT

Superhydrophobic (SH) surfaces arise from the cooperation between an appropriate surface roughness, consisting of a hierarchical topography with features at micro and nano-levels, and a unique surface chemistry, namely a low surface energy. Herein, a simple and fast strategy to produce SH magnetic surfaces is reported. To this end, polyamide microcapsules (MIC) exhibiting surface nanofeatures and entrapping magnetic iron microparticles were produced by activated anionic ring-opening polymerization in solution. Afterwards, to attain a low surface energy, MIC were coated with a fluorosilane precursor, yielding Sil-MIC. By simply depositing Sil-MIC as a powder above any solid substrate a hierarchical topography was formed exhibiting contact angles around 150° and 140° for water and diiodomethane, respectively. The presence of magnetic microparticles within the Sil-MIC allows for controlling their arrangement and temporal fixation through an external magnetic field. Complete recuperation of both substrate and Sil-MIC without any loss is possible after elimination of the magnetic field. Additionally, robust and stable SH magnetic membranes were fabricated by carefully sintering Sil-MIC. Such Sil-MIC could be useful in fabrication of highly versatile water/oil repellent surfaces, to produce liquid marbles or microfluidic channels and as templates for microspheres fabrication.

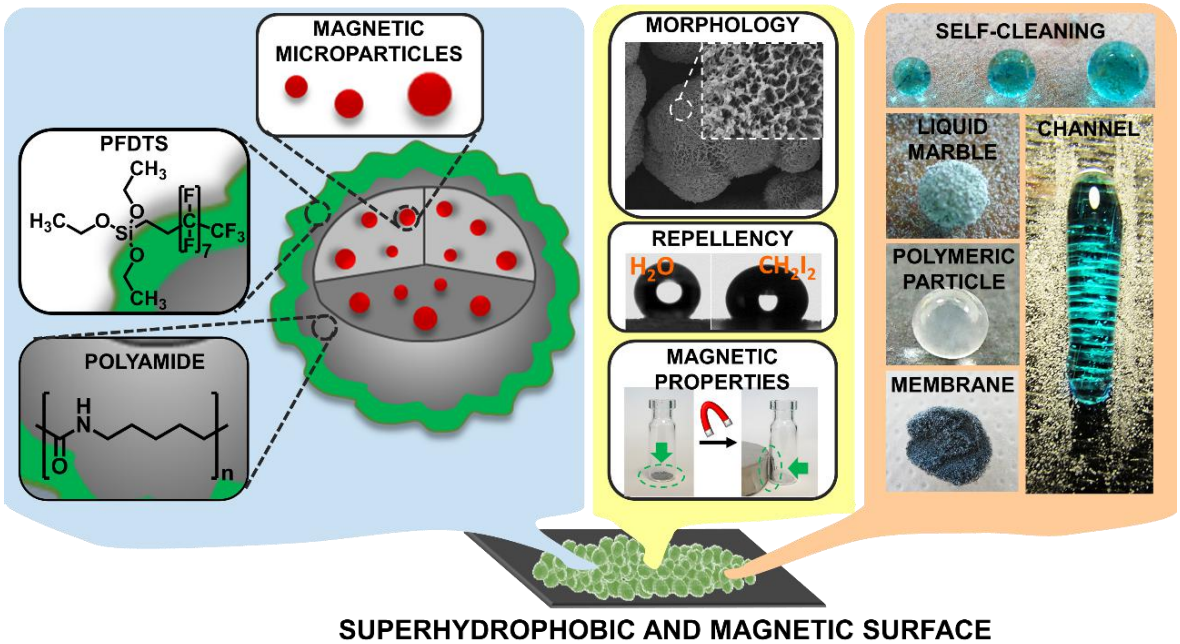

[4] Based on the publication: Ana M. S. Costa, Nadya V. Dencheva, Sofia G. Caridade, Zlatan Z. Denchev, João F. Mano, Moldable Superhydrophobic Surfaces, *Advanced Materials Interfaces* **2016**, 3 (16), 1600074.

1. Introduction

There are several applications that require liquid repellence such as in self-cleaning textiles and surfaces, electronic and medical devices, microfluidics, and high-throughput screening systems [1]. Examples of surfaces with special wettability can be found in nature, being the one of the lotus leaf and its self-cleaning ability the most well-known [2]. Surfaces with high water repellency exhibiting WCA higher than 150° and sliding angles lower than 10°, are commonly referred as superhydrophobic surfaces [3]. The desired wettability can be achieved by controlling the surface properties including its topography and chemical composition, which in case of the lotus leaf is conferred by the presence of branch-like nanostructures on the top of micropapillae and by their coating with an epicuticula wax, respectively [4]. It is well-accepted that the multiscale roughness at both micro and nano levels is responsible for promoting higher WCA as well as a more stable composite solid–liquid–air interface. On the one hand, the microstructures support the droplet in the Cassie wetting state through air entrapment within the valleys between the asperities while, on the other hand, the nanostructures prevent the valleys filling by small droplets and, hence, the droplet collapse into the Wenzel wetting state.

Considerable efforts have been devoted to the creation of bio-inspired artificial surfaces with special wettability [4a,5], including electrospinning, plasma etching, and lithography [6]. However, most of these methods require expensive equipment and materials [7], complex processes and/or harsh conditions [8], which are all major disadvantages for practical production and application. Moreover, most of these strategies are done in an irreversible way, in the sense that the structure of the substrate is fixed after the modification.

The concept presented in this work is based on the use of specifically designed microcapsules (MIC) to create a non-permanent SH surface. For the proof-of-concept, such surfaces were fabricated by covering a substrate with polyamide MIC coated with a perfluorinated hydrocarbon precursor, 1H,1H,2H,2H-perfluorodecyltriethoxysilane (PFDTS),

and entrapping metallic magnetic microparticles (coated MIC will be referred as Sil-MIC) (Scheme 7.1). The main advantage of using magnetically responsive Sil-MIC particles is the ability to control their arrangement and fixation over the substrate by applying an external magnetic field. An easy separation between the Sil-MIC particles and the substrate, *i.e.,* a complete recuperation of both is possible after elimination of the external field. As shown in this work, in such a way virtually any solid surface may become highly repellent to liquids after freely depositing on it such particles and fixing them appropriately by magnetic attraction. Such technology may also be used to produce robust and stable SH films. The potential usefulness of the developed SH surfaces was also assessed by producing droplets, solid particles, marble particles, and microfluidic channels.

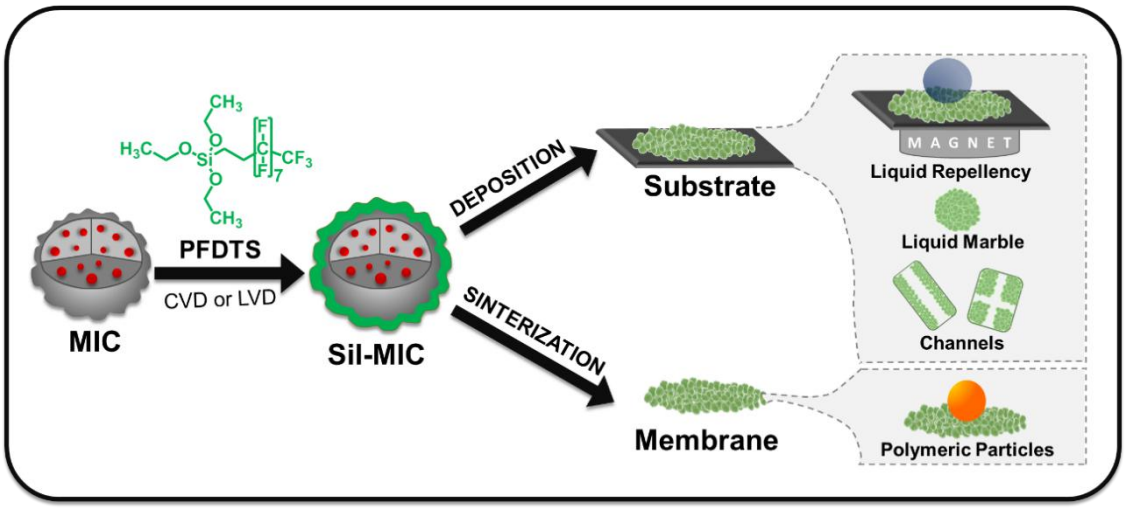

Scheme 7.1 - Schematic representation of the methodology followed to produce Sil-MIC through the coating of MIC with PFDTS to attain the adequate surface chemistry. SH surfaces with magnetic properties were obtained either by freely depositing the Sil-MIC particles above a substrate or after applying a controlled sinterization process. The unique properties of the former surfaces were assessed by testing the ability to repel both water and oil-based liquids, and by producing liquid marbles, microfluidics channels, and polymeric particles.

2. Materials & Methods

2.1. Materials

1H,1H,2H,2H-perfluorodecyltriethoxysilane (PFDTS, 97%), phosphate buffer saline (PBS), Dulbecco's Modified Eagle's Medium without phenol red (DMEM), diiodomethane (99%), alcian blue, calcium chloride ($CaCl_2$) and low viscosity sodium alginate from brown algae (ALG, ~250 cP) were purchased from Sigma-Aldrich (U.S.A.). MTS (3-(4,5-dimethylthiazol-2-yl)5-(3-carboxymethoxy-phenyl)-2-4-sulfophenyl)-2-4-sulfophenyl)-2H-tetrazolium), acetic acid and sodium bicarbonate were supplied from VWR (Belgium). TrypLE Express, fetal bovine serum (FBS), penicillin/streptomycin solution were purchased from Alfagene (Portugal). All materials were used as received. Unless otherwise stated, water purified in an 18 MΩ cm MilliQ Plus water system was used throughout.

2.2. Preparation and Characterization of Coated Microcapsules (Sil-MIC)

The methodology to produce Fe-loaded polyamide MIC is described in Section S8.1 (SI.8). Afterwards, two approaches were used to lower the surface energy of the resultant MIC either (i) by immersing the particles (10 (w/v)%) in a PFDTS (1 (v/v)%) solution in deionized water for 48 h or (ii) by CVD inside a desiccator containing a PFDTS solution (150 µL) for 48 h. The obtained Sil-MIC were characterized for their morphology, elemental composition, and wettability by SEM (JSM-6010LV, JEOL, Japan), EDS, and static WCA measurements (OCA15+ goniometer, DataPhysics, Germany), respectively. In order to prepare the samples for SEM analysis, both the MIC and Sil-MIC were sputter-coated with gold and the images were acquired in high-vacuum by tracking the signal of secondary electrons employing an accelerating voltage of 15 kV and a working distance of 14 mm. On the other side, the EDS profile of the samples was obtained without gold coating. The static WCA was determined on the basis of the sessile drop method by dispensing a 8 µL droplet of either water or diiodomethane over Sil-MIC previously placed above a substrate at RT. The values were

obtained using the SCA 20 software and correspond to 30 replicates carried out on different areas of the surface. Four different substrates were used, namely, paper, plastic, metal, and glass, which were cleaned with detergent, ethanol, and deionized water and dried with compressed air, with the exception of paper, which any possible contaminant was removed by compressed air.

The surface contact area (SCA) and the fractional area (FA) were measured to further confirm the water repellency of the produced Sil-MIC. SCA was calculated as the area of the circle with radius (R) in contact with the SH surface as described in ref. [17], with r is given by the following equation:

$$r = R\,sin\,(\theta) \qquad (1)$$

,where R represents the radius of the dispensed droplet and θ its WCA. On the other hand, FA was determined by the ratio between SA and the surface area of the sphere.

2.3. Fabrication of Sil-MIC Membranes

500 µL of MIC suspension (20% (w/v) in water) were heated in a furnace (FornoCerâmica, Portugal) under air atmosphere for 30 min at 150 °C to obtain a sintered Sil-MIC membrane. The samples were cooled to RT and washed with ethanol in an ultrasound bath for 15 min to remove non-attached Sil-MIC. The washed substrates were immersed in a PFDTS solution at 1% (v/v) in deionized water for 48 h and, then dried in air.

2.4. Assessment of the cytotoxicity of the developed Sil-MIC

Sil-MIC cytotoxicity was evaluated through the extract test following the guidelines described in ISO 10993-5(2009). Briefly, an immortalized mouse lung fibroblast cell line (L929, European Collection of Cell Cultures) was cultured in complete DMEM medium supplemented with 3.7 g/L sodium bicarbonate, 10% FBS and 1% penicillin-streptomycin (pH 7.4). L929 cells were grown in 150 cm^2 tissue culture flasks and incubated at 37 °C in a humidified air

atmosphere of 5% CO_2. The culture medium was exchanged every 3 days. Upon reaching 90% of confluence, L929 cells were washed with PBS and chemically detached from tissue culture flasks using 0.05% Tryple Express solution for approximately 5 min at 37°C in a humidified air atmosphere of 5% CO_2. Later, fresh medium was added to inactivate the Tryple Express effect and the cells were centrifuged at 200g for 3 min. Then, the medium was decanted followed by the cells re-suspension in complete culture medium at density of 1×10^5 cells per mL. 100 µL of the former cell suspension were dispensed in each well of a 96 well-culture plate and incubated at 37°C in a humidified air atmosphere of 5% CO_2. Simultaneously, Sil-MIC and MIC (0.4 mg in 2 mL of DMEM) were incubated at 37°C and 60 rpm to extract possible leachables. After 24h, the cell culture medium was replaced by 100 µL of the different extraction fluids and left in incubation for 24h (n=3). Both positive (C+; latex rubber) and negative (C-; tissue culture polystyrene plates (TCPS)) controls were extracted under the same conditions. The extract cytotoxicity was quantified by measuring the activity of mitochondrial dehydrogenases of viable cells [3]. This parameter was assessed using a tetrazolium salt, namely MTS [4], which yields a water-soluble brown formazan product in the presence of mitochondrial dehydrogenase enzymes. The amount of formazan generated is directly proportional to the total mitochondria activity per cell. Briefly, the extracts were removed and 100 µL of 1:5 MTS/DMEM (without phenol red) was added to each well containing L929 cells. The samples were cultured for 3 h at 37 °C in dark. After that, the absorbance was measured at a wavelength of 490 nm using a microplate reader (Sinergy HT, BioTek, USA).

2.5. Statistical Analysis

The level of significant differences between the average WCA and between the MTS values for each condition was assessed using one-way ANOVA (SPSS software) with Tukey's post hoc test, after verifying homogeneity of variances and normality distribution criteria. The homogeneity of variances criterion was tested using Levene's test, while the Shapiro–Wilk test

was used to study the data normality. P-values lower than 0.05 were considered statistically significant. The results are presented as mean ± standard deviation.

3. Results and Discussion

MIC with a magnetic particle content of 10 wt% were synthesized by a previously developed one-step *in-situ* activated anionic polymerization (AAP) process —see Section S8.1 (SI.8) for more details. The former process led to porous Fe-loaded MIC with an almost spherical shape, equivalent diameters in the 30–40 μm range and a BET surface area of 7.5 m^2 g^{-1}. The fabrication steps and the underlying chemistry are schematically shown in Figure S8.1 (SI.8).

Interestingly, when placed above a substrate, MIC mimic the hierarchical structure of natural SH surfaces with features at both micro and nano levels [1a,2], as shown by SEM (Figure 8.1A). Besides the appropriate surface roughness, MIC were rendered hydrophobic through their coating with PFDTS, yielding Sil-MIC [12]. It is worth noticing that after applying the former coating process, the initial multiscale structure was preserved, which is crucial to obtain a SH surface (Figure 8.1B). The successful immobilization of PFDTS was assessed through EDS (Figure 8.1C) by observing the presence of both silicon and fluorine characteristic peaks on the Sil-MIC spectrum and their absence on the MIC one. This coating is needed to decrease the MIC surface energy as the CA of a surface covered by these particles is *ca.* 80° (Figure 8.1A; left bottom corner and Figure 8.1E). PFDTS coating was carried out either by a chemical vapor deposition (CVD) [13] or liquid phase deposition (LPD) method [12c,14]. Nevertheless, it was observed that after 48 h both methodologies resulted in the increase of the WCA values to around 150°, this value being reached faster with the LPD method (Figure S8.3A, SI.8). The produced Sil-MIC were spread above four different substrates, namely, paper, metal, glass, and plastic (Figure 8.1D). The wettability of the resulting covered substrates was measured by the WCA (Figure 8.1E) and compared with the uncoated substrates (Figure S8.3B,

SI.8). WCA values around 150° reflect the high-water repellency of the formed surfaces, and the low contact area of the droplet with the produced SH substrates (corresponding to a fractional area (FA) value of *ca.* 3.2%). By applying the same PFDTS surface modification only on the uncoated substrates, namely, on paper, metal, glass, and plastic, the WCA values significantly increased however it was not enough to obtain a SH surface due to the lack of a hierarchical morphology (Figure S8.3B, SI.8). Moreover, Sil-MIC water repellency can be observed at different scales, as displayed in Figure 8.1F, where different droplet sizes were dispensed above the produced superhydrophobic surface (Movie S8.1, SI.8). Besides water, diiodomethane was also dispensed above the obtained Sil-MIC reaching contact angles of 138.3° ± 5.8° and highlighting their quasi superamphiphobic character, simultaneously superhydrophobic and superoleophobic [15] (Figure S8.4, SI.8). This behavior may be ascribed to the presence of over-hanging structures and reentrant/convex geometries on the produced Sil-MIC (Figure 8.1B inset) as already reported on literature [13c,16].

The successful incorporation of Fe-magnetic particles within Sil-MIC was further proved by the presence of the iron characteristic peak on the EDS spectra of both MIC and Sil-MIC (Figure 8.1C). Importantly, the magnetic properties were preserved after the coating (Figure 8.1G,H and Movie S8.2, SI.8). Taking advantage of the loaded Fe particles, Sil-MIC can be temporarily fixed on different substrates using a permanent magnet. Consequently, by a simple elimination of the magnetic field, both the substrate and Sil-MIC are completely recovered.

Summarizing, the contact angle measurements and the magnitudes obtained thereof further confirm the formation of quasi superamphiphobic substrates by simply spreading Sil-MIC above a surface and immobilizing them using a simple magnet. The possibility of spreading the developed powder in virtually any solid substrate and the instantaneously fixing of the interest area with a simple external magnetic field permit to develop a new concept of “movable,” or “reconfigurable” SH surfaces.

To further assess the potential of the developed Sil-MIC, these particles were used to produce liquid marbles and microfluidic channels/patterns. Liquid marbles, which were first

introduced by Aussillous and Quéré, are composed of liquid droplets protected from the external environment by a hydrophobic shell [17]. Owing to their low dimensions and the easiness of manipulating liquids inside them, liquid marbles can be used to miniaturize processes, making them attractive as microreactors and sensors [18].

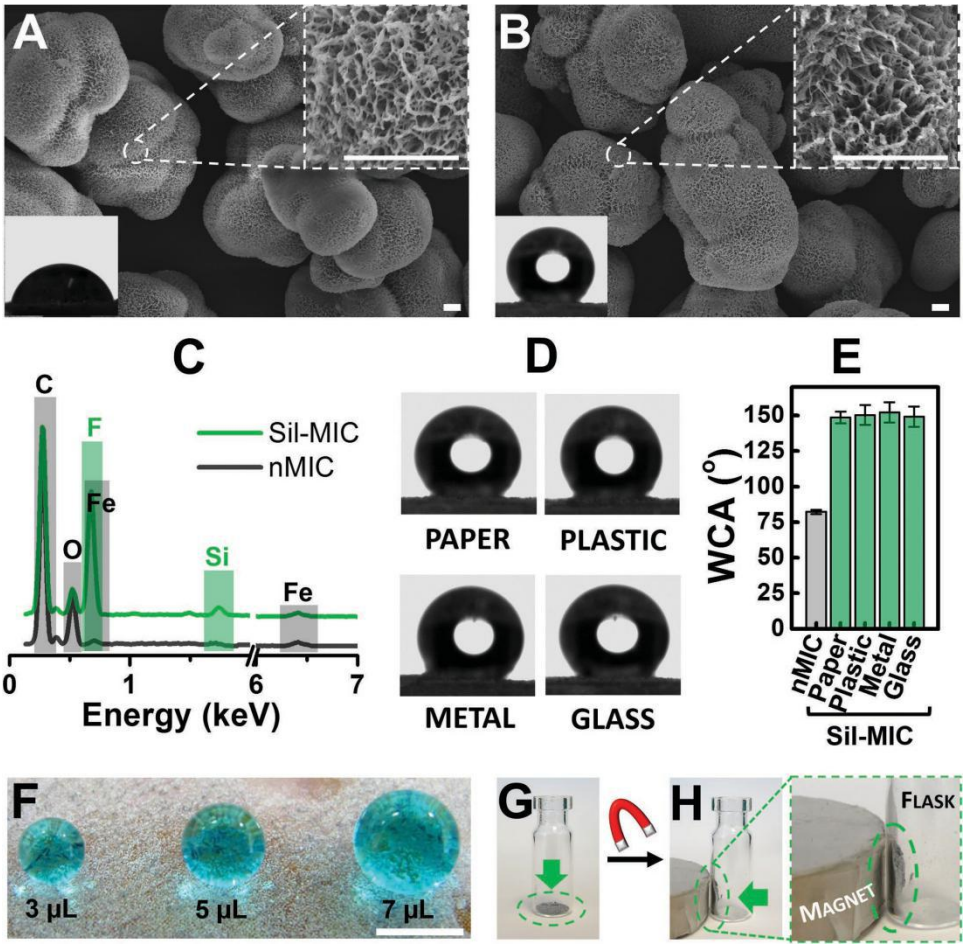

Figure 8.1 - SEM images of the fabricated **A)** MIC and **B)** Sil-MIC composite powders. The insets include representative images of the lateral profiles of water droplets placed above surfaces covered with Sil-MIC (left bottom corner) and magnifications of the SEM images, revealing the nanotopography of the particles (right upper corner). The scale bars correspond to 5 µm. **C)** EDS spectra of both MIC and Sil-MIC. **D)** Representative images of water droplets over Sil-MIC powder above four types of substrates, namely, paper, plastic, metal, and glass. **E)** WCA values of MIC and Sil-MIC above the four types of substrates. nMIC correspond to non-modified MIC. **F)** Droplets, containing alcian blue dye for better visualization, with different sizes above the Sil-MIC powder. The scale bar corresponds to 1 mm. Evaluation of the Sil-MIC magnetic properties by comparing their behavior in the **G)** absence or **H)** presence of a magnet (surface magnetic intensity of 0.075 T).

Liquid marbles were produced by dropping a liquid containing alcian blue dye above Sil-MIC previously spread above a watch glass (Figure 8.2A). Afterwards, the previous droplet was rolled above this Sil-MIC powder, yielding liquid marbles (Figure 8.2B and Movie S8.3, SI.8). These particles can be used to produce stable spherical miniaturized bioreactors due to their ability to inject or remove liquid without destroying their integrity as shown in Figure 8.2C and Movie S8.4 (SI.8). The magnetic responsiveness of the produced liquid marbles constitutes an advance in this kind of systems, conferring easiness on handling; for example, their motion can be controlled remotely using a permanent magnet (Figure 8.2D and Movie S8.5, SI.8). The size of these systems can be tuned by controlling the dispensed volume above the Sil-MIC particles (Figure 8.2E). Moreover, a cytotoxicity test was performed to assess the ability of the developed liquid marbles to support living cell encapsulation using the developed SH powder. As shown in Figure 8.2F, the developed Sil-MIC do not present any cytotoxicity compared with the negative control due to the high hydrophobicity of the powder, resulting in a low interaction with water-based liquids such as the culture medium.

Taking advantage of the mobility and spatial control of these surfaces, other adaptive devices can be constructed such as microfluidic channels (Figure 8.2G,H and Movie S8.6, SI.8) or patterns (Figure 8.2I,J). By fixing such particles with an external magnetic field, a liquid may be confined or forced to flow in the exposed regions.

Inspired by the hierarchical morphology of the Sil-MIC above a substrate, these particles were carefully sintered at 150 ºC for 30 min in order to retain the surface roughness and yield a robust and stable membrane. Afterwards, the produced films were coated with a low-surface-energy PFDTS compound to achieve superhydrophobicity (Figure 8.3A). This process must be carefully performed as the overheating may result in the loss of the hierarchical topography (Figure 8.3B), which is responsible for the SH character. Contrarily, the particles must partially melt in order to get a stable membrane. Otherwise, the membrane lacks robustness and is easily fragmented as can be observed in Figure 8.3C. The sintering temperature was chosen to

be in the very early stage of the melting process of the polyamide particles and above the glass transition of this polymer (Figure S8.2, SI.8).

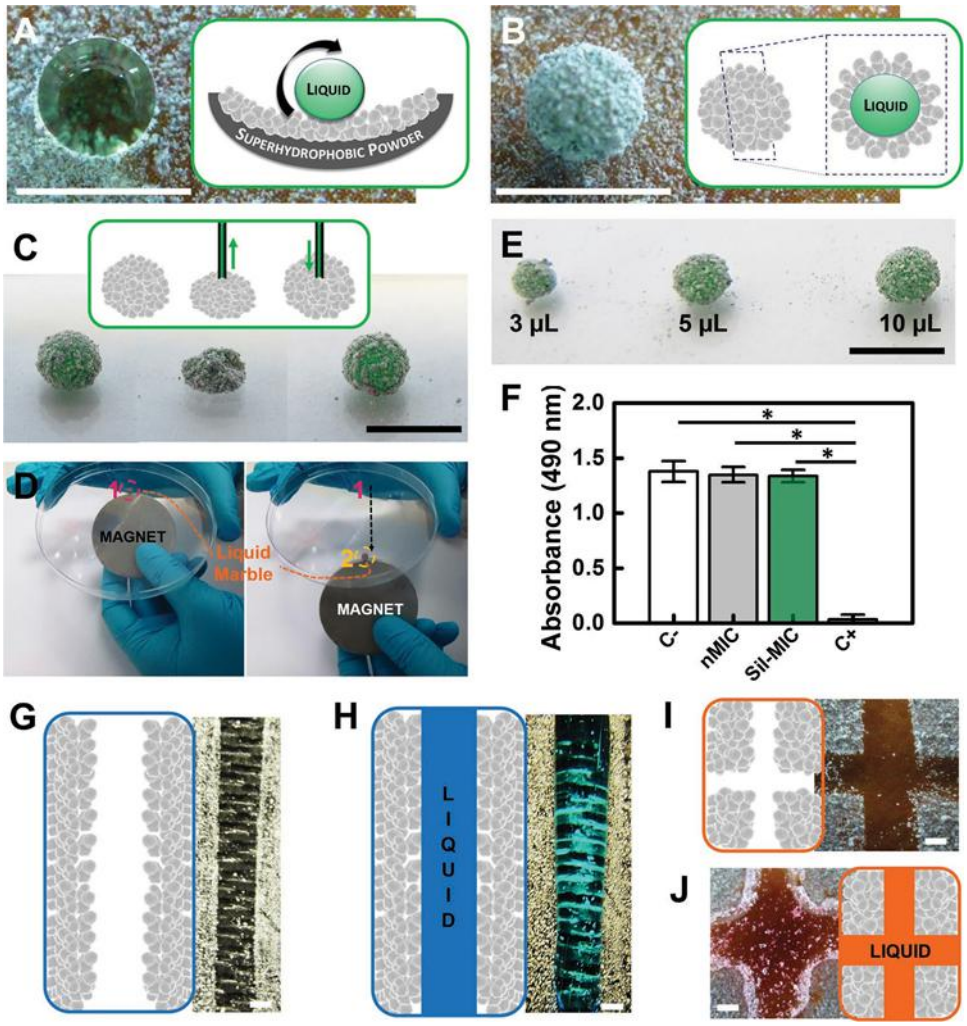

Figure 8.2 - A) Liquid marble fabrication process by dispensing a liquid droplet containing alcian blue dye above a watch glass covered with Sil-MIC and **B)** then, by carefully rolling it above the Sil-MIC powder. **C)** Assessment of the ability to inject or remove liquid from the produced marbles without compromising their integrity. **D)** Motion control of the produced liquid marbles using a permanent magnet. **E)** Liquid marbles with different sizes produced by dispensing controlled volumes of water containing alcian blue dye above Sil-MIC powder. **F)** Cytotoxicity of both MIC and Sil-MIC powders using L929 cell line and evaluated through an MTS assay. The positive (C^+) and negative (C^-) controls correspond to latex rubber and TCPS, respectively. **G,H)** Hydrophilic channel and **I,J)** patterns printed on glass slide covered with Sil-MIC powders. The scale bars correspond to 2 mm.

After their exposure to high temperatures, Sil-MIC films were obtained, preserving their magnetic properties and the shape of the pulverized powder (Figure 8.3D). Therefore, they can be used to reversibly cover any substrate, even when it is vertically oriented (Movie S8.7, SI.8). These substrates can also be used to produce polymeric particles. The technology using SH surfaces to obtain spherical particles comprises the dispensing of a polymeric solution on a surface, which yields spherical-shaped droplets [19]. Afterwards, the former liquid droplets are hardened into a hydrogel through a crosslinking process and collected from the SH surface by tilting it. Overall, this technique presents two main advantages over the currently available methodologies to create spherical systems. First, since it avoids the use of any solvents/process liquids, it allows the encapsulation of virtually any kind of molecules and biological cargo with efficiencies of almost 100%. Second, this technique is cheaper and simpler inasmuch as it does not involve the use of complex apparatus [19a]. As a validation, ALG particles were produced above the obtained SH membranes using $CaCl_2$ as crosslinker (Figure 8.3E), giving rise to stable spherical hydrogel particles (Figure 8.3F).

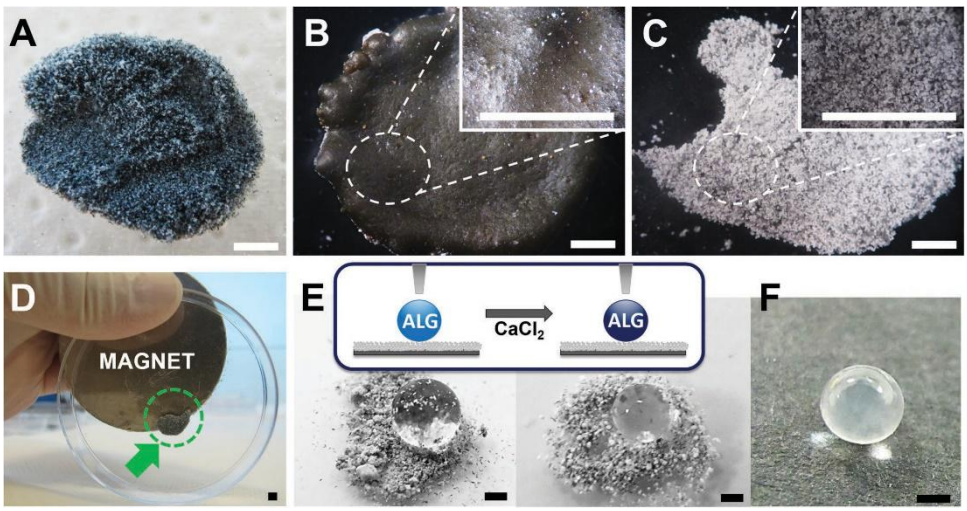

Figure 8.3 - Sil-MIC membranes produced by a sintering process at: **A)** 150 °C for 30 min, **B)** 200 °C for 30 min, and **C)** 100 °C for 30 min. **D)** Motion control and fixation ability of the produced sintered SH membranes using a permanent magnet**. E)** Polymeric particles fabrication process using the developed SH powder as a supportive platform. **F)** Example of an ALG hydrogel sphere fabricated following the former methodology. The scale bars correspond to 300 µm.

4. Conclusion

In conclusion, this paper discloses a fast and simple strategy to produce SH surfaces by simply spreading hydrophobized Fe-loaded composite corrugated microcapsules over a substrate. Moreover, the presence of the magnetic particles within the former microcapsules allows for their motion and fixation control through an external magnetic field as well as for the complete recycling of both substrate and microcapsules without any loss. Based on the obtained results, this methodology is envisioned to constitute an innovative approach for the cost-effective production of SH reconfigurable surfaces for direct applications in a large spectrum of fields including biomedicine, biotechnology, and agriculture to prepare liquid marbles, microfluidic channels, and as templates for polymeric particles fabrication.

Acknowledgements

This work was funded by FCT through the grants SFRH/BD/101748/2014 and SFRH/BPD/96797/2013, and through nSTEP project NORTE-07-0124-FEDER-000039.

Supplementary Information (SI.8)

S8.1. Preparation and characterization of polyamide microcapsules (MIC)

Polyamide MIC with a Fe-particle content of 10 wt% were synthesized by a developed one-step *in situ* process according to the process described in [20, 21]. Briefly, the polymerization was carried out in a 250 mL glass flask fitted with thermometer, magnetic stirrer, Dean-Stark attachment for azeotropic distillation with reflux condenser and an inlet for dry N_2. In a typical synthesis, 0.5 mol of ε-caprolactam (ECL, product of Brüggemann, Germany) and 5 wt%, in respect to ECL, of carbonyl iron powder (non-insulated, donated by BASF, Ludwigshafen, Germany, containing +99.8% Fe, grain size of 3-5 μm) were added to 100

mL of a 1:1 volume ratio of toluene/xylene while stirring, under a N_2 atmosphere, refluxing the reaction mixture for 10-15 min. Then, 3 mol% of initiator (dicaprolactamato-bis-(2-methoxyethoxo)-aluminate, Katchem, Czech Republic) and 1.5 mol% of activator (Brüggolen C20 of Brüggemann, Germany) were added. The reaction time was set in 1 hour, the temperature kept in the 125-135°C range and a constant stirring rate of *ca.* 800 rpm was applied. The Fe-loaded MIC were formed as a fine powder and were separated from the reaction mixture by hot vacuum filtration. Afterwards, the obtained MIC were washed several times with methanol and dried for 30 min in a vacuum oven at 100°C (Yield: 72%). The fabrication steps are schematically shown in Figure S8.1A and the underlying chemistry – in Figure S8.1B.

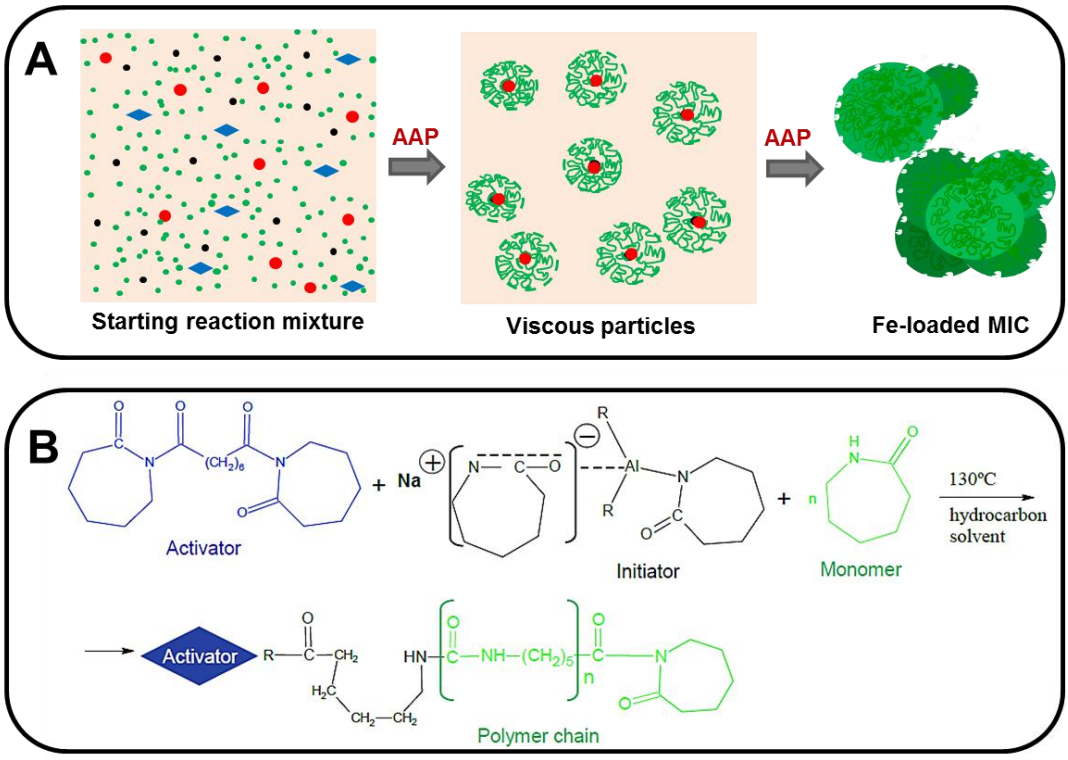

Figure S8.1 - (A) Schematic representation of the various steps of AAP process used to produce Fe-loaded MIC: the starting reaction mixture contains the monomer ●, the activator ◆, the initiator molecules ●, and the Fe particles ●; all of them were suspended in a hydrocarbon solvent ■. The final Fe-loaded MIC are porous objects produced after coalescence of viscous particles and a solid state crystallization. The Fe particles are in the MIC interior. **(B)** Simplified chemical reactions of AAP: the activator (blue) is a bis-caprolactam imide compound that starts any PA6 macromolecule (green). The initiator (black) is a caprolactamate anion stabilized by an organoaluminum ligand.

The average viscometric molecular weight of the MIC is 37.5 kg/mol as determined by intrinsic viscosity measurements at 25 °C.

The differential scanning calorimetry (DSC) measurements were carried out in a 200 F3 equipment of Netzsch (Selb, Germany) at a heating and cooling rates of 10 °C/min under N_2 purge. The typical sample weights were in the 10-15 mg range. The results suggested that MIC melting temperature was of 208.9°C.

The effective load of Fe inside the produced MIC was established by means of thermogravimetric analysis (TGA) in a Q500 gravimetric balance (TA Instruments, New Castle, USA) heating the samples to 600 °C at 10 °C/min in a N_2 atmosphere. The real load (R_L) of Fe was of 9.8 % and was calculated according to:

$$R_L = R_{Fe} - R_{PA6}\,[\%] \qquad (1)$$

where R_{PA6} is the carbonized residue at 600 °C of empty MIC and R_{Fe} corresponds to that of the respective loaded MIC measured by TGA.

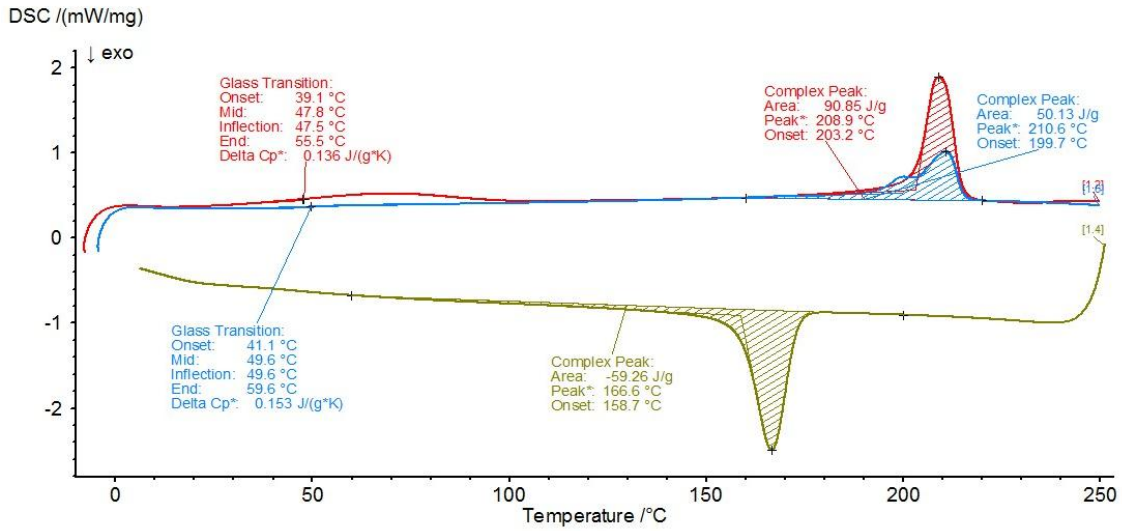

Figure S8.2 - DSC curves of the produced MIC used to identify their thermal transitions including the glass transition and the melting process ("complex peak").

S8.2. WCA measurements employing different PFDTS coating methodologies above different substrates

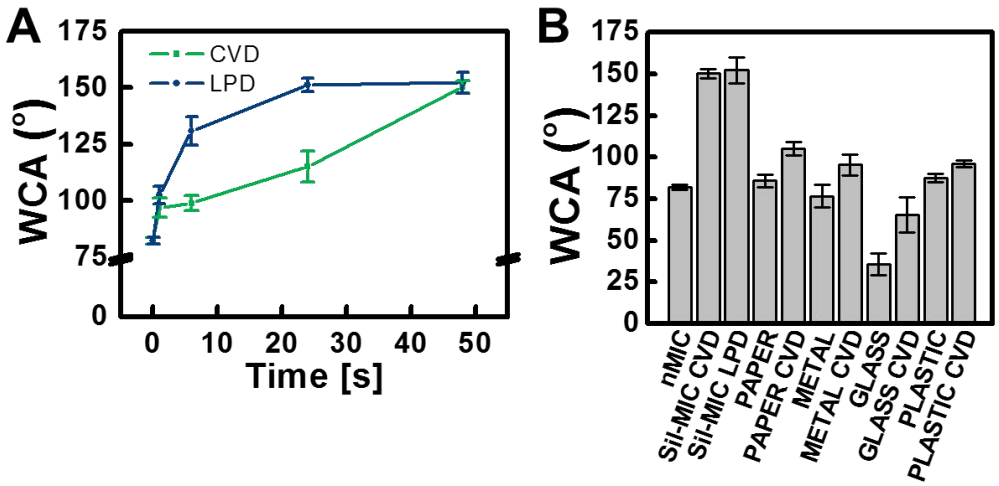

Figure S8.3 - (A) WCA values obtained using a chemical vapor deposition (CVD) or a liquid phase deposition (LPD) process for different PFDTS exposure times. **(B)** WCA values of non-modified microcapsules (nMIC), PFDTS coated microcapsules through CVD (Sil-MIC CVD), PFDTS coated microcapsules through LPD (Sil-MIC LPD), paper (PAPER), PFDTS coated paper through CVD (PAPER CVD), metal (METAL), PFDTS coated metal through CVD (METAL CVD), glass (GLASS), PFDTS coated glass through CVD (GLASS CVD), plastic (PLASTIC) and PFDTS coated plastic through CVD (PLASTIC CVD).

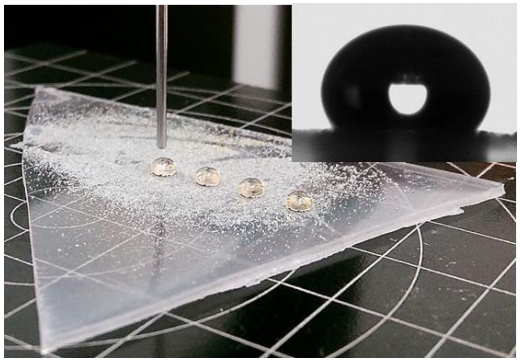

Figure S8.4 - Representative image of the contact angle of Sil-MIC powder above a plastic substrate using diiodomethane.

Movie S8.1. Wettability of Sil-MIC placed above a glass substrate: dispensing a water droplet; **Movie S8.2.** Motion control of Sil-MIC: using a permanent magnet; **Movie S8.3.** Liquid marble production process: using Sil-MIC; **Movie S8.4.** Control of liquid content present on the produced liquid marble: removing or adding water using a needle; **Movie S8.5.** Motion control of the liquid marble: using a permanent magnet; **Movie S8.6.** Production of a microfluidic channel using Sil-MIC; and **Movie S8.7.** Motion control of Sil-MIC membranes: using a permanent magnet; are available online using DOI: 10.1002/admi.201600074.

References

[1] a) S. Wang, K. Liu, X. Yao, L. Jiang, Bioinspired Surfaces with Superwettability: New Insight on Theory, Design, and Applications, *Chem. Rev.* **2015**, 115, 8230; b) A. C. Lima, J. F. Mano, Micro-/nano-structured superhydrophobic surfaces in the biomedical field: part I: basic concepts and biomimetic approaches, *Nanomedicine* **2015**, 10, 103; c) A. C. Lima, J. F. Mano, Micro/nano-structured superhydrophobic surfaces in the biomedical field: part II: applications overview, *Nanomedicine* **2015**, 10, 271; d) M. Nosonovsky, B. Bhushan, Superhydrophobic Surfaces and Emerging Applications: non-adhesion, energy, green engineering, *Curr. Opin. Colloid Interface Sci.* **2009**, 14, 270.

[2] W. Barthlott, C. Neinhuis, Purity of the sacred lotus, or escape from contamination in biological surfaces, *Planta* **1997**, 202, 1.

[3] P. Roach, N. J. Shirtcliffe, M. I. Newton, Progess in superhydrophobic surface development, *Soft Matter* **2008**, 4, 224.

[4] a) X. Zhang, F. Shi, J. Niu, Y. Jiang, Z. Wang, Superhydrophobic surfaces: from structural control to functional application, *J. Mater. Chem.* **2008**, 18, 621; b) A. B. D. Cassie, S. Baxter, Wettability of porous surfaces, *J. Chem. Soc., Faraday Trans.* **1944**, 40, 546; c) R. N. Wenzel, Resistance of solid surfaces to wetting by water, *Ind. Eng. Chem. Res.* **1936**, 28, 988.

[5] X. Deng, L. Mammen, Y. Zhao, P. Lellig, K. Müllen, C. Li, H.-J. Butt, D. Vollmer, Transparent, thermally stable and mechanically robust superhydrophobic surfaces made from porous silica capsules, *Adv. Mater.* **2011**, 23, 2962.

[6] a) H.-J. Choi, S. Choo, J.-H. Shin, K.-I. Kim, H. Lee, *J. Phys. Chem. C* **2013**, 117, 24354; b) D. Han, A. J. Steckl, Superhydrophobic and Oleophobic Fibers by Coaxial Electrospinning, *Langmuir* **2009**, 25, 9454; c) D. Zhu, X. Lu, Q. Lu, Electrically conductive PEDOT coating with self-healing superhydrophobicity, *Langmuir* **2014**, 30, 4671.

[7] Y. Zhu, J. C. Zhang, J. Zhai, Y. M. Zheng, L. Feng, L. Jiang, Multifunctional Carbon Nanofibers with Conductive, Magnetic and Superhydrophobic Properties, *Chem. Phys. Chem.* **2006**, 7, 336.

[8] Z. Huang, Y. Zhu, J. Zhang, G. Yin, *Stable Biomimetic Superhydrophobicity and Magnetization Film with Cu-Ferrite Nanorods, J. Phys. Chem. C* **2007**, 111, 6821.
[9] A. M. Costa, M. Alatorre-Meda, N. M. Oliveira, J. F. Mano, Biocompatible polymeric microparticles produced by a simple biomimetic approach, *Langmuir* **2014**, 30, 4535.
[10] T. Mosmann, Rapid colorimetric assay for cellular growth and survival: application to proliferation and cytotoxicity assays, *J. Immunol. Methods* **1983**, 65, 55.
[11] J. A. Barltrop, T. C. Owen, A. H. Cory, J. G. Cory, 5-(3-Carboxymethoxyphenyl)-2-(4,5-dimethylthiazolyl)- 3-(4-sulfophenyl)tetrazolium, Inner Salt (MTS) and Related Analogs of 3-(4,5-dimethylthia-zolyl)-2,5-diphenyltetrazolium Bromide (MTT) Reducing to Purple Water-Soluble Formazans as Cell-Viability Indicators, *Bioorg. & Med. Chem. Lett.* **1991**, 1, 611.
[12] a) J. Zhang, S. Seeger, Superoleophobic coatings with ultralow sliding angles based on silicone nanofilaments, *Angew. Chem., Int. Ed.* **2011**, 50, 6652; b) K. Zhao, K. S. Liu, J. F. Li, W. H. Wang, L. Jiang, Superamphiphobic CaLi-based bulk metallic glasses, *Scr. Mater.* **2009**, 60, 225; c) N. M. Oliveira, R. L. Reis, J. F. Mano, Superhydrophobic surfaces engineered using diatomaceous earth, *ACS Appl. Mater. Interfaces* **2013**, 5, 4202.
[13] a) S. M. Ramos, A. Benyagoub, B. Canut, C. Jamois, Superoleophobic behavior induced by nanofeatures on oleophilic surfaces, *Langmuir* **2010**, 26, 5141; b) V. A. Ganesh, S. S. Dinachali, H. K. Raut, T. M. Walsh, A. S. Nair, S. Ramakrishna, Electrospun SiO2 nanofibers as a template to fabricate a robust and transparent superamphiphobic coating, *RSC Adv.* **2013**, 3, 3819; c) X. Deng, L. Mammen, H. J. Butt, D. Vollmer, Candle soot as a template for a transparent robust superamphiphobic coating, *Science* **2012**, 335, 67.
[14] a) C. Aulin, S. H. Yun, L. Wågberg, T. Lindström, Design of highly oleophobic cellulose surfaces from structured silicon templates, *ACS Appl. Mater. Interfaces* **2009**, 1, 2443; b) T. Fujii, H. Sato, E. Tsuji, Y. Aoki, H. Habazaki, *Important Role of Nanopore Morphology in Superoleophobic Hierarchical Surfaces, J. Phys. Chem. C* **2012**, 116, 23308.
[15] Q. Xie, J. Xu, L. Feng, L. Jiang, W. Tang, X. Luo, C. C. Han, Facile Creation of a Super - Amphiphobic Coating Surface with Bionic Microstructure, *Adv. Mater.* **2004**, 16, 302.
[16] A. Tuteja, W. Choi, M. Ma, J. M. Mabry, S. A. Mazzella, G. C. Rutledge, G. H. McKinley, R. E. Cohen, Designing superoleophobic surfaces, *Science* **2007**, 318, 1618.
[17] P. Aussillous, D. Quéré, Liquid marbles, *Nature* **2001**, 411, 924.
[18] a) N. M. Oliveira, C. R. Correia, R. L. Reis, J. F. Mano, The Potential of Liquid Marbles for Biomedical Applications: A Critical Review, *Adv. Healthcare Mater.* **2015**, 4, 264; b) T. Arbatan, L. Li, J. Tian, W. Shen, Liquid Marbles as Micro-bioreactors for Rapid Blood Typing, Adv. *Healthcare Mater.* **2012**, 1, 80; c) J. Tian, N. Fu, X. D. Chen, W. Shen, Respirable liquid marble for the cultivation of microorganisms, *Colloids Surf., B* **2013**, 106, 187.
[19] a) W. Song, A. C. Lima, J. F. Mano, Bioinspired methodology to fabricate hydrogel spheres for multi-applications using superhydrophobic substrates, *Soft Matter* **2010**, 6, 5868; b) A. M. S. Costa, M. Alatorre-Meda, C. Alvarez-Lorenzo, J. F. Mano, Superhydrophobic Surfaces as a Tool for the Fabrication of Hierarchical Spherical Polymeric Carriers, *Small* **2015**, 11, 3648.

[20] F. M. Oliveira, N. Dencheva, P. Martins, S. Lanceros-Méndez, Z. Denchev, Reactive microencapsulation of carbon allotropes in polyamide shell-core structures and their transformation in hybrid composites with tailored electrical properties, *Express Polym. Lett.* **2016**, 10,160.
[21] N. Dencheva, Z. Denchev, S. Lanceros-Méndez, T. A. Ezquerra, One - Step In Situ Synthesis of Polyamide Microcapsules With Inorganic Payload and Their Transformation into Responsive Thermoplastic Composite Materials, *Mat. Eng.* **2015**, 301.

Chapter IX: Results & Discussion

Biocompatible Polymeric Microparticles Produced by a Simple Biomimetic Approach[5]

ABSTRACT

The use of superhydrophobic surfaces to produce polymeric particles proves to be biologically friendly since it entails the pipetting and subsequent crosslinking of polymeric solutions under mild experimental conditions. Moreover, it renders encapsulation efficiencies of ~100%. However, the obtained particles are 1 to 2 mm in size, hindering to a large extent their application in clinical trials. Improving on this technique, we propose the fabrication of polymeric microparticles by spraying a hydrogel precursor over superamphiphobic (SA) surfaces followed by photo-crosslinking. The particles were produced from methacrylamide chitosan (MACHI) and characterized in terms of their size and morphology. As demonstrated by optical and fluorescence microscopy, the designed strategy led, for the first time, to the production of spherical particles with diameters in the order of micrometers, nominal sizes not attainable by pipetting. Particles such as these may be suitable for medical applications such as drug delivery and tissue engineering.

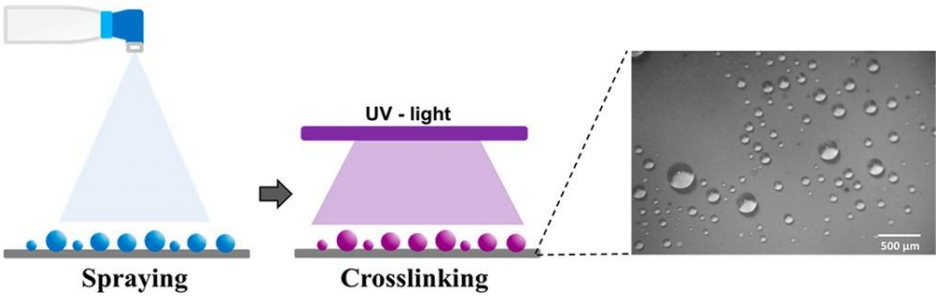

[5] Based on the publication: Ana M. S. Costa, Manuel Alatorre-Meda, Nuno M. Oliveira, João F. Mano, Biocompatible Polymeric Microparticles Produced by a Simple Biomimetic Approach, *Langmuir* **2014**, 30 (16), pp. 4535–4539.

1. Introduction

Polymeric particles for biomedical applications can be produced by a plethora of different routes, including emulsion polymerization, solvent evaporation/extraction, and phase separation (coacervation), among others; all of which are indeed effective for their massive production but might also present major limitations related to the use of organic/toxic solvents or high temperature, compromising the encapsulation of certain bioactive materials [1, 2]. Recognizing the aforementioned drawbacks of conventional protocols, our group has recently proposed the implementation of biomimetic synthesis procedures based on the utilization of SH surfaces for the production of polymeric mono- and multilayered particles [3, 4], also inspiring the work of others [5]. The strategy, encompassing the pipetting and subsequent crosslinking of polymeric solutions containing the drug to be released, is rather simple and reproducible, allowing the production of totally biocompatible materials with encapsulation efficiencies of ~100%. However, the minimum size and shape of the produced particles are strongly dependent on the viscosity/volume of the dispensed polymeric solution and substrate conditions, resulting in the production of particles not smaller than 1 mm in diameter, hampering in consequence their tentative use in clinical trials.

Improving on this biomimetic technique, here we demonstrate, for the first time, the production of polymeric microparticles on top of SA surfaces. The particles were produced from aqueous solutions of MACHI by spraying followed by photo-crosslinking. On the one hand, MACHI is anticipated to endow the particles with the favorable biological properties of CH such as its outstanding biocompatibility [6-8] and biodegradability [9, 10] while being soluble in water, and presenting methacrylic groups necessary for crosslinking [11]. On the other hand, we prove that spraying onto SA surfaces is conducive to the production of increasingly smaller particles with nominal diameters in the order of micrometers.

2. Materials & Methods

2.1. Materials

Glass microscope slides were from Medline (Spain). Acetic acid was from VWR (Belgium). Tetraethyl orthosilicate (TEOS, 98%), methacrylic anhydride (MA, ≥92%), ammonium hydroxide solution (30–33%), 2-hydroxy-4-(2-hydroxyethoxy)-2-methylpropiophenone (I2959, 98%), and 1H,1H,2H,2H-perfluorodecyltriethoxysilane (silane, 97%) were from Sigma-Aldrich. Chitosan 95/20 was from Heppe Medical Chitosan GmbH (Germany). KBr powder was from PIKE Technologies (USA). Deuterium oxide was from Cambridge Isotope Laboratories (USA). All materials were used as received. Unless otherwise stated, water purified in an 18 MΩ cm Milli-Q Plus water system was used throughout.

2.2 Synthesis of SA Surfaces

SA surfaces were produced as described elsewhere with subtle variations [12]. Briefly, glass microscope slides were held above the flame of a paraffin candle in order to form a soot layer. Afterwards, the soot coated substrates were exposed to the chemical vapor deposition (CVD) of TEOS (4 mL) in the presence of ammonia (4 mL) for 24 h in a desiccator, followed by the calcination of the hybrid carbon/silica network at 600 °C for 2 h. Finally, the hydrophilic silica shell was coated with silane (150 µL) by CVD for 3 days. The surfaces were characterized for their topography and water contact angle (WCA) by Scanning Electron Microscopy (SEM, Leica Cambridge S360 operated at 15 kV) and Static WCA measurements (OCA15+ goniometer, DataPhysics, Germany), respectively. For the SEM characterization, the surfaces were sputter-coated with gold and palladium. The surface microstructure was determined from SEM pictures by drawing intensity plot profiles across the obtained image and defining a threshold of 150 (gray scale from 0 to 255) with the Image J software. The distance between two peaks was defined as the micro-feature size. Results are the mean of 30 measurements using 6 different intensity plots. On the other hand, the WCA characterization

was conducted on the basis of the sessile drop method. In a typical experiment 3 µL water droplets were dispensed on every surface and angles were measured after drop stabilization using the SCA 20 software supplied with the instrument. The experiments were carried out in triplicate on different areas of the surfaces at RT.

2.3. Synthesis of MACHI

As described by Yu et al. [11], CHI (3 w/v %) was dissolved in a 2 wt% acetic acid aqueous solution overnight at RT with constant stirring. Then, MA was added at 0.4 molar equivalents per CHI repeat unit and left for 3 h at RT. The mixture was dialyzed against distilled water for 3 days, changing the water twice a day. The MACHI solution was then freeze-dried and stored at -20 °C until use. Fourier Transform InfraRed Spectroscopy (FTIR, IRPrestige 21; Shimadzu) was used to infer about the correct CH methacrylation (SI.9, Section S9.1). Transmission spectra for CHI, MA, and MACHI were recorded in KBr pellets within the range of 4000-400 cm^{-1} using 32 scans, with a resolution of 2 cm^{-1}.

2.4. Synthesis and Characterization of MACHI Microparticles

On the day of the experiment, 2.5 w/v % MACHI was dissolved in water containing 0.25 w/v% I2959. To produce the MACHI microspheres, we dispensed this solution with a generic spray (nozzle sectional area = 7.55×10^{-4} cm^2, input pressure ~400 mbar; SI.9, Section S9.2) by spraying once 25 cm above the SA surface (Figure 9.1). Afterwards, the obtained polymeric droplets were crosslinked using UV light (365 nm, 11.4 mW/cm^2) for 1 min. The sprayed droplets were observed by optical (TR500; VWR) and fluorescence microscopy (Axio Imager Z1m; Zeiss) before and after crosslinking. The mean particle size (diameter) and shape factor (SF, ratio between diameters of particles orthogonal and parallel to the surface) of 90 different particles were obtained from 14 independent optical images by using ImageJ. For fluorescence

microscopy, images were recorded using a fluorescence emission of 505 nm and analyzed using the ZEN software supplied with the instrument.

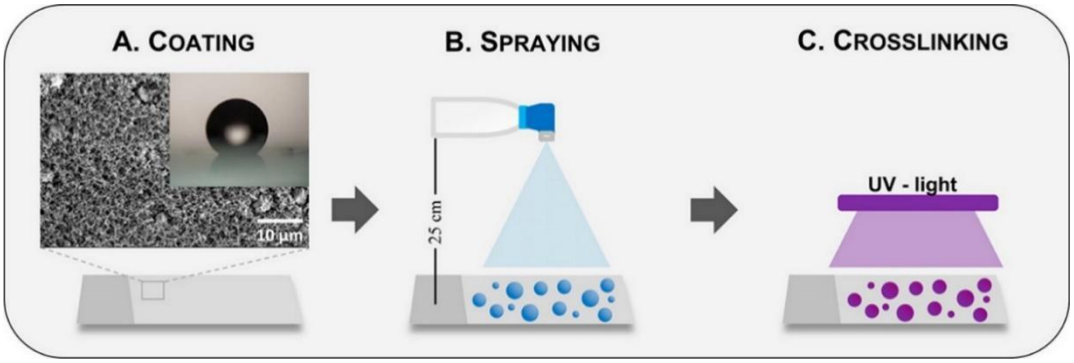

Figure 9.1 - Scheme depicting the strategy developed to produce MACHI microparticles. **(A)** Microscope glass slides were coated with a carbon/silica/silane network in order to obtain a SA surface. WCA and SEM images of the surface structure are shown. **(B)** MACHI solution was dispensed using a generic spray placed 25 cm above the SA surface. **(C)** MACHI particles were crosslinked using UV light for 1 min in the presence of I2959.

2.5. Statistical Analysis

Statistical significance was considered for $p < 0.05$ using the Student's t-test.

3. Results and Discussion

3.1. General Overview of the Proposed Technology

Polymeric microparticles were produced for the first time on top of superantiwetting surfaces. The microparticles were produced from MACHI, a well-known biopolymer, and crosslinked upon light irradiation in the presence of I2959, a cytocompatible crosslinker [13, 14]. The obtained particles were characterized before and after crosslinking in order to assess the feasibility of the proposed method.

The first step in our study was devoted to finding the optimal experimental conditions, in particular, those relative to the MACHI concentration, crosslinking time, spraying height for the

chosen spray, and particle recovery mechanism. With respect to the MACHI concentration and crosslinking time, preliminary studies with particles produced by pipetting demonstrated that polymer concentrations below 1% gave rise to weak gels even after crosslinking times greater than 10 min. By contrast, when the concentration of MACHI was increased to *ca.* 3%, the gels were found to adopt a more solid structure at crosslinking times of around 1 min. As a result, the MACHI concentration and crosslinking time were chosen to be 2.5% and 1 min, respectively. The selected concentration was the highest one allowing a free flow of the polymeric solution through the spray nozzle. Regarding the spraying height, it was decided to set it at 25 cm above the surface since shorter heights (*ca.* 5–10 cm) rendered particles equivalent to those obtained by pipetting, easily seen by naked eye, and higher ones (*ca.* 30–40 cm) reduced the quantity of dispensed solution given the restricted area of the surfaces. Finally, concerning particle recovery, we concluded that the best way to remove the particles from the surfaces was by mechanical methods such as by a slight tapping by the noncoated face of the SA surfaces. In this context, we also verified that the removal of particles is facilitated while working under humidified-air conditions so that the particles remain hydrated. The chosen experimental conditions made possible the administration of 17 ± 1 mg of polymeric solution per cycle (n = 6), resulting in a final weight of particles after crosslinking of 13 ± 2 mg (n = 6) (that is, a shrinking ratio of 23.5%). Inferred from optical micrographs of the surfaces after particle recovery, the process yield was determined to be *ca.* 100% inasmuch as almost no particle was observed all along the inspected surfaces.

3.2 Particle Characterization by Optical and Fluorescence Microscopy

Figure 9.2 presents optical and fluorescence micrographs of the produced microparticles before and after crosslinking. Regarding the optical characterization, panel A shows that dispensed particles (before crosslinking) were distributed all along the sprayed SA substrates with a well-defined spherical shape, although presenting a rather broad size distribution spanning from *ca.* 80 to 400 μm. The spherical shape (SF = 0.92 ± 0.06) is promoted by the

topography of the surfaces described in the SI.9, Section S9.3. It is well accepted that rough surfaces prompt the formation of a solid–air interface by the inner parts of asperities. Then, when water droplets are dispensed over SA surfaces, they organize preferentially by this interface, reducing to a high extent the solid–liquid contact area and therefore liquid adhesion. Referred to as the Cassie–Baxter state [15], this regime proves to preserve the spherical shape of droplets as long as their diameters are larger than the pitch between asperities and no external forces such as pressure are applied [16, 17]. Thus, the spherical shape of our particles is a consequence of the observed pitch between asperities (Figure S9.1B), which was found to amount to *ca.* 2 µm, a characteristic length at least 1 order of magnitude shorter than the diameter of the smallest sprayed droplets. Interestingly, this particle sphericity combined with their small dimensions, proved to guarantee a lower surface interaction with the SA substrates. As shown in Table 9.1, the fractional contact area (FA) of microparticles was determined to be *ca.* 4 times smaller than that of particles dispensed by pipetting.

Table 9.1 - Surface Contact Area (SCA) and FA in Contact with the Substrates (FA) for Microdroplets and Macrodroplets.[a]

	SCA (mm^2)	**FA (%)**
microdroplet ($R \cong 0.1$ mm)	5.8×10^{-4}	0.4
macrodroplet ($R \cong 1$ mm)	1.9×10^{-1}	1.7

[a] R stands for the particle radius. For details on these calculations, the reader is referred to the SI.9, Section S9.4.

On the other hand, regarding the broad size distribution of sprayed particles (80–400 µm), we speculate it to result from droplet fragmentation, namely, the formation of smaller droplets from larger ones due to their high-speed collision onto solid surfaces during spraying [18]. This is likely to occur considering the already-cited simplicity of the experimental setup by which physical variables such as spraying pressure and nozzle dimensions were not varied. At this point, it is noteworthy that other techniques arguably avoid fragmentation by spraying directly

onto liquid media [19]. Yet, they show the major drawback of requiring additional washing steps devoted to the removal of residual counterions from the bulk (originally present in excess for crosslinking), impacting to a high extent the process yield and not guaranteeing 100% encapsulation efficiencies [19, 20]. As mentioned before, this is not a problem in the current protocol. In our case, the mere implementation of more sophisticated sprays enabling the tuning of the aforementioned variables could be used to achieve a better control over the size distribution of the droplets (*i.e.,* better control of fragmentation).

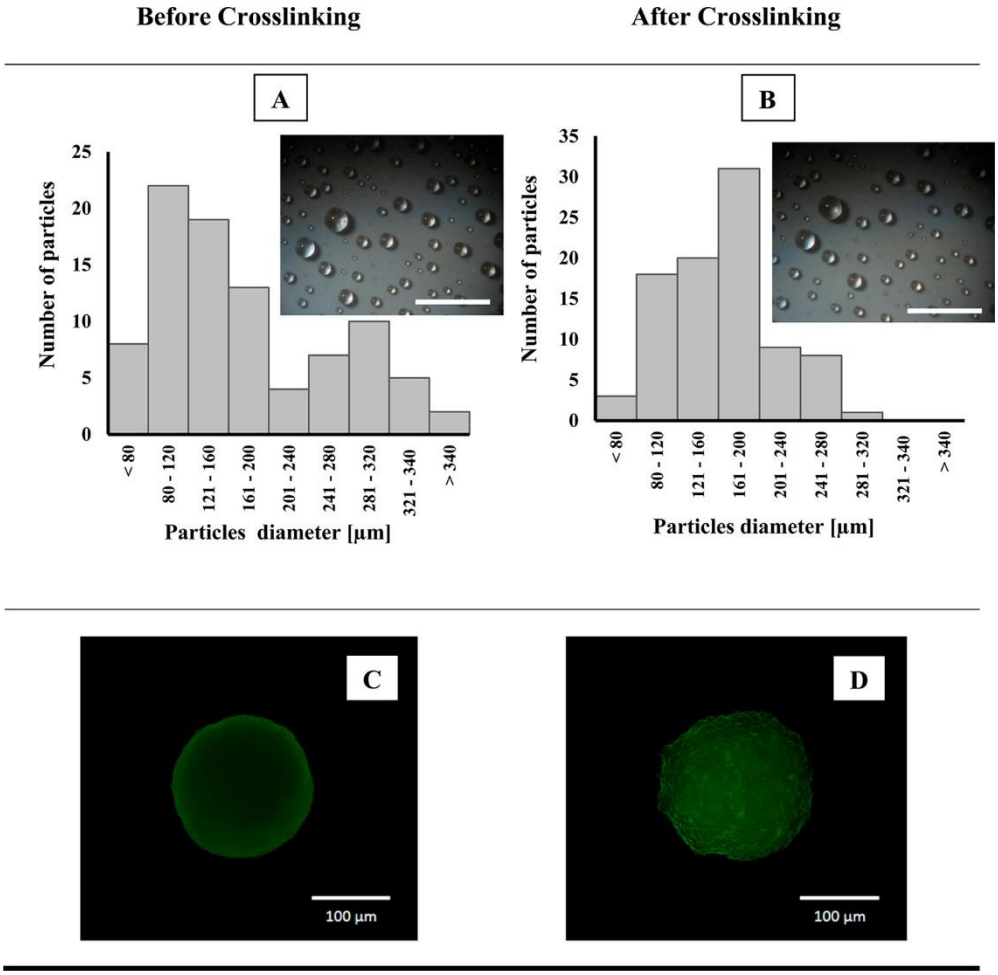

Figure 9.2 - Characterization of MACHI particles before and after crosslinking by optical (**A** and **B**) and fluorescence microscopy (**C** and **D**). Size distribution histograms in panels A and B were calculated from the measurement of the mean diameter (parallel to the surface) of imaged particles. The scale bar in optical micrographs of panels A and B stands for 1 mm.

With respect to particle evolution after crosslinking, panel B depicts two features worth stressing. First, the particles preserved the well-defined spherical geometry exhibited before crosslinking (SF = 0.93 ± 0.08), highlighting the advantages of employing a noninvasive procedure for particle processing [1]. Second, compared to sprayed particles, the width of the size distribution was slightly shortened to the 80–300 μm interval, which can fairly be attributed to water expulsion from the crosslinked polymeric core and the partial dehydration of free water from the surface of already-formed hydrogels [21, 22].

Taking advantage of the natural fluorescence of CH [23], fluorescence microscopy experiments were also carried out in order to gain insight into the inner structure of the produced particles, as shown in panels C and D. These panels confirm the spherical geometry and size of the particles revealed by optical microscopy; however, they also reveal clear differences in the fluorescence emission from samples before (panel C) and after crosslinking (panel D). Panel C displays the imaged particle as having a well-defined contour but a faint core; meanwhile, panel D shows a particle with a well-defined core structure, reflecting a homogeneous distribution of fluorescence emission points. Regarding panel C, the observed blurred profile suggests the presence of a comparatively higher quantity of water, distorting the fluorescence emission of CH. Technically speaking, such a distortion can result from background emission, spherical aberration, and/or a combination of both [22, 24]. Concerning panel D, on the other hand, the observed, more defined profile provides evidence of (i) the confinement of CH chains to a sound spatial restructuring because of crosslinking [25], leading to an enhanced intensity of the in-focus fluorescence related to the accumulation of emission points within a restricted area [26], and (ii) water expulsion from the particle core and the eventual evaporation of superficial water (as also inferred by optical microscopy) [21, 22], diminishing to a high extent the appearance of the aforementioned image artifacts. Interestingly and highlighting our particles as suitable vehicles for drug delivery, NMR results demonstrated that the practiced conditions led to a 76.3% conversion of methacrylic groups, providing evidence of the right crosslinking of CHI chains (SI.9, Section S9.5). As widely cited in

literature, the spatial restructuring of CHI chains within the particles after crosslinking constitutes the driving mechanism by which therapeutic molecules can be encapsulated [27]. Such reorganization is mandatory not only for the initial protection of encapsulated cargos but also for their subsequent controlled release [1].

Taken together, all of these observations ratify that despite the simplicity of the spray system used, which is in part responsible for the obtained size distribution, this method proves to be suitable for obtaining polymeric particles with sizes *ca.* 1 order of magnitude smaller with respect to the current methodology, namely, by pipetting [3, 4], reaching a high process yield of around 100%. Importantly, contrary to the wet-chemistry procedures commonly employed to produce polymeric microparticles [1], our proposed protocol is also demonstrated to be biologically friendly, straightforward, and cost-effective. In fact, we anticipate that the process can be scalable by employing surfaces with larger sectional areas and also by optimizing the experimental conditions for more robust sprays operating at varying spraying pressures, with different nozzles, and allowing, in consequence, to achieve tunable flow rates. Moreover, the simplicity of the concept and the attainable SA character of the surfaces [18] make it possible to expand this technology to other purposes such as cosmetics, agriculture, and electronics, where solvents different than water are often required. On the other hand, regarding the particles *per se*, the biocompatible properties of CHI combined with the mild processing conditions point them out as suitable microcarriers for many bioactive molecules such as cells and proteins, which is beneficial for different fields such as biology and tissue engineering [28, 29].

4. Conclusion

This work proposes a new strategy to produce polymeric particles based on the use of SA surfaces and spraying. Compared to other methodologies, the sketched approach proved to be simple, fast, cost-effective, and totally biocompatible, allowing the production of polymeric microparticles under mild experimental conditions without using any kind of harsh materials.

As such, the proposed strategy is anticipated to constitute a new, versatile tool for producing microcarriers for both science and technology. It must be noted, however, that the possibility of producing particles with increasingly smaller dimensions and narrower size distributions will rely directly on the optimization of the present process and/or the use of more robust dispensing systems. As previously mentioned, the process can be scalable by employing SA surfaces with larger sectional areas.

Acknowledgements

This work was funded by FCT through PhD grants SFRH/BD/101748/2014 and SFRH/BD/73172/2010, by CONACyT (Mexico) through post-doc grant 203732, by the European Union's Seventh Framework Programme (FP7/2007-2013) under grant agreement no. REGPOT-CT2012-316331-POLARIS, by FEDER through the Competitive Factors Operation Program—COMPETE, and by national funds through FCT in the scope of project PTDC/CTM-BIO/1814/2012.

Supplementary Information (SI.9)

S9.1. Characterization of MACHI polymer

Figure S9.1 reveals that the IR spectra of CHI and MA show the typical peaks of each component, namely the CHI bands at *ca.* 3700-2900 (-NH_2 and -OH groups); 2872 (-CH_2-); 1648 and 1581 (amide I and II, respectively); and 1058 (C-O) cm^{-1} [30,31]; and the MA bands at *ca.* 3110 (=CH_2); 2985 and 2961 (asymmetrical C-H stretching vibrations in CH_3); 2931 and 2855 (symmetrical C-H vibrations in CH_3); 1783 and 1731 (anhydride groups); 1637 (C=C); 1454 and 1379 (asymmetrical and symmetrical CH_3 vibrations from C-CH_3, respectively); 1402 (in plane =CH_2 vibration bending); 1297 (C-H in plane modes); 1048 (C-O-C stretching

vibrations of anhydride); 1004 (C-O vibrations in ester groups); 946 (out of plane vibrations of =CH2); and 814 cm^{-1} (C=C-H) [32,33].

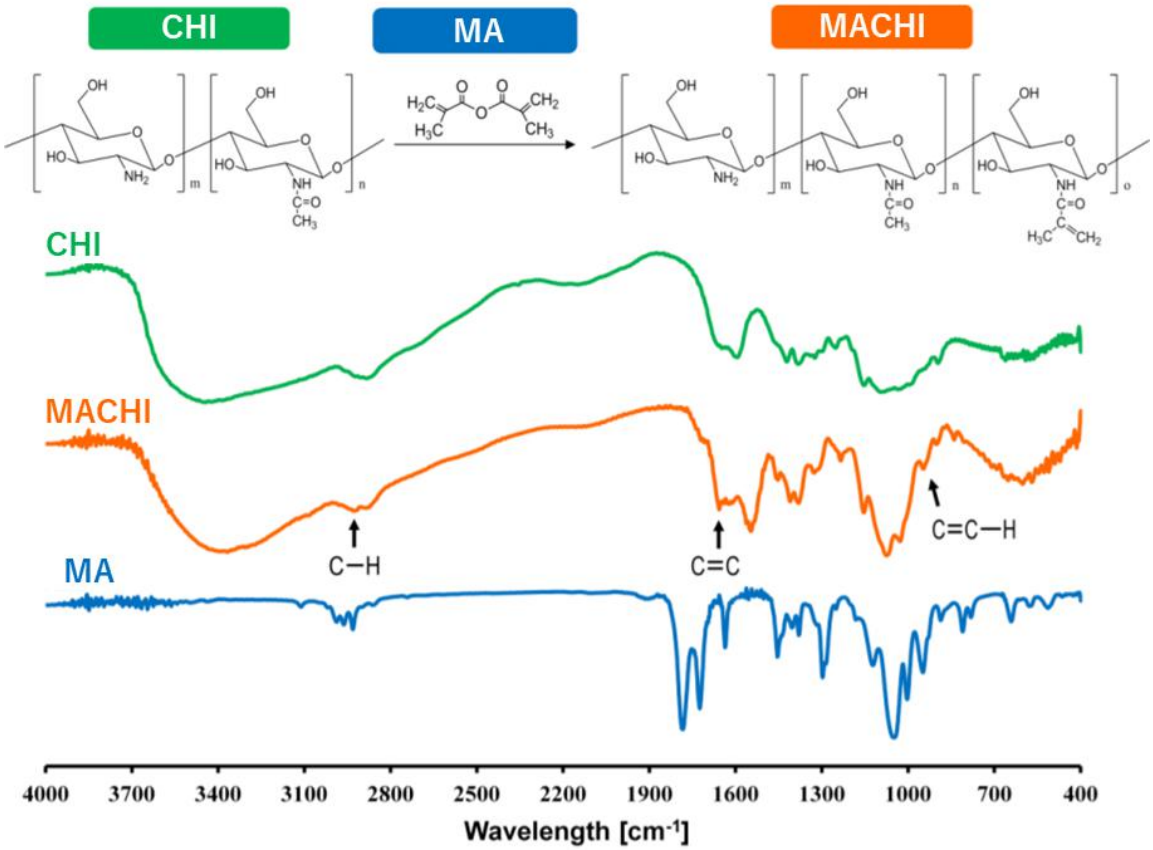

Figure S9.1 - FTIR spectra of CHI, MA and MACHI. Results are presented in %T. Marked with arrows are the chemical groups from MA attached to the modified MACHI polymer. A schematic representation of the chemical reaction occurring is also depicted in top of the image.

By contrast, the MACHI spectrum displays, in addition to those characteristic of CHI, the appearance of some distinctive peaks of MA (marked with arrows), specifically those located at 1656 and 814 cm^{-1}. As previously demonstrated for the methacrylation of dextran [32], these bands correspond respectively to C=C-H (the first one) and pendant vinyl groups (the second one) [34]. One final band also appearing in the MACHI spectrum is that at 2930 cm^{-1}. This band reflects the presence of pendant methyl groups, also related to the methacrylation

process as described by others [35]. Taken together, these findings demonstrate the CHI modification as successfully executed.

S9.2. Mechanical Characterization of the spray system used

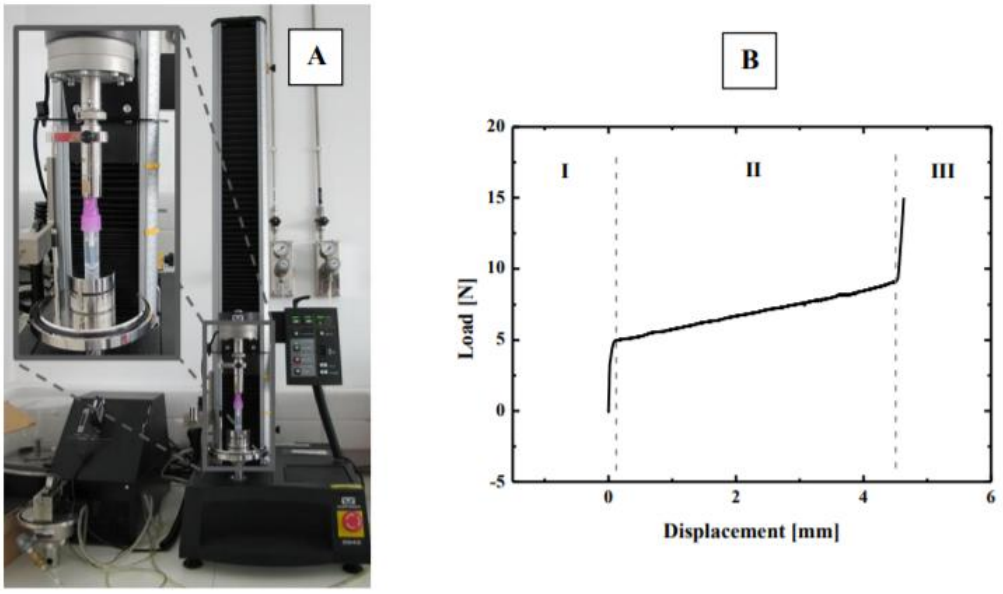

Figure S9.2 - A) Experimental set-up for mechanical testing: the spray is clamped by anvils for compression to occur. **B)** Load-displacement curve. The spray was tested while filled with MACHI solution.

The mechanical characterization was carried out on the basis of compression tests employing a Universal Mechanical Testing Machine (INSTRON 5540) equipped with a load cell of 1 kN and operating at a constant compression speed of 1 mm/min, as shown in Figure S9.2. Panels A and B show the experimental setup used and the load-displacement curve obtained upon examination, respectively. Zones I, II, and III in panel B correspond to the threshold load required to move the piston down, to the region at which piston is being moved by the applied load, and to the region at which the piston reaches the maximum limit of movement and consequently, the spray skeleton starts to be compressed, respectively. Accordingly, the input

pressure (P ~ 400 mbar) was calculated as the load required to move the spray piston down (*ca.* 5 N) divided by its cross-sectional area (1.33 cm^2).

S9.3. Characterization of SA surfaces

Figure S9.3 shows the morphology of the SA surfaces as imaged by SEM. It is clear from this figure that the treated substrates present a rough profile with microscopic pores all along their surfaces resulting from the deposition of carbon particles (soot layer) which have been demonstrated to be ordered in the form of a 3D fractal network that proves to be preserved after the silica coating and calcination [12]. This network-like structure endows the surface with focal points (*i.e.* gradients in surface roughness and microscopic pores) allowing the formation of air pockets on top of which water droplets are able to rest [17,15].

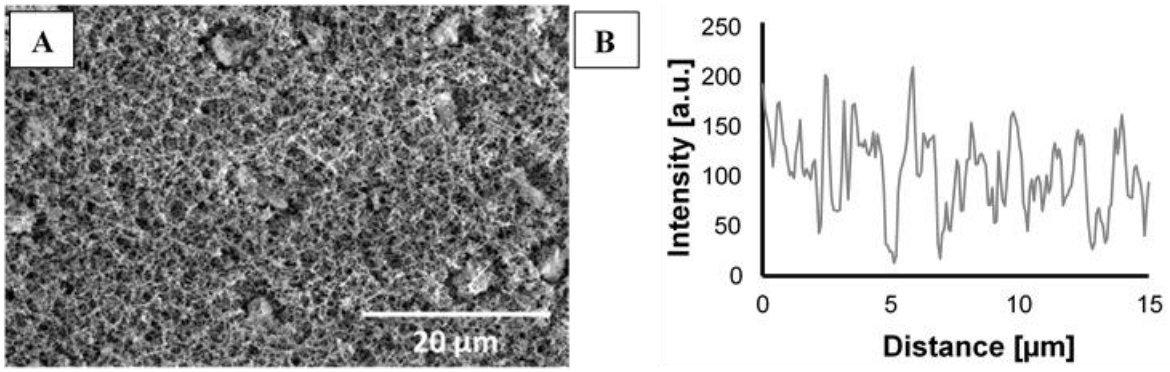

Figure S9.3 - A) Representative SEM image of coated surfaces. **B)** Topographic profile of the imaged surface as obtained all along the X-axis for a given Y-coordinate.

Generally speaking, this composite interface (solid-air-liquid) leads to an increase in the macroscopic CA and a reduced contact angle hysteresis [12]. Obviously, in order for the surface features to readily promote the formation of this interface, they must present nominal pitches smaller than the actual diameter of the given droplet [16]. As observed from panel B,

textural features resulting from surface coating present average pitches of around 2.37 ± 1.00 µm, proving themselves as suitable resting places for the produced micro-droplets.

On the other hand, with respect to wettability, our characterization proved the SA character of the produced surfaces leading to WCA values of (164.1 ± 0.9)° (see also water droplet profile in the inset image of Figure 9.1A). These values are in fair agreement with others previously reported for droplets equivalent in volume (3 µL) [12]. Important to our purposes, the WCA was also measured for the sprayed droplets. Obtained results demonstrated that smaller droplets yielded higher WCA values of around (172.5 ± 1.2)° ($p < 0.05$). One possible explanation for this result is that gravity exerts a lower influence on these smaller particles [36].

S9.4. Determination of the MACHI droplets' shape factor and surface contact area

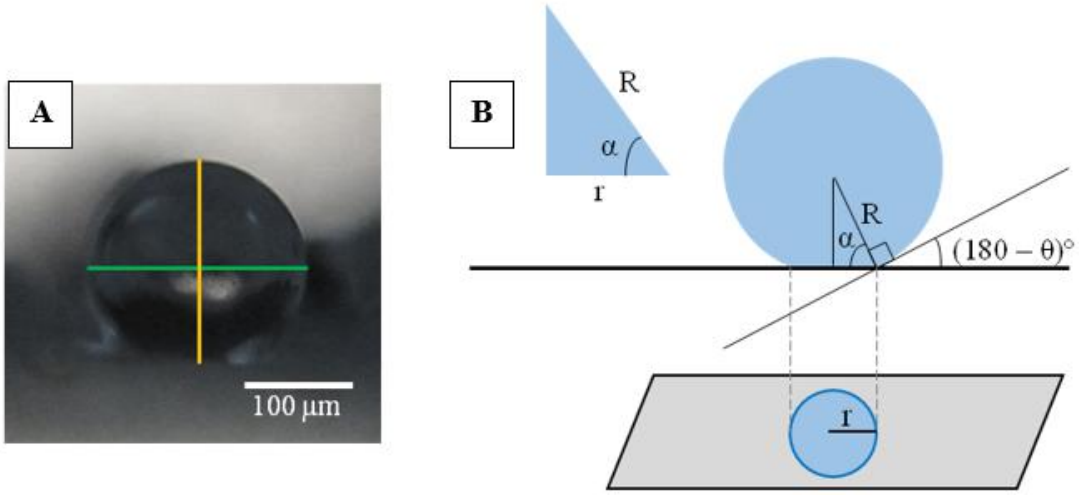

Figure S9.4. A) MACHI microparticle as observed from a lateral view. Bars represent the horizontal and vertical diameters measured to determine the shape factor. **B)** Schematic representation of the droplet contact area measurement. R and θ stand for the droplet radius and the contact angle, respectively.

The shape factor (SF) and surface contact area (SCA) of the produced microparticles were determined from the lateral view of optical micrographs in order to further confirm the

sphericity of the particles. SF was calculated as the ratio between the orthogonal and parallel to the surface diameters. Meanwhile, SCA was calculated as the area of a circle with radius (R) in contact with the surface, according to the following equation:

$$r = R\sin(\theta) \quad (1)$$

,where R and θ represent the radius of the dispensed particle and its WCA, respectively.

Figure S9.4 shows a schematic representation of how SF and FA were calculated. In addition, the fractional area (FA) was calculated as SA divided by the surface area of the sphere.

S9.5. Determination of the crosslinking degree

25 mg of MACHI were dissolved in 1 mL of deuterium oxide containing 0.25 w/v% I2959 and placed inside a 5 mm diameter NMR tube (Sigma-Aldrich). Afterwards, the MACHI solution was photocrosslinked using UV-light (365 nm, 11.4 mW/cm^2) for 1, 5, and 15 min. The ^{1}H-NMR spectra of non-crosslinked and crosslinked MACHI samples were recorded on a Bruker Avance instrument operating at 300 MHz and 27 ºC. Chemical shifts were expressed in ppm (δ units). Data were processed using the Mestre Nova software.

Figure S9.5 displays the ^{1}H NMR spectra of the MACHI solution before (panel A) and after 1 min crosslinking (panel B). As a result of the UV-light exposure, the photoinitiator (I2959) forms free radicals needed to initiate the polymerization process between the pendant vinyl groups of the MACHI. As the reaction proceeds, these vinyl groups are consumed. Accordingly, the crosslinking degree was determined as the decrease in the area under the curve of the peaks corresponding to the two hydrogens adjacent to C=C double bond (located at 5.7 and 5.4 ppm [32,14]) relative to the H2 peak at 3 ppm (GluN, glucosamine) [37]. Results from integration are shown in Table S9.1, also including experiments after 5 and 15 min of crosslinking.

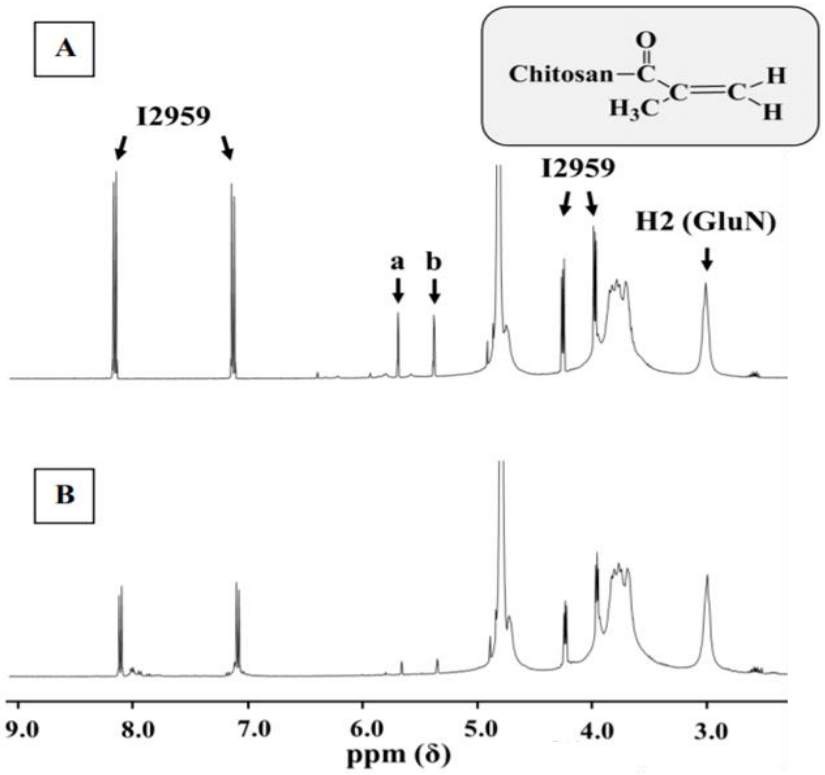

Figure S9.5 - ^{1}H NMR spectra of MACHI solution before (**A**) and after (**B**) 1 min crosslinking. The box on top of the graphs shows the chemical structure of MACHI.

Table S9.1. MACHI crosslinking degree as a function of the crosslinking time.

Crosslinking time [min]	**Integrated area at 5.7 ppm** [%]	**Integrated area at 5.4 ppm** [%]	**Integrated area at 3 ppm** [%]	**Crosslinking Degree** [%]
0	5.78	5.79	88.44	0
1	1.52	1.49	96.99	76.30
5	0.40	0.38	99.21	94.04
15	-	-	>99	>99

As observed from Table S9.1, the hydrogels under study present a crosslinking degree of *ca.* 76%. Interestingly, the chemical reaction further evolved at higher times, leading to crosslinking degrees of *ca.* 94% and > 99% at 5 and 15 min, respectively.

References

[1] Varde N. K., Pack D. W., Microspheres for controlled release drug delivery, *Expert Opin. Biol. Ther.* **2004**, 4, 35.
[2] Lima A. C., Sher P., Mano J. F., Production methodologies of polymeric and hydrogel particles for drug delivery applications, *Expert Opin. Drug Delivery* **2012**, 9, 231.
[3] Song W. L., Lima A. C., Mano J. F., Bioinspired methodology to fabricate hydrogel spheres for multi-applications using superhydrophobic substrates, *Soft Matter* **2010**, 6, 5868.
[4] Lima A. C., Custódio C. A., Alvarez-Lorenzo C., Mano J. F., Biomimetic Methodology to Produce Polymeric Multilayered Particles for Biotechnological and Biomedical Applications, *Small* **2013**, 9, 2487.
[5] Deng X., Paven M., Papadopoulos P., Ye M., Wu S., Schuster T., Klapper M., Vollmer D., Butt H.-J., Solvent-Free Synthesis of Microparticles on Superamphiphobic Surfaces, *Angew. Chem., Int. Ed.* **2013**, 52, 11286.
[6] Rodríguez-Velázquez E., Silva M., Taboada P., Mano J. F., Suárez-Quintanilla D. Alatorre-Meda, M., Enhanced Cell Affinity of Chitosan Membranes Mediated by Superficial Cross-Linking: A Straightforward Method Attainable by Standard Laboratory Procedures, *Biomacromolecules* **2014**, 15, 291.
[7] Alatorre-Meda M., Taboada P., Hardl F., Wagner T., Freis M., Rodriguez J. R., The influence of chitosan valence on the complexation and transfection of DNA: The weaker the DNA-chitosan binding the higher the transfection efficiency, *Colloids Surf., B* **2011**, 82, 54.
[8] Alves N. M., Mano J. F., Chitosan derivatives obtained by chemical modifications for biomedical and environmental applications, *Int. J. Biol. Macromol.* **2008**, 43, 401.
[9] Krajewska B., Wydro P., Jańczyk A., Probing the Modes of Antibacterial Activity of Chitosan. Effects of pH and Molecular Weight on Chitosan Interactions with Membrane Lipids in Langmuir Films, *Biomacromolecules* **2011**, 12, 4144.
[10] Krajewska B., Kyzioł A., Wydro P., Chitosan as a subphase disturbant of membrane lipid monolayers, The effect of temperature at varying pH: II. DPPC and cholesterol. *Colloids Surf., A* **2013**, 434, 359.
[11] Yu L. M. Y., Kazazian K., Shoichet, M. S. Peptide surface modification of methacrylamide chitosan for neural tissue engineering applications*, J. Biomed. Mater. Res., Part A* **2007**, 82A, 243.
[12] Deng X., Mammen L., Butt H.-J., Vollmer D., Candle Soot as a Template for a Transparent Robust Superamphiphobic Coating, *Science* **2012**, 335, 67.
[13] Mironi-Harpaz I., Wang D. Y., Venkatraman S., Seliktar D., Photopolymerization of cell-encapsulating hydrogels: Crosslinking efficiency versus cytotoxicity, *Acta Biomater.* **2012**, 8, 1838.
[14] Jeon O., Bouhadir K. H., Mansour J. M., Alsberg, E., Photocrosslinked alginate hydrogels with tunable biodegradation rates and mechanical properties, *Biomaterials* **2009**, 30, 2724.

[15] Cassie A. B. D., Baxter S., Wettability of porous surfaces, *Trans. Faraday Soc.* **1944**, 40, 0546.
[16] Jung Y. C., Bhushan B., Wetting behaviour during evaporation and condensation of water microdroplets on superhydrophobic patterned surfaces, *J. Microsc. (Oxford, U.K.)* **2008**, 229, 127.
[17] Wenzel R. N., Surface roughness and contact angle, *J. Phys. Colloid Chem.* **1949**, 53, 1466.
[18] PasandidehFard M., Qiao Y. M., Chandra S., Mostaghimi J., Capillary effects during droplet impact on a solid surface, *Phys. Fluids* **1996**, 8, 650.
[19] Suksamran T., Opanasopit P., Rojanarata T., Ngawhirunpat T., Ruktanonchai U., Supaphol P., Biodegradable alginate microparticles developed by electrohydrodynamic spraying techniques for oral delivery of protein, *J. Microencapsulation* **2009**, 26, 563.
[20] Ramadan Q., Gijs M. A. M., Simultaneous magnetic particles washing and concentration in a microfluidic channel, *Procedia Chem.* **2009**, 1, 1499.
[21] Fondecave R., Wyart F. B., Wetting laws for polymer solutions, *Europhys. Lett.* **1997**, 37, 115.
[22] Yoshida H., Hatakeyama T., Hatakeyama H., Characterization of water in polysaccharide hydrogels by DSC, *J. Therm. Anal.* **1993**, 40, 483.
[23] Bhaskar S., Gibson C. T., Yoshida M., Nandivada H., Deng X. P., Voelcker N. H., Lahann J., Engineering, Characterization and Directional Self-Assembly of Anisotropically Modified Nanocolloids, *Small* **2011**, 7, 812.
[24] Egner A., Hell S., Aberrations in Confocal and Multi-Photon Fluorescence Microscopy Induced by Refractive Index Mismatch, In Handbook of Biological Confocal Microscopy, Pawley, J. B., Ed., *Springer*: New York, **2006**, pp 404.
[25] Berger J., Reist M., Mayer J. M., Felt O., Peppas N. A., Gurny R., Structure and interactions in covalently and ionically crosslinked chitosan hydrogels for biomedical applications, *Eur. J. Pharm. Biopharm.* **2004**, 57, 19.
[26] Waters J. C., Accuracy and precision in quantitative fluorescence microscopy, *J. Cell Biol.* **2009**, 185, 1135.
[27] Al-Qadi S., Alatorre-Meda M., Zaghloul E. M., Taboada P., Remunan-Lopez C., Chitosan-hyaluronic acid nanoparticles for gene silencing: The role of hyaluronic acid on the nanoparticles' formation and activity, *Colloids Surf. Bs* **2013**, 103, 615.
[28] Croisier F., Jérôme C., Chitosan-based biomaterials for tissue engineering, *Eur. Polym. J.* **2013**, 49, 780.
[29] Oliveira M. B., Mano J. F., Polymer-Based Microparticles in Tissue Engineering and Regenerative Medicine, *Biotechnol. Prog.* **2011**, 27, 897.
[30] Robles E., Villar E., Alatorre-Meda M., Burboa M. G., Valdez M. A., Taboada P., Mosquera V., Effects of the hydrophobization on chitosan–insulin nanoparticles obtained by an alkylation reaction on chitosan, *Journal of Applied Polymer Science* **2013**, 129, 822.

[31] Blanco-Fernandez B., Rial-Hermida M. I., Alvarez-Lorenzo C., Concheiro A., Edible chitosan/acetylated monoglyceride films for prolonged release of vitamin E and antioxidant activity, *Journal of Applied Polymer Science* **2012**, 129, 626.
[32] Kim S.-H., Chu C.-C., Synthesis and characterization of dextran–methacrylate hydrogels and structural study by SEM, *Journal of Biomedical Materials Research* **2000**, 49, 517.
[33] Naveau H. P., Infrared, NMR and Mass-spectra of methacrylates or methacrylate-anhydride of 5 phenolic compounds, *Spectrochimica Acta Part a-Molecular Spectroscopy* **1972**, A 28, 651.
[34] Lima A. C., Song W., Blanco-Fernandez B., Alvarez-Lorenzo C., Mano J. F., Synthesis of Temperature-Responsive Dextran-MA/PNIPAAm Particles for Controlled Drug Delivery Using Superhydrophobic Surfaces, *Pharmaceutical Research* **2011**, 28, 1294.
[35] Mohamadi S., Preparation and Characterization of PVDF/PMMA/Graphene Polymer Blend Nanocomposites by Using ATR-FTIR Technique, In Infrared Spectroscopy - Materials Science, Engineering and Technology, *Theophanides*, T., Ed. Intech: **2012**, Vol. 1, pp 213.
[36] Reznik S. N., Yarin A. L., Spreading of an axisymmetric viscous drop due to gravity and capillarity on a dry horizontal wall, *International Journal of Multiphase Flow* **2002**, 28, 1437.
[37] Fernandez-Megia E., Novoa-Carballal R., Quiñoá E., Riguera R., Optimal routine conditions for the determination of the degree of acetylation of chitosan by 1H-NMR, *Carbohydrate Polymers* **2005**, 61, 155.

Chapter X: Results & Discussion

Superamphiphobic surfaces as a tool for the fabrication of hierarchical spherical polymeric carriers[6]

ABSTRACT

A novel, simple, versatile and cytocompatible strategy to fabricate hierarchical polymeric carriers with high encapsulation efficiencies is developed using superamphiphobic (SA) surfaces. The carries are obtained by the incorporation of cell/BSA-loaded dextranmethacrylate (MA-DEXT) microparticles into alginate (ALG) macroscopic beads. Engineered devices like these are expected to boost the development of innovative and customizable systems for biomedical and biotechnological purposes.

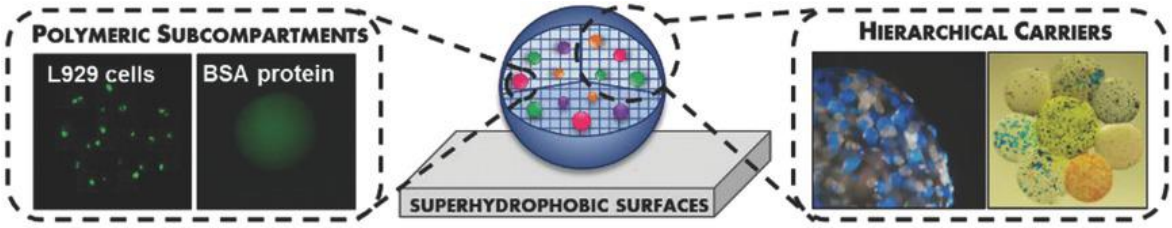

[6] Based on the publication: Ana M. S. Costa, M. Alatorre-Meda, C. Alvarez-Lorenzo, João F. Mano, Superhydrophobic Surfaces as a Tool for the Fabrication of Hierarchical Spherical Polymeric Carriers, *Small* **2015**,11 (30), pp. 3648-3652.

1. Introduction

Multicompartmentalized devices with a hierarchical arrangement constitute a new class of engineered assemblies with an enormous potential impact in the biomedical field [1]. Several efforts have been done in order to design such systems with the purpose of building multifunctional artificial cells [2]. In fact, the application area of these compartmentalized systems is much broader due to their ability to combine different reactions and functionalities in a confined volume [3], making them attractive as drug carriers [2b, 4] microreactors [5] and disease models [6].

To date, some strategies to fabricate hierarchical systems have been reported; for instance, a double emulsion process was proposed to produce bilayer polymeric multivesicle assemblies equipped with pH-responsive channels [2b]. Additionally, the layer-by-layer technique has been used to manufacture multifunctional polyelectrolyte capsules by sequential adsorption of interacting polymers followed by template dissolution [4b, 7]. Other methodologies include reversible ethanol-induced interdigitation of saturated bilayers and microfluidics [8]. The aforementioned methods present some drawbacks, for instance, the impossibility to encapsulate bioactive compounds such as globular proteins due to their incompatibility with organic solvents [2b, 7], the difficulty to tune the number of small compartments within the larger vessel [1a], and the need for intricate processes that may require the control of multiple flows [8b].

The technology using superhydrophobic (SH) surfaces constitutes an alternative to the previously stated methodologies [9]. It is inspired by the rolling of water drops on the Lotus leaf and involves the dispensing of a polymeric solution on a SH surface, which leads to spherical-shaped droplets. Afterwards, the liquid droplets are hardened into a hydrogel form by a crosslinking mechanism and collected from the SA substrate by tilting it. Overall, this technique presents three main advantages over the currently available methodologies to create spherical vesicles. First, since it avoids the use of any solvents/process liquids or another kind

of additive, it allows the encapsulation of bioactive molecules with efficiencies of almost 100%. Second, this technique is cheaper and simpler inasmuch as it does not involve the use of complex apparatus [9]. Third, this solvent-free strategy has already been proved to obtain particles with sizes in micrometer range by spraying followed by photocrosslinking [10].

In the present paper, versatile polymeric assemblies of microparticles within macroscopic beads were produced, for the first time, using SA surfaces as templates. To this end, MA-DEXT, a photocrosslinkable derivative of the biocompatible DEXT polysaccharide [11], was used to produce polymeric subcompartments containing L929 cells and BSA protein. Afterwards, hierarchical particles were produced by dispensing droplets of an ALG solution containing BSA-loaded MA-DEXT microparticles over a SA surface, which were, subsequently, crosslinked by calcium-mediated ionic gelation. Moreover, the possibility of packing several small compartments loaded with different molecules into larger polymeric containers was also evaluated.

2. Materials & Methods

2.1. Materials

Tetraethyl orthosilicate (TEOS, 98%), ammonium hydroxide solution (30-33%), 1H,1H,2H,2H-perfluorodecyltriethoxysilane (silane, 97%), dextran from Leuconostoc sp. (DEXT, MW 40 KDa), glicidyl methacrylate (GMA), dimethylamine pyridine (DMAP, 99%), hydrochloric acid (HCl, 37%), dimethyl sulfoxide (DMSO), 2-hydroxy-4'-(2-hydroxyethoxy)-2-methylpropiophenone (I2959, 98%), bovine serum albumin (BSA, ~66kDa, 96%), albumin–fluorescein isothiocyanate conjugate (BSA-FITC), phosphate buffer saline (PBS), alcian blue, Dulbecco's Modified Eagle's Medium without phenol red (DMEM), calcium chloride ($CaCl_2$), low viscosity sodium alginate from brown algae (ALG, ~250 cP) and HEPES hemisodium salt (HEPES) were from Sigma-Aldrich (U.S.A.). Acetic acid (Glacial), MTS (3-(4,5-dimethylthiazol-

2-yl)5-(3-carboxymethoxy-phenyl)-2-4-sulfophenyl)-2-4-sulfophenyl)-2H-tetrazolium) and sodium bicarbonate were supplied from VWR (Belgium). Deuterium oxide (D_2O) was purchased from Laborspirit (Portugal). TrypLE Express, fetal bovine serum (FBS), penicillin/streptomycin solution, calcein-AM, propidium iodide (PI) and α-MEM were from Alfagene (Portugal). Safranin T was from Fluka (U.S.A.). Toluidine blue O was purchased from Betalab (U.S.A). All materials were used as received. Unless otherwise stated, water purified in an 18 MΩ cm MilliQ Plus water system was used throughout.

2.2. Superamphiphobic surface fabrication and characterization

SA surfaces were prepared using a chemical vapor deposition (CVD) method as already described in literature [12]. Briefly, glass petri dishes were soot coated using a paraffin candle and then transferred into a desiccator containing TEOS (4 mL) and ammonia (4 mL) solutions. After a 24 h incubation period, the calcination of the carbon/silica coated substrates was performed at 600 °C for 2 h (Furnace EB4, FornoCerâmica, Portugal). Finally, the obtained surfaces were exposed to the CVD of a silane solution (150 µL) for 3 days.

The SA surfaces were characterized for their morphology, topography and WCA by Scanning Electron Microscopy (SEM, JSM-6010LV, JEOL, Japan), Atomic Force Microscopy (AFM, Multimode NanoScope IVA, Veeco, USA) and static WCA measurements (OCA15+ goniometer, DataPhysics, Germany), respectively.

In order to prepare the samples for SEM analysis, the SA surfaces were sputter-coated with gold and the images were acquired in high-vacuum by tracking the signal of secondary electrons employing an accelerating voltage of 15 kV and a working distance of 11 mm. For the topographic characterization, the SA substrates were mounted on top of magnetic discs and imaged using a RTESP probe (Bruker) with a spring constant of 20-80 Nm^{-1} and a typical resonance frequency in the range of 200-400 kHz. Tapping mode operating with decoupled XY (16 x 16 μm^2) and Z-scanner (3.8 µm) was selected. AFM images were scanned in topography, amplitude and phase mode with resolution of 512 x 512 pixels. The surface topography, the

root-mean-square roughness (RMS) and average film height (Hav) were evaluated from 10 x 10 μm^2 regions over different locations of the studied surfaces using the freeware Gwyddion 2.24 software after raw AFM data flattening and plane fitting. Unmodified glass (UG) petri dishes were used as control surfaces. The static WCA was determined on the basis of the sessile drop method by dispensing 3 µL water droplet over a SA surface at room temperature (RT). The values were obtained using the SCA 20 software and correspond to four replicates carried out on different areas of the surface. The surface contact area (SCA) and the fractional area (FA) were measured to further confirm the sphericity of the water droplets. SCA was calculated as the area of the circle with radius (r) in contact with the SA surface as described in [10], with r given by the following equation: r = R sin (θ), where R represent the radius of the dispensed droplet and θ its WCA. On the other hand, FA was determined by the ratio between SA and the surface area of the sphere.

2.3. MA-DEXT polymer synthesis

MA-DEXT was synthesized as already described in literature [13] by mixing DMAP catalyst (0.5 g) with a dextran solution (0.1 g/mL, 25 mL) in DMSO. Once dissolved, GMA (2.45 mL, 0.4 eq per hydroxyl group in the glucose unit) was added followed by the degassing of the previous solution with N_2 for 5 minutes. After a 48h incubation period, the DMAP was neutralized with HCl 1M and the solution was dialyzed (MWCO 12400 Da) against water over 4 days and freeze-dried. Molar substitution (MS) was estimated from ^{1}H-Nuclear Magnetic Resonance (^{1}H-NMR, Innova 750, 400 MHz, Varian, Australia) spectra of the freeze-dried powder dissolved in D_2O, which were analyzed using MestReNova software (MestreLab, Spain). MS was calculated by the ratio between the average value of the area of the peaks at 5.7 at 6.0 ppm (Figure S10.2Aa) and the area at 4.9 ppm (Figure S10.2Ab, anomeric proton) and, then, multiplied by 1.04 to normalize by the α-1,3 linkages of the dextran [14].

DEXT was functionalized with methacrylic groups through its reaction with GMA in the presence of DMSO and DMAP as shown in Fig S10.2A. During this process, the hydroxyl

groups of DEXT are ionized as a consequence of the alkaline pH, allowing the direct attachment of methacrylate esters to the 2- and 3- hydroxyl groups of the DEXT chain, in proportion of 1:1 [13]. As a result of this transesterification mechanism, MA-DEXT was obtained.

2.4. Production and characterization of MA-DEXT microparticles

MA-DEXT microparticles were synthesized by first dissolving 0.5 g of MA-DEXT in 10 mL of distilled water containing 0.25% w/v of I2959 photoinitiator. A Nisco Encapsulator Unit Var J30 system (Nisco Engineering, Switzerland) equipped with a 350 µm diameter nozzle was used to produce the polymeric droplets on the SA petri dish as depicted in Figure 10.1A (see the article). Briefly, a syringe pump (Harvard 11 Plus, Massachusetts, USA) was used to create a jet of the polymer solution which became instable due to the air pressure inside the nozzle chamber, generating a spray of polymeric droplets. The size of these droplets was tuned by changing both the polymer flow rate and the air pressure inside the nozzle. The distance between the nozzle and SA surface was kept constant at 15 cm (Figure 10.1AI in the article) and in each spray cycle 100 µL of polymeric solution were released. Afterwards, the obtained polymeric droplets were crosslinked under UV-light exposure (365 nm, 11.4 $mWcm^{-2}$) for 2 min inside a closed humidity chamber to limit the effects of evaporation (Figure 10.1AII). Lastly, the MA-DEXT microparticles were recovered from the surface by mechanical shaking of the SA petri dish (Figure 10.1AIII).

The obtained hydrogel microparticles were observed using an optical stereomicroscope (TR500, VWR, USA) equipped with a digital camera (G12 Olympus, Canon, Japan) and characterized for their morphology, size and size distribution by measuring a total of 450 particles from at least 20 independent optical images obtained in four different experiments (five different images per experiment) using Image J software.

The shape factor (SF) of the produced microparticles was determined from the lateral view of optical micrographs (Figure S10.3) in order to further confirm the sphericity of the

particles. SF was calculated as the ratio between the orthogonal and parallel to the surface diameters.

2.5. Cells Encapsulation inside the MA-DEXT microparticles

In Vitro Cell culture: An immortalized mouse lung fibroblast cell line (L929, European Collection of Cell Cultures) was cultured in complete α-MEM medium supplemented with 3.7 gL^{-1} sodium bicarbonate, 10% FBS and 1% penicillin-streptomycin (pH 7.4). L929 cells were grown in 150 cm^2 tissue culture flasks and incubated at 37 °C in a humidified air atmosphere of 5% CO_2. The culture medium was exchanged every 3 days.

L929 encapsulation in MA-DEXT microparticles: Upon reaching 90% of confluence, L929 cells were washed with PBS and chemically detached from tissue culture flasks using 0.05% Tryple Express solution for 5 min at 37°C in a humidified air atmosphere of 5% CO_2. Later fresh medium was added to inactivate the Tryple Express effect and the cells were centrifuged at 1200 rpm for 5 min. Then, the medium was decanted followed by the cells re-suspension in a 5% w/v MA-DEXT in PBS solution containing 0.25% w/v I2959 at density of 5 x 10^6 cells per mL of polymer solution. MA-DEXT microparticles with cells-enclosed were, then, produced using the method depicted in Figure 10.1A and placed in 12-well tissue culture plate at 37°C with a humidified air atmosphere of 5% CO_2. At 1, 2, 3, 5 and 7 day of culture, three different assays were performed: LIVE/DEAD, MTS and DNA quantification.

In order to qualitatively assess the effect of the developed technology combining spraying and SA surfaces on the cell viability inside the microparticles, the LIVE/DEAD assay was performed. This assay is based on the ability of viable cells' esterases to hydrolyze calcein- AM (membrane permeant dye) into calcein (green fluorescent dye), which is retained in the cytoplasm. In turn, propidium iodide (PI, red fluorescent dye) binds mainly to DNA of disrupted cells since it is membrane impermeant. At each time point, the culture medium was removed and replaced by 1 mL of PBS containing 2 µL of calcein-AM and 1 µL of PI. After 10 min of incubation at 37°C, samples were washed three times with PBS and visualized

immediately after by a fluorescence microscope (Axio Imager Z1m, Zeiss, Germany) using excitation and emission wavelengths of 494 and 535 nm and 517 and 617 nm for calcein-AM and PI, respectively.

Mitochondrial activity was evaluated by measuring the activity of mitochondrial dehydrogenases of viable cells [15]. This parameter was assessed using a tetrazolium salt, namely MTS [16], which yields a water-soluble brown formazan product in the presence of mitochondrial dehydrogenase enzymes. The amount of formazan generated is directly proportional to the total mitochondria activity per cell. Briefly, culture medium was removed and 1mL of 1:5 MTS/DMEM (without phenol red) was added to each well containing L929 cells encapsulated in MA-DEXT microparticles. The samples were cultured for 3 h at 37 °C in dark. After that, 100 μL aliquots of each well (in triplicate) were transferred to 96-well plates and the absorbance was measured at a wavelength of 490 nm using a microplate reader (Sinergy HT, BioTek, USA). MA-DEXT microparticles without cells were used as a control. The experiments were carried out in triplicate.

The DNA quantification assay was carried out to assess the ability of L929 cells to proliferate inside these microparticles. Therefore, in each time point, each well containing MA-DEXT microparticles with cells was washed with PBS and then, 1mL of ultrapure sterile water was added. Subsequently, L929 cells were incubated at 37 °C for 1 h followed by freezing at -80°C, in order to lyse all the encapsulated cells. The analysis of the DNA content was performed using a PicoGreen dsDNA quantification kit (Invitrogen Ltd., Paisley, UK). Briefly, 100 μL aliquots of each time point were transferred, in triplicate, to a 96 well white opaque plate. Then, PicoGreen reagent, 100 μL per well, was added 10 min prior reading the samples using a multiwall spectrophotometer (Synergy HT, BioTek, USA) at excitation and emission wavelengths of 485/20 and 528/20 nm, respectively. Each condition was prepared in triplicate and MA-DEXT microparticles without cells were used as a background control.

Statistical analysis: The significance of the differences on the average MTS and DNA values for each time point was assessed using One-Way ANOVA (SPSS software) with Tukey's

post hoc test, after verifying homogeneity of variances and normality distribution criteria. The homogeneity of variances criterion was tested using Levene's test, while the Shapiro-Wilk test was used to study the data normality. P-values < 0.05 were considered statistically significant. The results are presented as mean ± standard deviation.

2.6. BSA entrapment and release from hierarchical polymeric carriers

Both MA-DEXT microspheres and multicompartmentalized systems, entailing the entrapment of the produced MA-DEXT in an ALG matrix, were evaluated for its ability to release proteins, using BSA as model protein drug. Four different formulations were tested as depicted in Figure 10.1B (see the article): the first condition (MA-DEXT Mic + BSA) was done to study the ability of the MA-DEXT microspheres to entrap and then release BSA protein; the second condition (DEXT Mic + BSA) + ALG Matrix) was performed in order to evaluate the effect of the presence of an ALG matrix on the release of BSA from the MA-DEXT microspheres; the third condition (ALG Matrix + BSA) refers to the control of the BSA release from ALG matrix. Finally, the fourth condition (MA-DEXT Mic + (ALG Matrix + BSA)) constitute the control of the effect of the presence of MA-DEXT Mic on the BSA release from the ALG Matrix.

To produce the former polymeric systems, BSA protein was either dissolved in a MA-DEXT solution (Figure 10.1BI) or a in ALG solution (Figure 10.1BII). After the complete dissolution of BSA, the MA-DEXT microspheres (with or without BSA) were fabricated as described in Figure 10.1A and then, suspended in 1% (w/v) ALG matrix (with or without BSA). A 6 µL droplet of ALG solution containing the MA-DEXT Mic was dispensed using a pipette above a SA surface and crosslinked by incorporating Ca^{2+} ions into its structure (ionotropic gelation, 6 µL of 0.1 M $CaCl_2$). The size of these beads can be tuned by dispensing precise volumes of the polymeric precursor solution above the SA surface. In fact, Song et al. showed that by varying this volume from 2 µL to 20 µL, the particles diameters ranged from *ca.* 1 mm to

3 mm [9]. In this study, the ALG beads showed a mean diameter of 1.95 ± 0.18 mm, which corroborates with previous studies [9, 17].

In the preparations of all BSA-loaded formulations, the total mass of BSA was maintained constant at 0.250 mg. The obtained systems were suspended in 8 mL of HEPES buffer (10 mM, pH 7.4) and kept under agitation at 60 rpm and 37°C. At pre-established time periods, 150 µL of the supernatant were collected and replaced by fresh HEPES solution in order to maintain the total volume constant. The amount of BSA release in each time period was quantified by using the Micro BCA™ Protein assay (Pierce, USA). These experiments were repeated three times for each sample. In order to get insights into the BSA distribution inside all the formulations tested, FITC- labeled BSA was also encapsulated as previously described for the non-labeled BSA. The particles were observed by fluorescence microscopy (Axio Imager Z1m, Zeiss, Germany) and the images were recorded in the green channel (505 nm) and analyzed using the ZEN software supplied with the instrument.

2.7. Production of multicompartmentalized particles

MA-DEXT microparticles were specifically stained using 1mL of three different dyes commonly used in histology to stain the cartilage's glycosaminoglycans, namely: safranin O (0.1% (w/v) in distilled water; stains in red), toluidine (0.1% (w/v) in distilled water, stains in dark blue) and alcian blue (1% (w/v) in distilled water containing 3% (v/v) of acetic acid, stains in light blue). In order to produce hierarchical systems using ALG macroscopic beads as containers of MA-DEXT microparticles, the stained MA-DEXT hydrogels were mixed with a 1% (w/v) ALG in water solution. The former solution was dispensed using a pipette (6 µL) above a SA surface and then, the polymeric droplets were crosslinked by adding 6 µL of 0.1 M $CaCl_2$ solution on top of each droplet. The stained MA-DEXT microparticles and ALG vessels containing these microspheres were visualized by an optical stereomicroscope (TR500, VWR, USA) equipped with a digital camera (G12 Olympus, Canon, Japan).

3. Results and Discussion

Firstly, the SA templates were produced by CVD and characterized in terms of their WCA, which was found to be *ca.* 163º, and surface morphology by SEM and AFM, showing the presence of both nano- and microstructures required for superhydrophobicity (Figure S10.1). Regarding the polymeric precursors, DEXT was successfully modified into the photocrosslinkable MA-DEXT through its reaction with GMA. The degree of substitution was found to be *ca.* 71%, meaning that 71% of glucoses bear a methacrylate moiety (Figure S10.2).

Polymeric microparticles were produced by spraying a MA-DEXT aqueous solution onto a SA petri dish (Figure 10.1AI). Immediately after, the petri dish with the microdroplets was transferred to a humidified chamber since for small droplets the effects of evaporation were found to be significant. The crosslinking process was driven by UV-light exposure in the presence of I2959, a cytocompatible photoinitiator [18], yielding the MA-DEXT hydrogel microspheres (Figure 10.1AII). Subsequently, the crosslinked microspheres were retrieved by a gentle shaking of the petri dish (Figure 10.1AIII). This methodology is based on previous work of our group [10] and was further improved in this paper by using a sophisticated spray system with aim of better controlling the particles' size. To this end, both the polymer solution flow rate and air pressure inside the nozzle were varied as shown in Figure 10.2A. The optical images of the obtained particles revealed the existence of two size populations for each condition. This may be explained by the overlapping of different droplets during spraying probably: (1) between the new arriving droplets and those already deposited on the SA surface and/or (2) due to high-speed collision either in the midair [19] or upon arrival to the SA surface [20], leading to an unavoidable fragmentation of larger droplets into smaller ones. Nevertheless, it was clear that by decreasing the polymer flow rate and increasing the air pressure inside the nozzle, the two-size populations appeared to merge (Condition II), resulting in a narrow size distribution, which is extremely relevant for cell and drug encapsulation purposes. Based on these results, the parameters of Condition II (1mL/h, 500 mbar) were

selected for performing further studies, resulting in a particle mean diameter of *ca.* 226.8 ± 38.8 µm. Moreover, as a result of the high liquid repellency of the modified surfaces, the produced MA-DEXT particles presented an almost spherical shape as proved by a shape factor value close to 1 (0.91 ± 0.52; Figure S10.3).

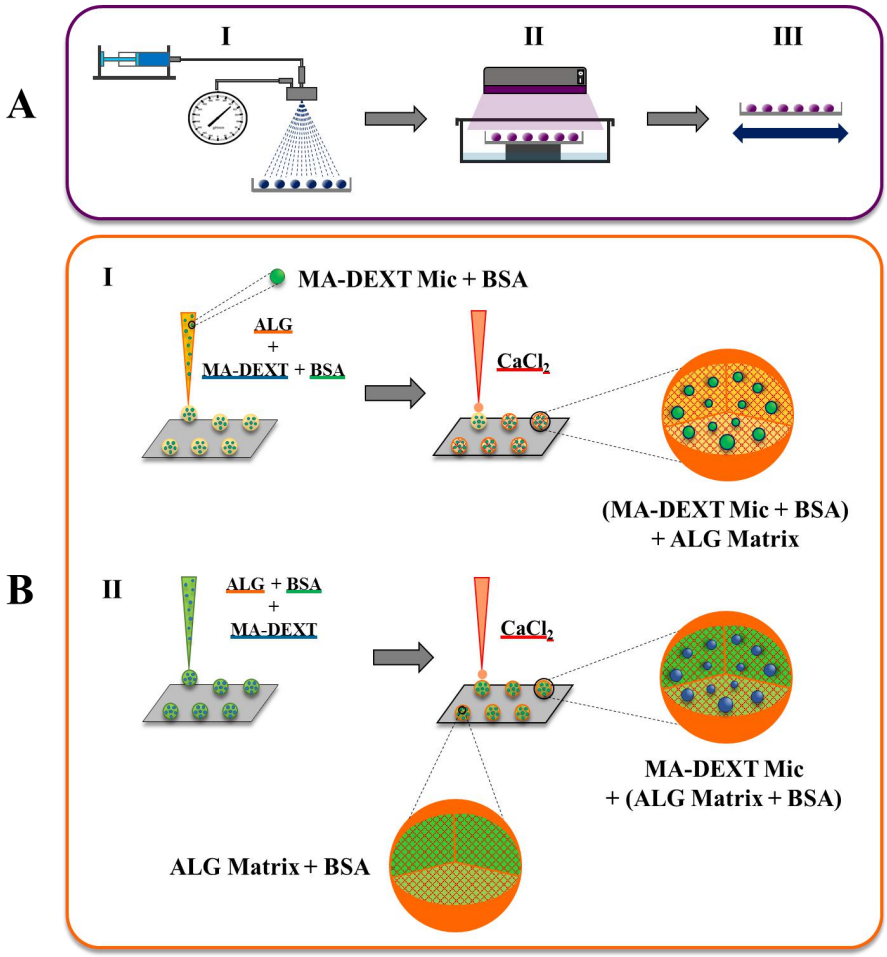

Figure 10.1 - Schematic representation of the subcompartments **(A)** and hierarchical polymeric carriers **(B)** synthesis routes. **AI)** MA-DEXT aqueous solution was sprayed over SA petri dishes. **AII)** MA-DEXT particles were crosslinked by UV-light exposure. **AIII)** Microparticles were collected by gently shaking. **BI)** BSA-loaded MA-DEXT microspheres were suspended in an ALG solution and dispensed over SA surface using a micropipette. Afterwards, the ALG matrix was crosslinked in the presence of Ca^{2+} ions, yielding ALG beads containing BSA-loaded MA-DEXT microspheres. **BII)** Non-loaded MA-DEXT microspheres were also incorporated into an ALG solution as stated previously in order to assess the effect of the presence of the microspheres on the BSA release from the ALG Matrix. Additionally, ALG beads without MA-DEXT microparticles e containing only BSA were also fabricated over SA surfaces and used as controls.

These microcompartments were subsequently loaded with cells to assess the suitability of employing the purposed strategy, combining spraying and SA platforms, for producing microcarriers for the encapsulation of highly sensitive bioactive compounds.

L929 cells were first suspended in a MA-DEXT solution and then, the hydrogel microcarriers were produced following the method described in Figure 10.1A. Several techniques were used to assess the cell behavior at distinct time points, namely cell viability by MTS and LIVE/DEAD assays and cell proliferation by DNA quantification. LIVE/DEAD fluorescence images (Figure 2BI) revealed a homogenous distribution of cells in the MA-DEXT particles with a good viability over the 7 days of incubation. In our opinion, this viability is ascribed to the mild processing conditions employed and the small size of the obtained particles, which allows an efficient exchange of nutrients, released products and oxygen with the surrounding environment [21]. In fact, a diameter of 400 μm has been described as the upper size limit for cell encapsulation within microparticles since it corresponds to twice the maximum diffusion distance of oxygen and nutrients from blood vessels to cells [22]. MTS results (Figure 10.2BII) showed an overall increase in the metabolic activity over the 7 days of assay, with a statistically significant increase when comparing day 1 with days 5 and 7 of culture (one-way ANOVA, Tukey's multiple comparison test, $p<0.05$). These outcomes are in good agreement with the observed LIVE/DEAD images, suggesting again a good cell viability inside the MA-DEXT particles. Similar results using MA-DEXT as polymeric matrix were already observed in literature [23]. Regarding DNA quantification assay, the number of cells inside these microparticles remained constant up to 5 days after the production of these cell-laden carriers. After this time, a statistically significant increase was observed when comparing day 1 with day 7 of culture (one-way ANOVA, Tukey's multiple comparison test, $p<0.05$). To boost both the cell adhesion and proliferation, the incorporation of bioactive motifs such as RGD (Arginine-Glycine-Aspartic Acid), which is recognized by integrin receptors on cellular membrane, could be envisaged. Such an approach was not considered here since it overpasses the scope of the present paper. As observed, the developed technique combining spraying with

SA substrates proved to be an attractive procedure to encapsulate cells in polymeric microparticles since factors such as the pressure inside the nozzle, the droplets collision onto SA surface and the crosslinking process using UV-light were quite mild and the cell viability was preserved.

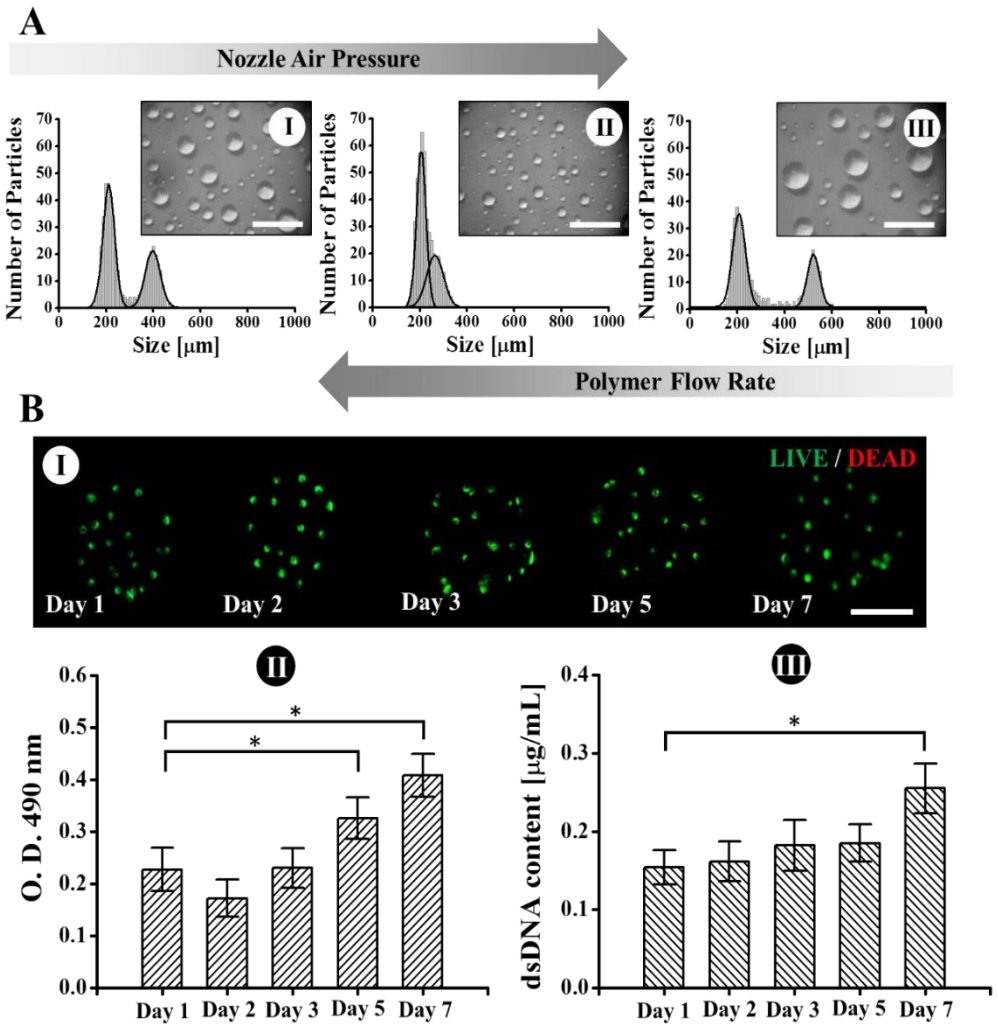

Figure 10.2 - **(A)** MA-DEXT microparticles production as a function of three different combinations of both the nozzle air pressure and polymer flow rate, namely: **(I)** 1 mL/h and 350 mbar; **(II)** 1 mL/h and 500 mbar; and **(III)** 3 mL/h and 500 mbar. The data was fitted to a Gaussian distribution using OriginPro 8 software and the scale bar corresponds to 1mm. **(B)** MA-DEXT microparticles with enclosed L929 cells. **(I)** LIVE/DEAD images obtained by fluorescence microscopy assay. Calcein and PI were used to stain green the living cells and red the dead cells, respectively. Scale bar corresponds to 100 μm**. (II)** L929 cells metabolic activity inside the MA-DEXT microparticles was quantified by a MTS assay. Optical density (O.D.) was measured at a wavelength of 490 nm. **(III)** DNA quantification assay obtained for each time point. Statistical differences were marked with * and correspond to a p-value < 0.05.

Once confirmed our technology as totally cytocompatible, the next step was devoted to characterizing the suitability of the obtained MA-DEXT microparticles to incorporate and release biomolecules, in particular proteins. These macromolecules are often degraded by the low pH in the stomach if orally administrated, or by proteases in case of intravenously delivery [24], highlighting the need for bioencapsulation strategies to ensure their successful delivery into the injured place [25]. To this end, BSA was chosen as a model drug protein and was dispersed in a MA-DEXT solution followed by its encapsulation as done with cells (Figure 10.1A).

In order to visualize the encapsulated protein, FITC-labeled BSA protein was used. As shown by fluorescence microscopy (Figure 10.3A), this protein was homogeneously distributed inside the spherical polymeric microcarriers, reveling its successful encapsulation. After the entrapment, which is expected to be almost 100% due to the solvent-free character of this technique, the ability of these loaded microparticles to release this protein was assessed at physiological conditions. The observed release profile (Figure 10.3E (green line)) presents a relatively fast release at earlier times (*ca.* 80% after 1h) followed by a sustained delivery, which is typical of hydrogel carrier systems. This condition might be favorable, for instance, in the beginning of wound treatment, where an initial burst of therapeutic drugs could provide an immediate relief and the following prolonged release could promote a gradual healing [26].

Later, hierarchical multicompartmentalized systems were constructed by incorporating the already formed BSA-loaded microparticles into ALG beads using a SA surface as a support. ALG was selected due to its biocompatibility and non-toxicity as well as for its ability to form hydrogels at mild conditions through ionic crosslinks between its carboxylic acid groups and divalent cations such as Ca^{2+} [27]. Besides the already discussed condition where BSA protein was loaded into MA-DEXT microparticles (MA-DEXT Mic + BSA), three more conditions were tested in order to study the *in-vitro* protein release from the hierarchical carriers. These

formulations differed in the presence or absence of microparticles and/or BSA protein inside the particles as displayed in Figure 10.1B.

FITC-BSA initial distribution inside these compartmentalized devices was clearly observed by fluorescence microscopy (Figure 10.3B-D). Panel B shows the packing of protein-loaded MA-DEXT microparticles inside the ALG matrix ((MA-DEXT Mic + BSA) + ALG Matrix). Interestingly, the microparticles preserved their quasi-spherical shape even after the second encapsulation process. This physical stability and the associated encapsulation efficiency of ≈ 100% of the proposed strategy are not commonly attained by conventional processing pathways involving more than one conditioning steps [28], highlighting the relevance of synthesizing hierarchical systems using SA surfaces. Conversely and as expected, panels C and D that show the encapsulation of the protein within the ALG matrix in the absence (ALG Matrix + BSA) and presence of non-loaded DEX-MA microparticles (MA-DEXT Mic + (ALG Matrix + BSA)), respectively, showed the homogeneous organization of the encapsulated protein inside the formed macro-bead as also observed for other related systems [9]. As observed from panel D, such homogeneous organization is interrupted by the presence of the non-loaded microparticles, which were depicted as non-filled (black) spots, further confirming the already cited outstanding stability of the DEX-MA inner compartments.

All the formulations showed an initial burst release of BSA within the first 20 min (*ca.* 28% for the ALG Matrix + BSA, 25% for MA-DEXT Mic + (ALG Matrix + BSA) and 16% for the (MA-DEXT Mic + BSA) + ALG) followed by a more sustained release (Figure 10.3 E). This initial burst release may be ascribed to the presence of some protein molecules attached or close to the surface of the hydrogel [29]. In particular, for the case of (MA-DEXT Mic + BSA) + ALG Matrix, the burst and the sustained release were separated by a lag time occurring between 20 min and 1 h. This phenomenon can be attributed to the time needed for the BSA to diffuse from MA-DEXT microparticles into ALG matrix and then through the ALG matrix to the surrounding environment [7]. Regarding the other two profiles (Figure 10.3E, represented by pink and blue lines), it is clear that they were very similar, with the latter showing the highest

level of protein retention. This can be related to the presence of empty MA-DEXT microparticles in formulation MA-DEXT Microparticles + (ALG Matrix + BSA), which allow BSA diffusion from the outer ALG matrix toward the center of these small spheres which competes with this protein diffusion from the ALG matrix to the surrounding medium. Additionally, attractions between the ALG carboxyl groups (-COOH) and the BSA amine groups (-NH2) as well as hydrogen bonds between the (-COOH) from the ALG and (-COOH) of BSA may also restrict this protein release from these polymeric carriers [29a].

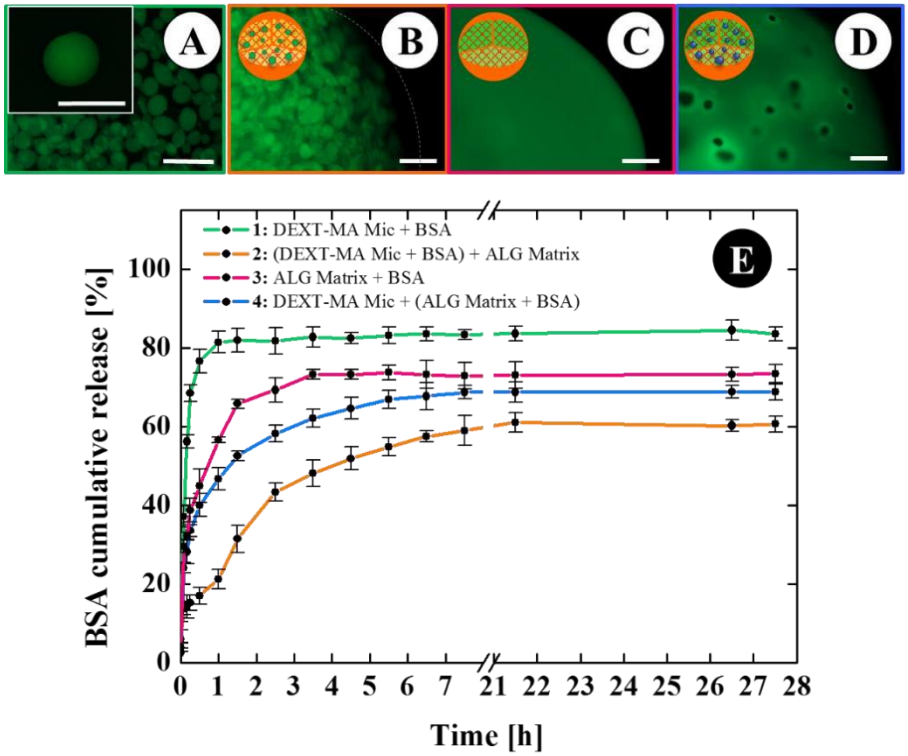

Figure 10.3 - BSA encapsulation in the developed polymeric devices. **(A)** MA-DEXT microparticles containing FITC-BSA. **(B)** FITC-BSA-loaded MA-DEXT microparticles incorporated in ALG beads **(C)** ALG beads containing FITC-BSA. **(D)** Non-loaded MA-DEXT microparticles encapsulation inside ALG beads containing FITC-BSA. The scale bar corresponds to 400 µm. **(E)** BSA release profiles for all the formulations tested in HEPES buffer (10 mM), pH 7.4 and at 37°C.

Finally, we also investigated the possibility of scaling up this process to create hierarchical hydrogel systems with multifunctional subcompartments. As proof of concept, three different dyes commonly used in histology were entrapped in the MA-DEXT

microparticles, namely: safranin O (Figure 10.4A), toluidine (Figure 10.4B) and alcian blue (Figure 10.4C), which in turn were incorporated inside an ALG matrix. The obtained hierarchical systems showed that the subcompartments were evenly distributed within the ALG matrix as visualized by an arrangement of colored dots along the bulk of the macroscopic polymeric bead, showing an outstanding structural stability of the inner microparticles (Figure 10.4D and 10.4E). Production of multilayered compartmentalized particles using SA platforms has been previously reported, but this process is difficult to execute as it needs the sequential individual layering steps [30].

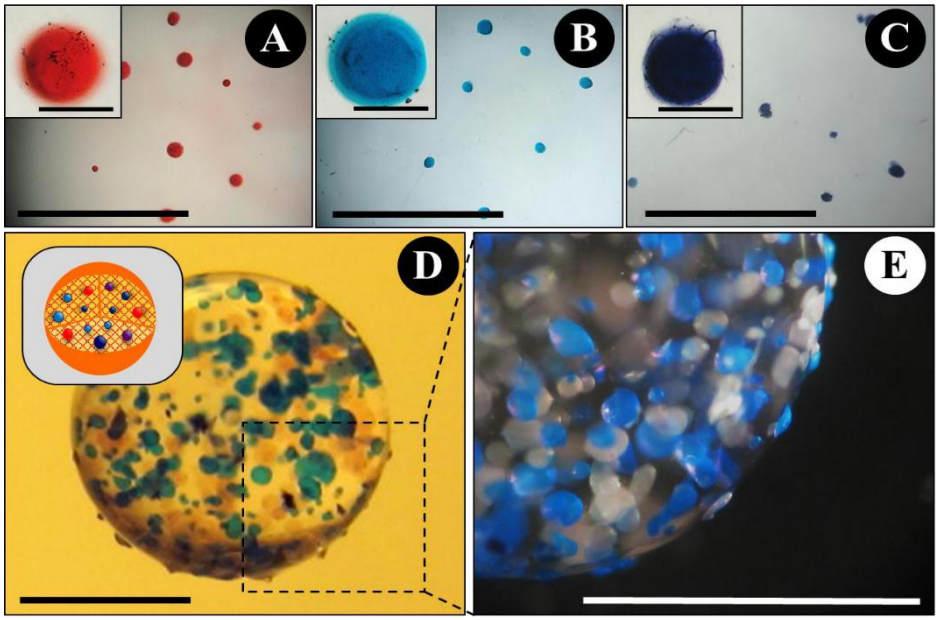

Figure 10.4 - MA-DEXT particles stained with safranin O (**A**; red), alcian blue (**B**; light blue) and toluidine (**C**; dark blue). **(D)** Hierarchical polymeric particles consisting of stained MA-DEXT microparticles embedded in an ALG Matrix. **(E)** Magnification of the hierarchical polymeric carriers. Scale bars for overviews and insets stand for 1 mm and 200 µm, respectively.

4. Conclusion

In conclusion, this work demonstrates the use of SA surfaces as a suitable tool to create hierarchical systems for the encapsulation of bioactive molecules and cells. Based on a

solvent-free methodology, the sketched technique proved to be simple, reproducible and totally biocompatible, allowing the production of polymeric carriers at physiological conditions. On the one hand, the optimization of experimental variables such as spraying pressures and polymer flow rate allow the production of robust microcompartments with homogeneous size distributions and, importantly, with the required characteristics to sustain cells in culture. On the other hand, the possibility of creating a second polymeric matrix demonstrated to be useful for drug delivery inasmuch as it proved to tune the release profile of encapsulated proteins. Based on the obtained results, this methodology is envisioned to constitute an innovative approach for the cost-effective production of hierarchical systems for direct applications in drug delivery. Moreover, the versatility of the technology could allow to include virtually any kind of elements in multi-scaled structures, including cells, microorganisms, objects with magnetic, electrical or optical activity or therapeutic substances.

Acknowledgements

This work was funded by FCT through PhD grants SFRH/BD/101748/2014 and SFRH/BD/73172/2010, by the European Union's Seventh Framework Programme (FP7/2007-2013) under grant agreement no. REGPOT-CT2012-316331-POLARIS, by FEDER through the Competitive Factors Operation Program - COMPETE, by IACOBUS Program (GNP-AECT), and by national funds through FCT in the scope of project PTDC/CTM-BIO/1814/2012 and by MICINN (SAF2011-22771).

Supplementary Information (SI.10)

S10.1. SA surface characterization

Figure S10.1A shows an example of a modified glass petri dish with a macroscopically smooth SA coating, which is typical of the executed treatment. In order to obtain a SA

substrate, which is defined by a WCA value greater than 150º [31], the presence of both surface roughness (usually originated from microscopic protrusions) and a low surface energy are required [32]. For instance, in case of the Lotus leaf, well-known for its self-cleaning character, the microstructures are provided by the presence of papillae while the epicuticula wax is responsible for the low surface energy [33]. These microscopic protrusions work as support points above which the droplet is suspended in the Cassie state, allowing for the creation of air pockets in the valleys between the asperities (composite solid-liquid-air interface). It is well-accepted that the spacing between asperities as well as the height of each protrusion have a critical role in preventing the collapse of the droplet into the Wenzel wetting state. To get an insight into the height of the asperities, AFM of the SH surface was performed, and the results are displayed in Figure S10.1. Untreated glass (UG) substrates were used as a control and clear differences are observed from the 3D profiles (Figure S10.1B and S10.1C). The coated surfaces display protrusions with height values of *c.a.* 1.32 μm, contrary to the UG ones, which present features 164 times smaller (c.a. 8.05 nm) (see panel S10.1D). This outcome demonstrates the successful modification of the glass petri dishes leading to the formation of microstructures, which were found to be present over the entire SA substrate (panel S10.1D). As displayed in panel S10.1E, the occurrence of these microscopic features gave rise to a 2-order increase in the RMS of the coated surfaces (from 0.002 to *ca.* 0.5 mm, as compared to non-treated ones). Surface roughness is known to be pivotal for the prevalence of the simultaneously superhydrophobic and superoleophobic character of the produced surfaces.

SEM characterization was carried out in order to elucidate the morphology of the obtained features resulting from the surface treatment. SEM images (panel S10.1F and S10.1G) revealed a fractal organization of the deposited carbon particles, in good agreement with other studies [12].

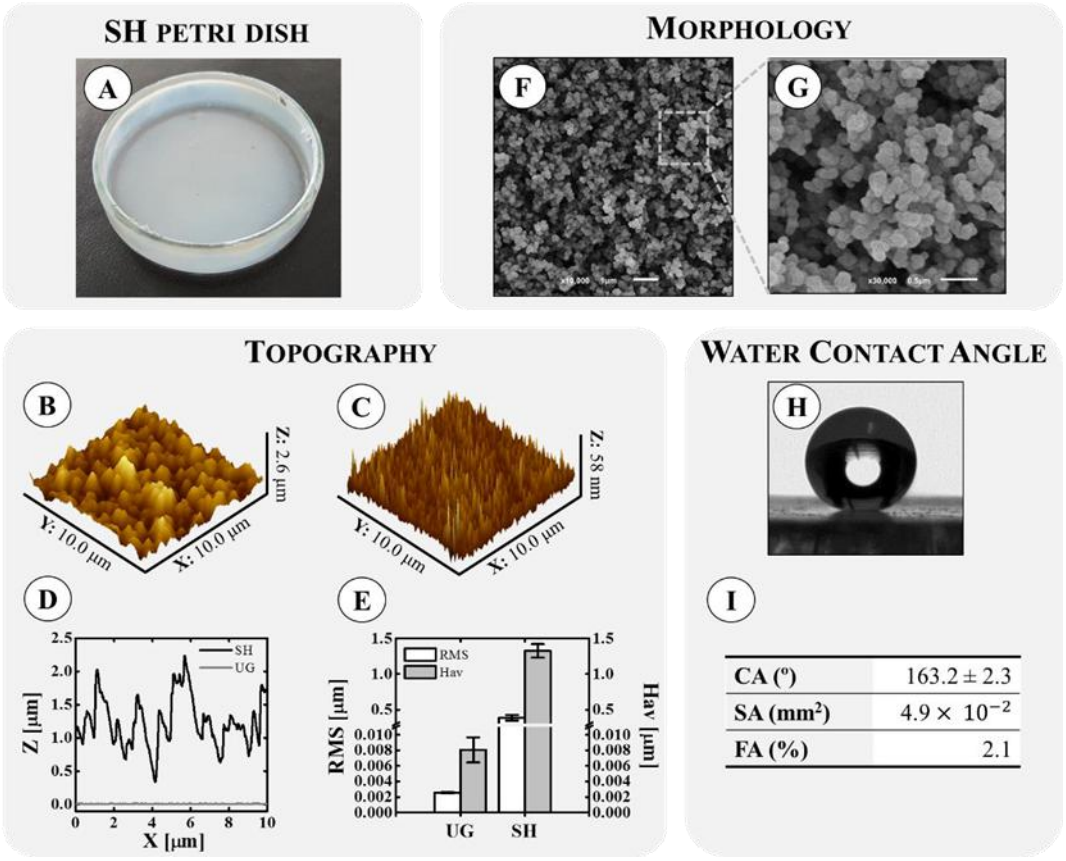

Figure S10.1 - SA petri dish characterization. **(A)** Photograph of a glass petri dish after the SA coating, showing a white, opaque SA layer typical of this treatment. Topography: **(B)** 3D AFM image of the SA **(C)** and UG surfaces; **(D)** Z profile of both surfaces obtained all along the X-axis at a fixed Y-coordinate; **(E)** Surface roughness (RMS) and average height (Hav) of the UG and SA substrates. Morphology: **(F)** SEM image of SA surface. The scale bar corresponds to 1 µm; **(G)** Zoom in of a certain region of the former SEM image. The scale bar corresponds to 0.5 µm. Water contact angle (WCA) results: **(H)** lateral image of a 3 µL water droplet deposited on the SA surface; **(I)** Table showing the values WCA, surface contact area (SCA) and fractional area (FA), as determined from SA surfaces.

Together with RMS, this network-like structure, combining both nano- and microstructures, is responsible for promoting a higher WCA as well as a more stable composite solid-liquid-air interface. On the one hand, the microstructures resist to the capillary waves while, on the other hand, the nanostructures prevent the valleys filling by small droplets [34]. These micro-to-nanoscale hierarchical structures are also observed in Nature, namely, in the Lotus leaf since the 5-9 µm size papillae present branch-like nanostructures with *ca.* 125 nm in diameter [35]. Another example is the water strider's leg, which due to the presence of

micrometer-scale needle-like setae with nanoscale grooves allow this insect to stand and walk quickly on water [36].

The extent of droplet contact with the SA surface was measured by the WCA and the obtained results are displayed in panel S10.1H and S10.1I. Higher WCA values, around 163º, reflect the low contact area of the droplet with the produced SA substrates, in compliance with other results found in literature [10,12]. The former outcome was further proved by the small surface contact area (SCA) obtained, which corresponds to a minute fractional are of the droplet in contact with the surface (*ca.* 2.1%, Figure S10.1I). In sum, the characterization of the WCA and the magnitudes obtained thereof further confirm the right formation of the SA substrates.

S10.2. MA-DEXT polymer characterization

Figure S10.2B depicts ^{1}H-NMR spectra of both DEXT and MA-DEXT using D_2O as a solvent.

Three new peaks appeared as a consequence of the chemical modification of DEXT, at 1.85 ppm from methyl protons (CH3, Figure S10.2Bc) and at 5.7 and 6.2 ppm corresponding to the protons of the double bond (C=C, Figure S10.2Ba) [11, 13]. The MS was calculated by dividing the average value of the area of the peaks at 5.7 at 6.2 ppm by the area at 4.9 ppm (Figure S10.2Bb), which corresponds to the anomeric proton, and, then, by multiplying by a factor of 1.04 to normalize by the α-1,3 linkages existing in the dextran [37, 16c]. The MS was found to be of *ca.* 71%, which indicates that the 71% of glucoses bear a methacrylate moiety.

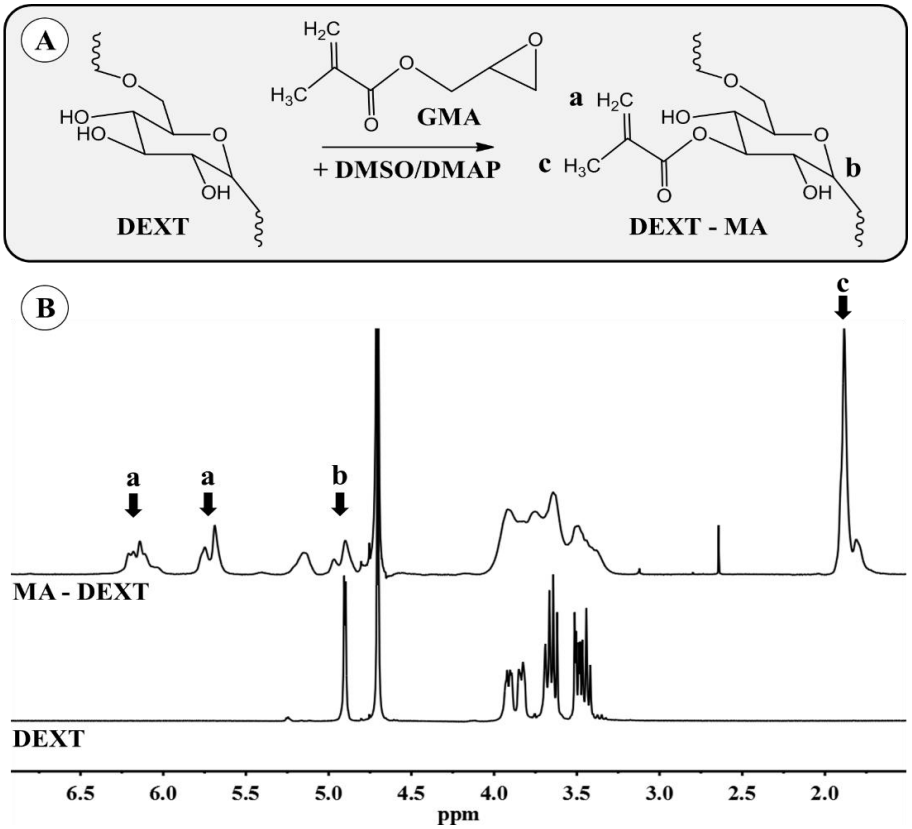

Figure S10.2 - MA-DEXT synthesis. **(A)** Schematic representation of the chemical reaction between DEXT and GMA in the presence of DMSO and DMAP catalyst. **(B)** ^{1}H-NMR spectra of both DEXT and MA-DEXT in D_2O. a), b) and c) correspond to the protons of the double bond (peaks at 5.7 and 6.2), the anomeric proton (peak at 4.9 ppm) and methyl protons (CH3, peak at 1.85 ppm), respectively.

S10.3. Characterization of MA-DEXT microparticles

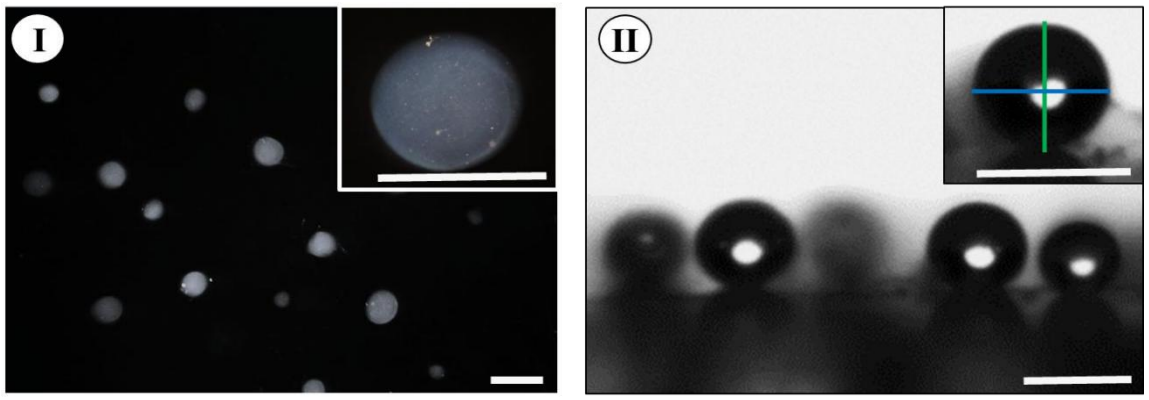

Figure S10.3 - MA-DEXT particles morphology: upper view **(I)** and side-view **(II)**. The lines in the inset represent the horizontal and vertical diameters measured to determine the shape factor (SF). The scale bars correspond to 250 µm.

References

[1] (a) M. Delcea, A. Yashchenok, K. Videnova, O. Kreft, H. Mohwald, A. G. Skirtach, Multicompartmental micro- and nanocapsules: hierarchy and applications in biosciences, *Macromol. Biosci.* **2010**, 10, 465; (b) R. Chandrawati, M. P. van Koeverden, H. Lomas, F. Caruso, Multicompartment Particle Assemblies for Bioinspired Encapsulated Reactions, *J. Phys. Chem. Lett.* **2011**, 2, 2639.

[2] (a) B. Städler, A. D. Price, R. Chandrawati, L. Hosta-Rigau, A. N. Zelikin, F. Caruso, Polymer hydrogel capsules: en route toward synthetic cellular systems, *Nanoscale* **2009**, 1, 68; (b) H.-C. Chiu, Y.-W. Lin, Y.-F. Huang, C.-K. Chuang, C.-S. Chern, Polymer vesicles containing small vesicles within interior aqueous compartments and pH-responsive transmembrane channels, *Angew. Chem. Int.* Ed. **2008**, 47, 1875.

[3] A. N. Zelikin, A. D. Price, B. Stadler, Poly(methacrylic acid) polymer hydrogel capsules: drug carriers, sub-compartmentalized microreactors, artificial organelles, *Small* **2010**, 6, 2201.

[4] (a) B. G. De Geest, S. De Koker, K. Immesoete, J. Demeester, S. C. De Smedt, W. E. Hennink, Self - Exploding Beads Releasing Microcarriers, *Adv. Mater.* **2008**, 20, 3687; (b) L. Hosta-Rigau, B. Städler, Y. Yan, E. C. Nice, J. K. Heath, F. Albericio, F. Caruso, Capsosomes with Multilayered Subcompartments: Assembly and Loading with Hydrophobic Cargo, *Adv. Funct. Mater.* **2010**, 20, 59.

[5] (a) A. D. Price, A. N. Zelikin, Y. Wang, F. Caruso, Triggered enzymatic degradation of DNA within selectively permeable polymer capsule microreactors, *Angew. Chem. Int. Ed.* **2009**, 48, 329; (b) P.-Y. Bolinger, D. Stamou, H. Vogel, An integrated self-assembled nanofluidic system for controlled biological chemistries, *Angew. Chem. Int. Ed.* **2008**, 47, 5544.

[6] O. Kulygin, A. D. Price, S. F. Chong, B. Stadler, A. N. Zelikin, F. Caruso, Subcompartmentalized polymer hydrogel capsules with selectively degradable carriers and subunits, *Small* **2010**, 6, 1558.

[7] R. R. Costa, E. Castro, F. J. Arias, J. C. Rodríguez-Cabello, J. F. Mano, Multifunctional compartmentalized capsules with a hierarchical organization from the nano to the macro scales, *Biomacromolecules* **2013**, 14, 2403.

[8] (a) H. C. Shum, A. R. Abate, D. Lee, A. R. Studart, B. Wang, C.-H. Chen, J. Thiele, R. K. Shah, A. Krummel, D. A. Weitz, Droplet microfluidics for fabrication of non-spherical particles, *Macromol. Rapid Commun.* **2010**, 31, 108; (b) R. Luo, Y. Cao, P. Shi, C. H. Chen, Near-infrared light responsive multi-compartmental hydrogel particles synthesized through droplets assembly induced by superhydrophobic surface, *Small* **2014**, 10, 4886.

[9] W. Song, A. C. Lima, J. F. Mano, Bioinspired methodology to fabricate hydrogel spheres for multi-applications using superhydrophobic substrates, *Soft Matter* **2010**, 6, 5868.

[10] A. M. Costa, M. Alatorre-Meda, N. M. Oliveira, J. F. Mano, Biocompatible polymeric microparticles produced by a simple biomimetic approach, *Langmuir* **2014**, 30, 4535.

[11] A. C. Lima, W. Song, B. Blanco-Fernandez, C. Alvarez-Lorenzo, J. F. Mano, Synthesis of temperature-responsive dextran-MA/PNIPAAm particles for controlled drug delivery using superhydrophobic surfaces, *Pharm. Res.* **2011**, 28, 1294.
[12] X. Deng, L. Mammen, H. J. Butt, D. Vollmer, Candle soot as a template for a transparent robust superamphiphobic coating, *Science* **2012**, 335, 67.
[13] L. M. Y. Yu, K. Kazazian, M. S. Shoichet, Peptide surface modification of methacrylamide chitosan for neural tissue engineering applications, *J. Biomed. Mater. Res. A* **2007**, 82A, 243.
[14] S. G. Levesque, R. M. Lim, M. S. Shoichet, Macroporous interconnected dextran scaffolds of controlled porosity for tissue-engineering applications, *Biomaterials* **2005**, 26, 7436.
[15] T. Mosmann, Rapid colorimetric assay for cellular growth and survival: application to proliferation and cytotoxicity assays, *J. Immunol. Methods* **1983**, 65, 55.
[16] J. A. Barltrop, T. C. Owen, A. H. Cory, J. G. Cory, 5-(3-carboxymethoxyphenyl)-2-(4,5-dimethylthiazolyl)-3-(4-sulfophenyl)tetrazolium, inner salt (MTS) and related analogs of 3-(4,5-dimethylthiazolyl)-2,5-diphenyltetrazolium bromide (MTT) reducing to purple water-soluble formazans As cell-viability indicators, *Bioorg. Med. Chem. Lett.* **1991**, 1, 611.
[17] A. C. Lima, P. Batista, T. A. M.Valente, A. S. Silva, I. J. Correia, J. F. Mano, Free and copolymerized γ-cyclodextrins regulate the performance of dexamethasone-loaded dextran microspheres for bone regeneration, *Tissue Eng Pt A* **2013**, 19, 1175.
[18] I. Mironi-Harpaz, D. Y. Wang, S. Venkatraman, D. Seliktar, Photopolymerization of cell-encapsulating hydrogels: crosslinking efficiency versus cytotoxicity, *Acta Biomater.* **2012**, 8, 1838.
[19] T. Vuong, A. Qi, M. Muradoglu, B. H.-P. Cheong, O. W. Liew, C. X. Ang, J. Fu, L. Yeo, J. Friend, T. W. Ng, Precise drop dispensation on superhydrophobic surfaces using acoustic nebulization, *Soft Matter* **2013**, 9, 3631.
[20] M. Pasandideh - Fard, Y. M. Qiao, S. Chandra, J. Mostaghimi, Capillary effects during droplet impact on a solid surface, *Phys. Fluids* **1996**, 8, 650.
[21] C. Schwinger, S. Koch, U. Jahnz, P. Wittlich, N. G. Rainov, J. Kressler, High throughput encapsulation of murine fibroblasts in alginate using the JetCutter technology, *J. Microencapsul.* **2002**, 19, 273.
[22] P. de Vos, M. M. Faas, B. Strand, R. Calafiore, Alginate-based microcapsules for immunoisolation of pancreatic islets, *Biomaterials* **2006**, 27, 5603.
[23] (a) H. Li, R. Niu, J. Yang, J. Nie, D. Yang, Photocrosslinkable tissue adhesive based on dextran, *Carbohydr. Polym.* **2011**, 86, 1578; (b) T. Wang, X. Mu, H. Li, W. Wu, J. Nie, D. Yang, The photocrosslinkable tissue adhesive based on copolymeric dextran/HEMA, *Carbohydr. Polym.* **2013**, 92, 1423; (c) A. C. Lima, A. M. Puga, J. F. Mano, A. Concheiro, C. Alvarez-Lorenzo, Free and copolymerized γ-cyclodextrins regulate the performance of dexamethasone-loaded dextran microspheres for bone regeneration, *J. Mater. Chem.* **2014**, 2, 4943.
[24] K. A. Black, D. Priftis, S. L. Perry, J. Yip, W. Y. Byun, M. Tirrell, Protein Encapsulation via Polypeptide Complex Coacervation, *ACS Macro Lett.* **2014**, 3, 1088.

[25] (a) S. Frokjaer, D. E. Otzen, Protein drug stability: a formulation challenge, *Drug discovery* **2005**, 4, 298; (b) S. P. Baldwin, W. Mark Saltzman, Materials for protein delivery in tissue engineering, *Adv. Drug Deliv. Rev.* **1998**, 33, 71.
[26] X. Huang, C. S. Brazel, On the importance and mechanisms of burst release in matrix-controlled drug delivery systems, *J. Control. Release* **2001**, 73, 121.
[27] O. Smidsrød, G. Skja˚k-Br˙k, Alginate as immobilization matrix for cells, *Trends Biotechnol.* **1990**, 8, 71.
[28] T. Suksamran, P. Opanasopit, T. Rojanarata, T. Ngawhirunpat, U. Ruktanonchai, P. Supaphol, Biodegradable alginate microparticles developed by electrohydrodynamic spraying techniques for oral delivery of protein, *J. Microencapsul.* **2009**, 26, 563.
[29] (a) J. Zhao, X. Zhao, B. Guo, P. X. Ma, Multifunctional interpenetrating polymer network hydrogels based on methacrylated alginate for the delivery of small molecule drugs and sustained release of protein, *Biomacromolecules* **2014**, 15, 3246; (b) G. D'Arrigo, C. Di Meo, L. Pescosolido, T. Coviello, F. Alhaique, P. Matricardi, Calcium alginate/dextran methacrylate IPN beads as protecting carriers for protein delivery, *J. Mater. Sci.* **2012**, 23, 1715.
[30] A. C. Lima, C. A. Custódio, C. Alvarez-Lorenzo, J. F. Mano, Biomimetic methodology to produce polymeric multilayered particles for biotechnological and biomedical applications, *Small* **2013**, 9, 2487.
[31] D. Öner, T. J. McCarthy, Ultrahydrophobic Surfaces. Effects of Topography Length Scales on Wettability, *Langmuir* **2000**, 16, 7777.
[32] (a) T. Sun, L. Feng, X. Gao, L. Jiang, Bioinspired surfaces with special wettability, *Acc. Chem. Res.* **2005**, 38, 644; (b) H.-J. Butt, C. Semprebon, P. Papadopoulos, D. Vollmer, M. Brinkmann, M. Ciccotti, Design principles for superamphiphobic surfaces, *Soft Matter* **2013**, 9, 418.
[33] W. Barthlott, C. Neinhuis, Purity of the sacred lotus, or escape from contamination in biological surfaces, *Planta* **1997**, 202, 1.
[34] M. Nosonovsky, B. Bhushan, Hierarchical roughness makes superhydrophobic states stable, *Microelectron. Eng.* **2007**, 84, 382.
[35] L. Feng, S. Li, Y. Li, H. Li, L. Zhang, J. Zhai, Y. Song, B. Liu, L. Jiang, D. Zhu, Super - Hydrophobic Surfaces: From Natural to Artificial, *Adv. Mater.* **2002**, 14, 1857.
[36] X. Gao, L. Jiang, Water-repellent legs of water striders, *Nature* **2004**, 432, 36.
[37] W. N. E. Vandijkwolthuis, O. Franssen, H. Talsma, M. J. Vansteenbergen, J. J. K. Vandenbosch, W. E. Hennink, Synthesis, Characterization, and Polymerization of Glycidyl Methacrylate Derivatized Dextran, *Macromolecules* **1995**, 28, 6317.

Chapter XI: Results & Discussion

Solvent-Free Strategy Yields Size and Shape-Uniform Capsules[7]

ABSTRACT

Capsules with a liquefied core were fabricated via the assembly of polymeric droplets induced by superamphiphobic (SA) surfaces. The use of these highly repellent substrates to produce liquified capsules presents several advantages over the current available strategies, such as: (i) an easy and precise control over the particle size and shape, (ii) a high encapsulation efficiency, (iii) mild processing conditions, and (iv) the possibility to include any object in either a water or oil-based liquid core. As proof of concept, a photocrosslinkable derivative of chitosan was used to produce the polymeric shell while a wealth variety of template cores were tested using a reversible crosslinking mechanism, interfacial gelation process or ice. Owing to the widespread application of polymeric capsules, the developed strategy is poised to usher the development of the next generation of materials not only for biomedical purposes but also for cosmetics, agriculture and electronics.

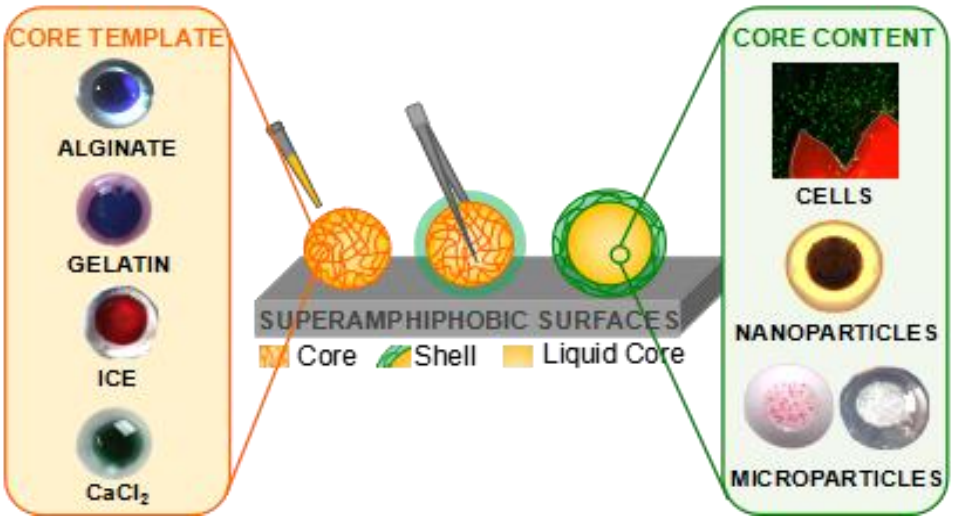

[7] Based on the publication Ana M. S. Costa, João F. Mano, Solvent-Free Strategy Yields Size and Shape-Uniform Capsules, *Journal of American Chemical Society* **2017**, 139(3), pp. 1057-1060.

1. Introduction

A significant research interest is being devoted toward the use of hollow materials as encapsulation devices for a plethora of different fields, spanning from electronics to cosmetics, including biomedical applications [1]. Core–shell structured particles with a liquid core exhibit (i) a more efficient and homogeneous transfer of solutes, (ii) a higher loading capacity provided by their internal ample space, and (iii) a lighter weight when comparing with their crosslinked-core counterparts [2]. Drawn by these appealing features, distinct strategies to fabricate polymeric capsules have been devised [3]. However, most of them are based on complex and harsh synthesis procedures, eluding the use of coagulating baths, which can ultimately compromise the cargo stability and loading efficiency. Thus, the absence of a simple and solvent-free methodology to prepare liquid-core capsules under mild conditions was the motivation of this work.

Herein, highly repellent substrates were used to design monosized and spherical polymeric capsules with a (i) hydrogel shell made of methacrylamide chitosan (MACHI), a biocompatible and light-sensitive derivative of CHI, and (ii) a liquefied core, wherein different molecules can be dispersed. Recently, surfaces with low wettability were successfully employed to produce compact spherical particles, from a wide range of materials and under mild conditions, by crosslinking pregel spherical droplets formed when in contact with these substrates [4]. However, the use of this solvent-free technology to attain liquefied capsules have not been reported [5].

2. Materials & Methods

2.1. Materials

Glass microscope slides were from Medline (Spain). Poly(L-lactic acid) (PLLA; Mw ~1600 – 2400, 70% of crystallinity) was purchased from Polysciences (Germany). Methylene

chloride (CH_2Cl_2) was obtained from Fisher Chemical (U.K.). Polyvinyl alcohol (PVA), tetraethyl orthosilicate (TEOS, 98%), ammonium hydroxide solution (30-33%), 1H,1H,2H,2H-perfluorodecyltriethoxysilane (silane, 97%), ethylenediaminetetraacetic acid (EDTA), 2-hydroxy-4'-(2- hydroxyethoxy)-2-methylpropiophenone (I2959, 98%), methacrylic anhydride (MA, ≥92%), phosphate buffer saline (PBS), penicillin/streptomycin solution, ethanol (EtOH), sodium carbonate (Na_2CO_3, ≥99.5%), calcium chloride ($CaCl_2$, ≥96%), low viscosity sodium alginate from brown algae (ALG, ~250 cP), antibiotic/antimycotic, gelatin from porcine skin, glycerol (≥ 99%), iron(II) chloride tetrahydrate (ferrous, $FeCl_2.4H_2O$, 98%), iron(III) chloride hexahydrate (ferric, FeCl3.6H2O, 98%) and 2-(N-morpholino)ethanesulfonic acid hydrate (MES, ≥99.5%) were from Sigma-Aldrich (U.S.A.). Chitosan 95/20 was from Heppe Medical Chitosan GmbH (Germany). Acetic acid (Glacial) was supplied from VWR (Belgium). TrypLE Express were from Alfagene (Portugal). Fibroblast Growth Kit (L-glutamine, hydrocortisone hemisuccinate, rh FGF β, rh EGF/ TGF β1 supplement, rh insulin, ascorbic acid and HLL supplement which, in turn, contained human serum albumin, linoleic acid and lecithin) was obtained from ATCC (U.K.). Fetal bovine serum was obtained from Merck Milipore (U.S.A). LIVE/DEAD Viability/Cytotoxicity Kit was from Molecular Probes Invitrogen (U.S.A.). Dyes (E102, E129, E133) were purchased from Elveflow (France). All materials were used as received. Unless otherwise stated, water purified in an 18 MΩ cm MilliQ Plus water system was used throughout.

2.2. Preparation and Characterization of Superamphiphobic Surfaces

The methodology followed to produce these SA surfaces has already been reported in literature [4b,6,7]. In short, glass slides were soot coated above a paraffin candle followed by a CVD procedure within a desiccator containing both TEOS solution (4 mL) and ammonia (4 mL). Calcination of the coated substrates was performed 24h after the CVD procedure by placing

them at 550ºC for 2h. Immediately after, the obtained surfaces were exposed to another CVD process using a silane solution (150 µL) for 3 days and stored until use.

These substrates were previously characterized by others and us [4b,8,9] in terms of their morphology, topography and water contact angle (WCA) by Scanning Electron Microscopy (SEM), Atomic Force Microscopy (AFM) and static WCA measurements, respectively. Herein, we extended the topographic characterization by using a profilometer. To this end, the samples were covered with a carbon layer to render them opaque to light and after analyzed to assess its roughness (root mean square - RMS value) using the SensoSCAN 5.3 software supplied with this equipment. The surface microstructure was also determined from the aforementioned images by drawing intensity plot profiles across the obtained pictures and defining a threshold. The distance between two peaks was defined as the micro-feature size. Results are the mean of 20 measurements using 10 different intensity plots.

2.3. Fabrication of the Polymeric Capsules

Liquid-core methacrylamide chitosan (MACHI) capsules were fabricated as shown in Figure 11.1. First, controlled volumes of a 1.5% (w/v) ALG in water solution (pH 7.0) were dispensed over a SA substrate using a micropipette. Different volumes were tested in order to tune the particle size. The obtained pre-gel droplets were subsequently hardened into a hydrogel upon adding other droplet containing Ca^{2+} ions (ionotropic gelation, 0.1 M $CaCl_2$ in 25 mM MES solution, pH 7.0) for 15 min in a humidified atmosphere to prevent water evaporation. It is worth noticing that, only for visualization purposes, the obtained ALG microparticles were stained by introducing a food dye in the polymer precursor solution (E133, 0.1% (v/v) in water, stains in dark blue). In order to produce polymeric capsules using ALG as sacrificial template, a droplet of MACHI polymer (2% (w/v) in a 16% (v/v) glycerol/water solution containing 0.25% (w/v) I2959, pH 7.0) was dispensed above a SA surface. With the aid of superhydrophobic tweezers, the ALG hydrogel core was entrapped within the previous droplet followed by its exposure to UV-light (365 nm, 2.8 mW/cm^2) for 1 min. Finally, the crosslinked ALG core was

dissolved by performing an EDTA treatment (20 mM in a 25 mM MES buffer solution, pH 7.0) for 5 min, yielding liquefied MACHI capsules. The obtained ALG cores and MACHI capsules were observed using an optical stereomicroscope (Stemi 508, Zeiss, Germany) equipped with a digital camera and characterized for their morphology, size and size distribution by measuring the diameter of 12 particles obtained in three different experiments using ImageJ^{TM} software.

Moreover, the static WCA was assessed in order to confirm the wettability of the produced substrates and was conducted on the basis of the sessile drop method. In a typical experiment, 3 µL water droplets were dispensed over a SA surface and the angles were measured after drop stabilization using the SCA 20 software. The experiments correspond to three replicates carried out on ten different surface regions at RT. The shape factor (SF) of the produced droplets was determined from their lateral view and used to further confirm their sphericity. Indeed, SF was calculated as the ratio between the orthogonal and parallel diameters in relation to the SA surface.

2.4. Methacrylamide Chitosan synthesis process, characterization and UV-mediated crosslinking

CHI, a polycationic biopolymer widely used in the biomedical field, is attractive because of its biocompatibility and chemical versatility [9]. Herein, 3 %(w/v) CHI was dissolved in 2 %(v/v) acetic acid overnight at RT with constant stirring as previously reported on literature [10]. Afterwards, MA was added at 0.4 molar equivalents per chitosan repeat unit and left for 3h at RT. The mixture was dialyzed against distilled water for 7 days, changing the water twice a day. The MACHI solution was, then, freeze-dried and stored at -20°C until use. Fourier Transform InfraRed Spectroscopy (FTIR, Bruker Tensor-27) was used to infer about the correct CHI methacrylation. Transmission spectra for both CHI and MACHI were recorded using the ATR mode (Golden Gate Acccessory, SPECAC) within the range of 4000-400 cm^{-1} using 256 scans, with a resolution of 4 cm^{-1}.

2.5. Cell encapsulation inside Polymeric Capsules

2.5.1. In Vitro Cell culture

Human adult primary dermal fibroblasts (ATCC® PCS–201–012™) were cultured in a Fibroblast Growth Kit medium supplemented with 10% FBS (heat-inactivated) and 1% penicillin-streptomycin (pH 7.4). Cells were grown in 150 cm^2 tissue culture flasks and incubated at 37 °C in a humidified air atmosphere of 5% CO_2. The culture medium was exchanged every 3 days.

2.5.2. Fibroblast encapsulation within MACHI capsules

Upon reaching 90% of confluence, fibroblasts were washed with PBS and chemically detached from tissue culture flasks using 0.05% Tryple Express solution for 5 min at 37°C in a humidified air atmosphere of 5% CO_2. Later, fresh medium was added to inactivate the Tryple Express effect and the cells were centrifuged at 1200 rpm for 5 min. Then, the medium was decanted followed by the cells re-suspension in different polymer in MES solution (pH 7.4) at a density of 1 x 10^6 cells per mL of polymer solution.

Five different formulations were tested as depicted in Figure S11.4: the first condition (A: ALG core+Cells) was done to study the ability of the produced ALG cores to entrap cells with high viability rates and was performed by ressuspended cells in 1.5% (w/v) ALG solution followed by Ca^{2+}-mediated crosslinking for 15 min (ionotropic gelation, 2 µL of 0.1 M $CaCl_2$) in a container with saturated humidity; the second condition (B: (ALG core+Cells) + MACHI shell) was performed in order to evaluate the effect of a MACHI external matrix on viability of cells entrapped within ALG crosslinked particle and was performed by entrapping a (ALG core+Cells) within a 2% (w/v) MACHI droplet containing 0.25% (w/v) I2959 photoinitiator and 16% (v/v) glycerol followed by UV curing for 1 min; the third condition (C: ((ALG core+Cells) + MACHI shell) + EDTA) was done to assess the effect of dissolution of the ALG core inside the MACHI

shell on cell viability and was performed by adding a droplet of EDTA solution (chelating agent, 6 µL of 20 mM) above a ((ALG core+Cells) + MACHI shell) for 5 min; the fourth condition (D: MACHI particle + Cells) refers to the control of the ability of cells to maintain viable after their encapsulation within a MACHI matrix and was performed by ressuspend the cells within a 2% (w/v) MACHI droplet containing 0.25% (w/v) I2959 photoinitiator and 16% (v/v) glycerol followed by UV curing for 1 min. Finally, the fifth condition (ALG core + (MACHI shell+Cells) + EDTA) constitute the control of the presence of ALG liquefied core on the cell viability within the MACHI shell and was performed by incorporating an ALG core within a MACHI droplet containing cells followed by UV curing for 1 min. The sacrificial core was obtained from a 2 µL droplet of an ALG pre-gel solution whereas a 4 µL droplet of a MACHI precursor solution was used to produce the polymeric shell. The MACHI + Cells particles (E) were done by dispensing a 6 µL droplet above a SA surface in order to attain the same size as the one of the polymeric capsules. Then, the produced particles were placed inside a 12-well tissue culture plate at 37°C with a humidified air atmosphere of 5% CO_2.

2.5.3. Cell Viability Assessment: LIVE/DEAD Assay

After 24h, the effect of the developed technology on the cell viability inside the different five formulations was qualitatively assessed by performing a LIVE/DEAD assay. This assay is based on the ability of viable cells' esterases to hydrolyze calcein-AM (membrane permeant dye) into calcein (green fluorescent dye), which is retained inside the cytoplasm. In turn, ethidium homodimer (EthD-1, red fluorescent dye) binds mainly to DNA of disrupted cells since it is membrane impermeant. Briefly, the culture medium was removed and replaced by 1 mL of PBS containing 0.5 µL of a 4 mM calcein AM stock solution and 2 µL of a 2 mM EthD-1 stock solution. After 30 min of incubation at RT, samples were washed three times with PBS and visualized immediately after by a fluorescence microscope (Z1m Inverted Microscope, Zeiss, Germany) using excitation and emission wavelengths of 494 and 535 nm and 517 and

617 nm for calcein-AM and EthD-1, respectively. These experiments were repeated three times for each sample.

2.6. MACHI Liquid-core Capsules: Multiple template cores

2.6.1. Gelatin

Gelatin is well-known for its biocompatibility, biodegradability and non-immunogenicity as well as for exhibiting cell-adhesive motifs all along its backbone [10-13]. A 2 µL droplet of a 2% (w/v) gelatin in water solution (with food dye 50:50 E133/E129, 0.1% (v/v), stains in purple) was dispensed over a SA surface and, subsequently, harden into a hydrogel by decreasing the temperature to 4ºC. Afterwards, a 2% (w/v) MACHI in water solution containing 0.25% (w/v) of I2959 photoinitiator and 16% (v/v) glycerol solution (with food dye E129, 0.01% in water, stains in light red) was used to produce a polymeric shell around the gelatin sacrificial core upon its UV-light crosslinking (365 nm, 2.8 mW/cm^2) for 1 min. The gelatin crosslinked core was turned into a liquid by increasing the temperature to 37ºC, yielding in liquid-core MACHI capsules.

2.6.2. Ice

A 2 µL water droplet containing a food dye (E129, 0.1% (v/v) in water, stains in red) was deposited above a SA surface and, subsequently, frozen at -80ºC for 15 min. Meanwhile, MACHI polymer was dissolved in 15% (v/v) EtOH in water solution (2% (w/v)) containing 0.25% (w/v) I2959 photoinitiator and placed at 4ºC. Polymeric capsules using ice as sacrificial template were produced by placing with superhydrophobic tweezers the core inside a 4 µL droplet of a MACHI solution above a SA surface. Then, the particle was crosslinked under UV-light (365 nm, 2.8 mW/cm^2) for 1 min using an ice bath below to avoid the core melting prior to the capsule formation. Afterwards, the fabricated particle was placed at RT, which resulted in the ice melting and, hence, on the production of liquid-core MACHI capsule.

2.6.3. Interfacial Gelation around a $CaCl_2$ droplet

In a first step, a 2 µL droplet of $CaCl_2$ (1 M in MES buffer) was pipetted to the interior of a 4 µL droplet of diluted ALG solution (0.1% (w/v) in water) in order to produce a flexible layer of ALG around the $CaCl_2$ liquid core by spontaneous ionotropic gelation. In a second step, the coated $CaCl_2$ core was retrieved from the SA surface with hydrophobic tweezers and placed on top of a 4 µL droplet of MACHI (2 w/v% in 16% (v/v) glycerol in water solution containing 0.25% (w/v) I2959 photoinitiator). The obtained system was subjected to UV-light irradiation (365 nm, 2.8 mW/cm^2) for 1 min to harden the MACHI polymer shell entrapping the liquid core.

2.7. Hierarchical Polymeric Capsules: Micro/Nanoparticles

2.7.1. Fabrication of the subcompartments

$CaCO_3$ microparticles were synthesized following a well-known method [14]. Shortly, aqueous solutions of Na_2CO_3 and $CaCl_2$ were prepared at 1 M. Coprecipitation of both solutions was performed under vigorous stirring (≈1000 rpm) by mixing 1 mL of each solution. After 30 s, stirring was stopped and the suspension of newly synthesized $CaCO_3$ microparticles, as result of growth of polycrystalline spherical vaterite particles [15], was left to react and precipitate for 15 min. The supernatant was removed and the particles washed twice with ultrapure water to remove residual salts. The obtained capsules were dried at 70°C until use.

PLLA microparticles were produced by emulsion solvent evaporation technique as elsewhere described with minor modifications [16]. Briefly, 1 g of PLLA was dissolved in 20 mL of CH_2Cl_2 containing a hydrophobic dye, Nile Red. Afterwards, this solution was added under agitation to 100 mL of 0.5% (w/v) PVA and left to stir for 2 days at RT to evaporate the organic solvent. The produced stained PLLA microparticles were collected by filtration and washed several times with distilled water. Ultimately, microparticles were subsequently frozen at -80 °C and lyophilized (Cryodos, Telstar) for 3 days. Prior to usage, microparticles were stored at 4 °C. Prior to usage, microparticles were stored at 4 °C.

The production of the Fe_3O_4 nanoparticles was based in a previously described protocol [17]. Shortly, Fe_3O_4 magnetic nanoparticles were synthesized by the co-precipitation reaction of $FeCl_2 \cdot 4H_2O$ and $FeCl_3 \cdot 6H_2O$ salts in the presence of NH_4OH under a nitrogen atmosphere at 60 °C. The obtained nanoparticles were then washed with deionized water and ethanol for several times, and ultimately dried in a VD23 (Binder, Germany) vacuum oven.

2.7.2. Fabrication of Hierarchical MACHI Capsules

In order to produce hierarchical systems using MACHI capsules as containers of each one of the three types of produced subcompartments, the produced micro/nanoparticles were suspended in a 1.5% (w/v) ALG in water solution. The former solution was dispensed using a pipette (2 µL) above a SA surface and then, the polymeric droplets were crosslinked by adding 2 µL of 0.1 M $CaCl_2$ solution on top of each droplet. Afterwards, the obtained monodisperse templates were assembled inside a MACHI shell followed by the hardening of this polymer coating by UV-exposure for 1 min, yielding capsules after the removal of the template by applying an EDTA treatment. It is worth noticing that glycerol (20% v/v) was added to compensate for the density mismatch.

2.7.3. Capsule Mechanical Stability Test

The mechanical stability of the produced capsules was tested as previously described using a rotational stress test [18]. Two types of capsules thickness were tested, namely 250 µm and 350 µm. The experiments were conducted in triplicates (n=4 for experiment). Therefore, MACHI capsules containing PLLA microparticles were placed inside centrifuge tubes with 5 mL of PBS and, then, centrifuged at 200 rpm for 60 min at RT. Every 15 min, the rotation was stopped in order to assess the number of damage capsules by visual inspection as the shell rupture will be translated on the release of previously entrapped PLLA microparticles inside the ALG sacrificial core. The intact capsules were placed again inside the centrifuge tubes to continue the rotational test.

2.8. Statistical Analysis

The significance of the differences on the average RMS values obtained from AFM and profilometer was assessed using the Student's t-test. P-values < 0.05 were considered statistically significant. The results are presented as mean ± standard deviation.

3. Results and Discussion

First, the liquefied core was obtained by dispensing a predefined volume of an ALG solution onto a SA surface, which is characterized by contact angles higher than 150° for both water and oil-based liquids (Figure 11.1I and SI.11; S11.2). ALG was selected due to its biocompatibility as well as for its ability to reversibly form hydrogels at mild conditions, making it a great candidate for the capsule liquid core (SI.11, S11.1). As shown in Figure 11.1a, pregel ALG droplets remained suspended above SA substrates, acquiring an almost spherical shape (SI.11; S11.2, shape factor of 0.95 ± 0.02). This shape was induced by the extreme wettability of these surfaces, which, in turn, is the result of the presence of a hierarchical topography with micro- and nanofeatures and a low surface energy (SI.11; S11.2).

Afterwards, $CaCl_2$ was added above the preformed ALG droplets to prompt their gelation (Figure 11.1I). Figure 11.1a shows the possibility of controlling the ALG particle size with high precision by simply tuning the dispensed volume above the SA surface.

By changing the droplet volume from 2 to 8 µL, the particle size increased from 0.5 ± 0.05 mm to 1.0 ± 0.05 after 15 min of Ca^{2+}-mediated crosslinking, which corroborates with previous studies ($R^2 \approx 0.99$) [19].

The preformed ALG hydrogel particles were then entrapped within a larger volume of MACHI solution, previously dispensed above a SA surface, to form a shell around it (Figure 11.1II). As shown in Figure 11.1b (upper panel), the ALG core sank almost instantaneously onto the SA due to a density mismatch between the MACHI solution (liquid) and the ALG particle

(hydrogel). Consequently, the external MACHI droplet may not completely surround the ALG core, forming a hole from which the immobilized cargo may be released in an uncontrolled way (SI.11; S11.3).

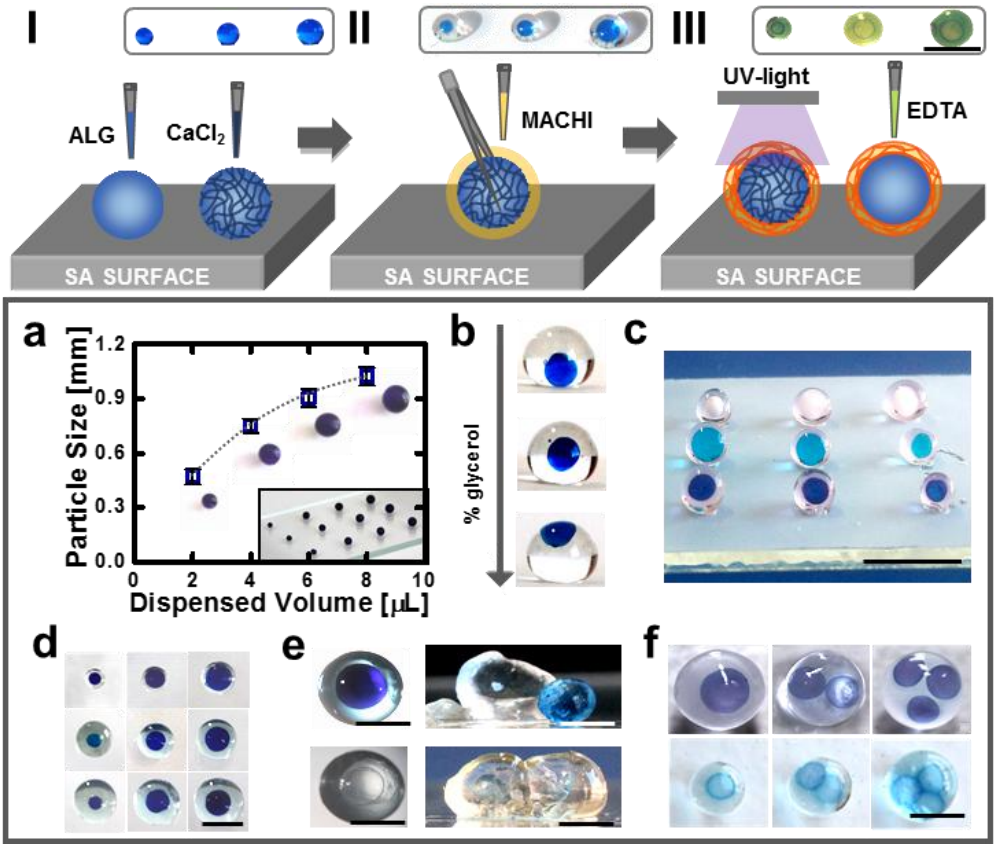

Figure 11.1 - **(I)** Spherical ALG droplet induced by a SA surface and their subsequent Ca^{2+}-mediated crosslinking. **(II)** Entrapment of an ALG core within a MACHI droplet. **(III)** UV-mediated crosslinking of the MACHI shell followed by the core dissolution via EDTA action. Scale bar stands for 1.2 mm. **(a)** Effect of the dispensed volume of ALG solution on the size of the obtained ALG particles after 15 min of Ca^{2+}-mediated gelling. Scale bar corresponds to 6 mm. **(b)** Effect of glycerol on the position of the ALG core inside a MACHI pregel droplet (0, 16 and 20% (v/v) of glycerol/water). **(c)** Scale-up of the developed strategy to attain simultaneously polymeric capsules containing cores with different sizes and entrapping different compounds. Scale bar stands for 2 mm. **(d)** Multicompartmental hydrogel particles with distinct shell thickness. Scale bar is 1.2 mm. **(e)** MACHI capsule before (upper panel) and after (lower panel) the EDTA treatment. Scale bar stands for 400 µm. **(f)** Hydrogel particles with a multicore structure before (upper panel) and after (lower panel) EDTA treatment. Scale bar corresponds to 700 µm.

To overcome this main issue, glycerol was used to increase the density of the external MACHI solution and compensate for the higher density of the ALG particle. As can be observed in Figure 11.1b, the ALG particle position inside the MACHI droplet can be tuned by adjusting the amount of glycerol added. Moreover, the inclusion of this compound ensures the scale-up of this process to attain simultaneously polymeric capsules with different core sizes (Figure 11.1c).

Afterwards, the MACHI hydrogel shell was crosslinked upon exposing this photosensitive polymer to UV-light for 1 min (Figure 11.1III and SI; S1.4). By varying the dispensed volume of MACHI polymer, the capsule thickness ranged from around 100 to 400 μm (Figure 11.1d).

Finally, the ALG core was dissolved upon dropping an EDTA solution above the previous particle, yielding a MACHI capsule with a liquid core (Figure 11.1III). EDTA, a divalent ion chelating agent, can disrupt the ALG/Ca^{2+} matrix as demonstrated by the conversion of the ALG solid core into a liquid (Figure 11.1e and SI; S11.2). Further control over the internal structure was demonstrated by synthesizing capsules exhibiting multiple-cores (Figure 11.1f). To produce these particles, different number of the preformed ALG templates were assembled simultaneously within a droplet of a MACHI precursor solution, which was subsequently gelled by UV-light exposure (Figure 11.1f; upper panel) and its cores liquefied upon EDTA action (Figure 11.1f; lower panel). Capsules with a hierarchical architecture of more than two core assemblies could be useful for individual reagent loading in each of the created subcompartments, being attractive as artificial organelles, bioreactors for confined synthesis or as drug carries [20].

Capsules with a core–shell structure were subsequently loaded with cells to assess the suitability of the purposed strategy to encapsulate highly sensitive compounds. To this end, the viability of human fibroblasts entrapped in five distinct cell carrier formulations was assessed. First, cells were homogeneously distributed within an ALG/Ca^{2+} matrix, exhibiting good viability rates due to (i) the mild processing conditions used, (ii) the efficient exchange of essential molecules with the surroundings provided by the particle small size, and (iii) the ALG

biocompatible character (Figure 11.2A). Then, these cell carriers were entrapped within a second polymeric layer made of MACHI. As shown in Figure 11.2B, some nonviable cells appeared on the core center after the incorporation of this barrier between the core and the culture medium. This may be ascribed to the increase of the overall diameter of the particle, which hampered the diffusion of nutrients/O_2/waste metabolites and, hence, compromising the cell viability. Therefore, these particles were subjected to an EDTA step to create liquefied cell-laden capsules. The results suggest the formation of a cell-friendly liquid environment wherein cells are metabolically active, highlighting the potential of these capsules as cell encapsulation devices (Figure 11.2C). Indeed, previous works have shown higher cell viability rates for higher core dissolution degrees, which can justify the attained high viability levels [21]. Other alternative to enhance the diffusion rates was tested by entrapping fibroblasts within the thin (≈200 μm) MACHI shell (Figure 11.2D). When comparing with compact cell-laden MACHI particles, which revealed nonviable cells at the inner areas (Figure 11.2E), most of the cells enclosed on the MACHI shell were viable, which further strengths the potential of the developed liquefied capsules.

Figure 11.3 summarizes different strategies to produce polymeric capsules using different sacrificial cores along with distinct removal methods. Gelatin, the denaturated form of collagen protein, was used as a core due to its temperature-responsive behavior. At low temperatures, its chains undergo a conformational change from a random coil to a triple helix, resulting on the formation of a 3D crosslinked network (Figure 11.3a). Interestingly, this aggregation process can be reversibly disrupted above 30 °C to yield liquefied capsules (Figure 11.3b) [12]. The use of gelatin as template constitutes a simplification over the process described in Figure 11.1 because it avoids the addition of any compound to either crosslink or liquefy the core. Another strategy also based on the use of thermosensitive templates consists in using ice as template. Contrarily to crosslinked cores, an ice core floats when placed above a MACHI droplet (Figure 11.3c). Thus, ethanol was added to lower the density of the surrounding droplet (Figure 11.3d).

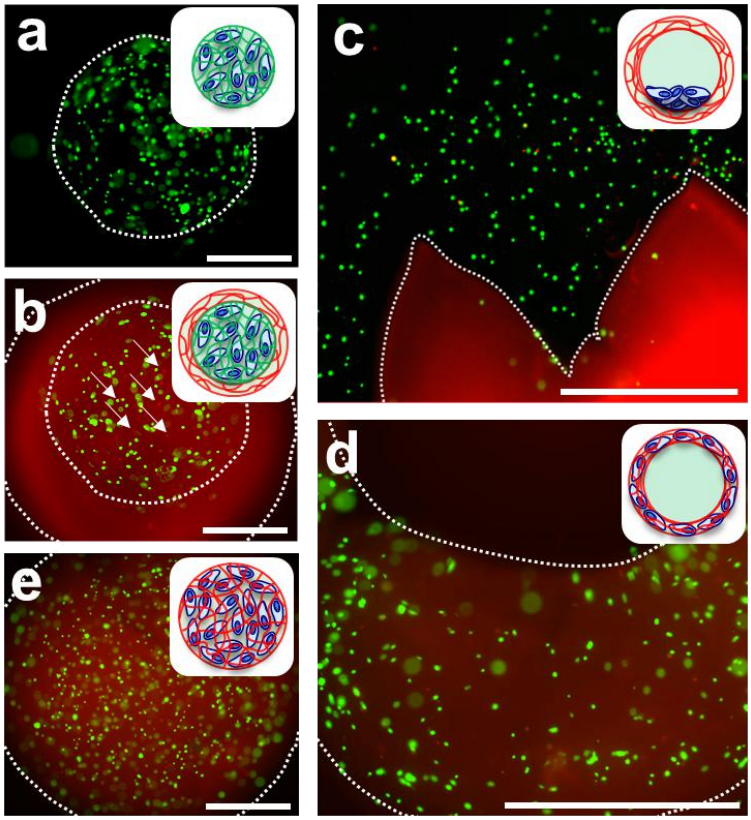

Figure 11.2 - LIVE/DEAD images of cell-laden ALG microparticles **(A)**, MACHI capsule with a crosslinked cell-laden ALG core (arrow indicates some nonviable cells) **(B)**, a ruptured MACHI capsule releasing the encapsulated cells **(C)**, cell-laden MACHI shell **(D)**, and cell-laden compact MACHI particle **(E)** using calcein (green; living cells) and Ethd-1 (red; dead cells) dyes. Scale bar corresponds to 200 μm.

Such capsules may be extremely attractive for the cryopreservation of living cells, an issue that has received increasing attention. Contrarily to some living organisms, most mammalian cells are unable to survive when exposed to subzero temperatures unless they are placed in solutions with specific additives and following defined freezing protocols [22]. Recently, the entrapment of the desired structures inside hydrogels emerged as an alternative to the established protocols since they allow the cell protection from mechanical damage upon ice crystallization and preserve the cell–cell interactions [23]. With this in mind, polymeric capsules containing both cells and cryopreservatives could be fabricated following this methodology, envisioning cell preservation for future outcomes. Polymeric capsules were also templated on a liquid core by depositing a $CaCl_2$ droplet above another of ALG, resulting on a

thin, elastic interfacial membrane (Figure 11.3II). Following this methodology, bicompartmental hydrogel particles were formed by assembling this core inside a MACHI shell (Figure 11.3e,f). Using this strategy, the addition of any compound to adjust the density or to remove the core is avoided.

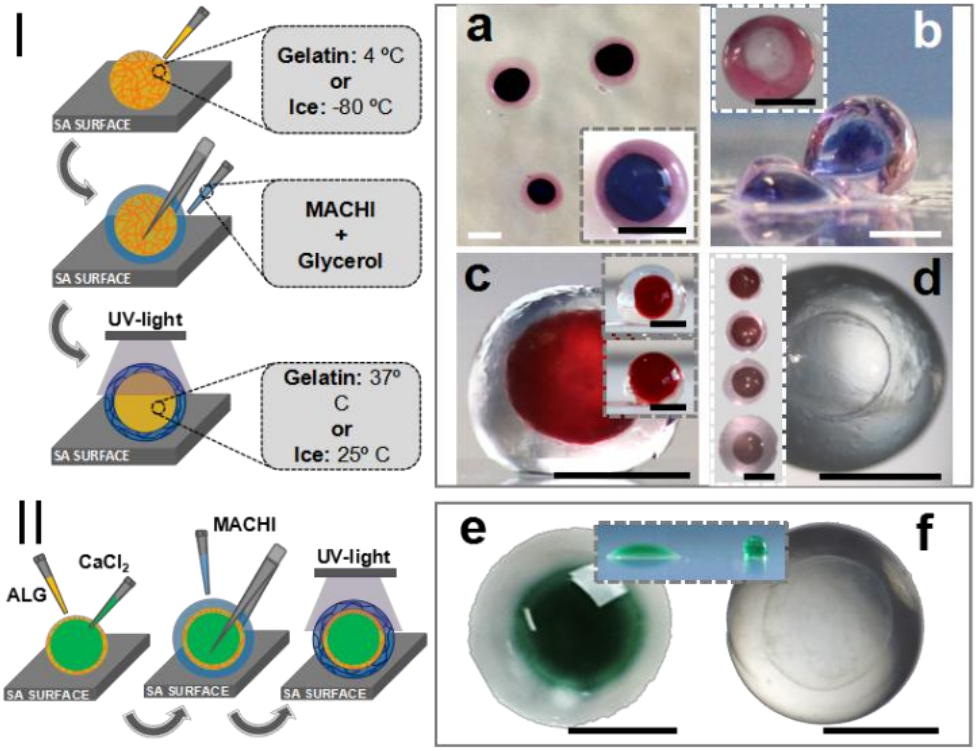

Figure 11.3 - Fabrication of polymeric capsules: **(I)** Thermoresponsive sacrificial cores: examples of MACHI capsules with a gelatin (a,b) or ice core (c,d) before (a,c) and after (b,d) the core removal, respectively. Regarding the ice-core capsules, ethanol was added to decrease the density of the surrounding MACHI solution (c, upper inset), the temperature was controlled to avoid the core melting (c, lower inset) and the shell thickness tuned by controlling the volume of MACHI solution dispensed (e, inset). **(II)** Interfacial gelation process: example of a MACHI capsule with a $CaCl_2$ liquid-core before (e) and after (f) the dye release. Scale corresponds to 400 µm.

Hierarchical systems were fabricated by incorporating different objects inside the core during the synthesis process, proving once more the versatility of this strategy. Herein, calcium carbonate ($CaCO_3$) particles were evenly distributed within the ALG core as visualized by an arrangement of white dots, characteristic of these particles (Figure 11.4a). These

subcompartments can also be disrupted through the action of EDTA, which turn the core into a liquid (Figure 11.4b). Such compartmentalized systems may find biomedical utility, which is imparted by their proven biocompatibility [24].

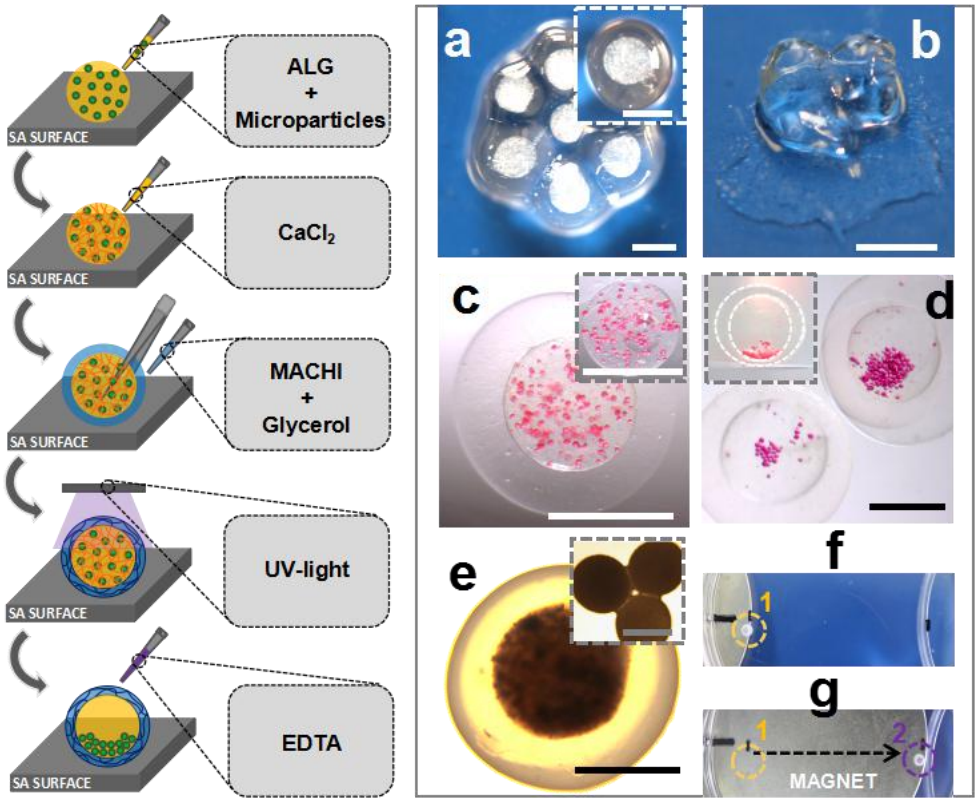

Figure 11.4 - Fabrication of hierarchical capsules containing either $CaCO_3$ **(a,b)** or PLLA microparticles **(c,d)**, or Fe_3O_4 nanoparticles before **(a,c,e)** and after **(b,d,f,g)** EDTA treatment. Motion control of the produced capsules using a permanent magnet (surface magnetic intensity of 0.075 T; f,g). Scale corresponds to 400 µm.

Similarly, PLLA microparticles were also enclosed within MACHI capsules and may have an increased importance, for example, as supporting points of anchorage-dependent cells as they are enable to grow in suspension (Figure 11.4c,d). Actually, it was previously reported higher cell viability levels when cells were encapsulated within particles containing anchorage points, highlighting the importance of these particulate devices for application in Tissue Engineering rather than be merely used as cell carriers [25]. Furthermore, the stability of the obtained capsules was assessed through a rotational test using capsules with two-layer

thicknesses, *i.e.,* 250 and 350 µm. Interestingly, after 1 h at 200 rpm, both capsules maintained their integrity avoiding the release of their contents, thus proving the production of stable capsules (S1.11, S11.6). Furthermore, Fe_4O_3 particles were successfully encapsulated within MACHI capsules (Figure 11.4e), empowering these capsules with magnetic-responsiveness that can be used to guide them over a surface (Figure 11.4f and 11.4g).

4. Conclusion

In summary, SA surfaces were successfully employed to fabricate ready-to-use and stable multiscaled liquefied capsules enclosing different objects. This strategy benefit from its (i) solvent-free character enabling a loading efficiency of almost 100%, (ii) reproducibility as demonstrated by the great control over the particle size and shape, (iii) versatility as shown by the fabrication of a wide variety of core–shell capsules, (iv) mild processing conditions as proved by the safe encapsulation of metabolically active cells, and (v) its cost-effective character inasmuch as it is based on a simple setup. Based on all these features, this simple, yet efficient strategy is envisioned to constitute an innovative approach to produce liquid-core polymeric systems to entrap a variety of sensitive molecules including not only cells but also proteins, genes, enzymes, and drugs, with minimal adverse effects on their functionality. Moreover, due to the simultaneously superhydrophobic and superoleophobic character of the used substrates, capsules may contain virtually any type of liquid make it possible to broad the application spectrum to diverse technological purposes such as agriculture, biotechnology, cosmetics, and electronics, where solvents different than water are often required. Owing to the widespread application of polymeric capsules like the produced ones, modifications to the conventional fabrication techniques are likely to have a strong impact and open new prospects for the development of the next generation of engineered polymeric assemblies for both science and technology.

Acknowledgements

This work was funded by FCT through the PhD grant SFRH/BD/101748/2014 and by European Research Council grant agreement ERC-2014-ADG-669858 for project ATLAS.

Supplementary Information (SI.11)

S11.1. Alginate polymer and Reversible Crosslinking Process

ALG, a polysaccharide mainly obtained from brown algae, is a linear copolymer composed of consecutive blocks of (1-4)-linked β-D-mannuronic acid (M-blocks) or its C-5 epimer α-L-guluronic acid (G-blocks) monomers or alternating M and G-residues (M-G blocks). This natural polymer tends to be negatively charged at a pH of around 7.4 (the physiological pH) since its pka value is of 3.4 and 3.7 for M and G acids, respectively [26]. Thus, ALG can yield gels when the carboxylic acid groups present on its backbone encounter divalent cations such as calcium ions. This bond occurs between G-blocks of adjacent ALG chains during gelling, creating an egg-box-like structure [27, 28]. In order to ensure the effective interaction between ALG and Ca^{2+} ions, several parameters such as the polymer and ion concentrations, and pH value need to be optimized. The values chosen were already reported in other publications [23]. A unique characteristic of ALG is its ability to reverse its gelling process, meaning that it is possible to return to ALG non-crosslinked form (liquid state), by simply adding Ca^{2+} chelators such as EDTA [29, 30]. The selected amount and time of EDTA treatment was based on other publications and was proved to be efficient in liquefying the ALG core [23]. All of these characteristics make ALG a great candidate to fabricate the capsule' liquid core under mild conditions.

S11.2. Preparation and Characterization of Superamphiphobic Surfaces

A superhydrophobic (SH) substrate is defined by a WCA value greater than 150° [8], which is conferred by the presence of both surface roughness (usually originated from microscopic protrusions with nano-scale features) and a low surface energy [31]. A behavior like this can be found in Nature, where several structures are able to repel water such as the case of the lotus leaf and its associated self-cleaning character, and also the case of the water strider's leg [32, 33]. Regarding the hierarchical structure, it is well known that the presence of microstructures allow the resistance to the capillary waves whilst the nanostructures are able to prevent the valleys filling by small droplets [34]. Besides these features, if a surface also exhibits overhanging structures, it can also repel oleo-based liquids, yielding SA surfaces.

Figure S11.1 displays the obtained results, suggesting the presence of a rough architecture resulting from the deposition of carbon particles (soot layer) with RMS values of 0.561 ± 0.065 mm. This outcome proves the successful modification of the microscope slides leading to the formation of microstructures, which were found to be homogeneously distributed over the entire SA substrate. Owing to this surface topography, when a water droplet is placed in contact with a SA surface, it exhibits a spherical shape. This shape is the result of the entrapment of air in the valleys between the microscopic protrusions above which the droplet is suspended in the Cassie state and, consequently, avoid its collapse into the Wenzel wetting state. Therefore, this composite interface (solid-air-liquid) leads to an increase in the macroscopic contact angle and a reduced contact angle hysteresis. Indeed, the WCA angle was measured to assess the extent of droplet contact with the SA surface and the obtained results are displayed in panel S11.1B. The high WCA values obtained, around 165°, reflect the low contact area of the droplet with the produced SH substrates, in compliance with other results found in literature [7, 4b]. Figure S11.1B inset shows an example of a droplet observed from the side view. By observing this image is possible to notice the characteristic spherical shape, which was further proved by the SF value obtained, which close to 1. Together with RMS, this

network-like structure is responsible for promoting a higher WCA as well as a more stable composite solid-liquid-air interface. In order for the surface features to readily promote the formation of this interface, they must present nominal pitches smaller than the actual diameter of the given droplet. As observed in Figure S11.2C, textural features resulting from this surface coating present average pitches of around 3.42 ± 1.61 mm, proving themselves as suitable resting places for the produced micro-droplets.

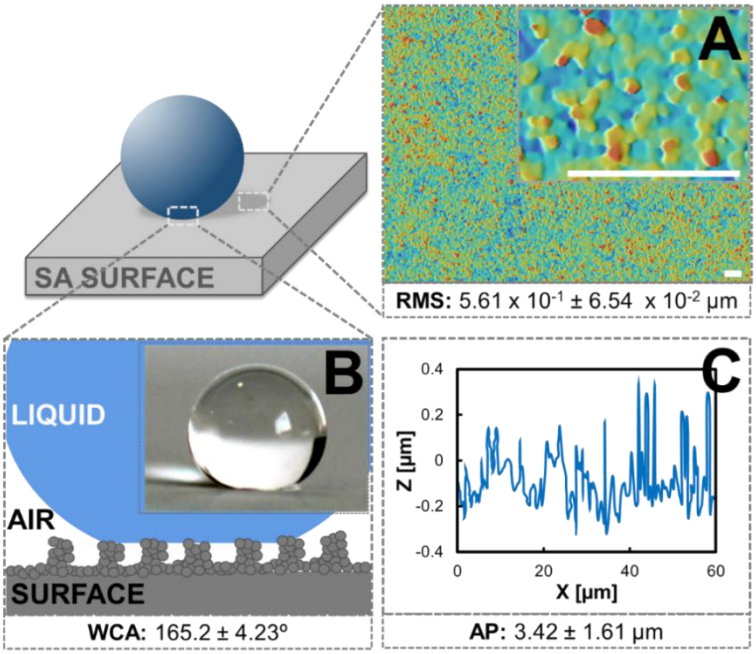

Figure S11.1 - Wettability character of the produced SA surfaces. **(A)** Representative topographic image obtained using a profilometer, depicting the surface roughness (RMS) value. The scale bar corresponds to 1 µm. The inset contains a zoom in of a certain region of the former image. The scale bar corresponds to 0.5 µm. **(B)** Schematic representation of a liquid droplet deposited on the fractal-like composite interface of the produced SA substrates. Inset corresponds to a lateral view of a 3 µL water droplet deposited on the SA surface. **(C)** Z profile of SA surfaces obtained all along the X-axis at a fixed Y-coordinate, showing the average pitch (AP) size values, as determined from these surfaces.

In sum, the characterization of these superamphiphobic surfaces was further extended by using a profilometer to assess the surface roughness. Although this technique has a lower resolution when compared with others such as AFM, it is quite simple as it does not require the adjusting and/or optimization of multiple parameters as well as rapid since it takes short

acquisition times. Interestingly, the obtained roughness (RMS; root mean square) values were not significantly different from the ones reported on literature ($p<0.5$; 0.498 ± 0.072 vs 0.56 ± 0.065 mm for AFM and profilometer, respectively). In sum, the characterization of the WCA and the magnitudes obtained thereof further confirm the right formation of the SA substrates.

Importantly, due to the simultaneously superhydrophobic and superoleophobic character of the used substrates, the capsules may contain virtually any type of liquid make it possible to broad the application spectrum to diverse technological purposes such as agriculture, biotechnology, cosmetics, and electronics, where solvents different than water are often required.

S11.3. Capsule Size and Density Mismatch: Glycerol and Hydrophobic Tweezers

The size of the produced hydrogel spheres can be controlled by dispensing precise volumes of the liquid using a micropipette. As shown in Figure 11.1a, the volume varied from 2 µL (minimum volume of ALG solution that was possible to dispense using a micropipette due to viscosity and surface tension constraints) to 8 µL (maximum volume of ALG solution dispensed to, after the addition of the MACHI polymer, avoid gravity effects on the capsule shape), corresponding to core diameters ranging between *ca.* 0.4 mm and 1 mm. Smaller particles may be obtained using spray-based methods or using other dispensing systems, which furthers strengths the importance of the dispensing mechanism used to tune the droplet size [7,4b]. The lower size limit is determined by various factors such as the dispensing method employed (*e.g.* spraying,...), the solution properties (*e.g.* viscosity,...), the substrate features (*e.g.* the distance between asperities on the surface) and the external conditions applied (*e.g.* pressure,...) [37]. It was shown that for relatively small volumes the shape of liquid drops on an extremely water repellent surface is almost spherical, tending to a more deformed geometry for the case of bigger droplets due to the effect of gravity, which is the main limiting factor to obtain bigger spherical particles. Herein, the capsule size ranged from *ca.* 500 µm to 2 mm since, besides the core size, the capsule also has a shell thickness.

Moreover, after the conversion of the polymeric droplet into a crosslinked particle, the size can also be different from the one of the initial droplet, due to the typical occurrence of shrinking during the crosslinking process and/or due to water evaporation from the droplet, for example. To avoid these former problems, the particle size was measured after 15 min of Ca^{2+}-mediated crosslinking and by incubating the particles under a humidified atmosphere. Regarding the shell thickness, it is challenging to attain a value lower than 100 μm due to the dispensing method used (by pipetting) and to ensure that the core was exactly in the middle position (Figure S11.2).

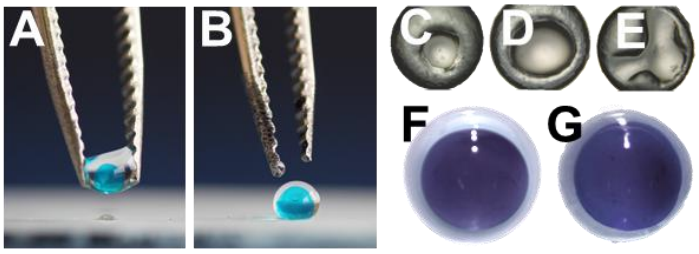

Figure S11.2 - Placement of an ALG crosslinked core (E133, stained in blue) inside a MACHI droplet using non-modified **(A)** and hydrophobic tweezers **(B)**. Due to the high repellency of the produced SA surfaces, the tweezers were modified using a waterproof spray to enable the deposition of the core within the MACHI droplet, as otherwise, the droplet would remain attached to them. **(C)** This step should be carried out in the presence of glycerol to avoid the sank of the ALG core into the surface, which may result on the formation of a hole after UV-mediated crosslinking. Moreover, owing to the low dimensions of this molecule, it is expected that once in solution glycerol will be able to diffuse into the surrounding medium, being released from the produced polymeric structures. **(D)** Typical appearance of the middle section of a MACHI particle by using glycerol. It is possible to observe that the produced capsule is hollow, resulting in a compartment that can be loaded with different compounds. **(E)** Other issue that need to be controlled is the stability of the capsule, which can be accomplished by increasing the UV-mediated crosslinking. After 20 s of UV crosslinking, a capsule is formed but it is not sufficiently robust to maintain its spherical shape, resulting on its collapse. **(F)** The sacrificial core must occupy the middle position in both directions vertical and horizontal in order to ensure a homogenous thickness, being critical for lower shell thickness (**G**, arrow).

S11.4. Methacrylamide Chitosan characterization and UV-mediated crosslinking

Figure S11.3 reveals that the IR spectra of CHI shows the typical peaks of each component, namely the CHI bands at *ca.* 3700-2900 (-NH_2 and -OH groups); 2872 (-CH_2-);

1648 and 1581 (amide I and II, respectively); and 1058 (C-O) cm^{-1} [35]. Meanwhile, the MACHI spectrum displays, in addition to those characteristic of CHI, the appearance of one distinctive peaks of MA (marked with arrows) at 1606 cm^{-1}. As previously demonstrated for the methacrylation of dextran, this band correspond pendant vinyl groups (the next two) [36, 37]. Taken together, these findings demonstrate that the CHI modification was successfully executed.

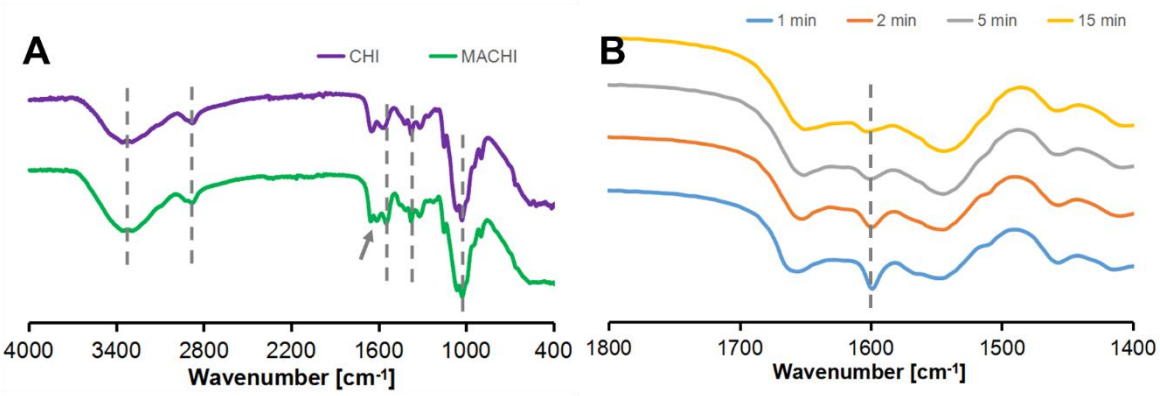

Figure S11.3 - (A) FTIR spectra of chitosan (CHI) and methacrylamide chitosan (MACHI). Marked with an arrow is the methacrylic group from MACHI polymer, which was attached to the modified CHI polymer. **(B)** FTIR spectra of MACHI polymer after its exposure to UV-light for 1,2,5 and 15 min. The decreasing of the characteristic (C=C) characteristic peak over time suggests the formation of a crosslinked 3D-structure. Results are presented in %T.

Moreover, the influence of the UV-crosslinking time on the crosslinking degree was also assessed. As a result of the UV-light exposure, the photoinitiator forms free radicals needed to initiate the polymerization process, namely the reaction between the methacrylated pendant groups on the MACHI. Therefore, the crosslinking degree of the MACHI was evaluated by the disappearance of the vinyl methylene groups on IR spectrum, after normalizing all the spectra. It is important to notice that FTIR was only used to evaluate qualitatively this process driven by UV-light. Its quantification was already provided in a previous publication resorting to NMR [7]. After 1 min, the characteristic peak of the methacrylic groups was still present but was lower, suggesting that MACHI chains have been crosslinked in order to create a hydrogel network. By

contrast, after 15 min this peak was almost completely removed, suggesting that almost all the groups were consumed to create a 3D-network. These results are in good agreement with previous publications [4b].

S11.5. Cell encapsulation inside Polymeric Capsules

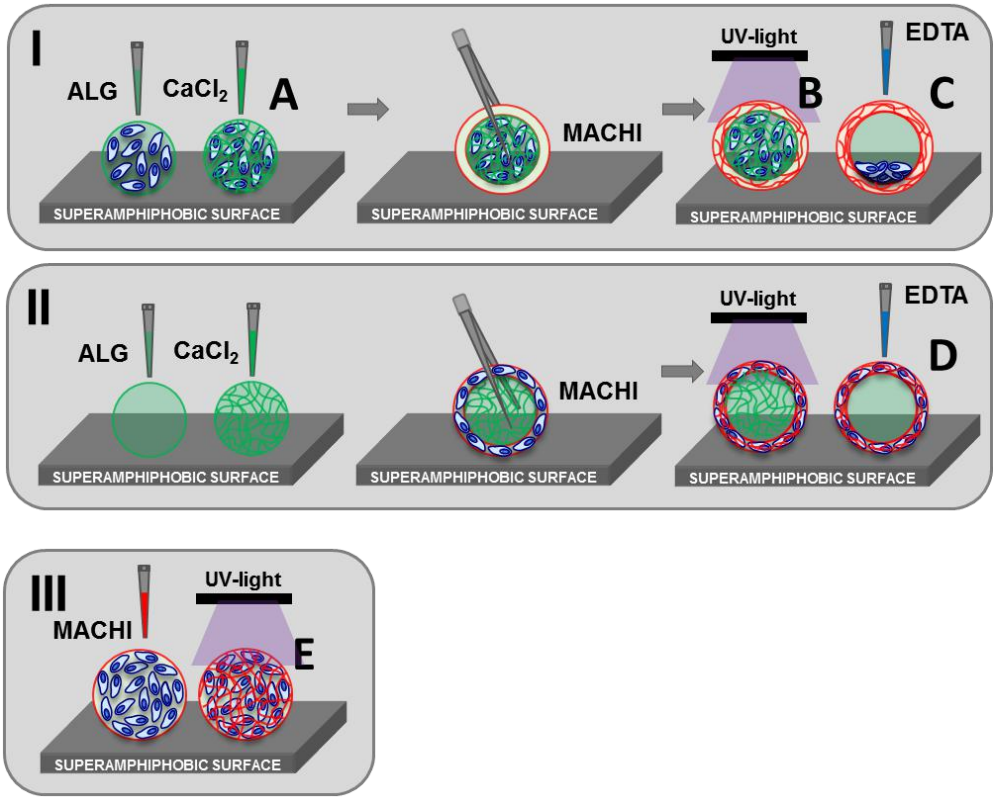

Figure S11.4 - Schematic representation of the synthesis route to attain cell-laden carriers. **(I)** Cell-laden ALG cores were crosslinked upon adding Ca^{2+} ions (A) and assembled into a MACHI droplet over a SA surface using superhydrophobic tweezers. Afterwards, the MACHI matrix was crosslinked by UV-light exposure (B) followed by the ALG core removal after an EDTA treatment, yielding MACHI capsules with a liquid-core containing cells (C). **(II)** Non-loaded ALG core was also incorporated into a droplet of MACHI with cells as stated before in order to obtain cell-laden MACHI capsules with a liquid-core (D). **(III)** Cell-laden MACHI carriers were also produced by suspending cells in this polymer precursor solution followed by its dispensing over a SA surface using a pipette and, its subsequent crosslinking by UV-light exposure (E).

S11.6. MACHI particles: Multiple template cores

Although the attained polymeric shell directly determines the capsules properties and, hence, their application, the template choice also plays an important role on the final characteristics of the obtained capsules as their size and shape are mainly dictated by the used sacrificial core [38, 39]. Therefore, special attention should be paid to the core composition, processing conditions and stability to allow its assembly within the MACHI droplet as well as to provide the appropriate conditions for its removal to not jeopardize the structure of both the capsule shell and the cargo [3,40,41]. In light of these facts, different templates along with different core removal methods were tested to evaluate the versatility of the developed strategy to obtain polymeric capsules with different physicochemical characteristics and, hence, making it possible their application in distinct fields. A schematic representation of the various strategies developed is shown in Figure 11.3.

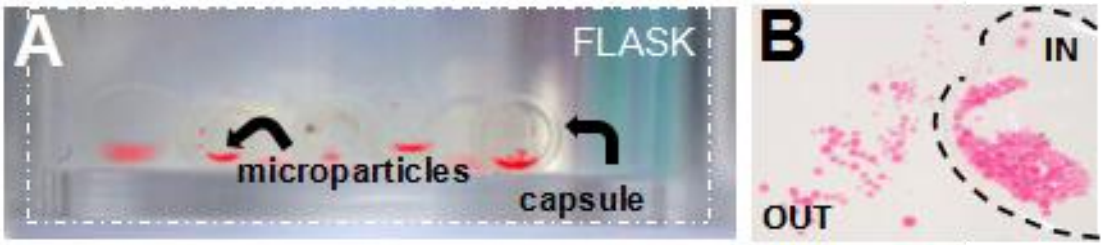

Figure S11.5 - Results of MACHI capsules stability assay: **A)** Capsules enclosing PLLA microparticles after the rotational assay. As it can be observed the PLLA particles deposited on the MACHI-capsule wall as result of the EDTA treatment. Moreover, non-ruptured capsules were observed since the PLLA particles remained inside the MACHI shell. **B)** Image of a hydrogel capsule which was ruptured to observe the release of its contents.

References

[1] a) X. W. Lou, L. A. Archer, Z. Yang, Hollow micro-/nanostructures: Synthesis and applications, *Adv. Mater.* **2008**, 20, 3987; b) W. Wei, G.-H. Ma, G. Hu, D. Yu, T. Mcleish, Z.-G. Su, Z.-Y. Shen, Preparation of Hierarchical Hollow CaCO3 Particles and the Application as Anticancer Drug Carrier, *J. Am. Chem. Soc.* **2008**, 130, 15808; c) B. J. Blaiszik, S. L. B. Kramer, M. E. Grady, D. A. McIlroy, J. S. Moore, N. R. Sottos, S. R. White, Autonomic restoration of electrical conductivity, *Adv. Mater.* **2012**, 24, 398; d) P. L. Lam, R. Gambari, Advanced progress

of microencapsulation technologies: In vivo and in vitro models for studying oral and transdermal drug deliveries, *J. Control. Release* **2014**, 1, 25.

[2] a) A.C. Lima, C. Alvarez-Lorenzo, J.F. Mano, Design advances in particulate systems for biomedical applications, *Adv. Healthc. Mater.* **2016**, 5, 1687; b) S.K. Verma, A. Amoah, U. Schellhaas, M. Winterhalter, S. Springer, T.A. Kolesnikova, "To Catch or Not to Catch": Microcapsule - Based Sandwich Assay for Detection of Proteins and Nucleic Acids, *Adv. Funct. Mater.* **2016**, 26, 6015.

[3] J. Cui, M.P. van Koeverden, M. Müllner, K. Kempe, F. Caruso, Emerging methods for the fabrication of polymer capsules, *Adv. Colloid Interface Sci.* **2014**, 207, 14.

[4] a) W. Song, A.C. Lima, J.F. Mano, Bioinspired methodology to fabricate hydrogel spheres for multi-applications using superhydrophobic substrates, *Soft Matter* **2010**, 6, 5868; b) A.M.S. Costa, M. Alatorre-Meda, N.M. Oliveira, J.F. Mano, Biocompatible polymeric microparticles produced by a simple biomimetic approach, *Langmuir* **2014**, 30, 4535.

[5] A.C. Lima, J.F. Mano, Micro/nano-structured superhydrophobic surfaces in the biomedical field: part II: applications overview, *Nanomedicine Lond.* **2015**, 10, 271.

[6] X. Deng, L. Mammen, H.-J. Butt and D. Vollmer, Candle soot as a template for a transparent robust superamphiphobic coating, *Science* **2012**, 335, 67-70.

[7] A. M. S. Costa, M. Alatorre-Meda, C. Alvarez-Lorenzo and J. F. Mano, Superhydrophobic Surfaces as a Tool for the Fabrication of Hierarchical Spherical Polymeric Carriers, *Small* **2015**, 11, 3648-3652.

[8] A. B. D. Cassie and S. Baxter, Wettability of porous surfaces, *J. Chem. Soc. Faraday Trans.* **1944**, 40, 546-551.

[9] M. Rinaudo, Chitin and chitosan: Properties and applications, *Prog. Polym. Sci.* ***2006***, 31, 603-632.

[10] L. M. Yu, K. Kazazian and M. S. Shoichet, Peptide surface modification of methacrylamide chitosan for neural tissue engineering applications, *J. Biomed. Mater. Res. Part A* **2007**, 82, 243-255.

[11] F. Bode, M. A. da Silva, A. F. Drake, S. B. Ross-Murphy and C. A. Dreiss, Enzymatically cross-linked tilapia gelatin hydrogels: physical, chemical, and hybrid networks, *Biomacromolecules* **2011**, 12, 3741-3752.

[12] A. Duconseille, T. Astruc, N. Quintana, F. Meersman and V. Sante-Lhoutellier, Gelatin structure and composition linked to hard capsule dissolution: A review, *Food Hydrocolloid.* **2015**, 43, 360-376.

[13] X. Liu and P. X. Ma, Phase separation, pore structure, and properties of nanofibrous gelatin scaffolds, *Biomaterials* **2009**, 30, 4094-4103.

[14] R. R. Costa, E. Castro, F. J. Arias, J. C. Rodríguez-Cabello and J. F. Mano, Multifunctional Compartmentalized Capsules with a Hierarchical Organization from the Nano to the Macro Scales, *Biomacromolecules* **2013**, 14, 2403-2410.

[15] J.-P. Andreassen, Formation mechanism and morphology in precipitation of vaterite - Nano-aggregation or crystal growth?, *J. Cryst. Growth* **2005**, 274, 256-264.

[16] R. Bodmeier and J. W. McGinity, Polylactic acid microspheres containing quinidine base and quinidine sulphate prepared by the solvent evaporation method. III. Morphology of the microspheres during dissolution studies, *J. Microencapsul.* **1988**, 5, 325-330.
[17] S. Gil, E. Castro and J. F. Mano, Synthesis and characterization of stable dicarboxylic pegylated Magnetite nanoparticles, *Mater. Lett.* **2013**, 100, 266-270.
[18] T. Haque, H. Chen, W. Ouyang, C. Martoni, B. Lawuyi, A. M. Urbanska and S. Prakash, *Superior cell delivery features of poly(ethylene glycol) incorporated alginate, chitosan, and poly-L-lysine microcapsules, Mol. Pharm.* **2005**, 2, 29-36.
[19] R. Luo, Y. Cao, P. Shi, C. H. Chen, Near-infrared light responsive multi-compartmental hydrogel particles synthesized through droplets assembly induced by superhydrophobic surface, *Small* **2014**, 10, 4886.
[20] a) R.J.R.W. Peters, I. Louzao and J.C.M. van Hest, From polymeric nanoreactors to artificial organelles, *Chem. Sci.* **2012**, 3, 335; b) W. Xu, P.A. Ledin, Z. Iatridi, C. Tsitsilianis and V.V. Tsukruk, Multicompartmental Microcapsules with Orthogonal Programmable Two-Way Sequencing of Hydrophobic and Hydrophilic Cargo Release, Angew. *Chem. Int. Ed.* **2016**, 55, 4908.
[21] R.L. Broughton and M.V. Sefton, Effect of capsule permeability on growth of CHO cells in Eudragit RL microcapsules: use of FITC-dextran as a marker of capsule quality, *Biomaterials* **1989**, 10, 462.
[22] J.M. Shaw, A. Oranratnachai and A.O. Trounson, Fundamental cryobiology of mammalian oocytes and ovarian tissue, *Theriogenology* **2000**, 53, 59.
[23] Y. Nie, V. Bergendahl, D.J. Hei, J.M. Jones and S.P. Palecek, Scalable culture and cryopreservation of human embryonic stem cells on microcarriers, *Biotechnol. prog.* **2009**, 25, 20.
[24] W. Wei, G.-H. Ma, G. Hu, D. Yu, T. McLeish, Z.-G. Su and Z.-Y. Shen, Preparation of hierarchical hollow CaCO3 particles and the application as anticancer drug carrier, *J. Am. Chem. Soc.* **2008**, 130, 15808.
[25] C.R. Correia, P. Sher, R.L. Reis and J.F. Mano, Liquified chitosan–alginate multilayer capsules incorporating poly(l-lactic acid) microparticles as cell carriers, *Soft Matter* **2013**, 9, 2125.
[26] F. Kurayama, S. Suzuki, T. Oyamada, T. Furusawa, M. Sato and N. Suzuki, Facile method for preparing organic/inorganic hybrid capsules using amino-functional silane coupling agent in aqueous media, *J. Colloid Interface Sci* **2010**, 349, 70-76.
[27] C. Li, Z.-Y. Li, J. Zhang, K. Wang, Y.-H. Gong, G.-F. Luo, R.-X. Zhuo and X.-Z. Zhang, Porphyrin containing light-responsive capsules for controlled drug release, *J. Mater. Chem.* **2012**, 22, 4623-4626.
[28] Q. Zhao, B. Han, Z. Wang, C. Gao, C. Peng and J. Shen, Hollow chitosan-alginate multilayer microcapsules as drug delivery vehicle: doxorubicin loading and in vitro and in vivo studies, *Nanomedicine* **2007**, 3, 63-74.

[29] I. Braccini and S. Pérez, Molecular Basis of Ca2+-Induced Gelation in Alginates and Pectins: The Egg-Box Model Revisited, *Biomacromolecules* **2001**, 2, 1089-1096.
[30] K. Y. Lee and D. J. Mooney, Alginate: properties and biomedical applications, *Prog. Polym. Sci.* **2012**, 37, 106-126.
[31] Y. C. Jung and B. Bhushan, Wetting behaviour during evaporation and condensation of water microdroplets on superhydrophobic patterned surfaces, *J. Microsc.* **2008**, 229, 127-140.
[32] W. Barthlott and C. Neinhuis, Purity of the sacred lotus, or escape from contamination in biological surfaces, *Planta* **1997**, 202, 1-8.
[33] X. Gao and L. Jiang, Water-repellent legs of water striders, *Nature* **2004**, 432, 36-36.
[34] M. Nosonovsky and B. Bhushan, Hierarchical roughness makes superhydrophobic states stable, *Microelectron. Eng.* **2007**, 84, 382-386.
[35] E. Robles, E. Villar, M. Alatorre-Meda, M. G. Burboa, M. A. Valdez, P. Taboada and V. Mosquera, Effects of the hydrophobization on chitosan-insulin nanoparticles obtained by an alkylation reaction on chitosan, *J. Appl. Polym. Sci.* **2013**, 129, 822-834.
[36] S. H. Kim and C. C. Chu, Synthesis and characterization of dextran-methacrylate hydrogels and structural study by SEM, *J. Biomed. Mater. Res.* **2000**, 49, 517-527.
[37] A. C. Lima, W. Song, B. Blanco-Fernandez, C. Alvarez-Lorenzo and J. F. Mano, Synthesis of temperature-responsive dextran-MA/PNIPAAm particles for controlled drug delivery using superhydrophobic surfaces, *Pharmaceut Res.* **2011**, 28, 1294-1305.
[38] B. V. Parakhonskiy, A. M. Yashchenok, M. Konrad and A. G. Skirtach, Colloidal micro- and nano-particles as templates for polyelectrolyte multilayer capsules, *Adv. Colloid Interface Sci* **2014**, 207, 253-264.
[39] H. Zimmermann, F. Ehrhart, D. Zimmermann, K. Müller, A. Katsen-Globa, M. Behringer, P. J. Feilen, P. Gessner, G. Zimmermann, S. G. Shirley, M. M. Weber, J. Metze and U. Zimmermann, Hydrogel-based encapsulation of biological, functional tissue: fundamentals, technologies and applications, *Appl. Phys. A* **2007**, 89, 909-922.
[40] F. Caruso, Hollow Capsule Processing through Colloidal Templating and Self - Assembly, *Chem. Eur. J.* **2000**, 6, 413-419.
[41] E. C. Goethals, A. Elbaz, A. L. Lopata, S. K. Bhargava and V. Bansal, Decoupling the effects of the size, wall thickness, and porosity of curcumin-loaded chitosan nanocapsules on their anticancer efficacy: size is the winner, *Langmuir* **2013**, 29, 658-666.

Chapter XII: Conclusions

SA surfaces were successfully employed to fabricate, under mild conditions, a variety of natural-based hydrogel systems with a spherical shape; all the obtained polymeric devices are summarized in Figure 12.1B. Previously, SH surfaces were proposed as biomimetic supports to yield spherical particles with sizes ranging from 1 to 3 mm. This technology comprises the pipetting of controlled volumes of a polymeric precursor solution onto a SH surface, which leads to spherical-shaped droplets. Afterwards, the previous liquid droplets are hardened into a hydrogel by employing one or more crosslinking steps (Figure 12.1A; Spherical). More recently, this strategy was further extended to yield multilayered millimeter-sized spherical particles containing different molecules to be released in a controlled manner as well as gathering the appropriate conditions to support the encapsulation of viable cells (Figure 12.1A; Multilayered). The main advantage of this methodology over the existent strategies to create spherical systems is the absence of an external liquid environment since the hydrogel particles are obtained mainly surrounded by air and under mild conditions. Consequently, sensitive bioactive molecules and living cells can be incorporated within these hydrogel spheres with encapsulation efficiencies of almost 100%, highlighting the potential of this bioinspired technology for biomedical purposes.

1. General Conclusion of the main results of Chapter VIII and XI

Despite all the advantages of using these liquid-repellent substrates, spherical particles with sizes in the micrometer range were inconceivable using a micropipette to dispense the polymeric solution. Improving on this technique, a novel, straightforward and cost-effective methodology, consisting in spraying followed by a crosslinking process, was developed to attain smaller spherical particles with diameters in the order of micrometers. The resultant microspheres were produced from aqueous solutions of MACHI, which was selected due to its cytocompatibility, solubility in water and its methacrylic groups necessary for crosslinking.

Importantly, the proposed strategy was proved to be suitable for obtaining hydrogel particles with sizes *ca.* 1 order of magnitude smaller when comparing with the current methodology using a micropipette. However, due to the to the simplicity of the spray system used, a broad particle size distribution was obtained.

For this reason, the previously described methodology was further optimized to produce polymeric microparticles with narrower size distributions. To this end, a MA-DEXT aqueous solution and an accurate dispensing system, consisting of a syringe pump and a nozzle, were used to generate a spray of polymeric droplets. By tuning both the polymer flow rate and the air pressure inside the nozzle, spherical hydrogel microparticles with a mean diameter of *ca.* 226.8 ± 38.8 μm were successfully fabricated after a photocrosslinking process (Figure 12.1B; Microparticle). Importantly, this technique, combining spraying with SA substrates, enabled the encapsulation of highly sensitive molecules such as proteins and viable cells inside the polymeric microparticles.

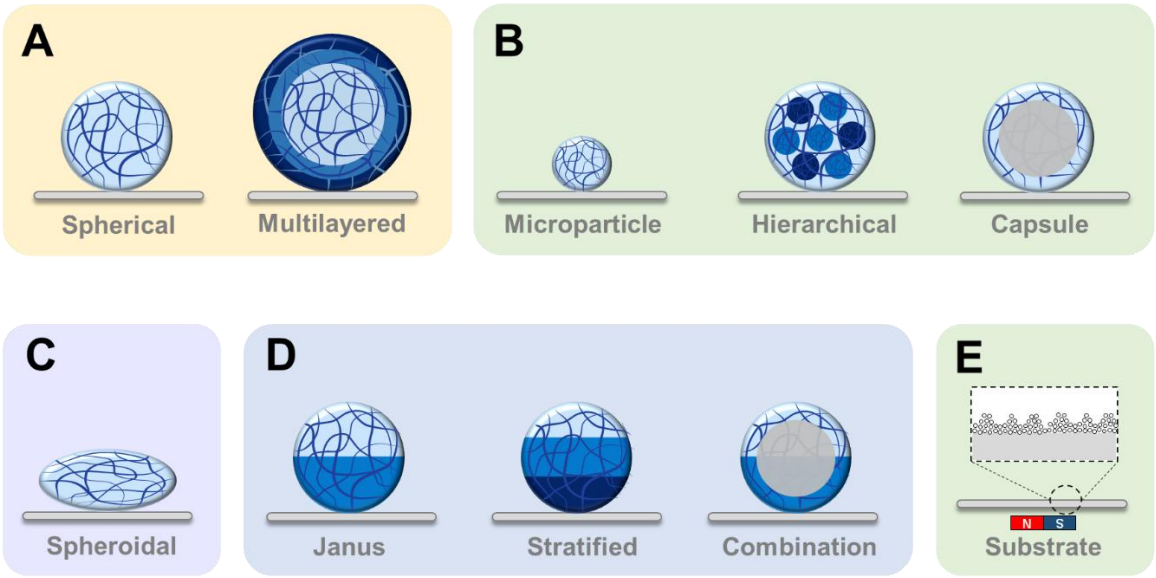

Figure 12.1 - Schematic overview of the use of liquid-repellent surfaces to produce polymeric particles. **(A)** Polymeric particles previously described in literature. **(B)** Polymeric particles advanced in this thesis; **(C)** Polymeric particles created in collaboration. **(D)** Polymeric particles that could be fabricated in future. **(E)** Schematic representation of the non-permanent SA surfaces designed in this thesis.

Spherical and hierarchical hydrogel systems were also produced over a SA surface by incorporating the MA-DEXT microparticles into ALG macroscopic beads crosslinked by ionic gelation (Figure 12.1B; Hierarchical). The suitability of the obtained hierarchical particles to incorporate and release biomolecules was evaluated. Indeed, the fabrication of this second ALG polymeric matrix demonstrated to be useful for drug delivery purposes inasmuch as it proved to tune the release profile of the encapsulated proteins.

Additionally, SA surfaces were successfully employed to fabricate ready-to-use and stable multiscaled polymeric capsules, comprising a: (i) hydrogel shell made of MACHI and (ii) a liquefied core, wherein different molecules can be dispersed (Figure 12.1B; Capsule). This strategy benefit from its (i) solvent-free character enabling a loading efficiency of almost 100%, (ii) reproducibility as demonstrated by the great control over the particle size and shape, (iii) versatility as shown by the fabrication of a wide variety of core–shell capsules using reversible crosslinking mechanisms, a interfacial gelation process or ice; (iv) mild processing conditions as proved by the safe encapsulation of metabolically active cells, and (v) its cost-effective character inasmuch as it is based on a simple setup. Capsules with a hierarchical structure were also fabricated by incorporating different objects inside the core during the synthesis process, proving once more the versatility of this strategy. Herein, $CaCO_3$ particles, PLLA microparticles, magnetic particles were successfully encapsulated within MACHI liquified capsules.

With the work performed in this thesis, it was also possible to further the design of SA surfaces by freely covering a solid substrate with specifically designed polyamide particles (Figure 12.1E; Substrate). On the one hand, when placed above a substrate, these particles mimicked the hierarchical structure of natural superhydrophobic surfaces, such as Lotus-leaf. On the other hand, their coating with a perfluorinated hydrocarbon precursor resulted in contact angle values of around 150° and 140° for water and diiodomethane, respectively, highlighting their quasi SA character. Additionally, magnetic particles were entrapped within these hydrophobized particles to allow their instantaneous and temporary immobilization above

the desired substrate as well as the complete recuperation of both substrate and microcapsules after elimination of the magnetic field. Worth noticing, the developed non-permanent SA surfaces did not present any cytotoxicity.

2. Future perspectives on the use of SA surfaces to produce spherical objects

2.1. Applications and future improvements of the produced multistructured particles

The strategies described in this thesis were proven successful in the design of multiple hydrogel-based systems, ranging from homogeneous noncompartmental microparticles to complex multicompartmental devices with distinct architectures. The versatility of the proposed strategy was demonstrated by using different natural-based materials such as chitosan, dextran, alginate and gelatin as well as various crosslinking mechanisms including photocrosslinking, ionotropic gelation and temperature-mediated crosslinking.

As previously mentioned, robust microparticles with homogeneous size distributions were produced for the first time above superantiwetting surfaces; this advance is anticipated to expand the use of this bioinspired technology in applications which require smaller sizes such as drug delivery and tissue engineering. Their potential for biomedical purposes was further reinforced by producing natural-based microspheres with the required characteristics to sustain the encapsulation of proteins and cells. Moreover, the simplicity of the concept and the attainable SA character of the used surfaces, make it possible to expand this technology to other purposes such as cosmetics, agriculture, food technology and electronics, where solvents different than water are often required. Future improvements could also include tuning the particle surface chemistry or physical properties. The bioactivity of these structures could be enhanced by incorporating bioactive sequences such as arginine-glycine-aspartic acid (RGD), which is recognized by integrin receptors on cellular membrane. Moreover, hydrogel spheres with better mechanical properties could be designed by combining this biomimetic strategy

with the DN-based methodology described in Section 1. It is also important to notice, that by applying the developed methodology, combining spraying and liquid repellent surfaces, several microparticles were produced simultaneously over a superantiwetting substrate, which can be advantageous for their massive production for industrial purposes.

Multicompartmentalized systems such as the ones described in this thesis can combine different reactions and functionalities in a confined volume. Therefore, they could be potentially used to create novel platforms, which could have direct applicability in building multifunctional artificial cells, drug carriers microreactors and disease models. Owing to their cytocompatibility and their mild processing conditions, these natural-based spherical particles are expected to be used as hydrogel carriers of many sensitive bioactive molecules such as cells and proteins in a plethora fields such as biology and tissue engineering. For drug delivery purposes, this compartmentalized architecture is envisioned to offer simultaneous release of various bioactive agents at different kinetics, which could potentially fulfill the therapeutic demands of a specific disease. In fact, their application range is diverse due to the versatility of the developed strategy, meaning that all the components of these multicompartmentalized particles can be easily replaced or combined with new features to meet the requirements of a specific application. Consequently, the developed hydrogel-based systems could potentially be applied in other fields rather than for biomedical purposes.

The production of hydrogel particles with complex structures is still challenging using the current available methodologies. Owing to the widespread application of engineered devices like these ones, modifications to the conventional fabrication techniques are likely to have a strong impact and open new prospects for the development of the next generation of customizable assemblies for both science and technology. In fact, it is expected the preparation of more sophisticated and complex systems using this bioinspired technique due to all its advantages. These modifications on the material macroscopic structure could include the fabrication of Janus (Figure 12.1D; Janus), stratified (Figure 12.1D; Stratified) or a combination of all the structure already attained (Figure 12.1D; combination). Besides the

production of spherical objects, hydrogels could be processed into other shapes above highly repellent surfaces. Indeed, a recent publication, demonstrated the possibility of creating spheroidal particles using this biomimetic methodology (Figure 12.1D; Stratified).

Finally, the use of SH or SA surfaces could be scalable for a continuous mass production by employing surfaces with larger areas and more automatic dispensing systems.

2.2. Improvements on the design of SA surfaces and future applications

The proposed versatile strategy to create non-permanent SA surfaces, by designing microparticles with a hierarchical composition, a low surface energy and magnetic properties, provides a consistent basis for the development of other devices based on this class of coatings. Such substrates could be prospective candidates for direct applications in a large spectrum of fields including biomedicine, biotechnology, and agriculture to prepare water/oil repellent surfaces, liquid marbles, microfluidic channels, and as templates for polymeric particles fabrication. The potential of the developed SA surfaces for the fabrication of the aforementioned systems was proved in this thesis. In particular, the produced liquid marbles could be used as stable spherical miniaturized bioreactors due to their ability to inject or remove liquid without destroying their integrity. Moreover, the magnetic responsiveness of the produced liquid marbles constitutes an advance in this kind of systems, conferring easiness on handling.

Future developments of these microcapsule-based SA surfaces may include testing other materials other than polyamide (for example, natural polymers) to confer, for instance, optical transparency that could be useful for several purposes such as in electronic and medical devices. Moreover, the stability of the obtained surfaces could be tuned by controlling, for instance, the amount of magnetic microparticles embedded inside the matrix of the hydrophobized microcapsules. The widespread implementation of this strategy for industry-related applications could also require a new deposition method of the microcapsules using techniques that cover larger areas.